BED LOAD DEPOSITS OF SHALLOW, UNIDIRECTIONAL CURRENTS

By A.J. Moss

VOLUME 2

CONTENTS:-

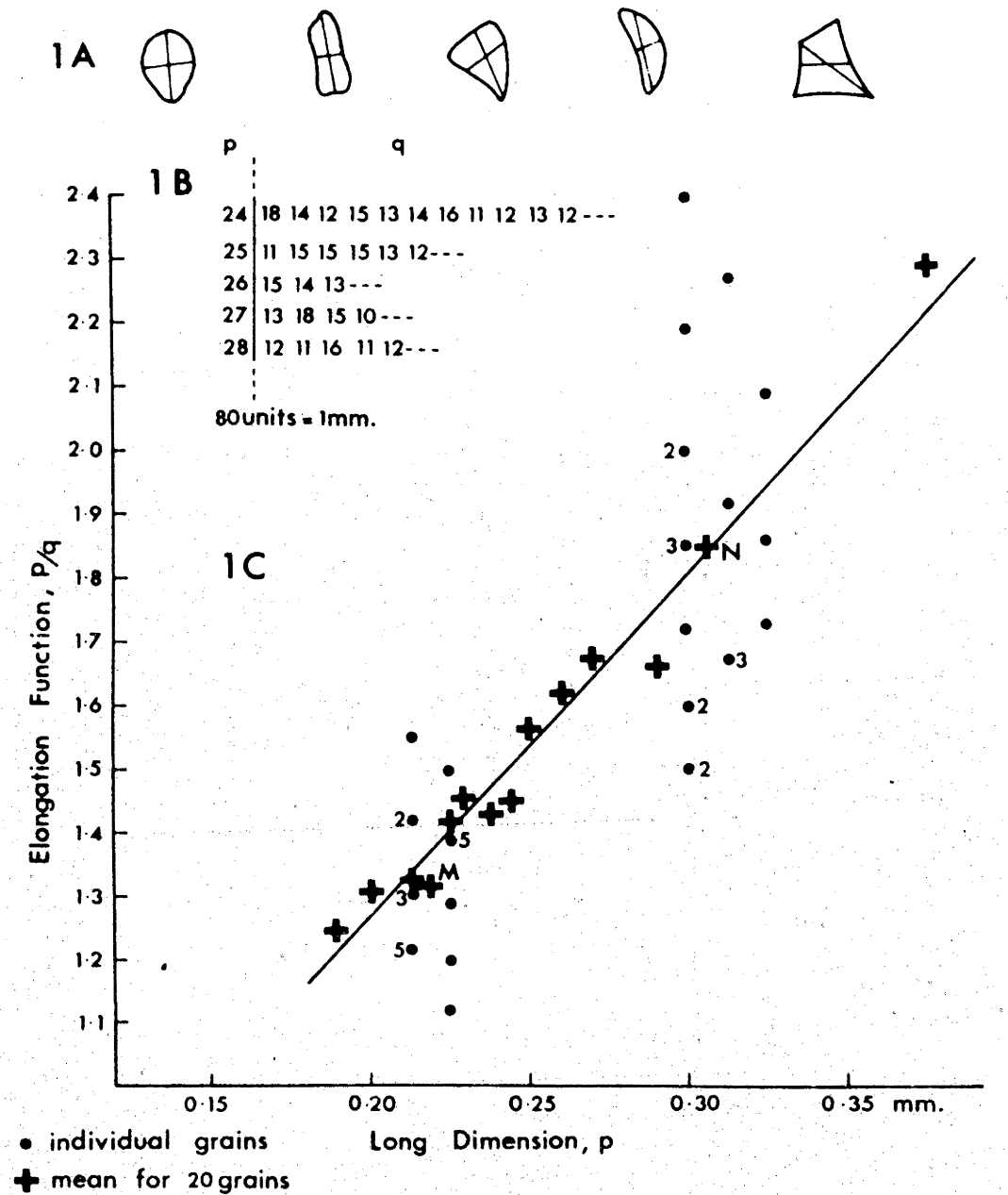

Fig. 1. Preparation of elongation function curve; A, - measurements made on particles B, - section of data sheet with values of q coded against values of p; C, - elongation function curve fitted to means of 20 grains of successive values of p. Points have appropriate figure if more than one grain has same dimensions. Those shown subscribe to means marked M and N.

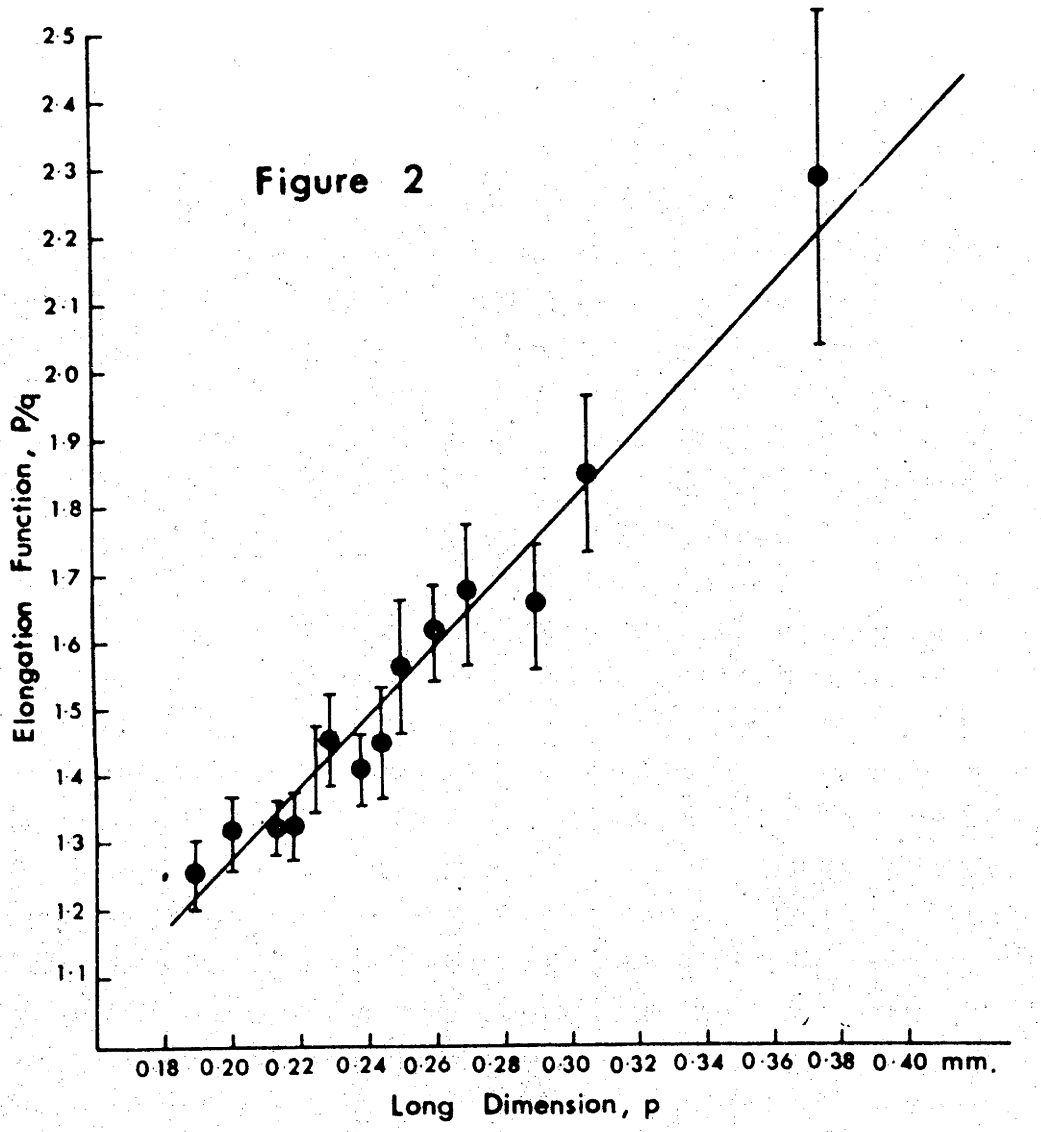

Fig. 2. Elongation function curve of 280 quartz grains with settling velocities between 0.74 and 0.82 cm/sec at 25°C. Points are means of 20 grains. 95% confidence limits are plotted for each point.

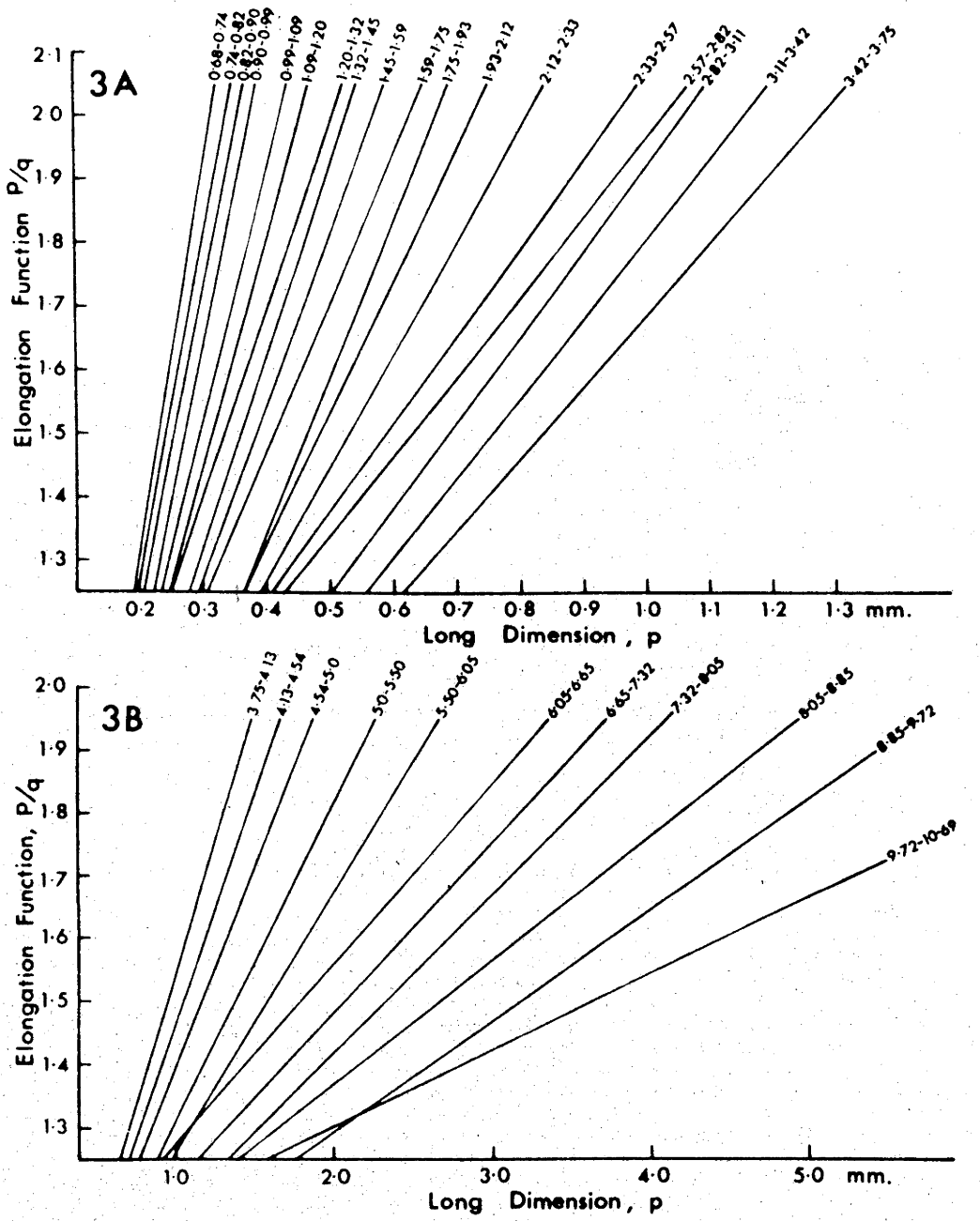

Fig. 3. Elongation function curves of successive suites of quartz grains with respect to settling velocity at 25°C. Each settling velocity range is covered by factor of 1.1. Ranges (cm/sec) are marked on curves.

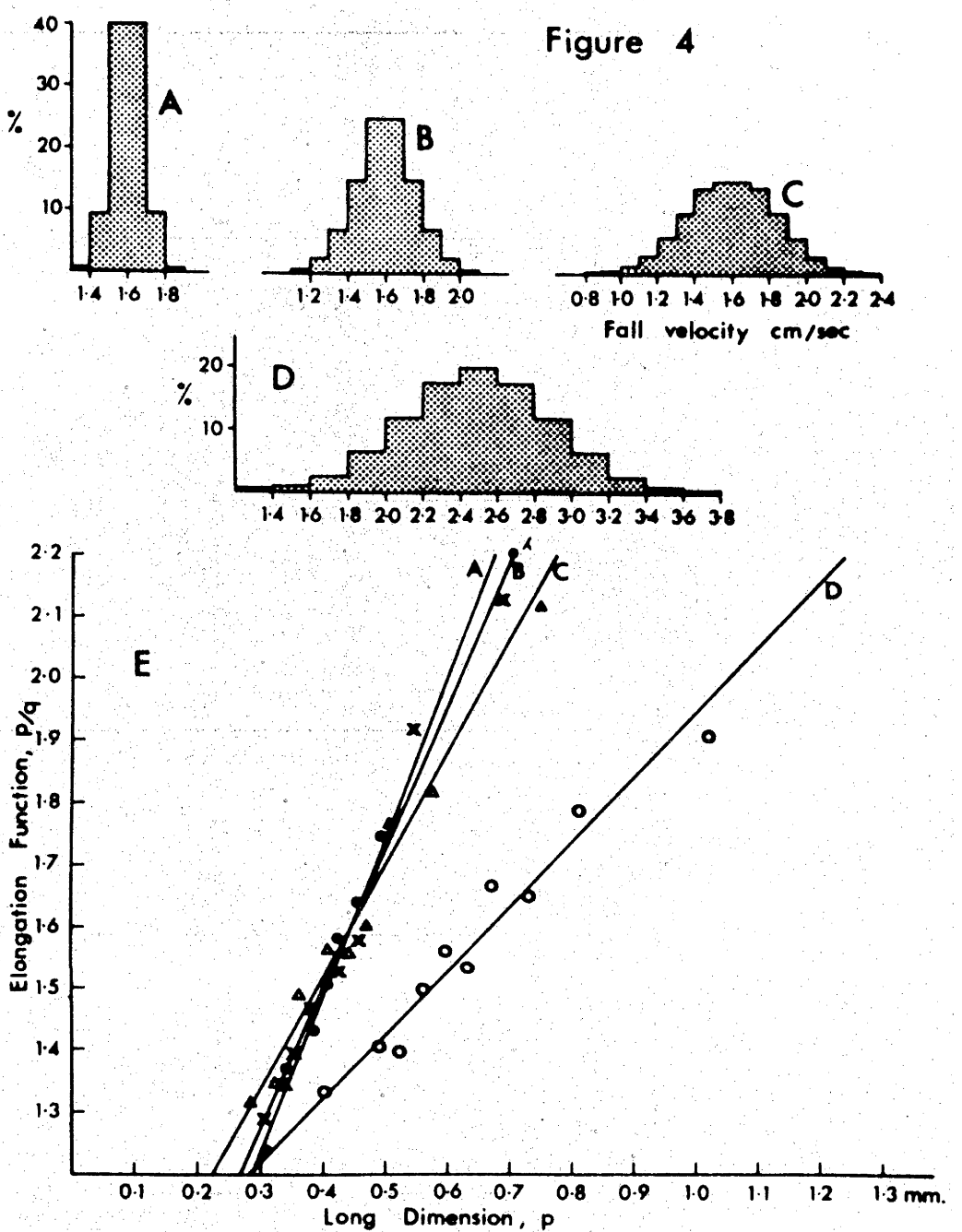

Fig. 4. Elongation function curves of quartz grain suites having gaussian distributions, with respect to settling velocity, of increasing dispersion.

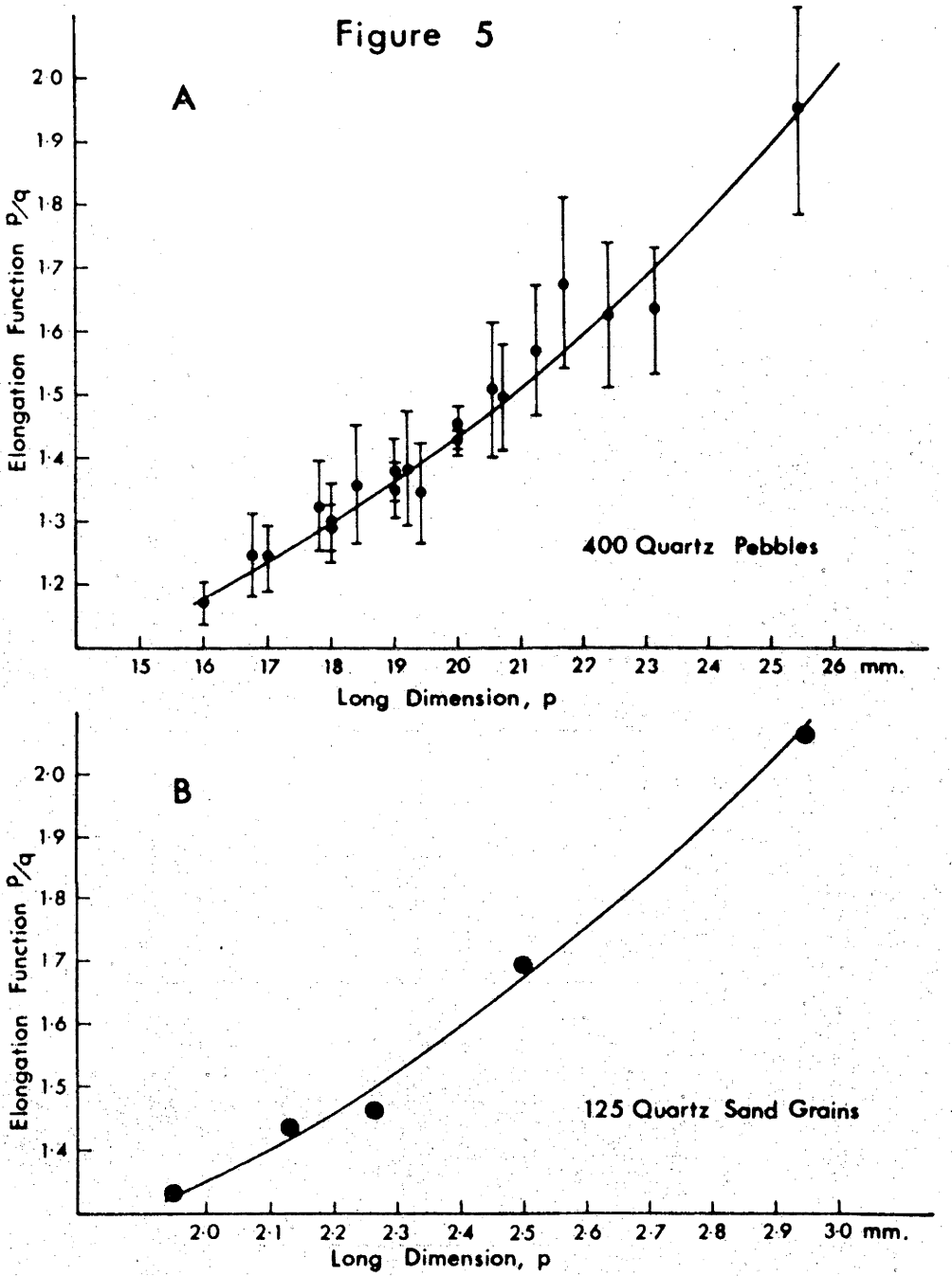

Fig. 5. Elongation function curves of suites of particles of nearly constant size. For quartz pebbles (above) points are means of 20 individuals and 95% confidence limits are given. Points for quartz sand grains are means of 25.

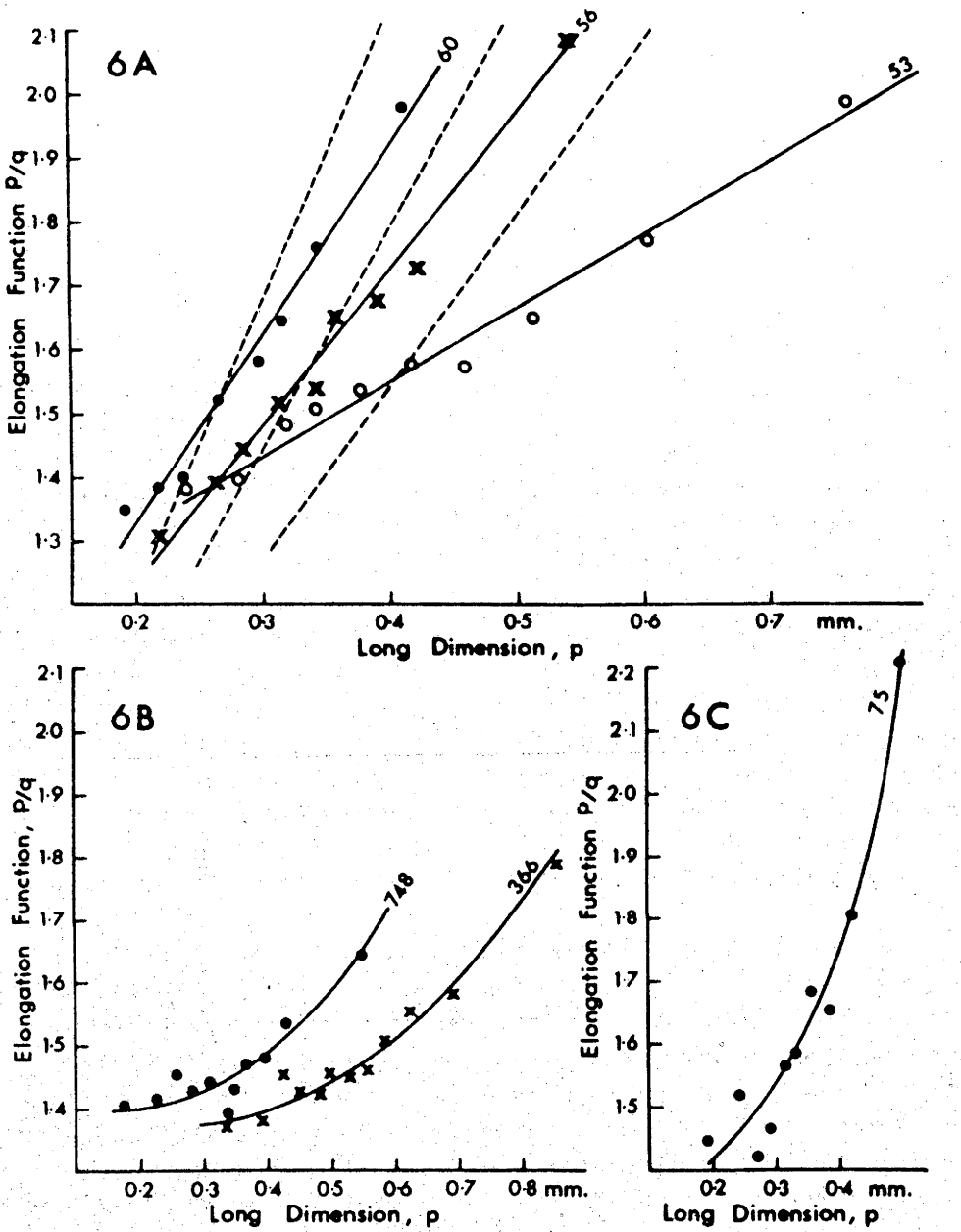

Fig. 6. A, - Elongation function curves of quartz grains from three natural beach sands compared with those of suites of quartz grains of nearly constant settling velocity (broken lines). Beach sands from Perranporth, Cornwall, U.K. B and C, - Elongation function curves of three wind laid sands; No. 748 from a desert dune in Abu Dhabi; No. 366 from Shoeburyness, Essex, U.K.; No. 75 from dune flanking beach yielding sands in 6A.

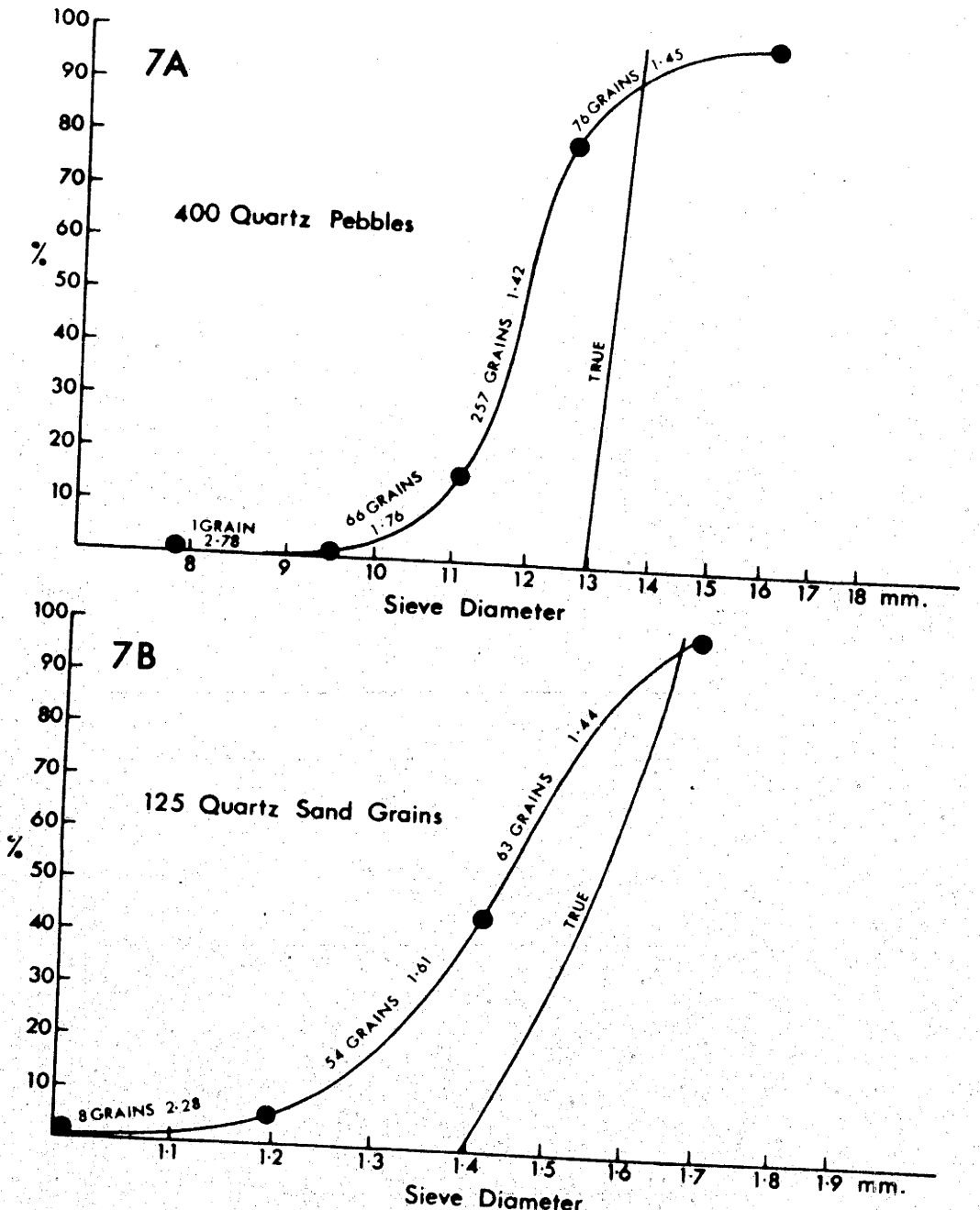

Fig. 7. A - Comparison of true size distribution and sieve size distribution for 400 quartz pebbles. Number of grains and mean elongation function are marked on each sieve fraction. 7B shows analogous results for 125 coarse sand grains.

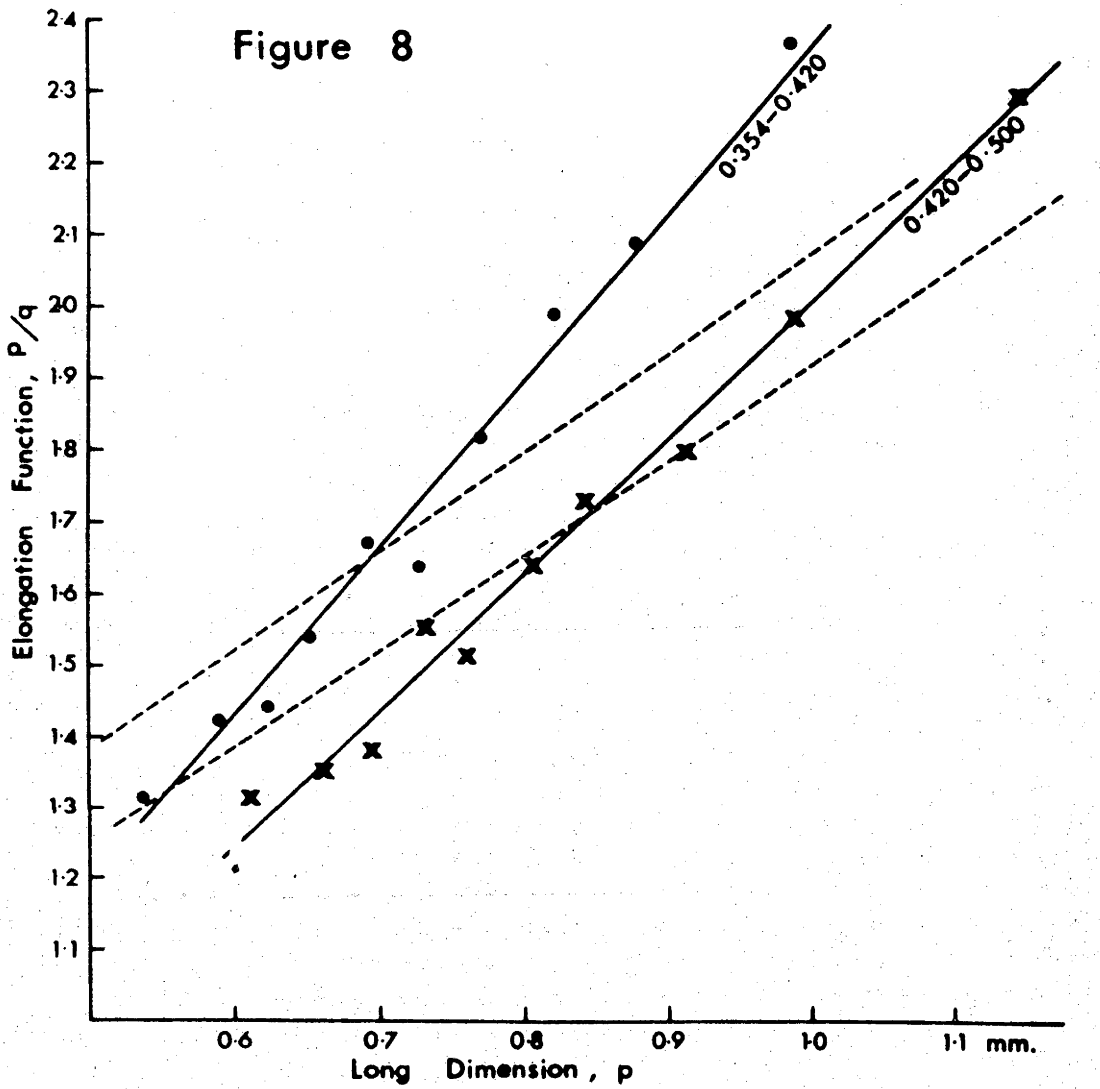

Fig. 8. Elongation function curves of two successive sieve fractions from a river sand. Superimposed are less steep curves of suites of quartz grains of almost constant settling velocity and similar mean size.

Figure 9

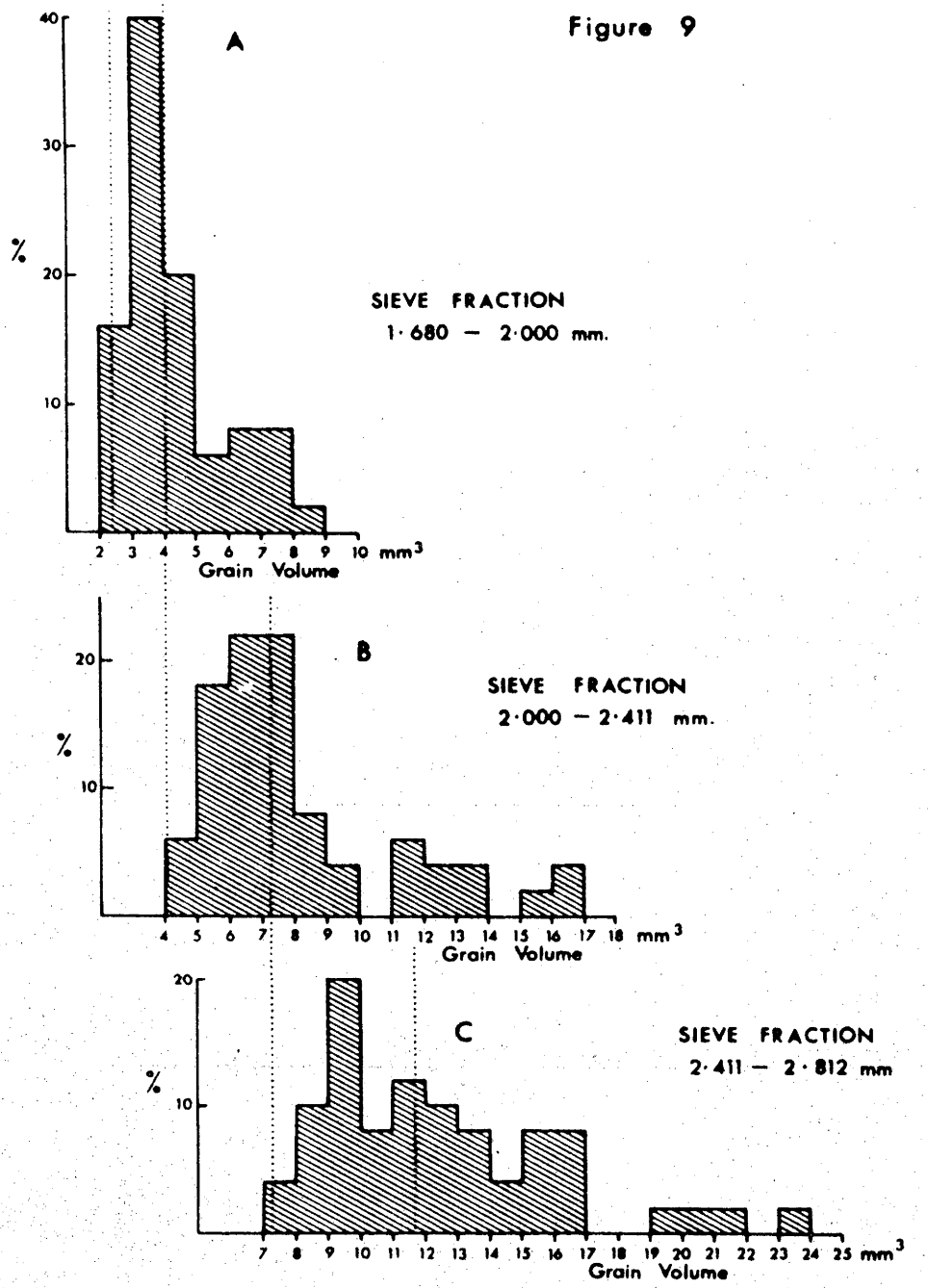

Fig. 9. Histograms of true sizes(volumes) of 50 quartz grains from each of three successive sieve fractions. The size ranges of spheres that could occur in the same fractions are indicated. Major size overlaps occur between successive fractions.

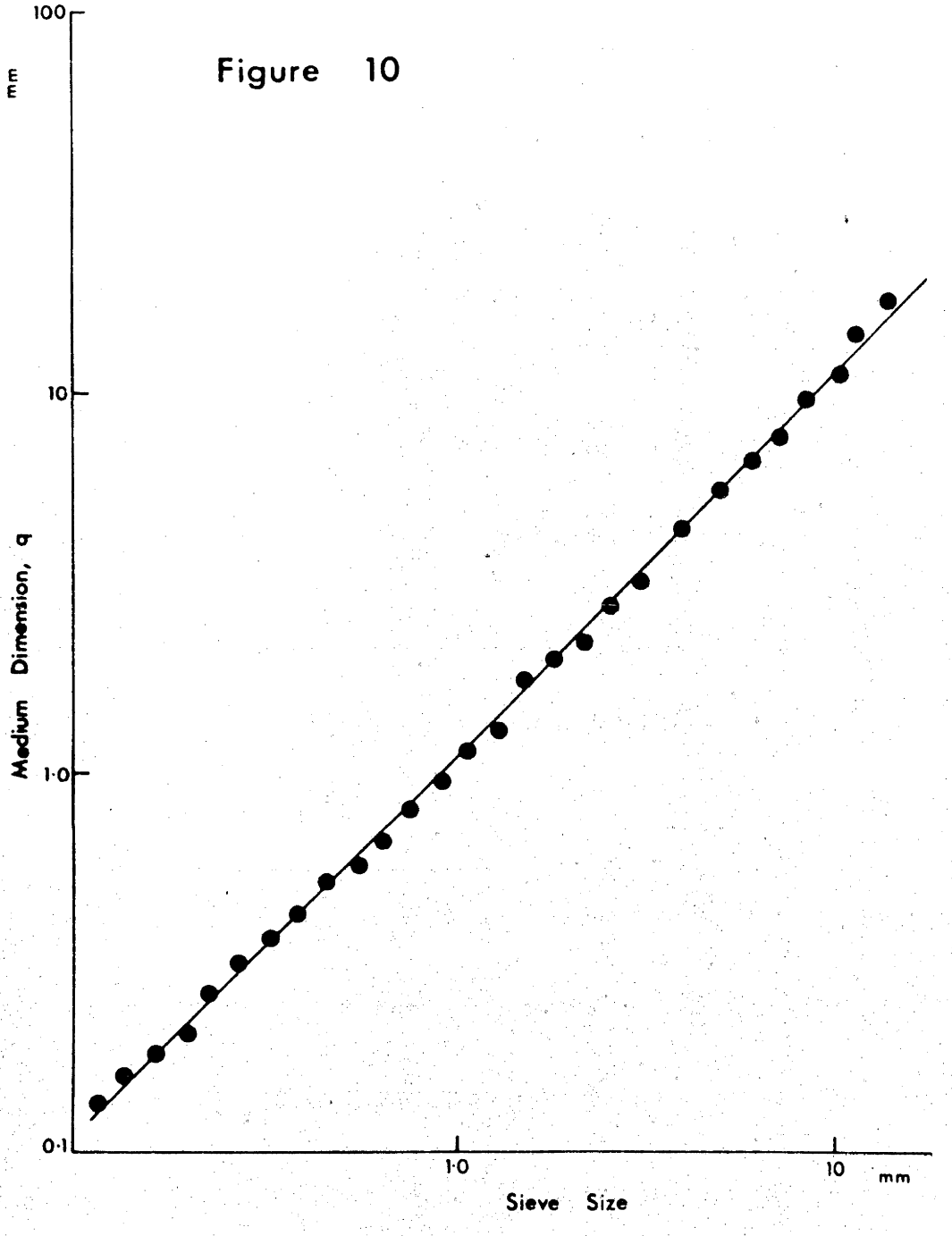

Fig. 10. Relationship between medium dimension (q) and sieve diameter for sand from the Molonglo River.

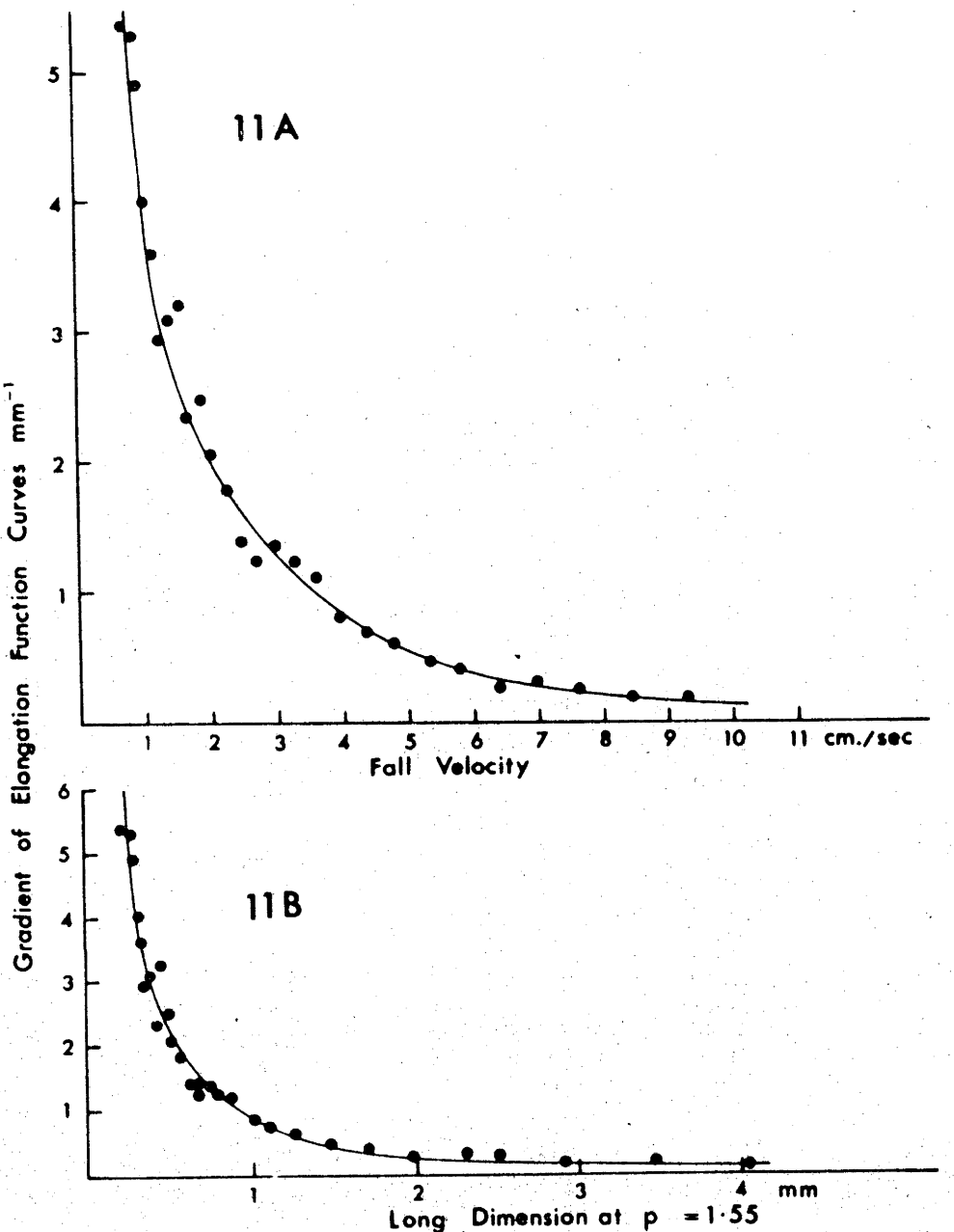

Fig. 11. A, - Gradients of elongation function curves of suites of grains of nearly constant settling velocity (shown in Fig. 3) plotted against fall velocity (settling velocity. B, - Relationship of gradients to long dimension value at p/q = 1.55.

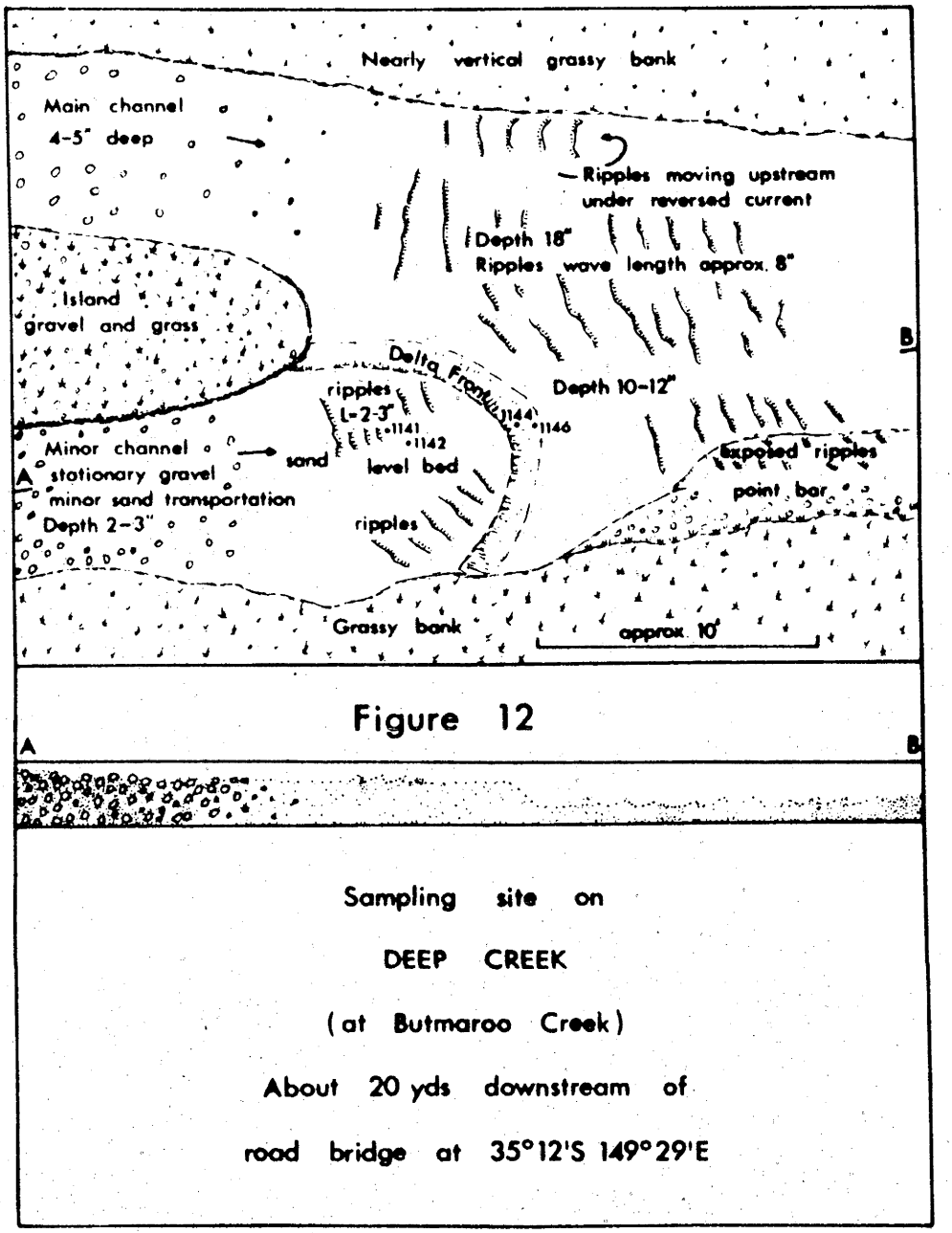

Figure 12

Fig. 12. Sampled site in Deep Creek. Reference numbers of samples studied are shown. A B is line of vertical section.

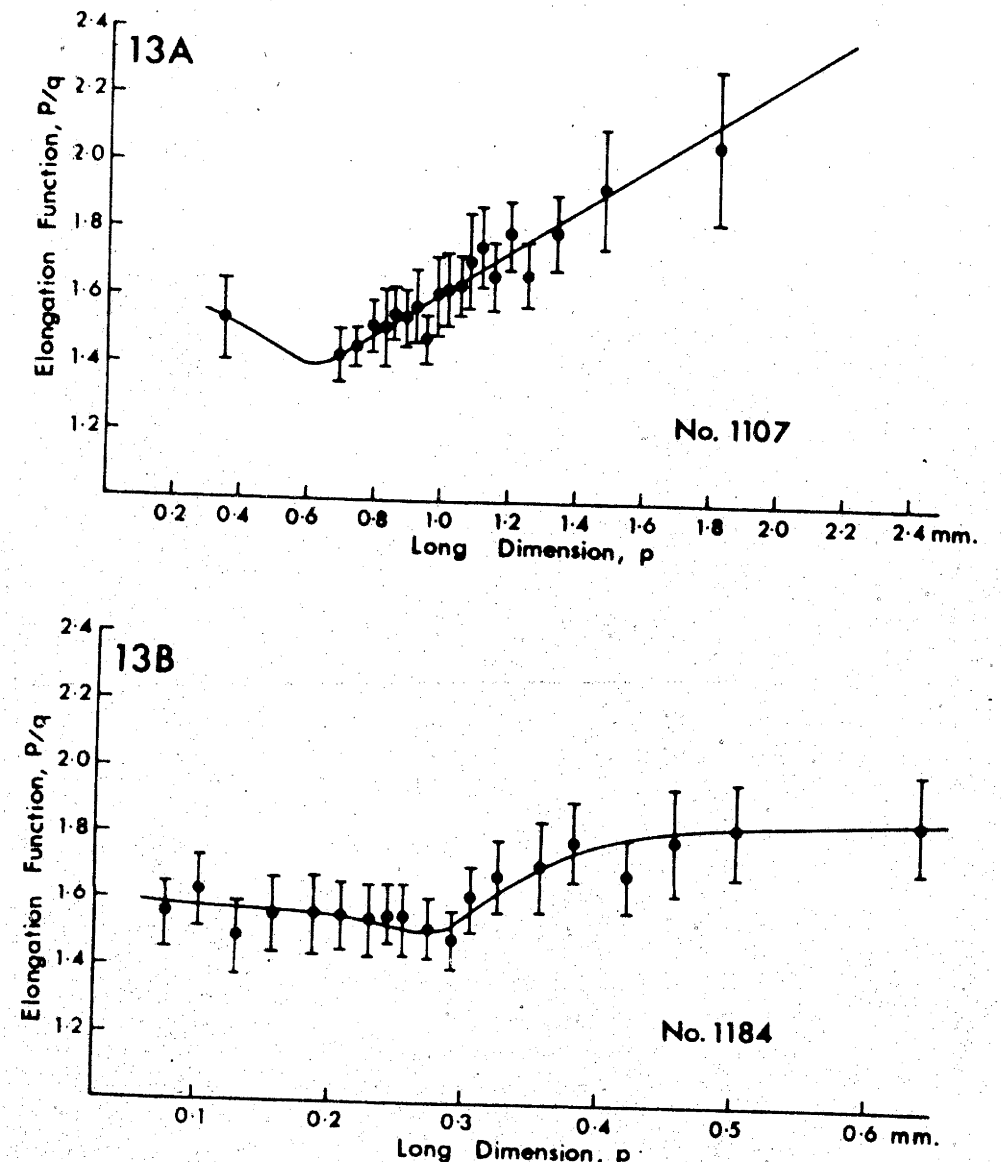

Fig. 13. Elongation function curves of two natural ripple stage sands, showing 95% confidence limits for mean points; points are means of 30 grains.

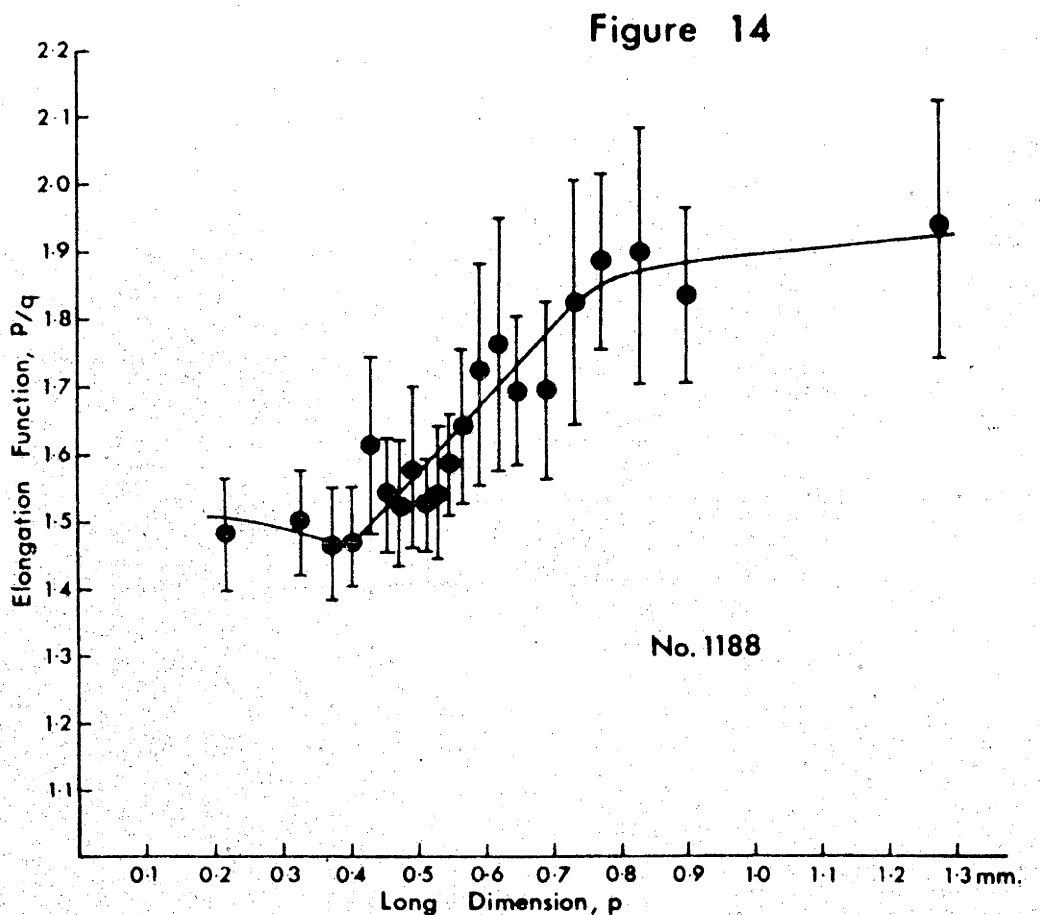

Fig. 14. Elongation function curve of a natural ripple stage sand showing 95% confidence limits for mean points.

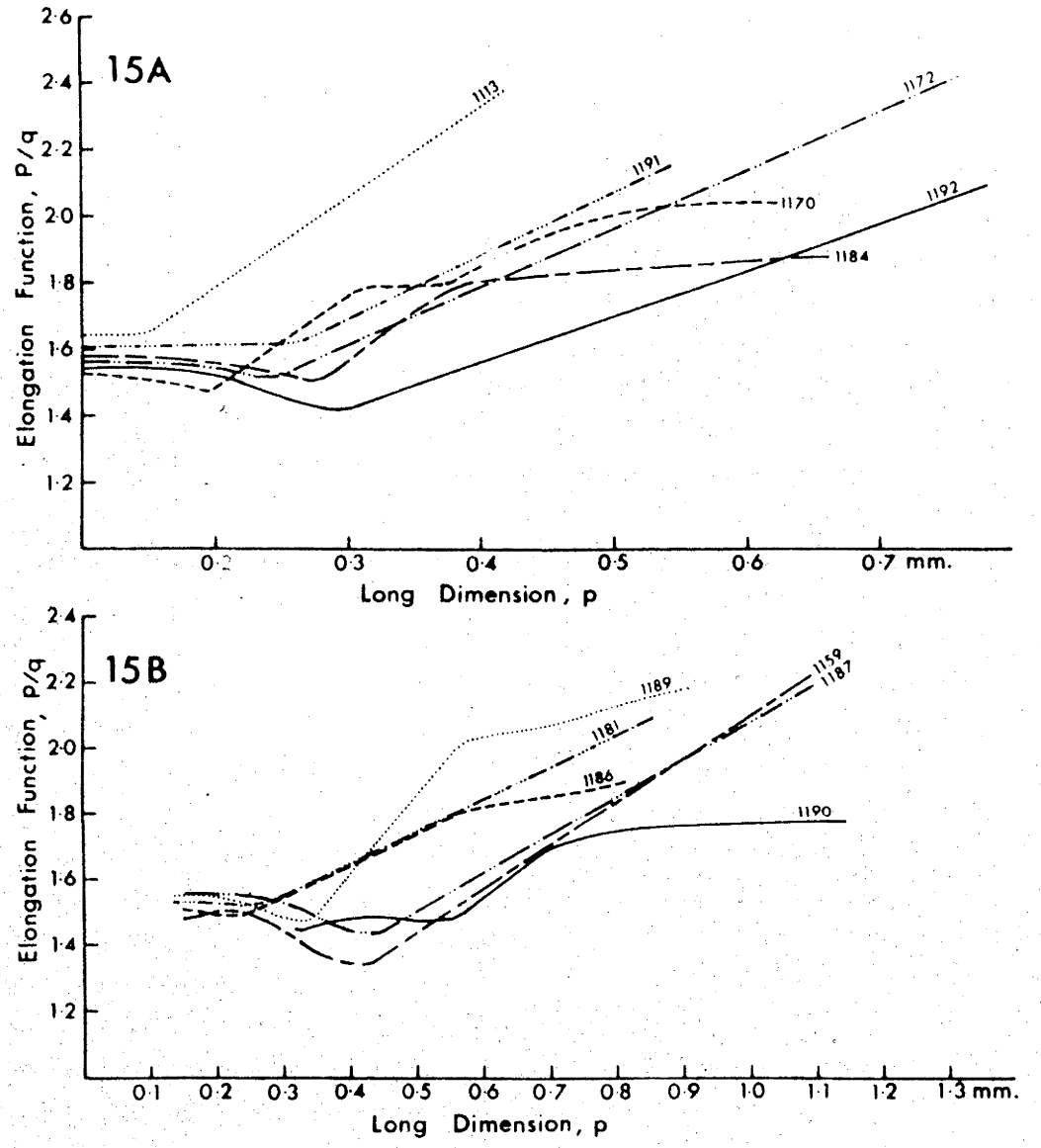

Fig. 15. Elongation function curves of ripple stage sands from rivers. Sediments described in Appendix 1.

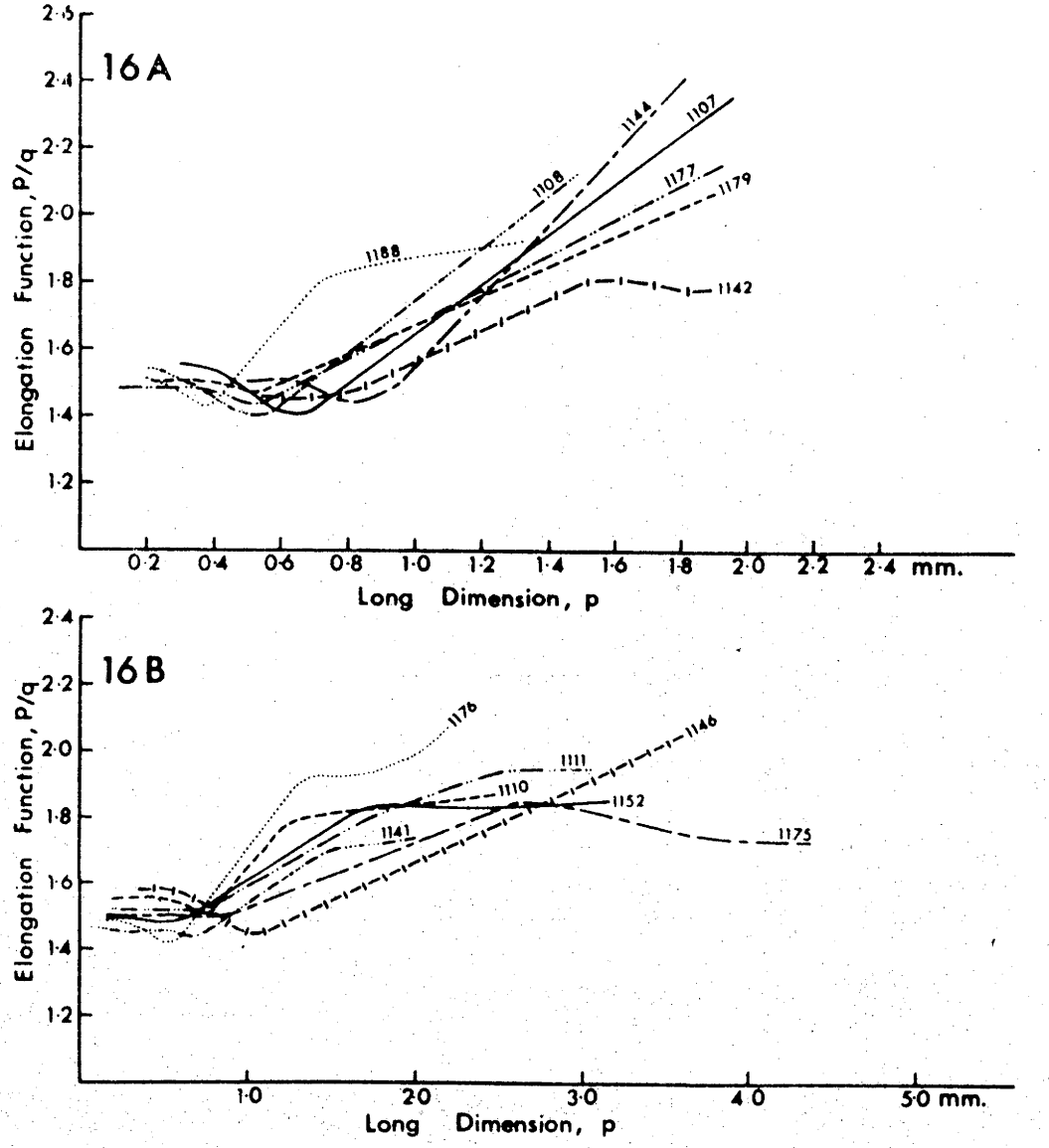

Fig. 16. Elongation function curves of ripple stage sands from rivers. Sediments described in Appendix 1.

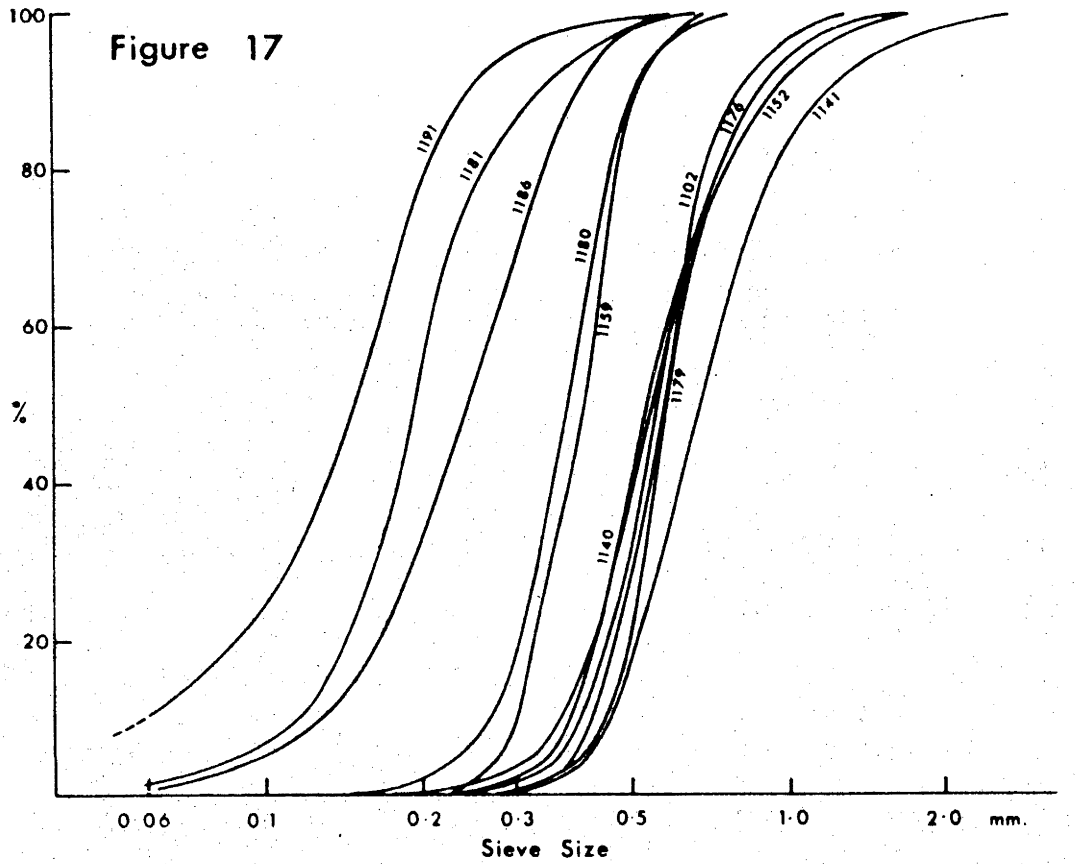

Fig. 17. Sieve cumulative curves for entire natural ripple stage sands.

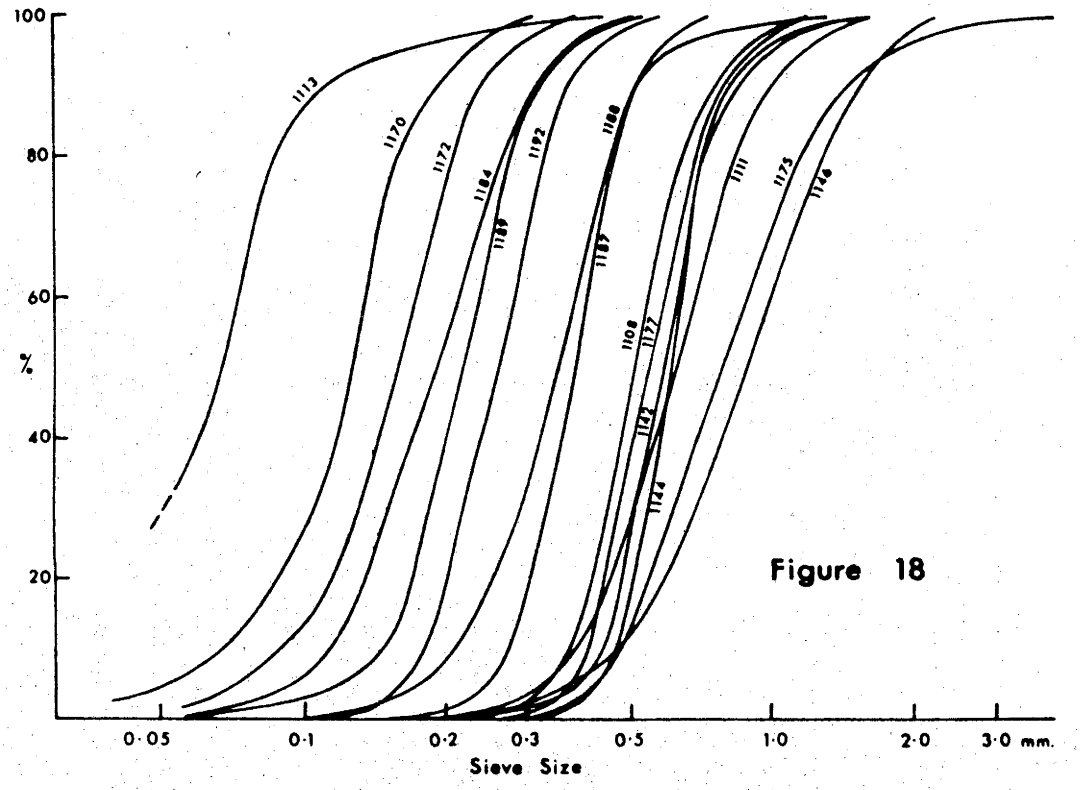

Fig. 18. Sieve cumulative curves for entire natural ripple stage sands.

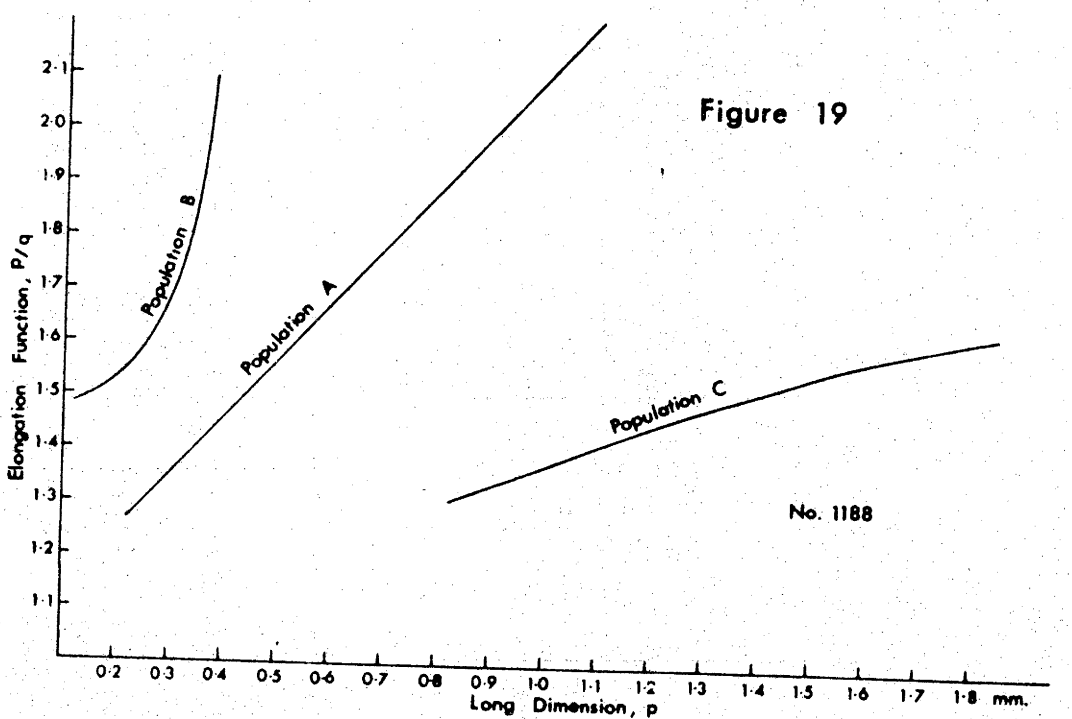

Fig. 19. Elongation function curves of the separated particle populations of No. 1188, a ripple stage sand.

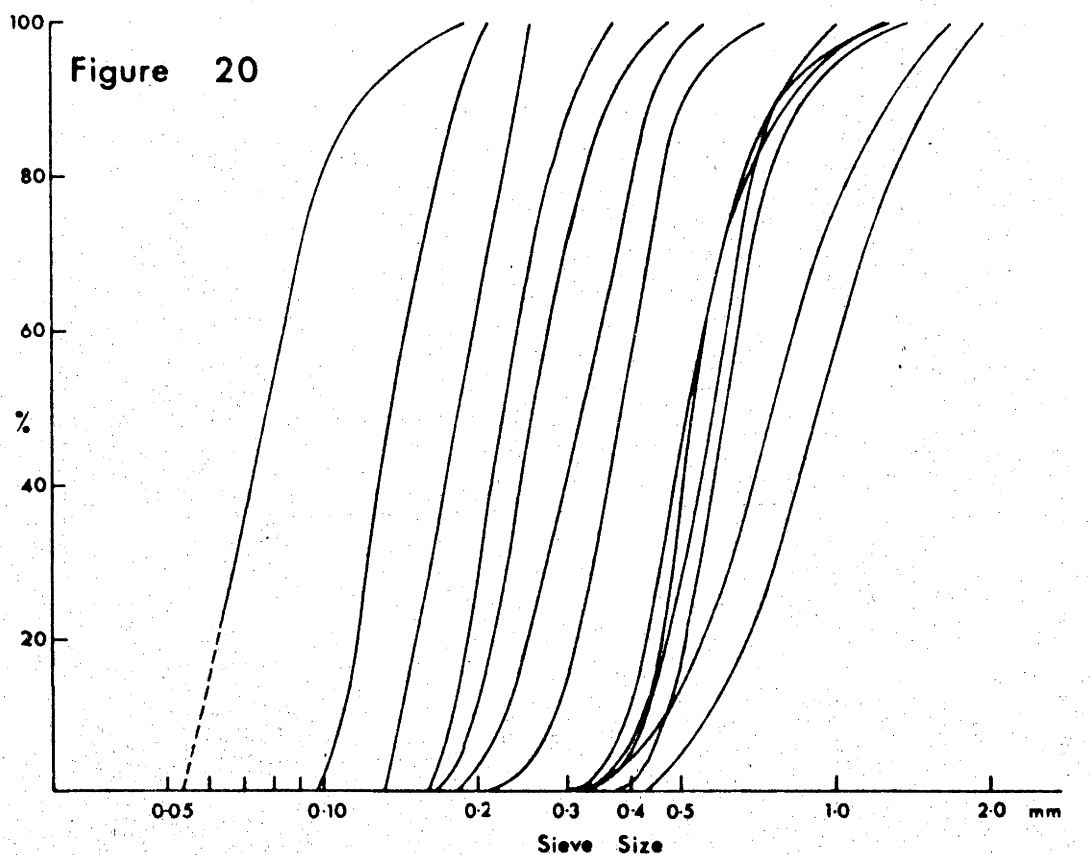

Fig. 20. Sieve cumulative curves for separated Population A's of natural ripple stage sands.

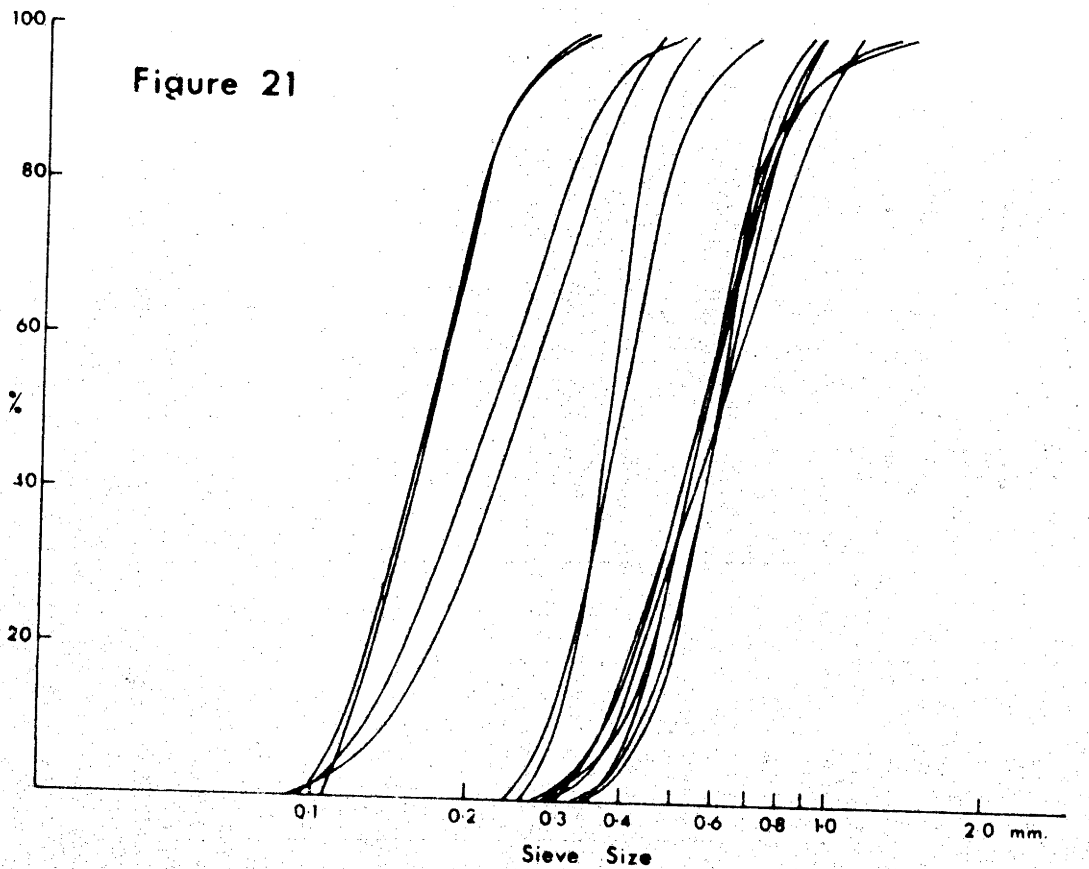

Fig. 21. Sieve cumulative curves for separated Population A's of natural ripple stage sands.

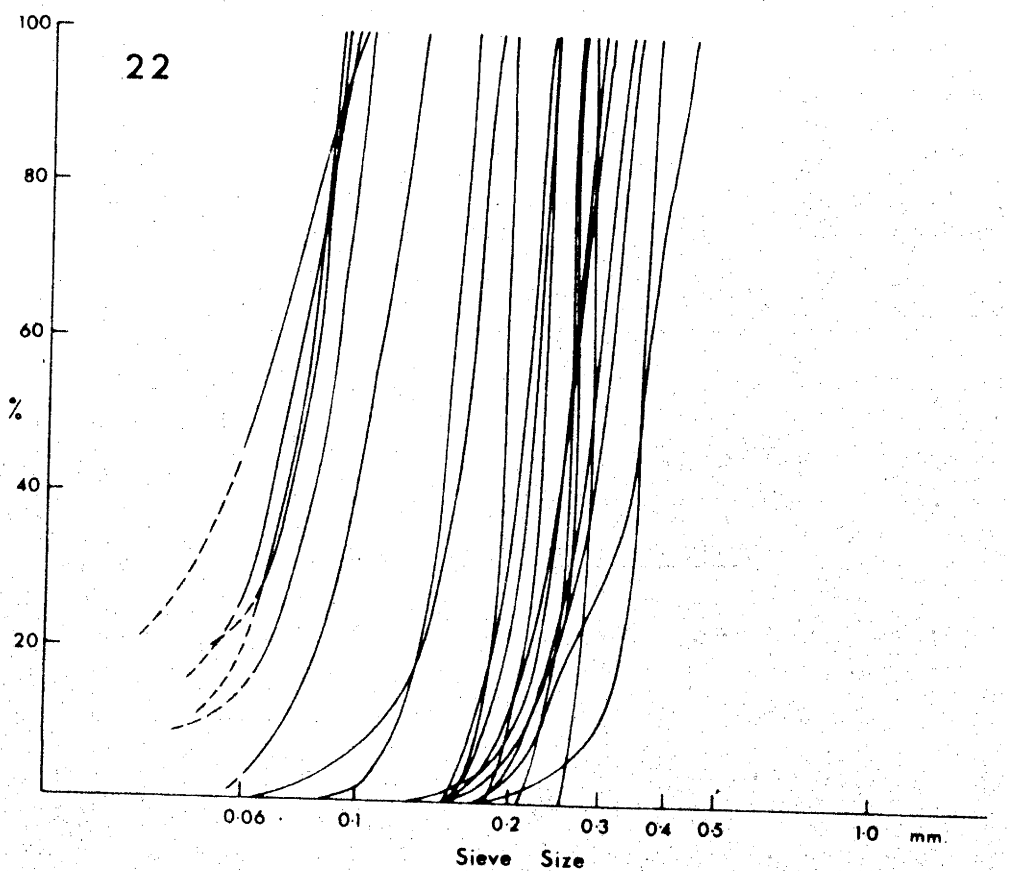

Fig. 22. Sieve cumulative curves for separated Population B's of natural ripple stage sands.

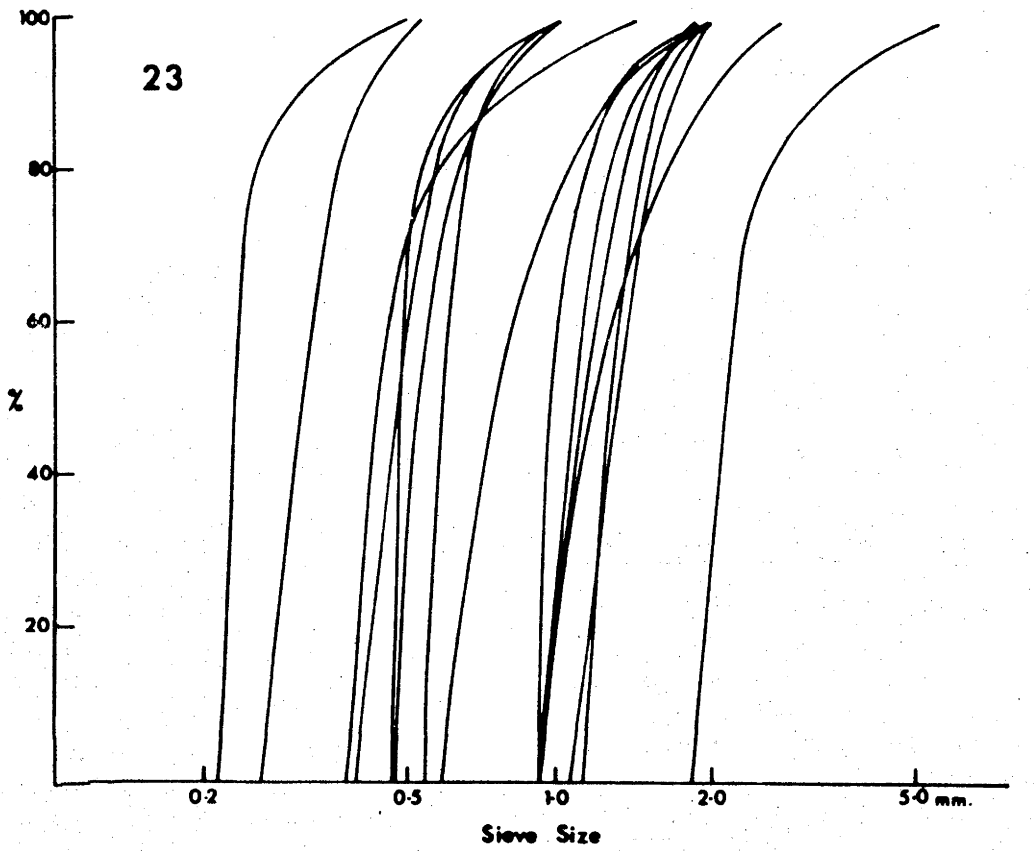

Fig. 23. Sieve cumulative curves for separated Population C's of natural ripple stage sands.

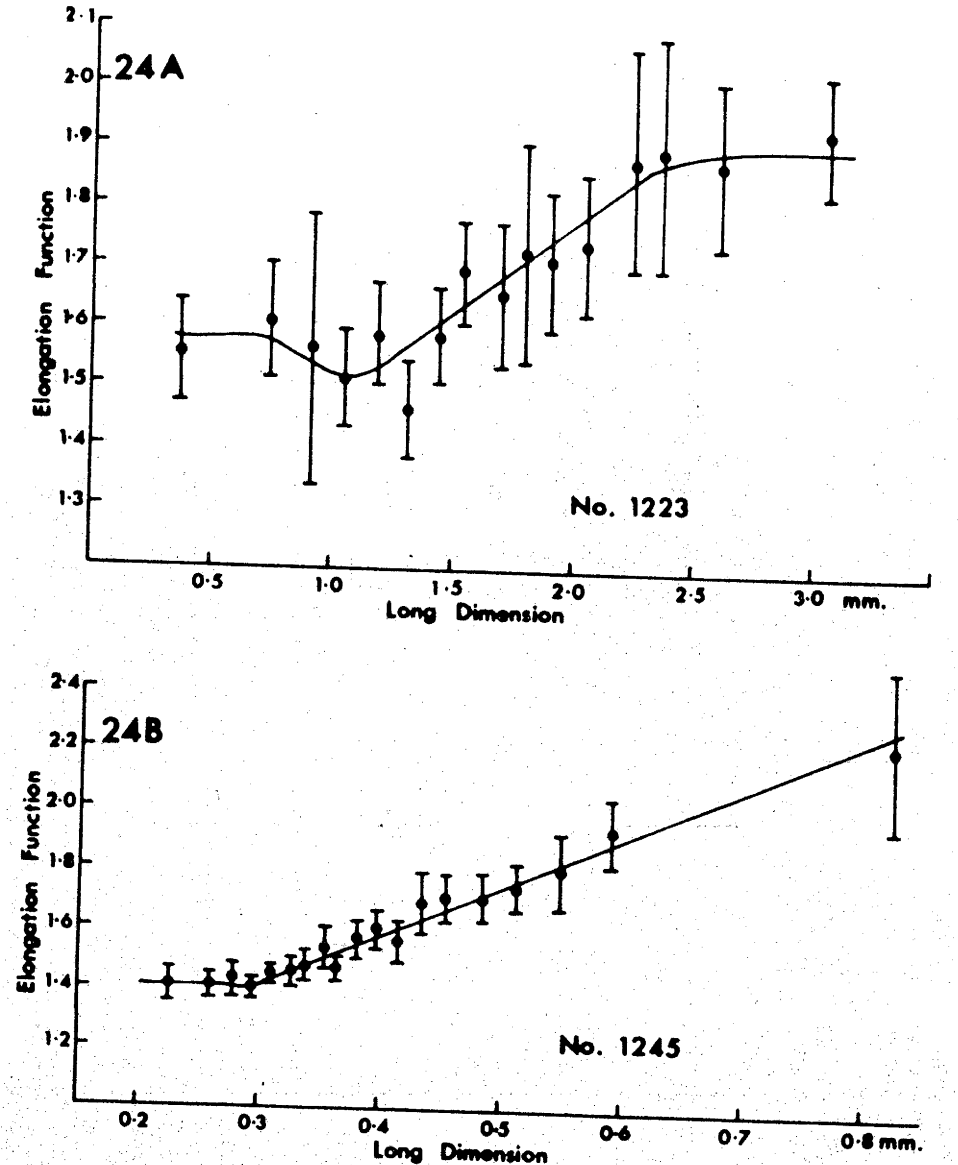

Fig. 24. Elongation function curves for two dune stage sands. 480 grains measured for No. 1223 (means of 30); 1140 for No. 1140 (means of 60). 95% confidence limits are given for the means.

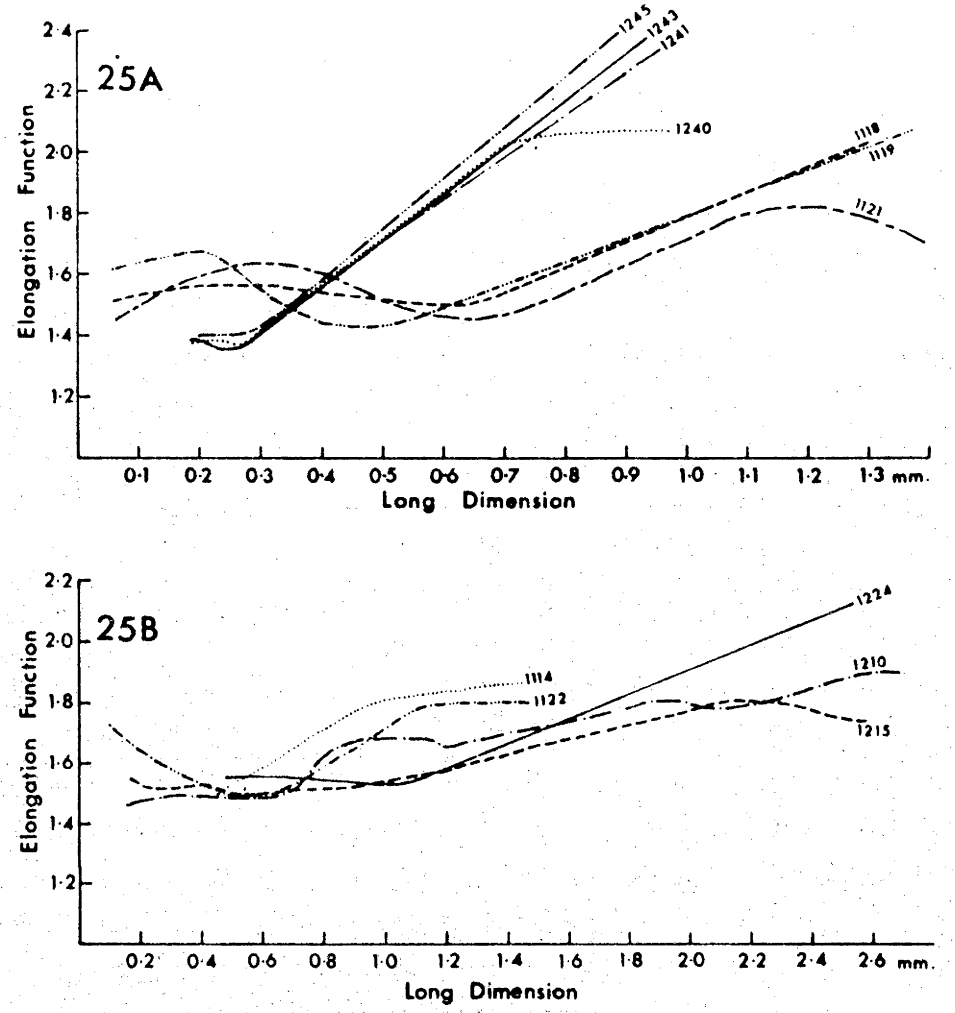

Fig. 25. Elongation function curves for natural dune stage sands.

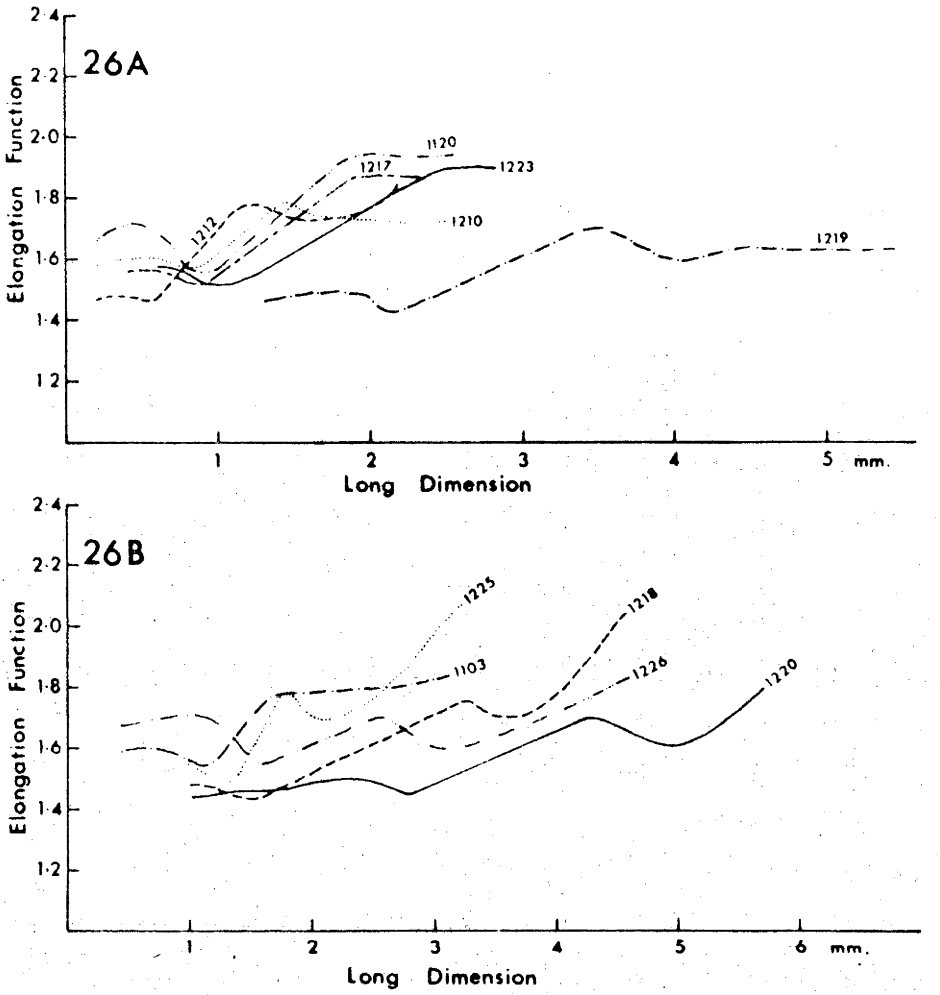

Fig. 26. Elongation function curves for natural dune stage sands.

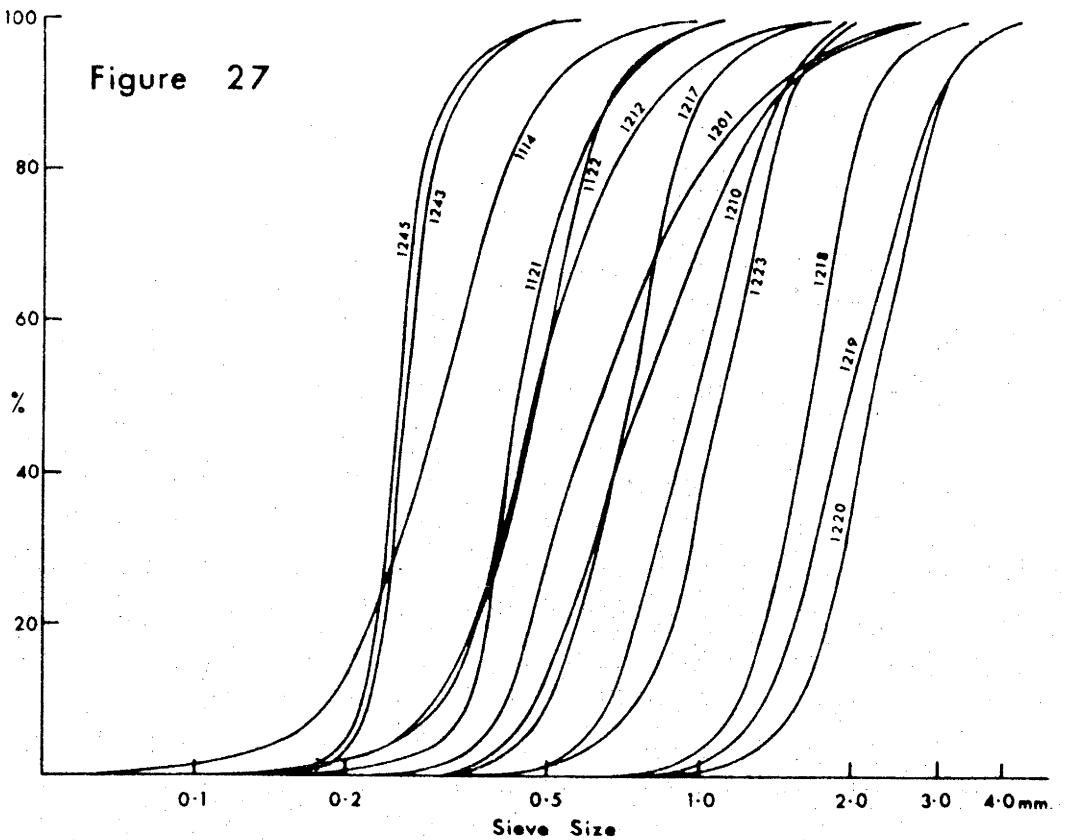

Fig. 27. Sieve cumulative curves for entire natural dune stage sands.

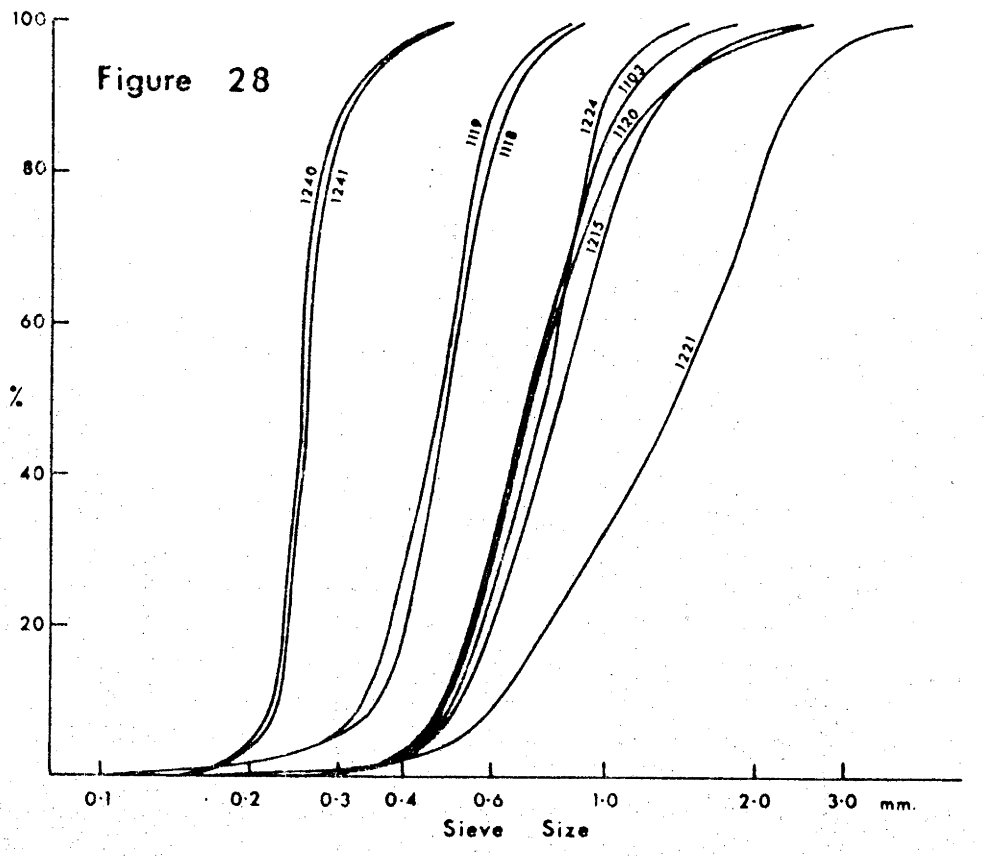

Fig. 28. Sieve cumulative curves for entire natural dune stage sands.

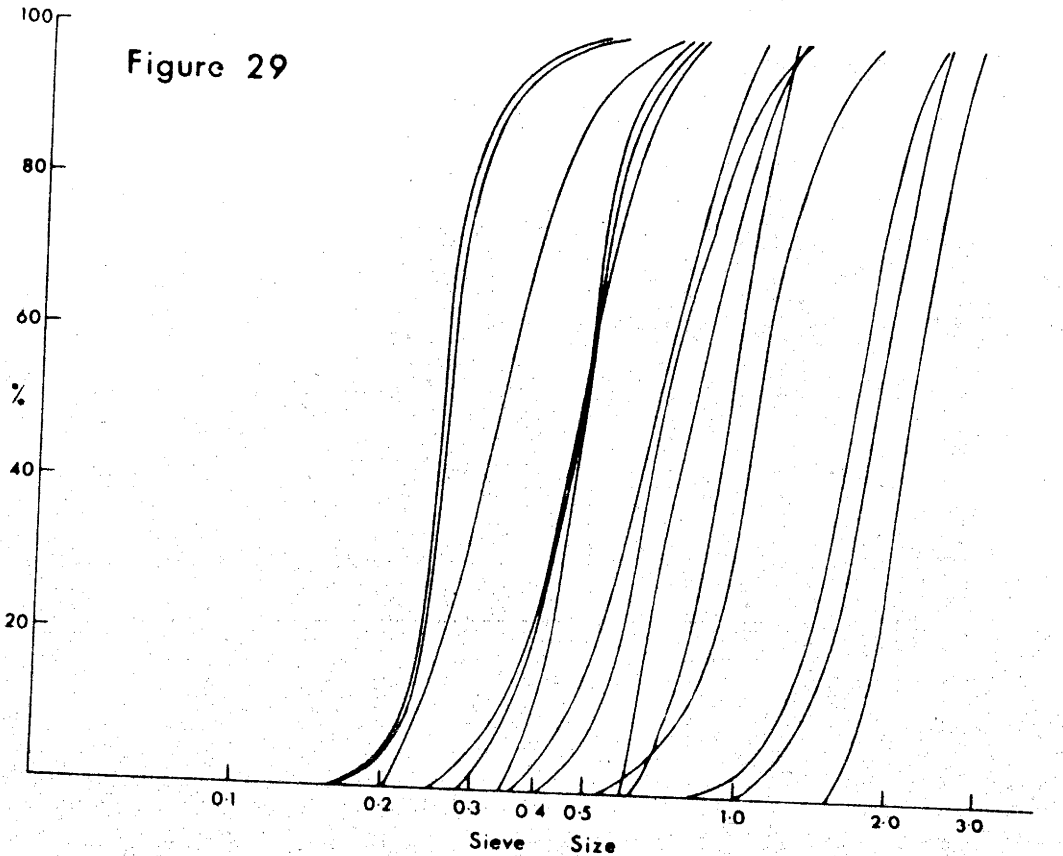

Fig. 29. Sieve cumulative curves for separated Population A's of natural dune stage sands.

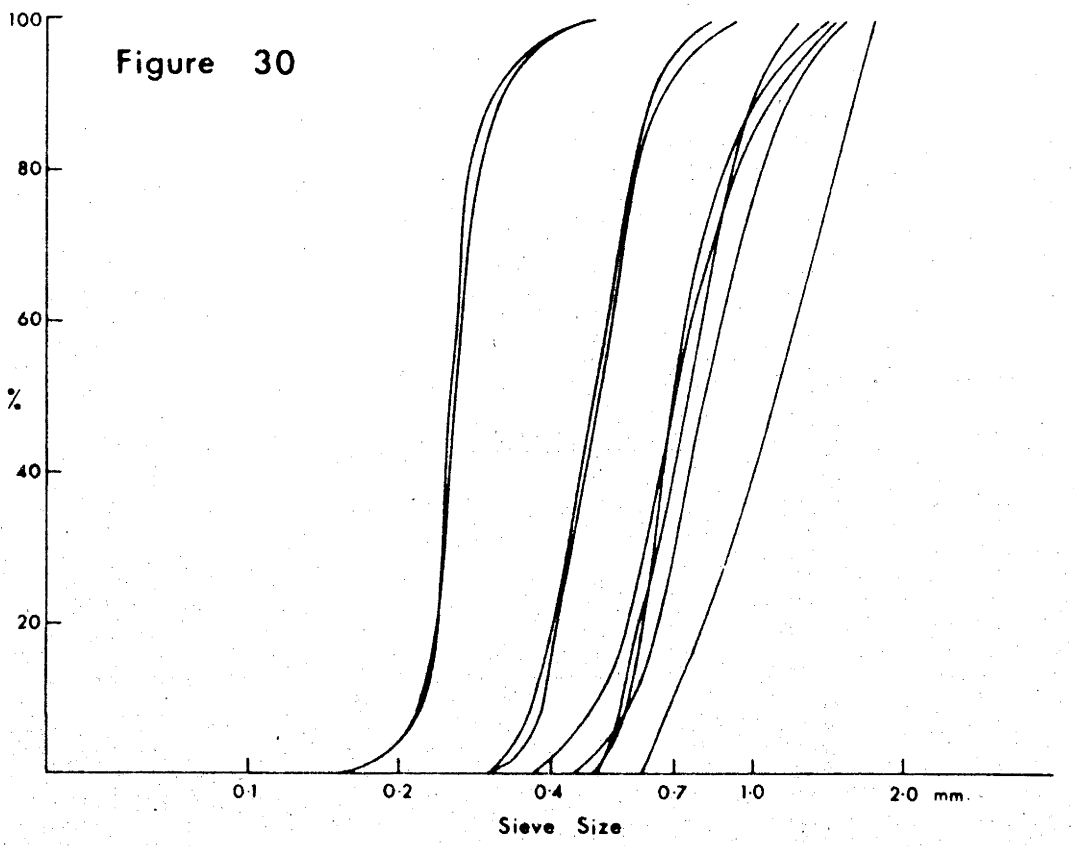

Fig. 30. Sieve cumulative curves for separated population A's of natural dune stage sands.

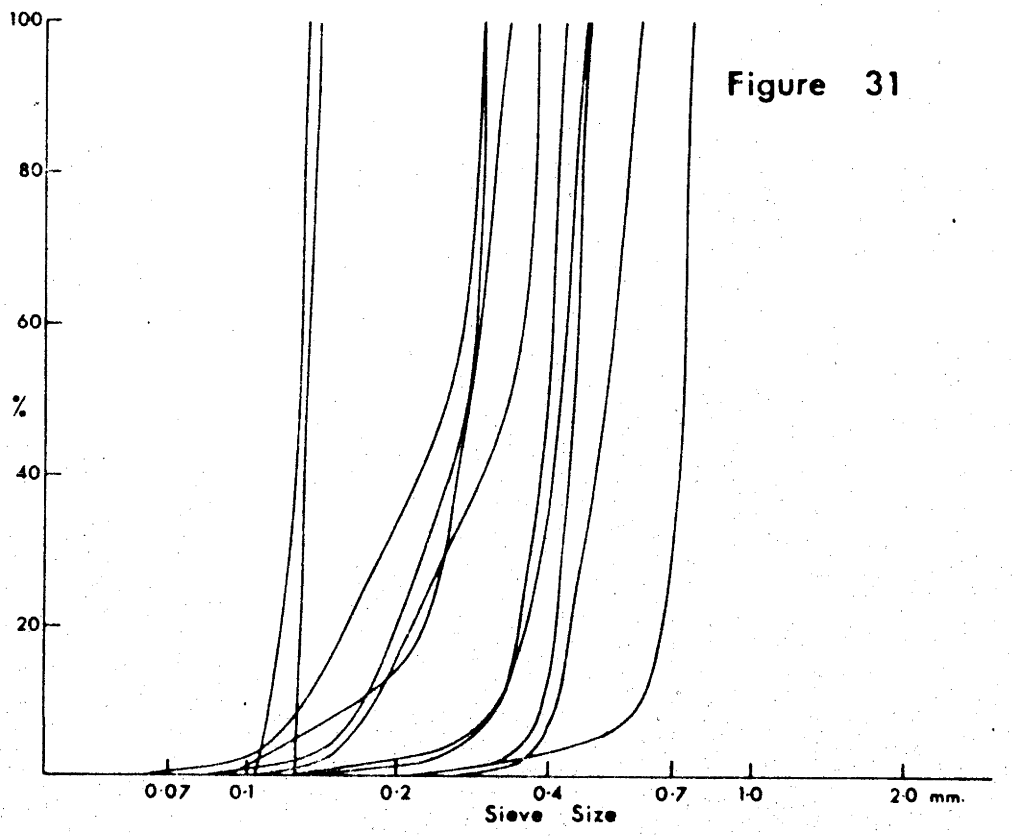

Fig. 31. Sieve cumulative curves for separated Population B's of natural dune stage sands.

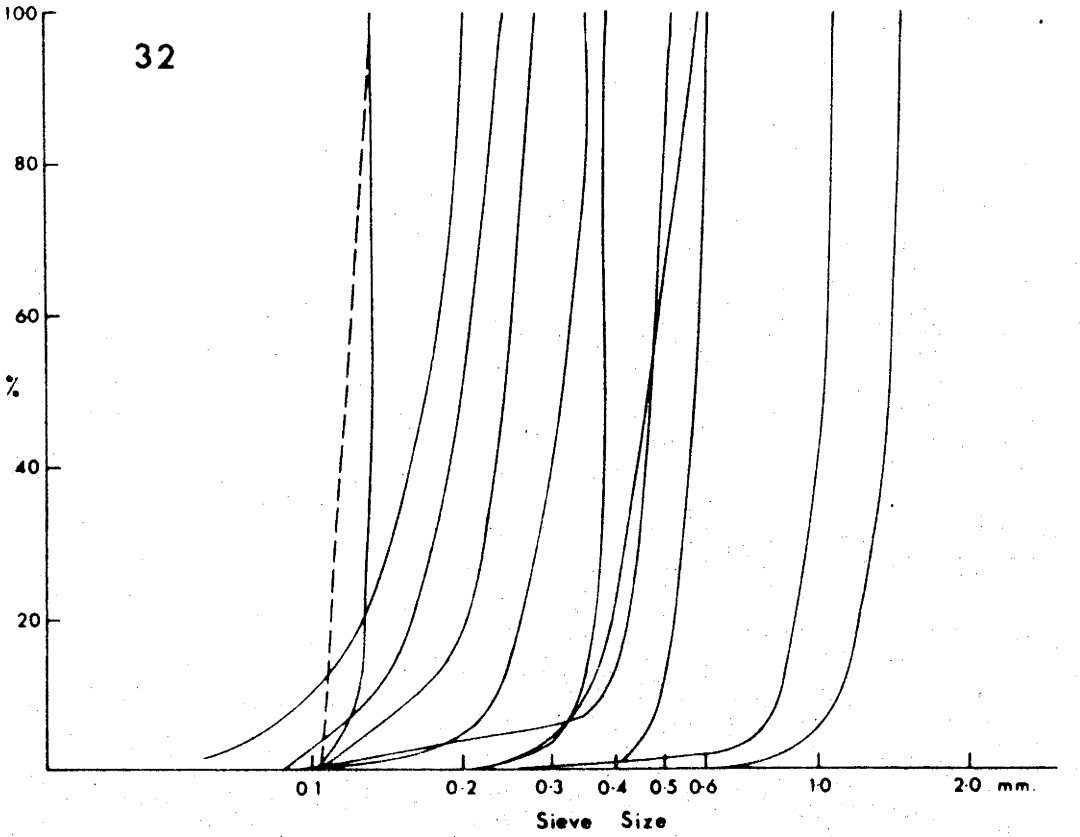

Fig. 32. Sieve cumulative curves for separated Population B's of natural dune stage sands.

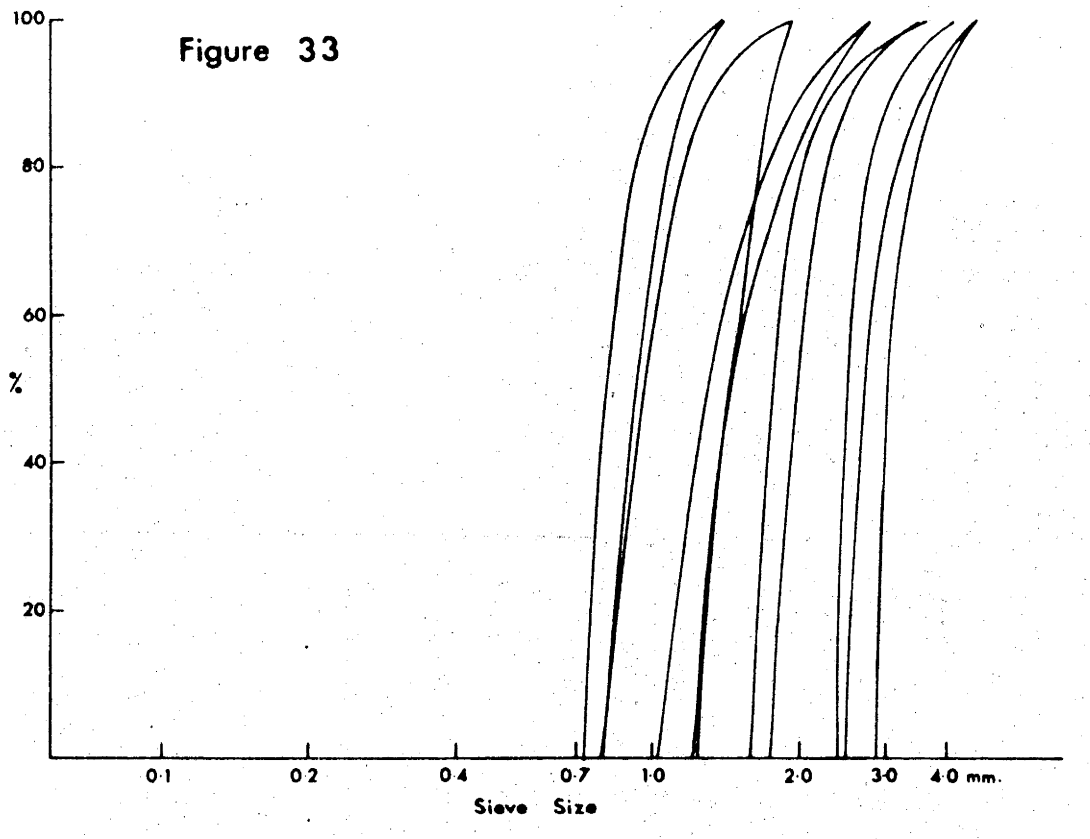

Fig. 33. Sieve cumulative curves for separated Population C's of natural dune stage sands.

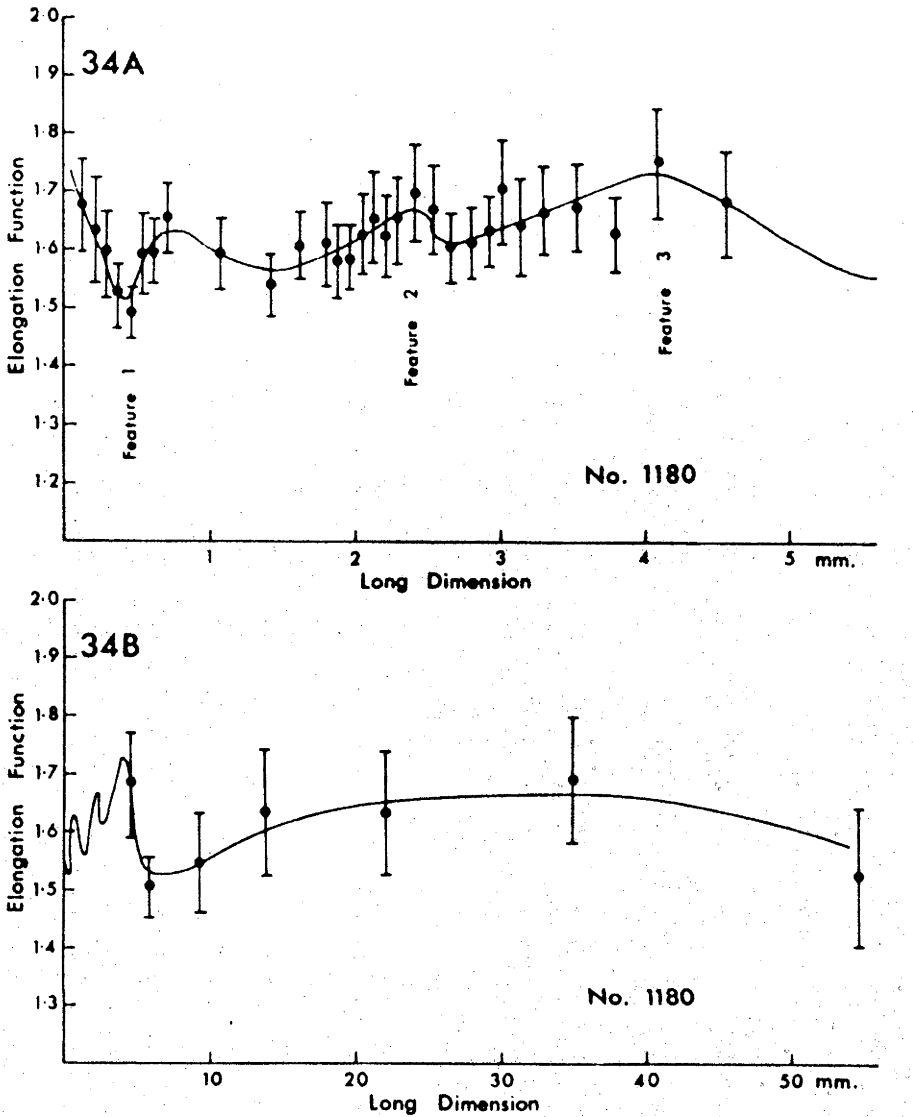

Fig. 34. Elongation function curve of No. 1180, a rheologic bed load deposit (river gravel) shown on two horizontal scales; 3180 particles measured; means of 90 for $p \leq 5$ mm; means of 30 for $p > 5$ mm; 95% confidence limits given for each point.

Figure 35

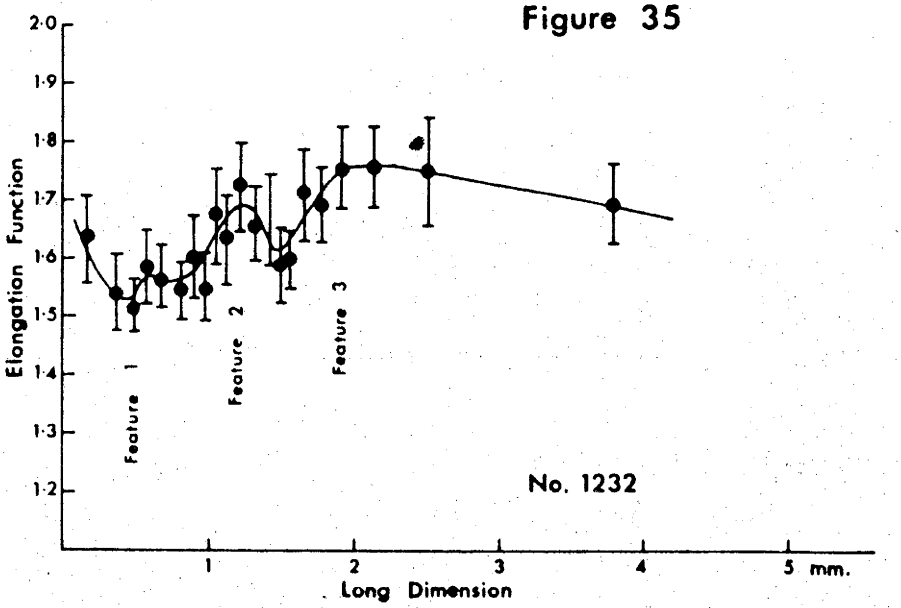

Fig. 35. Elongation function curve of No. 1232, a rheologic bed load sand; 2100 particles measured; means of 100 grains; 95% confidence limits given for each point.

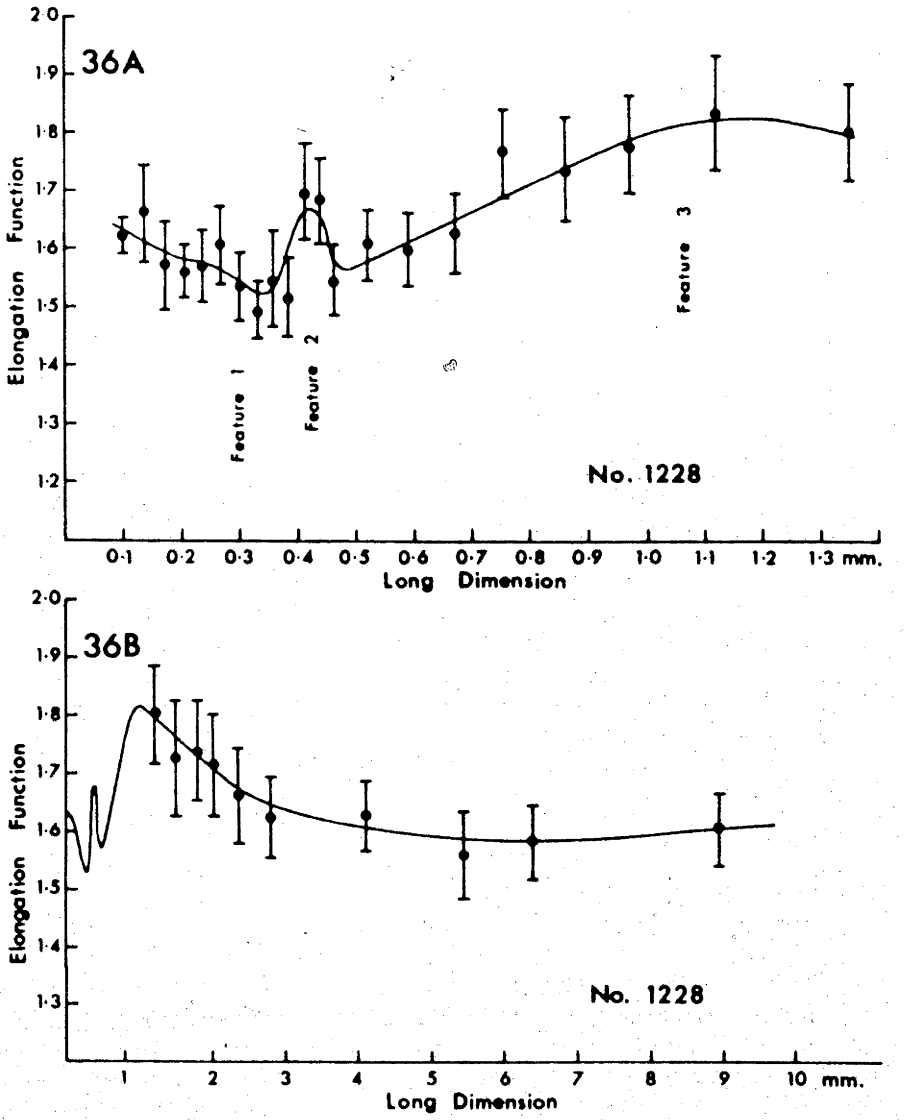

Fig. 36. Elongation function curve of No. 1228, a gravel. 3000 grains measured; means of 100 grains; 95% confidence limits given for each point. Curve shown on two horizontal scales.

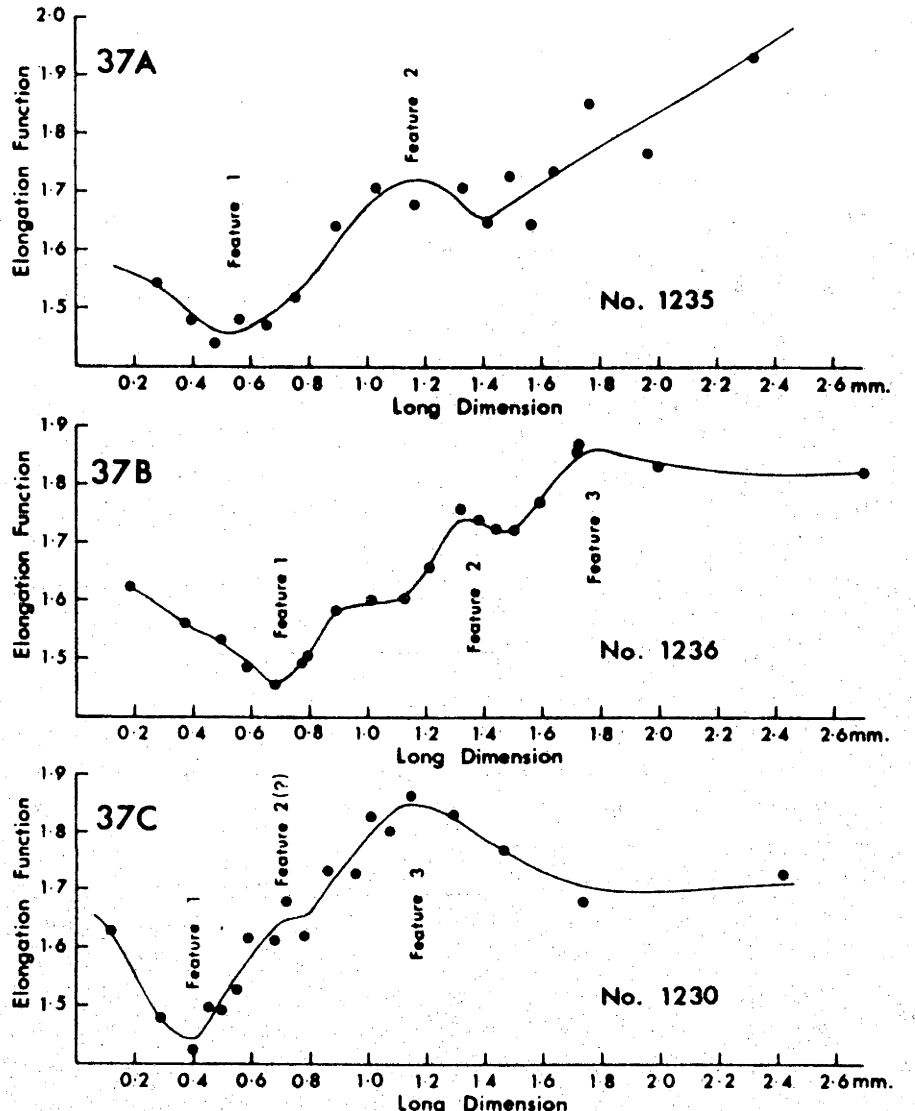

Fig. 37. Elongation function curves of three rheologic bed load sands; 1700 grains measured for No. 1235; 1740 for No. 1236 and 1140 for No. 1230.

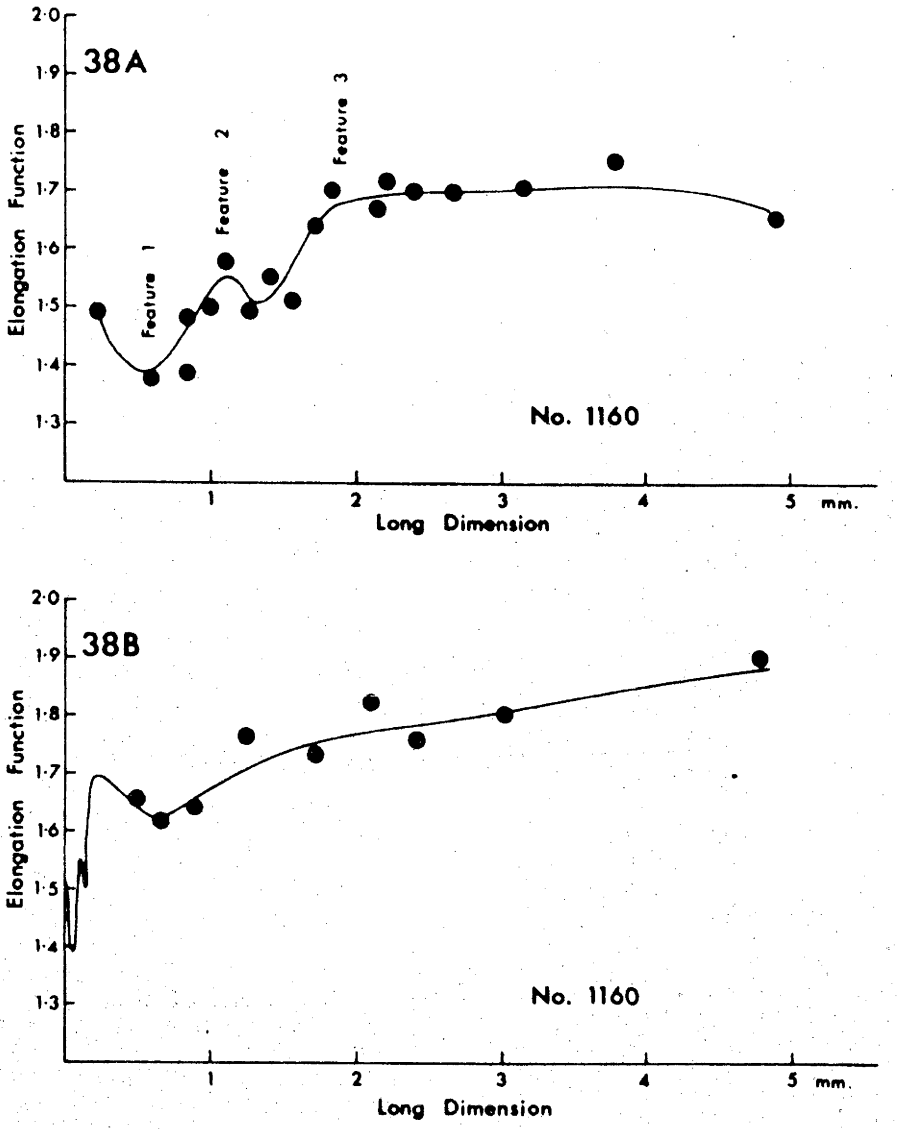

Fig. 38. Elongation function curve of a river gravel. 1410 particles measured; curve shown on two horizontal scales.

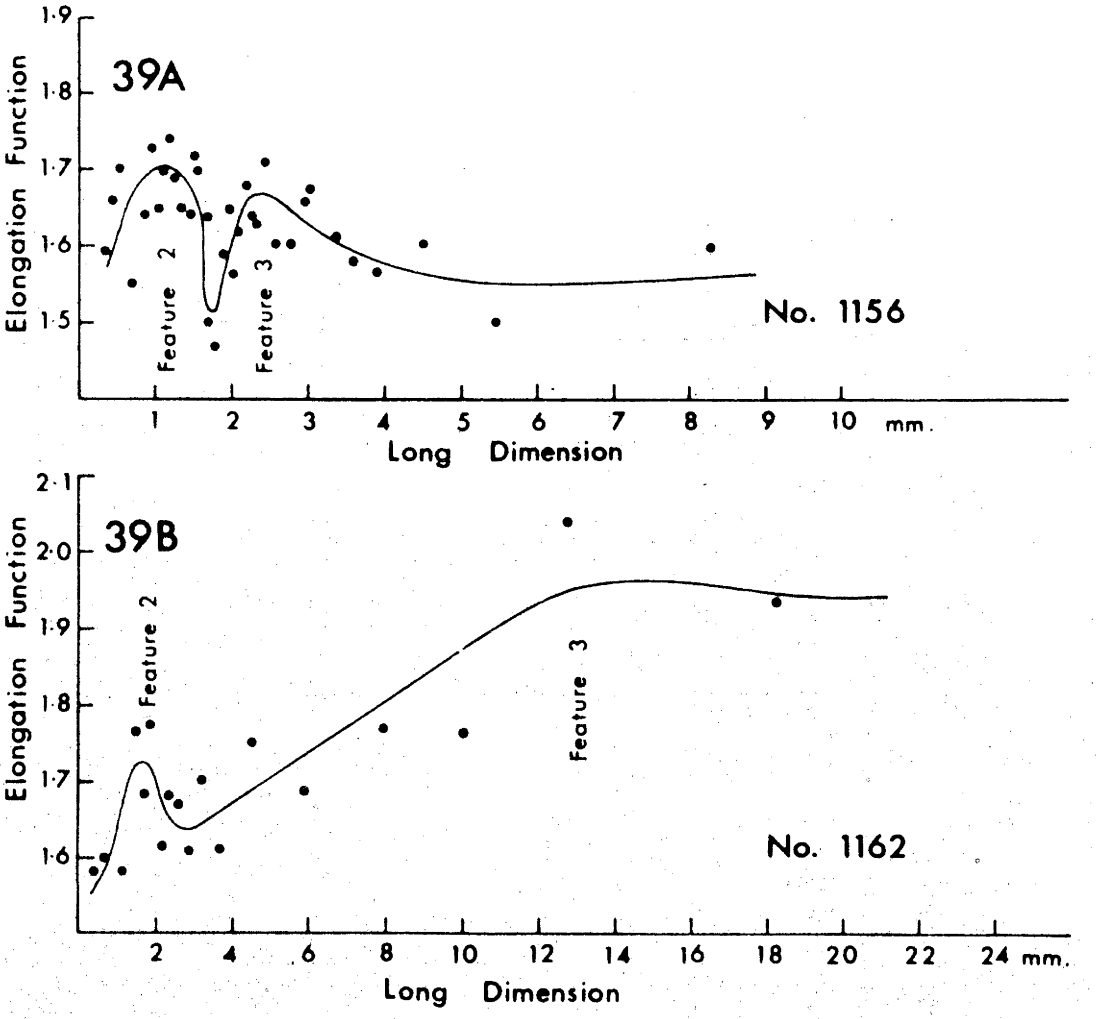

Fig. 39. Elongation function curves of two rheologic bed load deposits, 1080 particles measured both for No. 1156 and No. 1162.

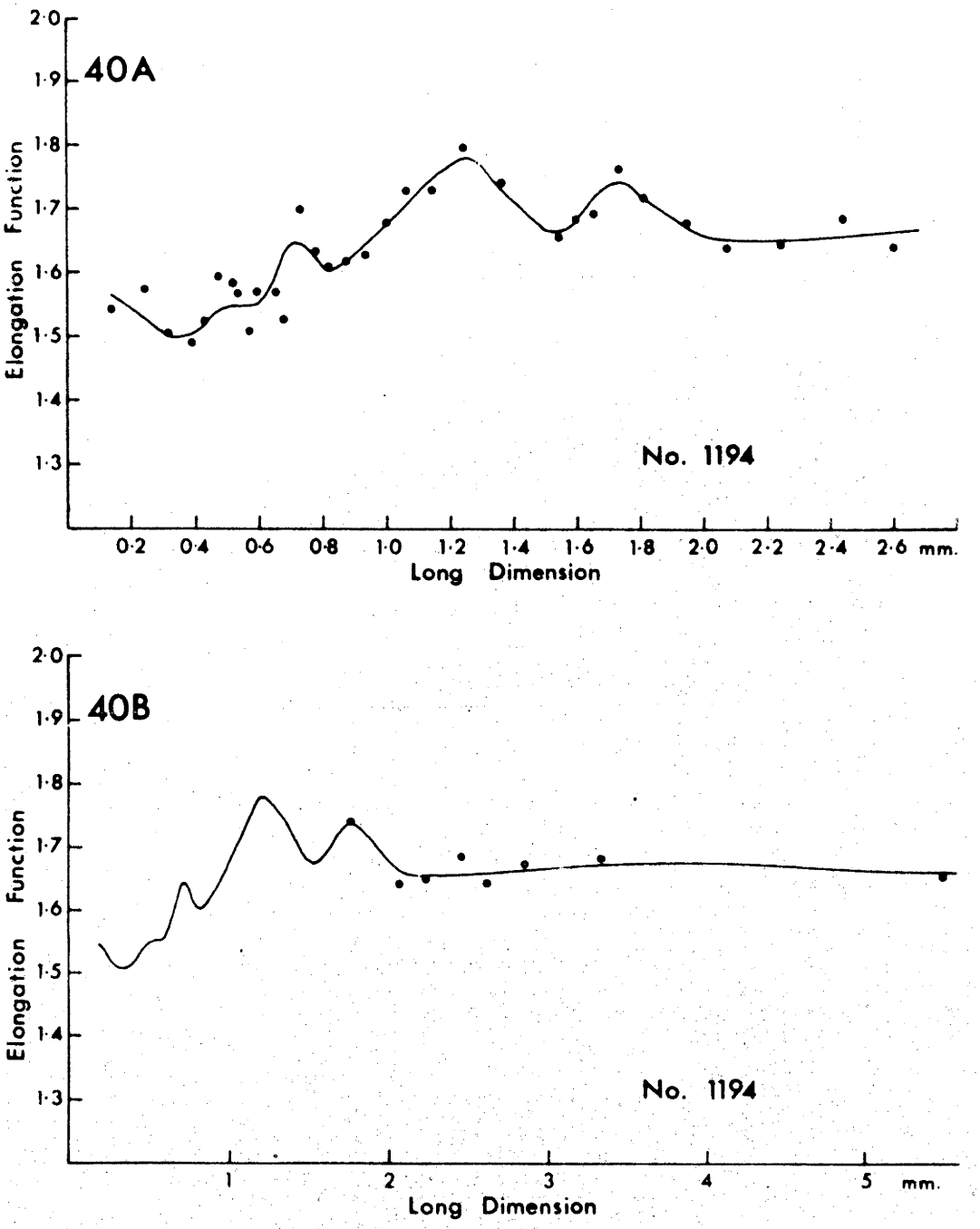

Fig. 40. Elongation function curve of No. 1194, a probable double sediment. 2100 particle measured.

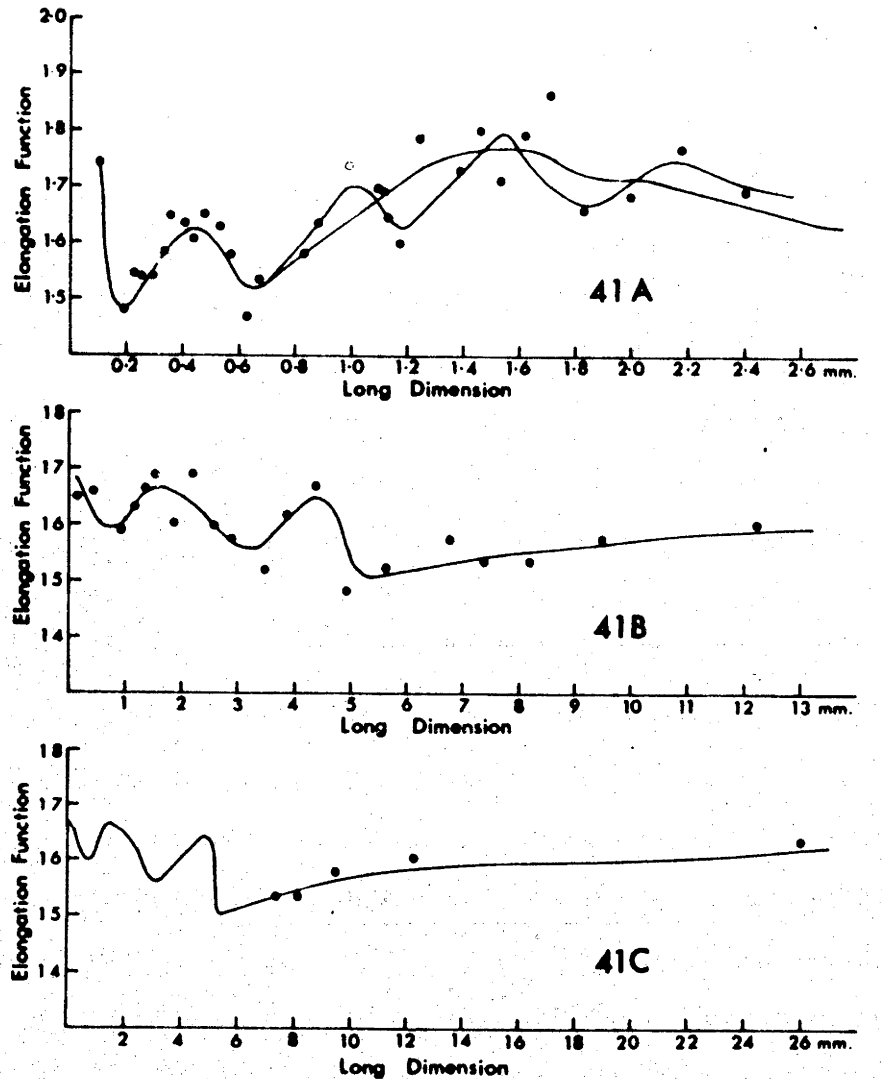

Fig. 41. Elongation function curve of a possible double sediment, No. 1193 with two possible interpretation of the 1840 data and the curve for No. 1153, shown on two horizontal scales and based on 1260 particles.

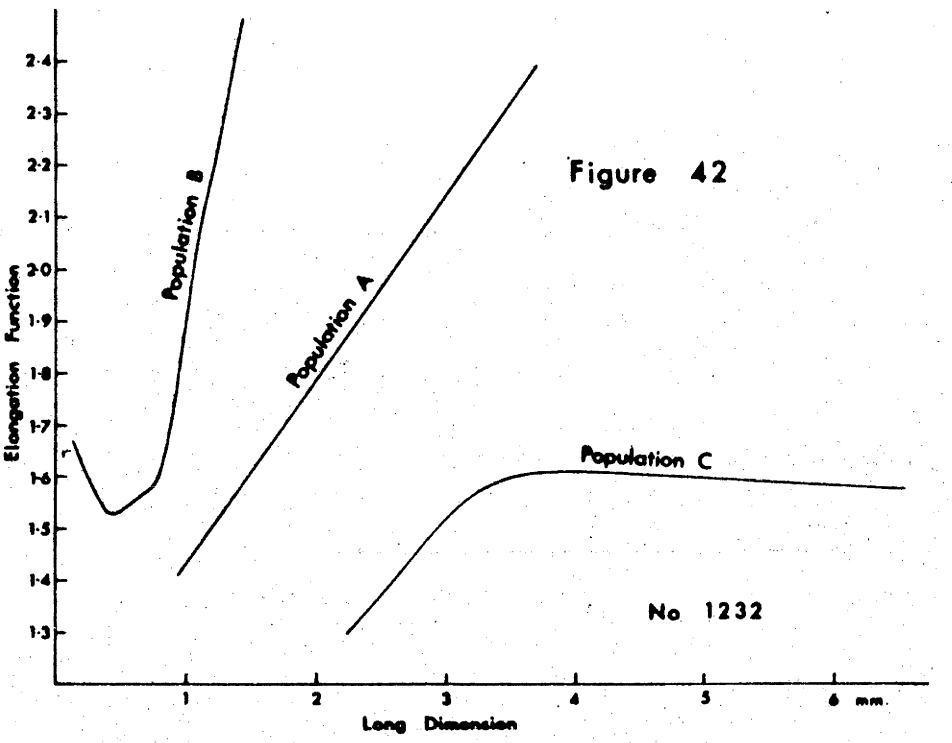

Fig. 42. Elongation function curves for Populations A, B and C of No. 1232, a rheologic bed load sand.

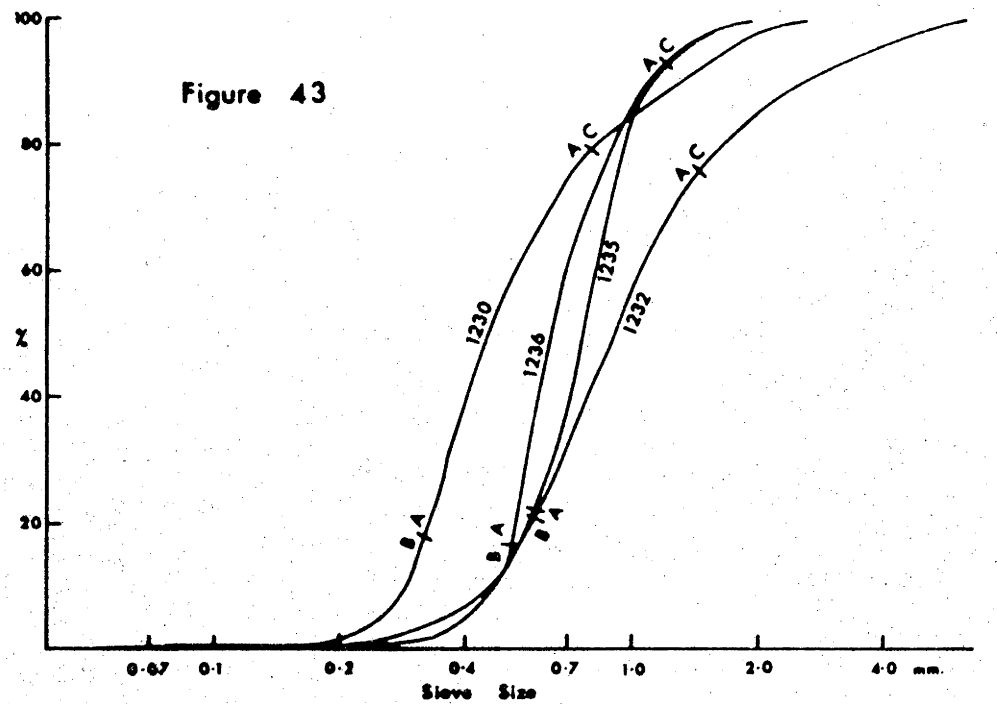

Fig. 43. Entire sieve cumulative curves for four rheologic bed load sands.

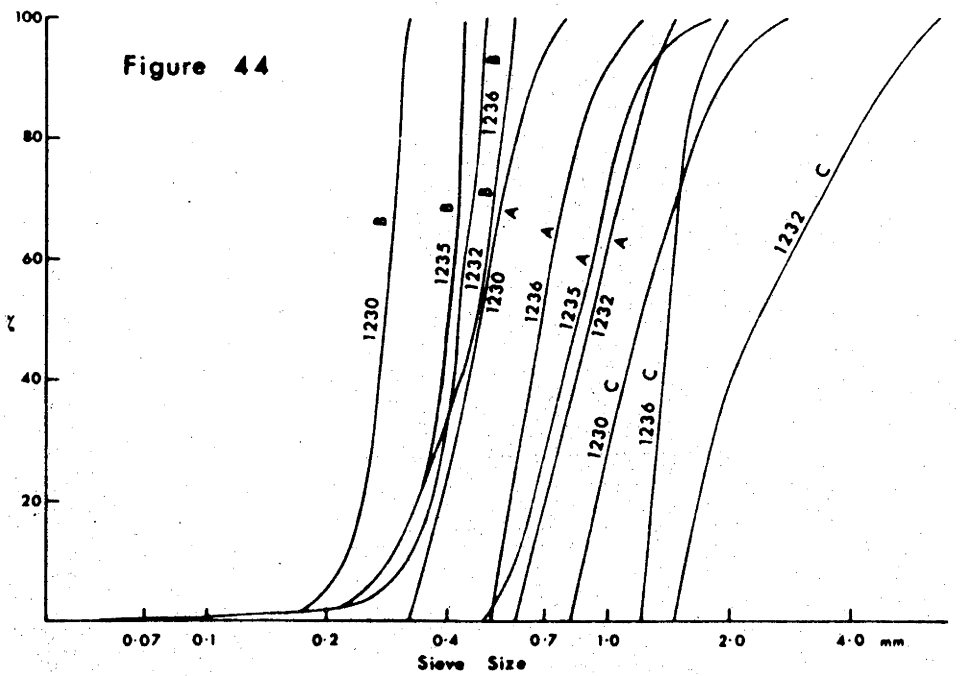

Fig. 44. Separate sieve cumulative curves for the populations of the sands of Fig. 43.

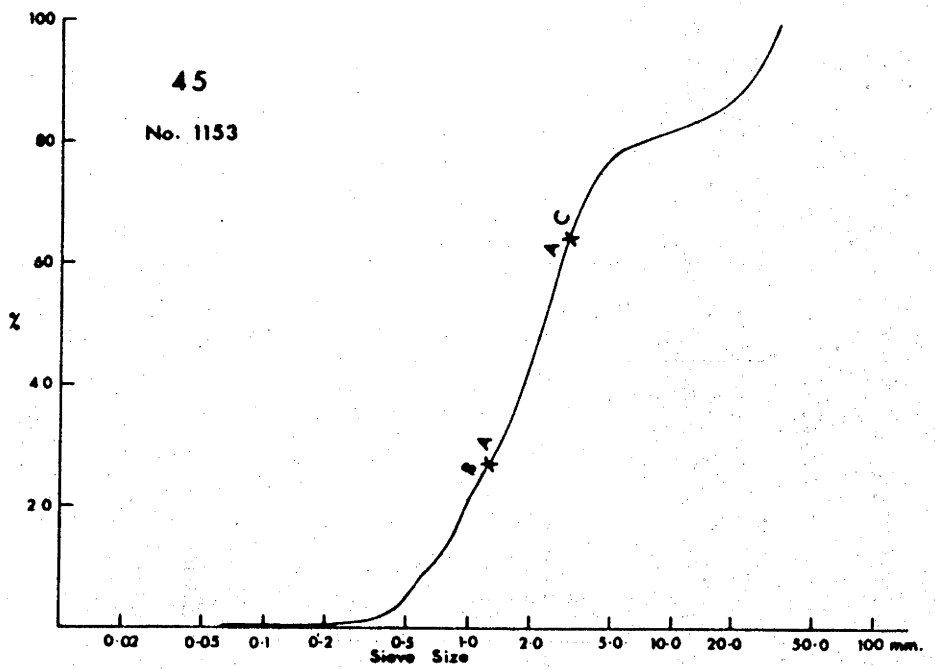

Fig. 45. Entire sieve cumulative curve for a river gravel, No. 1153.

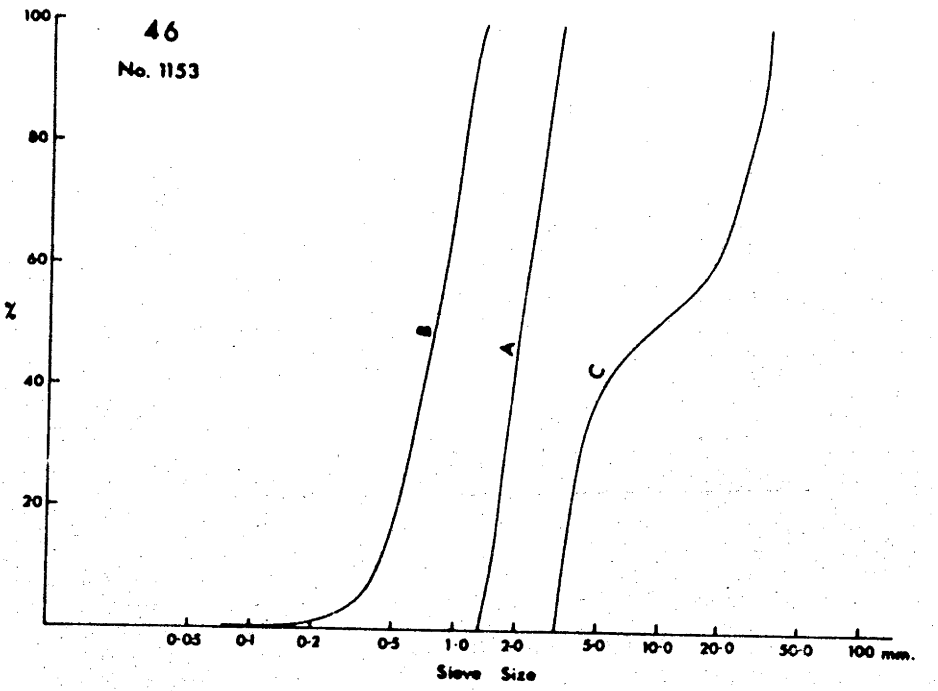

Fig. 46. Sieve cumulative curves for separated populations of No. 1153.

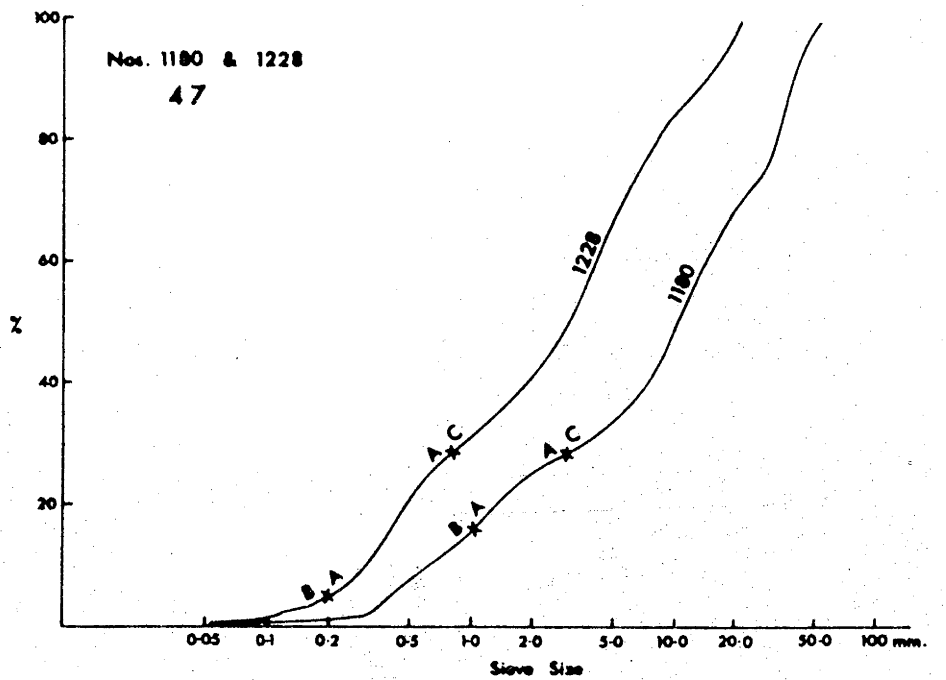

Fig. 47. Sieve cumulative curves for two river gravels, Nos. 1228 and 1180.

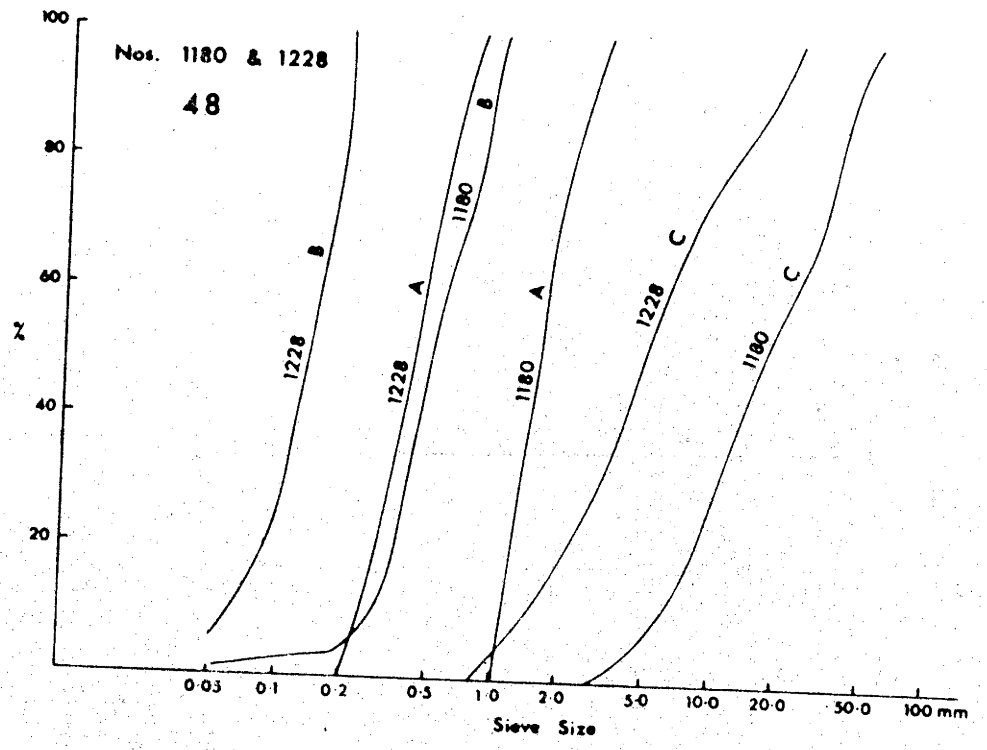

Fig. 48. Sieve cumulative curves for separated populations of two river gravels, Nos. 1228 and 1180.

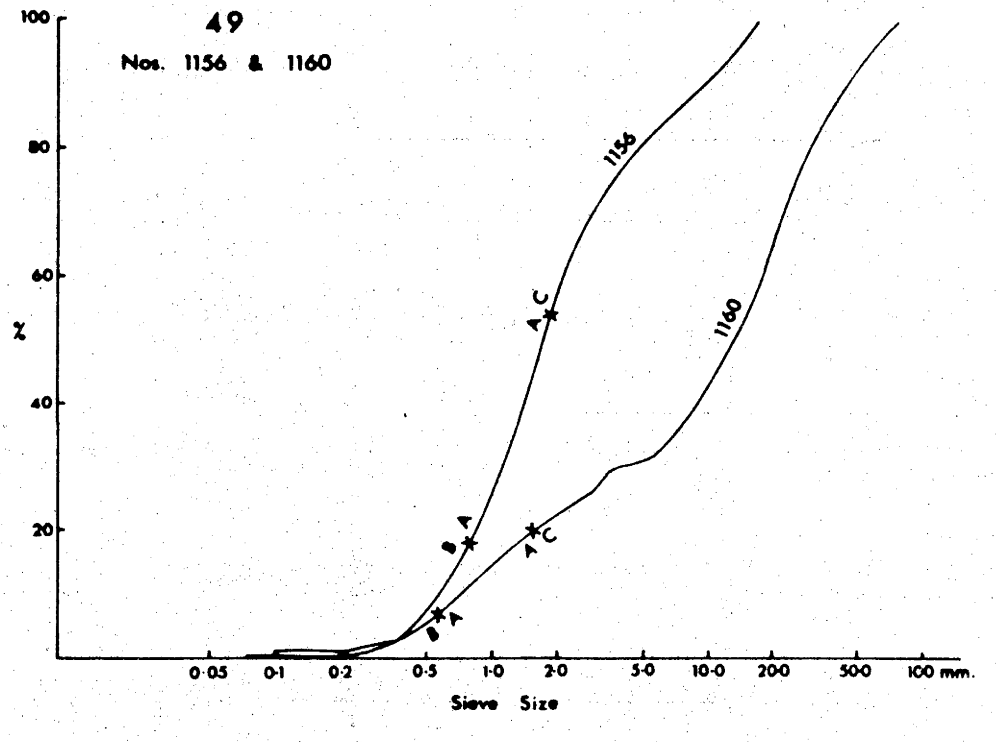

Fig. 49. Sieve cumulative curves for two river gravels, Nos. 1156 and 1160.

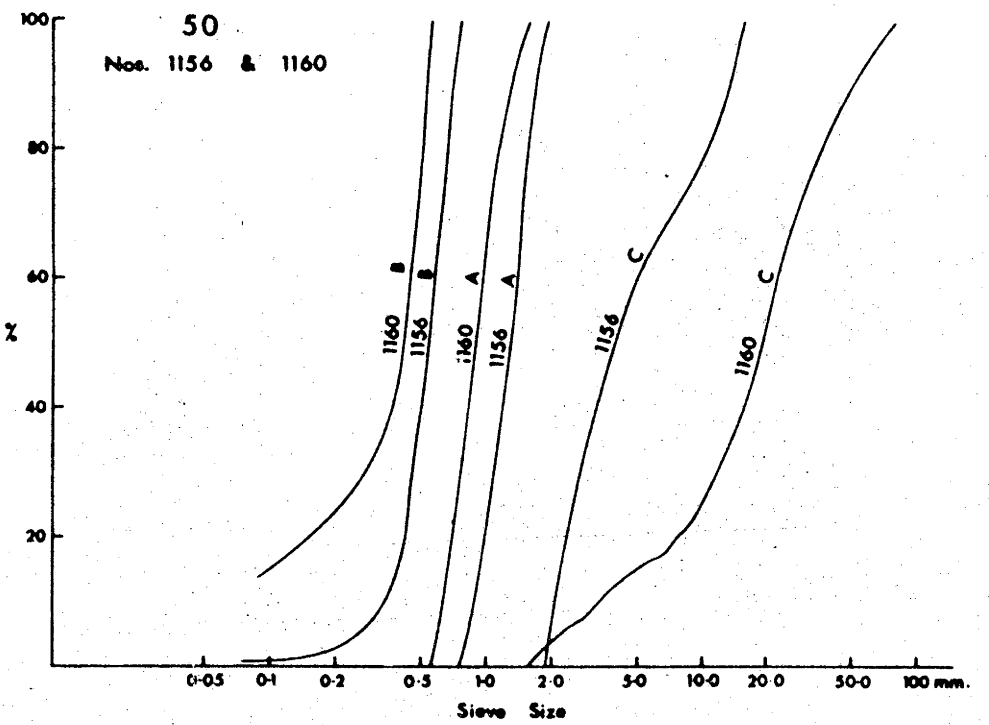

Fig. 50. Sieve cumulative curves for separated populations of two river gravels, Nos. 1156 and 1160.

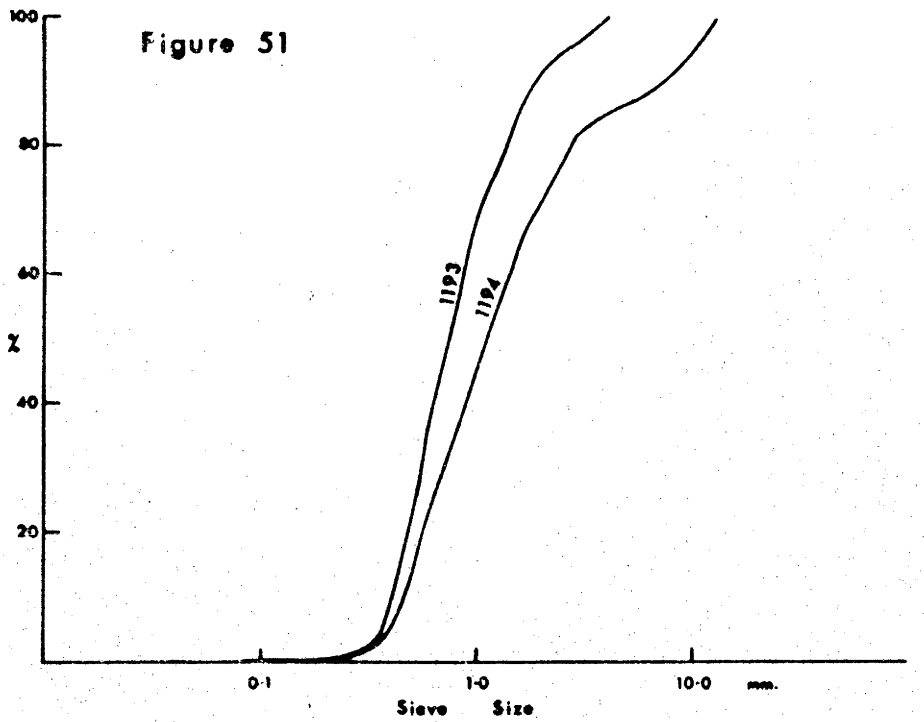

Fig. 51. Sieve cumulative curves for two probable double sediments, Nos. 1193 and 1194.

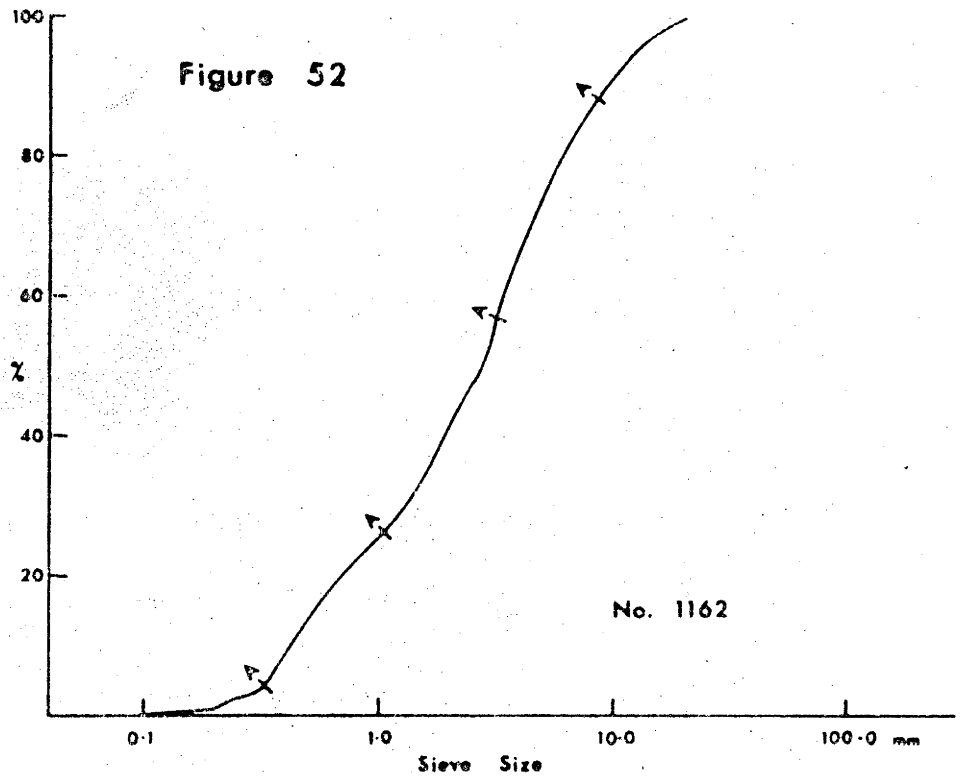

Fig. 52. Sieve cumulative curve for No. 1162, a probable double sediment.

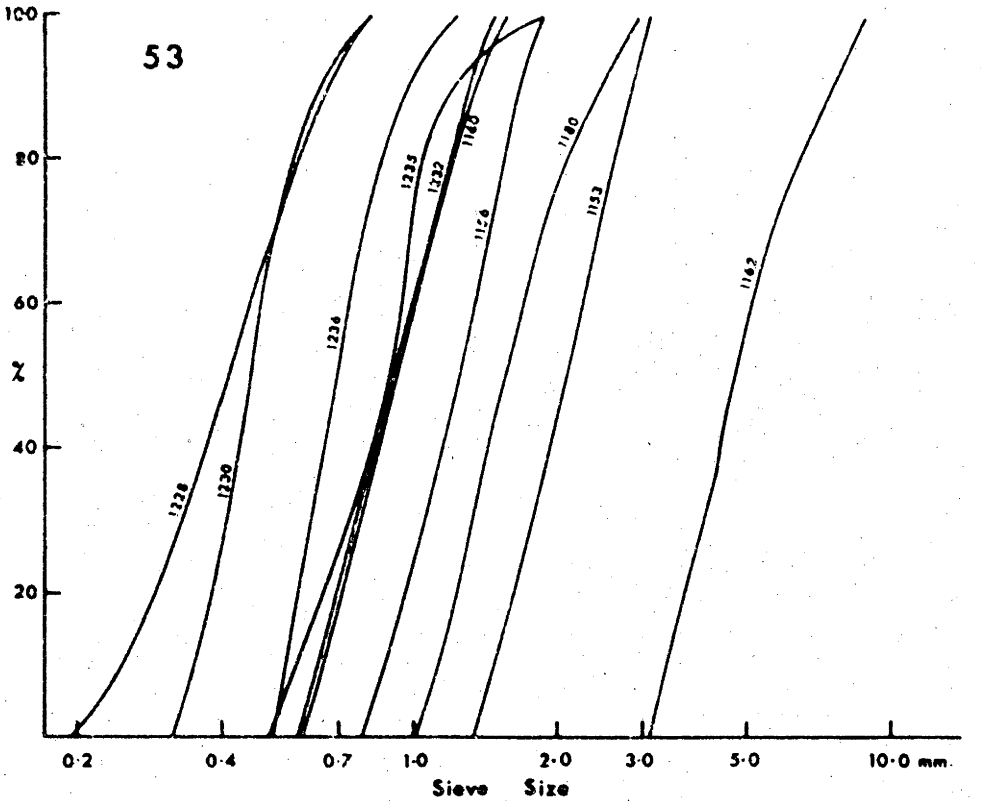

Fig. 53. Separated Population A sieve cumulative curves for natural rheologic bed load sediments.

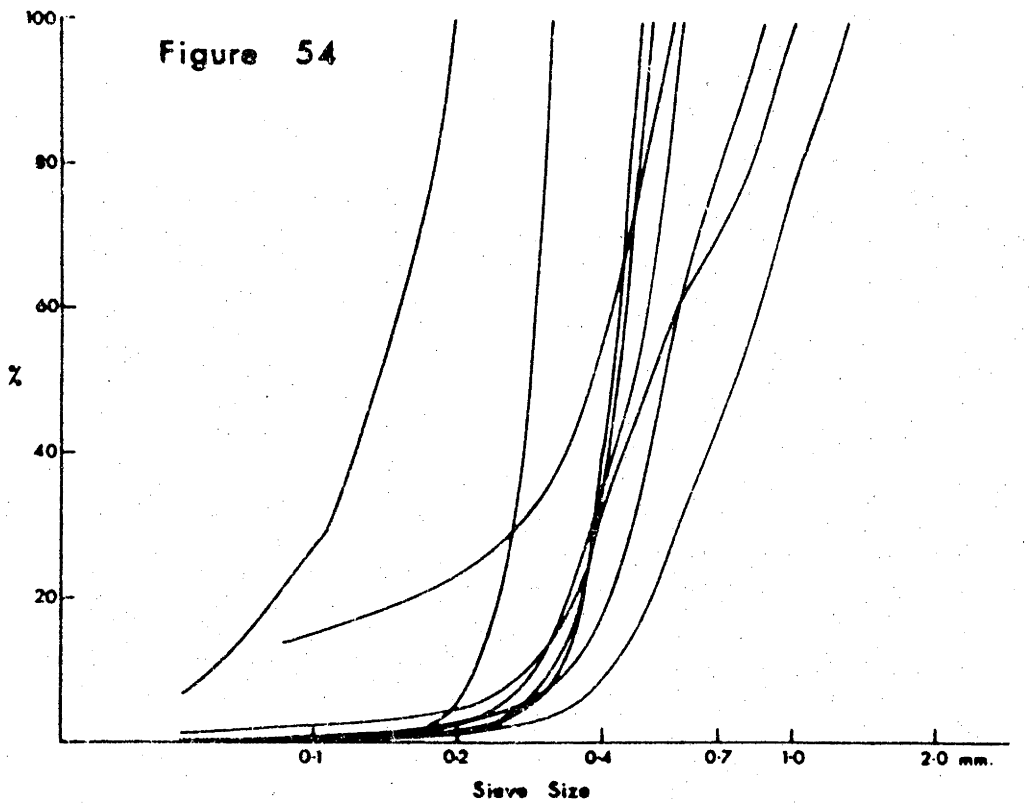

Fig. 54. Separated sieve cumulative curves (or Population B's of natural rheologic bed load sediments.

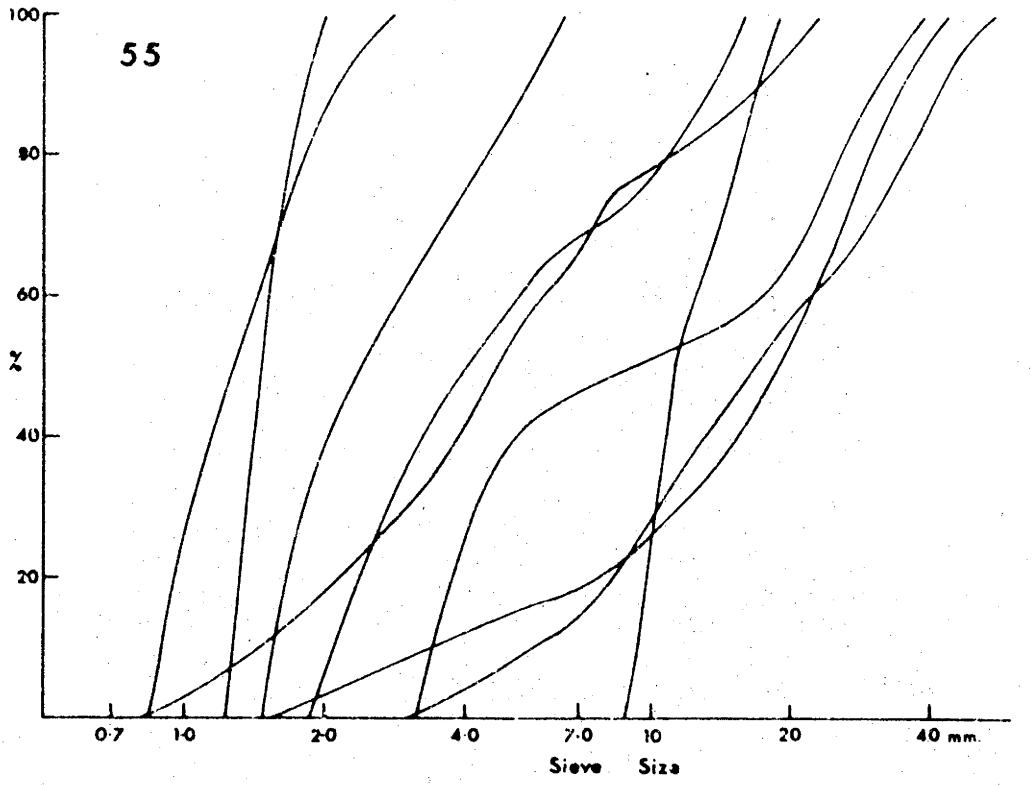

Fig. 55. Separated sieve cumulative curves for Population C's of natural rheologic bed load sediments.

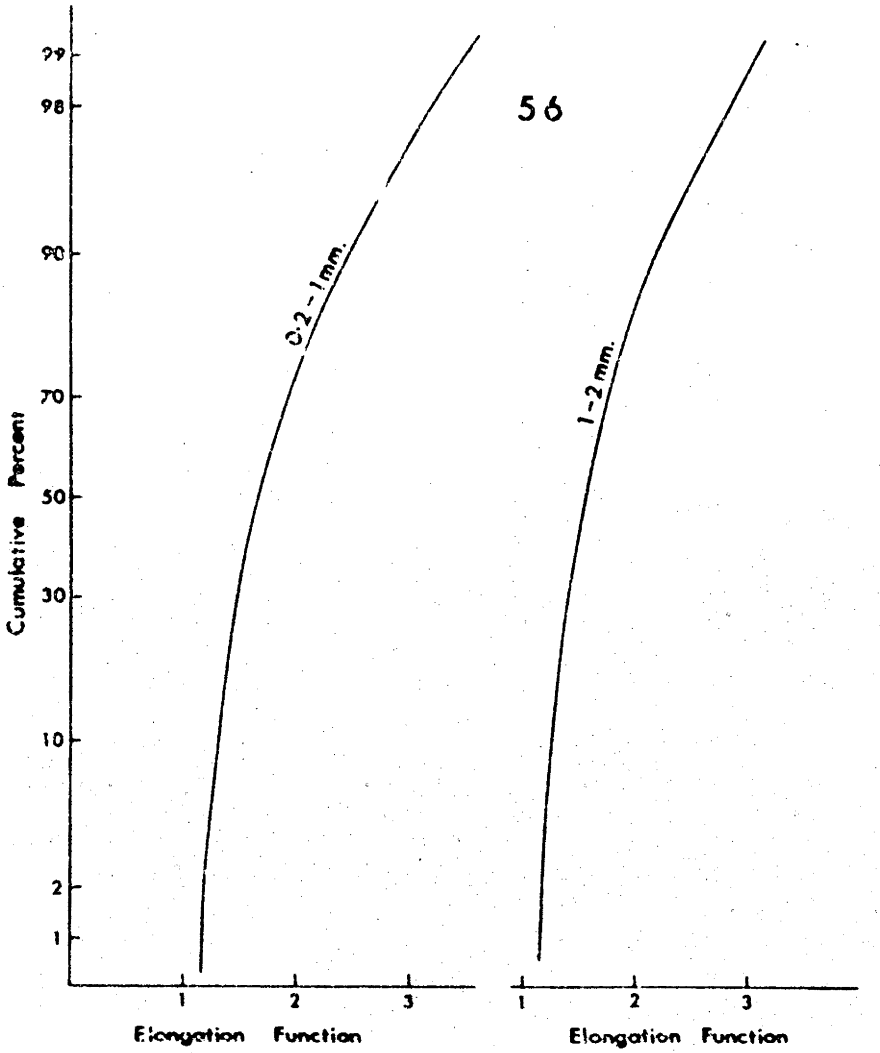

Fig. 56. Cumulative curves for the elongation function for granitic quartz in size ranges p = 0.2 - 1.0 mm and p = 1.0 - 2.0 mm. Data from Moss (1966).

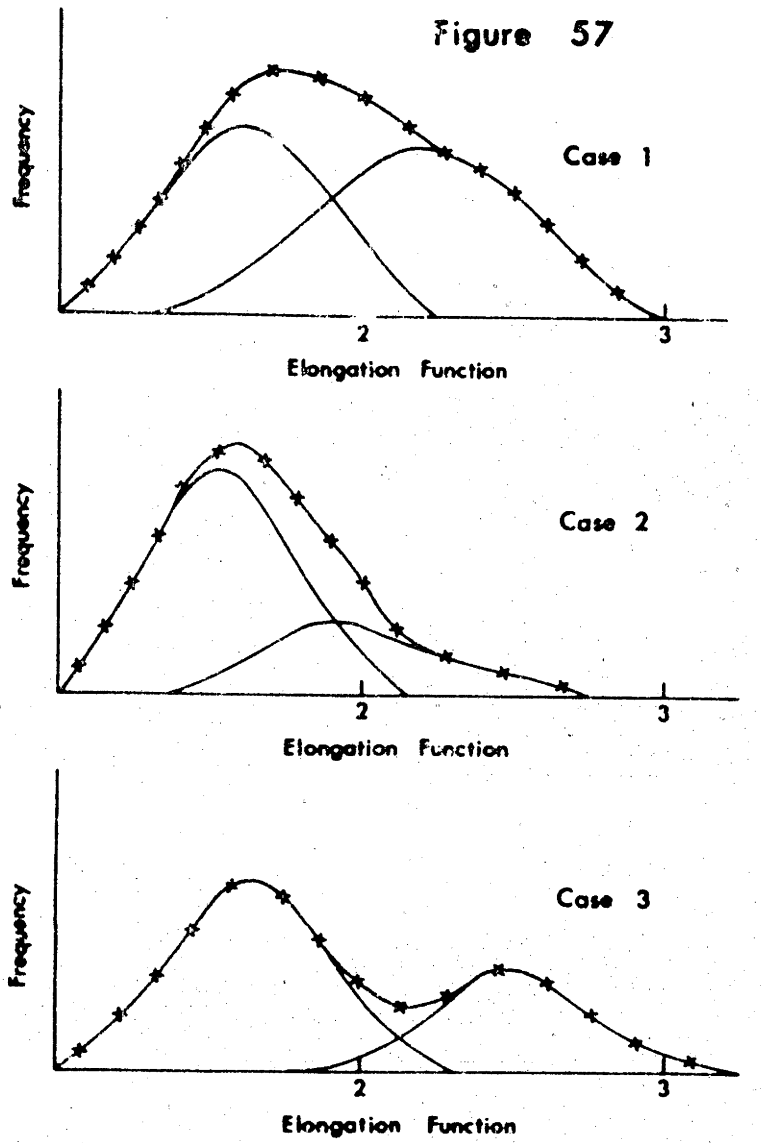

Fig. 57. Hypothetical frequency curves of overlapping distributions of the elongation function.

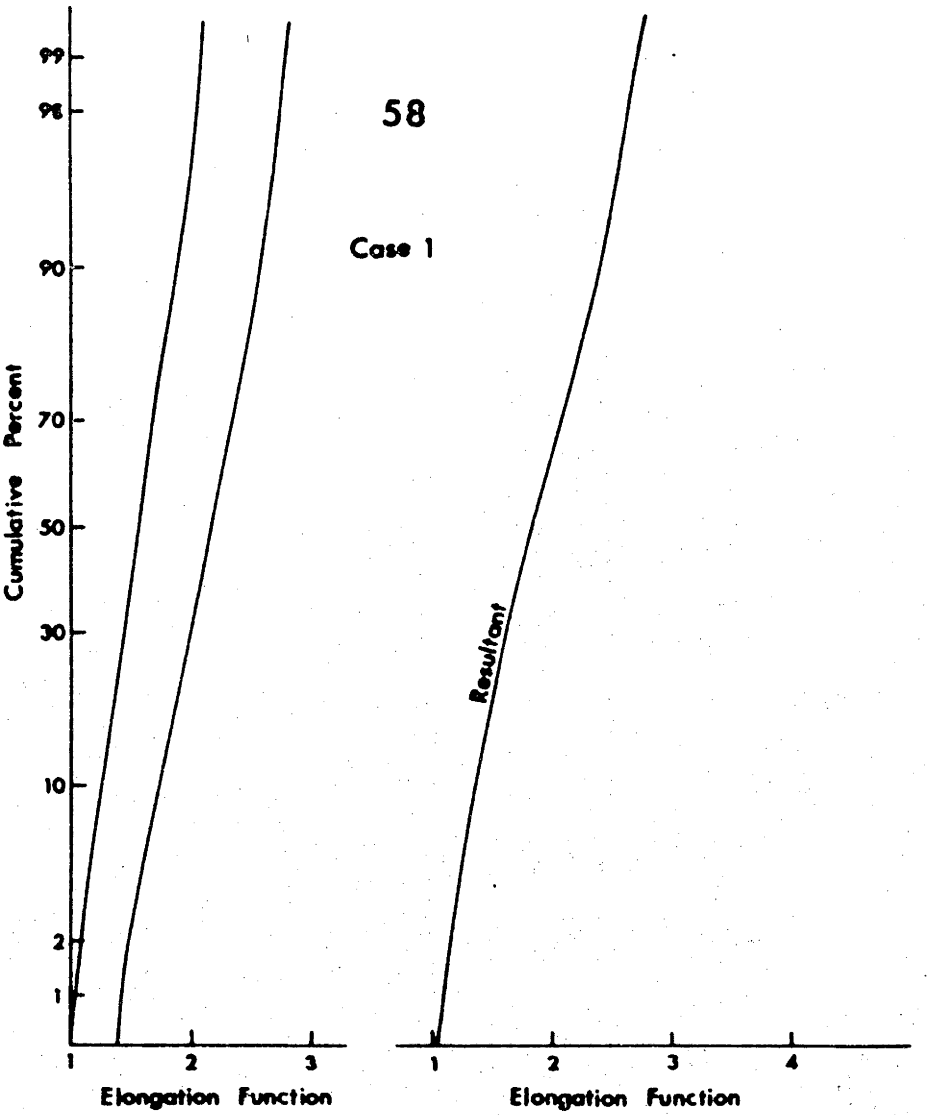

Fig. 58. Cumulative frequency curves for the elongation function; case 1 of Fig. 57.

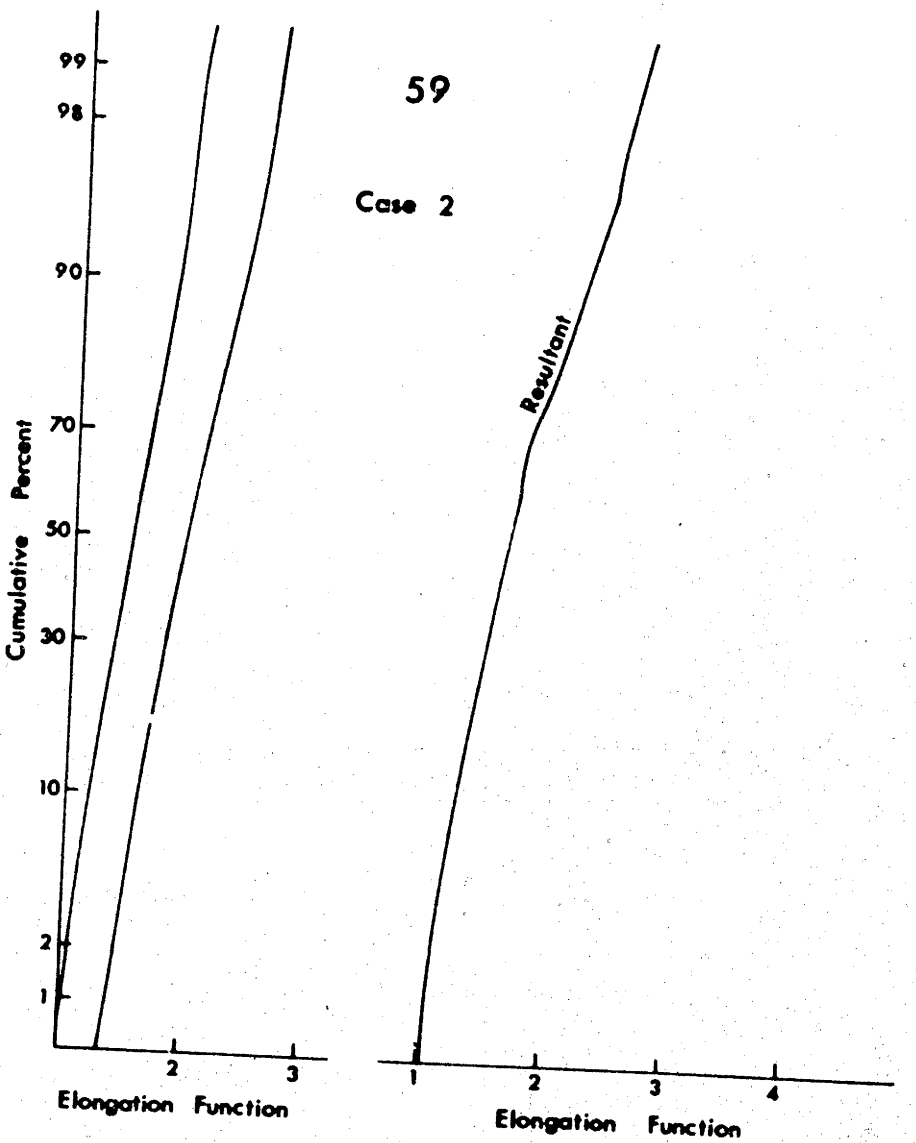

Fig. 59. Cumulative frequency curves for the elongation function; case 2 of Fig. 57.

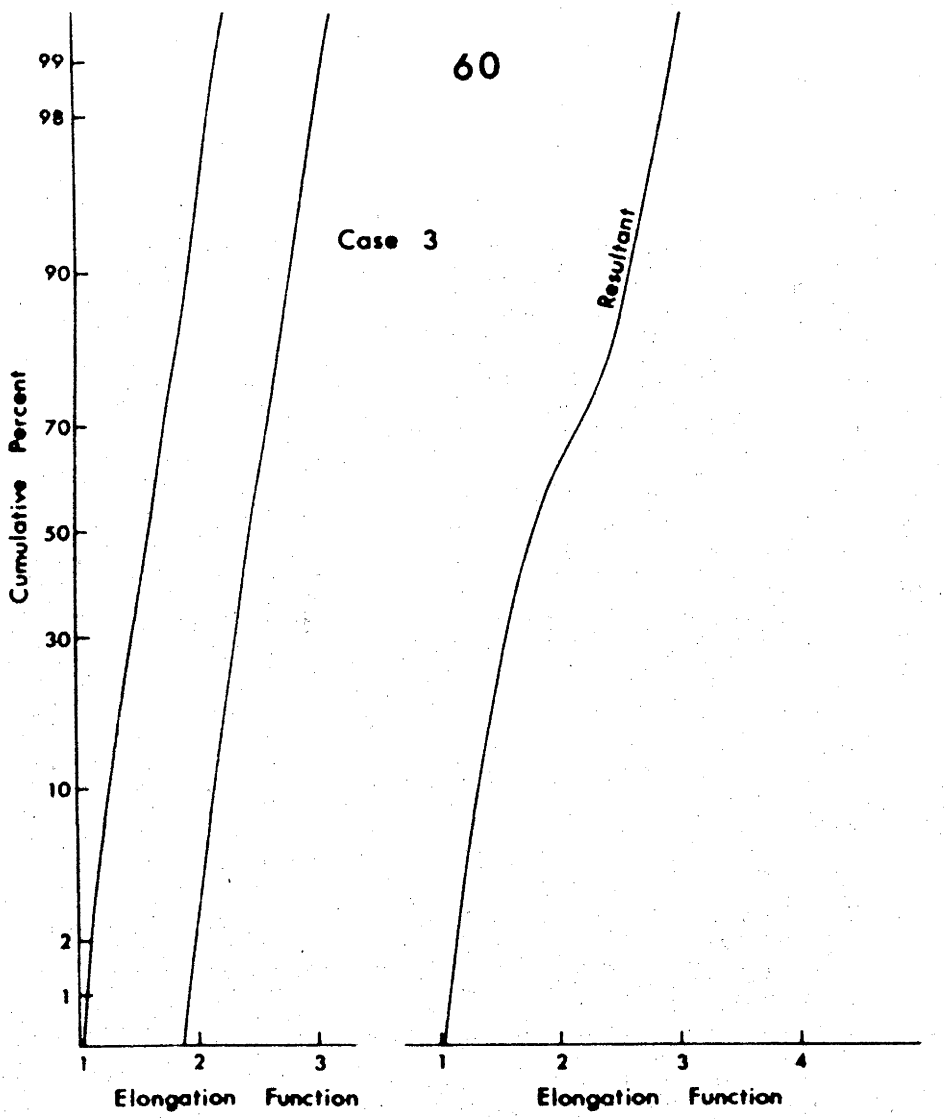

Fig. 60. Cumulative frequency curves for the elongation function; case 3 of Fig. 57.

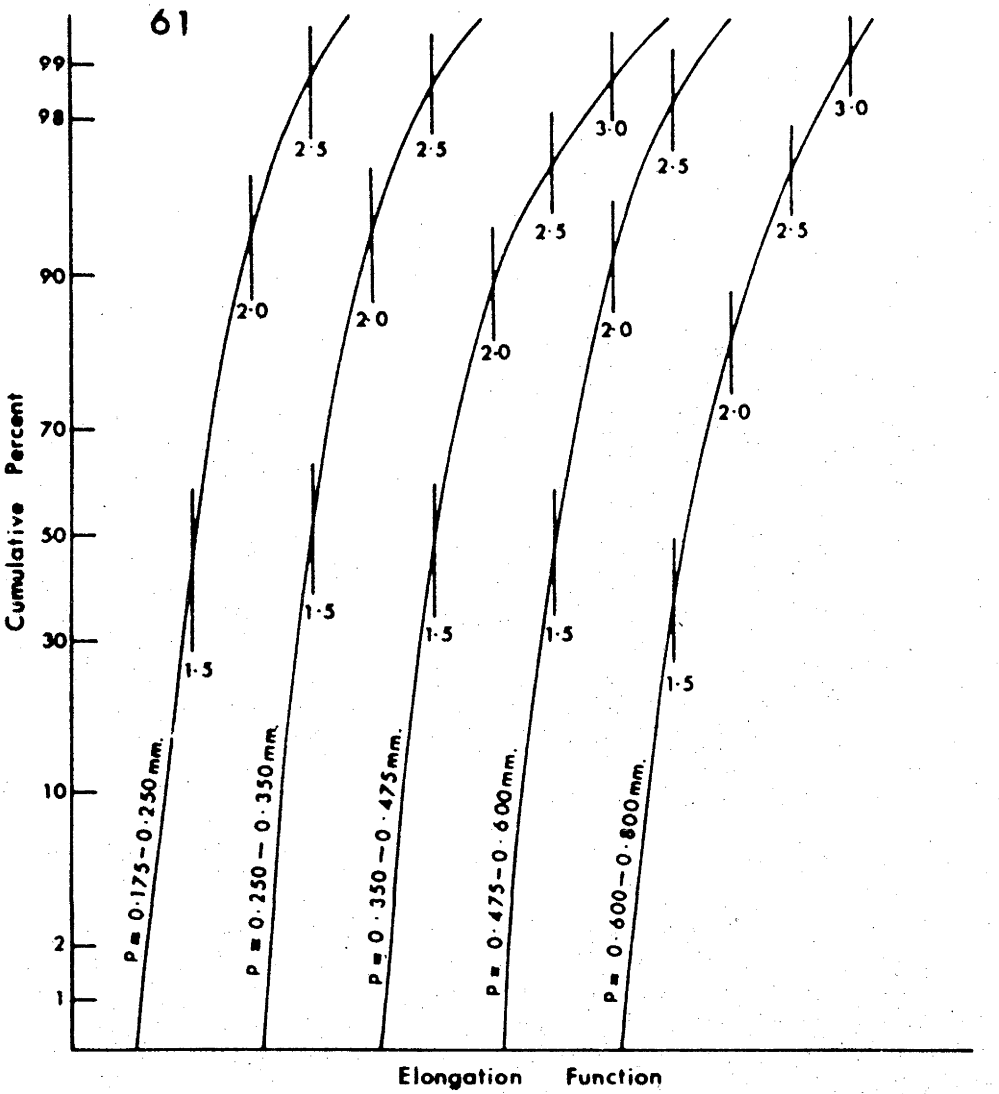

Fig. 61. Serial sections, with respect to the long dimension (range shown on each curve), of the overall distribution of the elongation function for No. 1228.

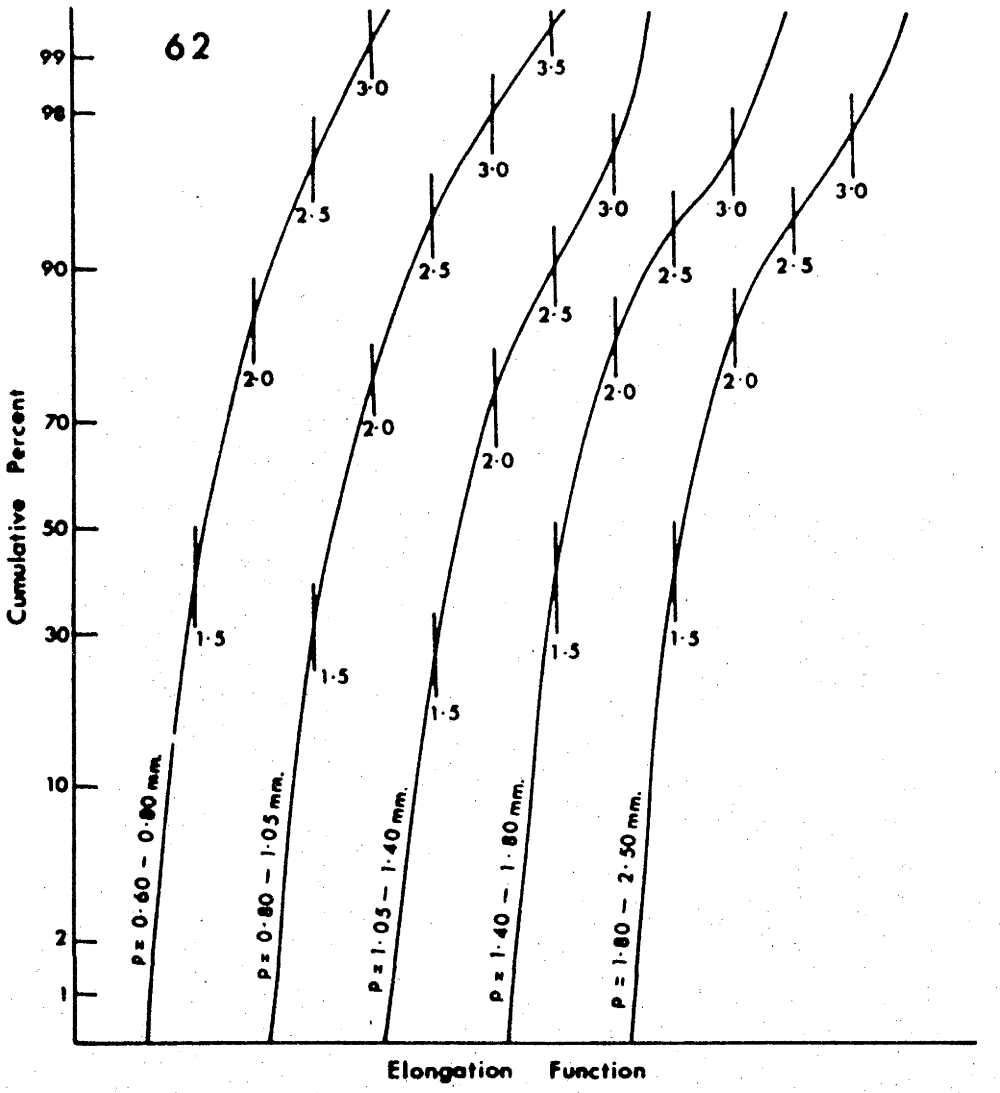

Fig. 62. Serial sections, with respect to the long dimension (range shown on each curve), of the overall distribution of the elongation function for No. 1228.

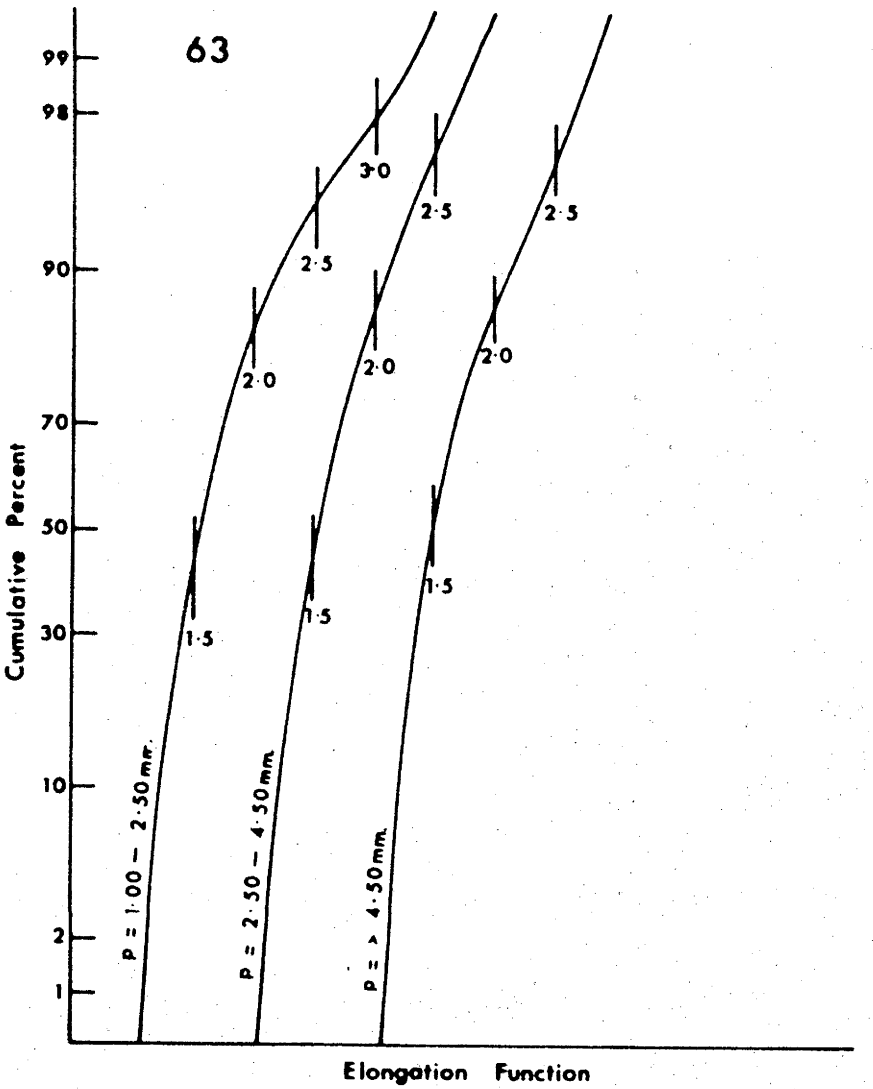

Fig. 63. Serial sections, with respect to the long dimension (range shown on each curve), of the overall distribution of the elongation function for No. 1228.

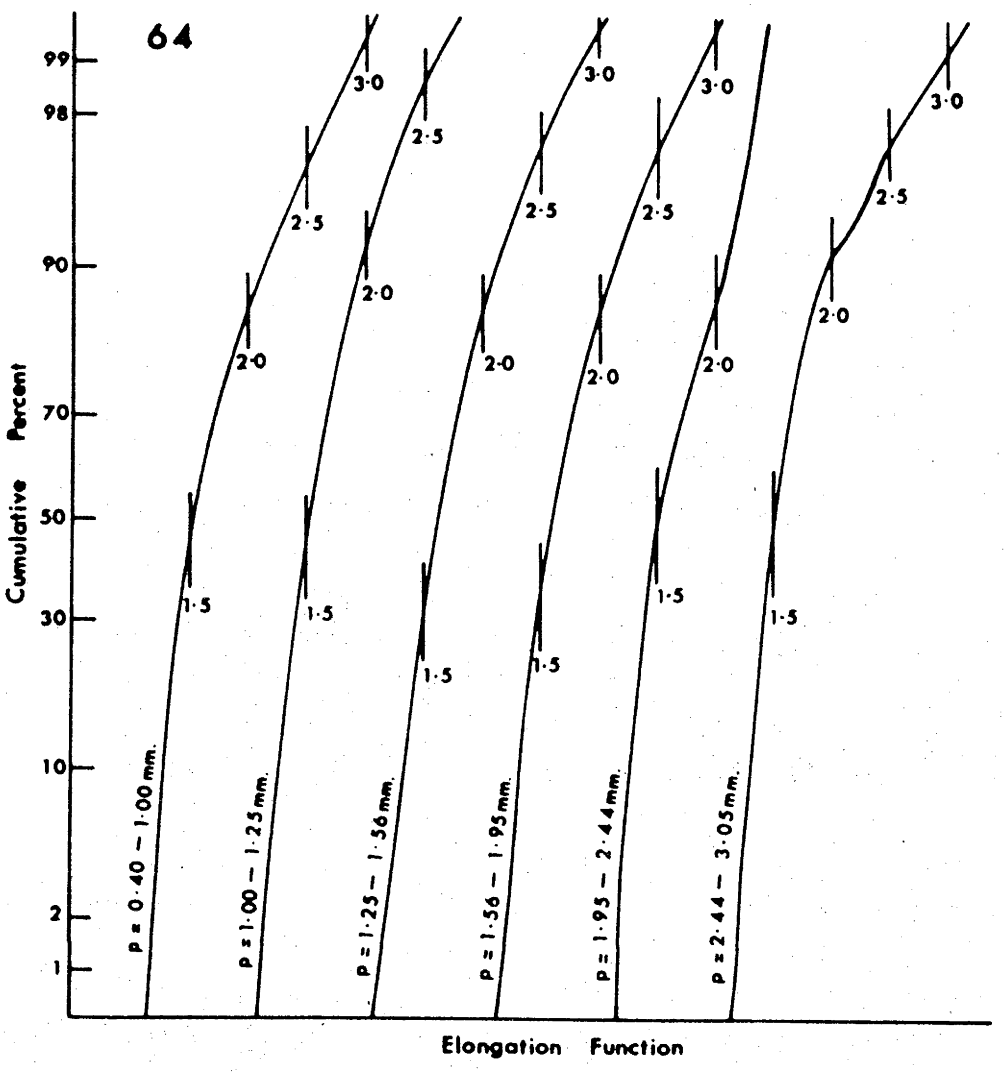

Fig. 64. Serial sections, with respect to the long dimension (range shown on each curve), of the overall distribution of the elongation function for No. 1153.

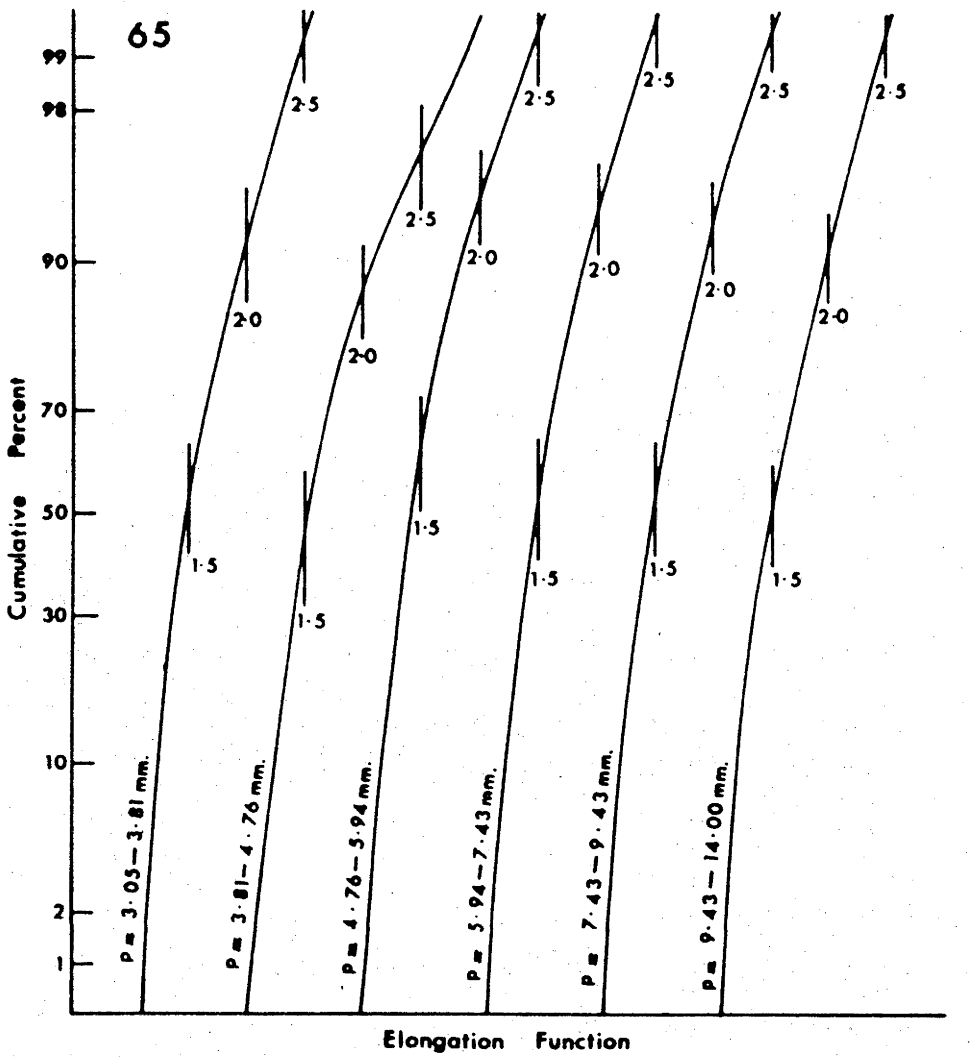

Fig. 65. Serial sections, with respect to the long dimension (range shown on each curve), of the overall distribution of the elongation function for No. 1153.

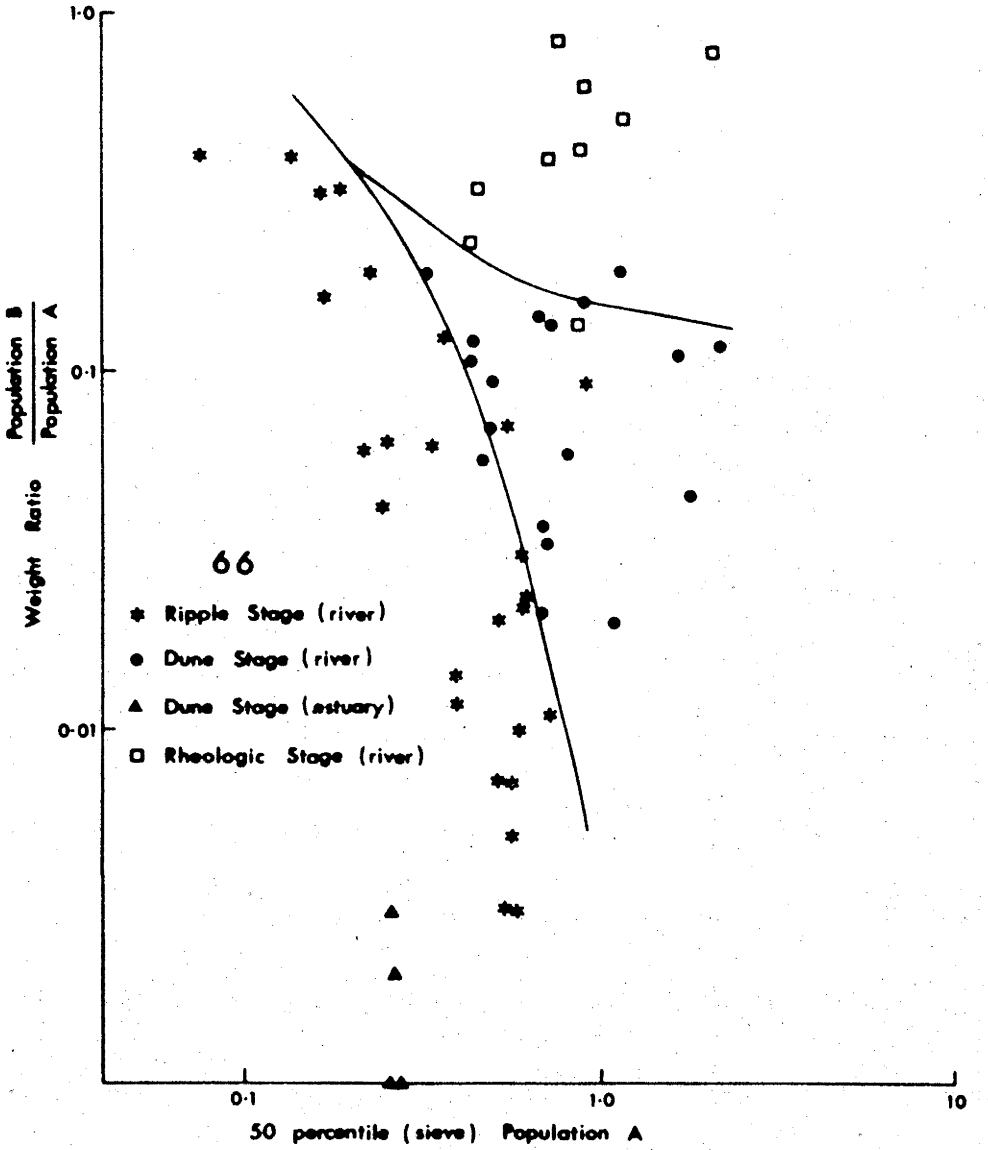

Fig. 66. The ratio of the weight of Population B to that of Population A versus the fifty percentile of Population A for natural sediment samples.

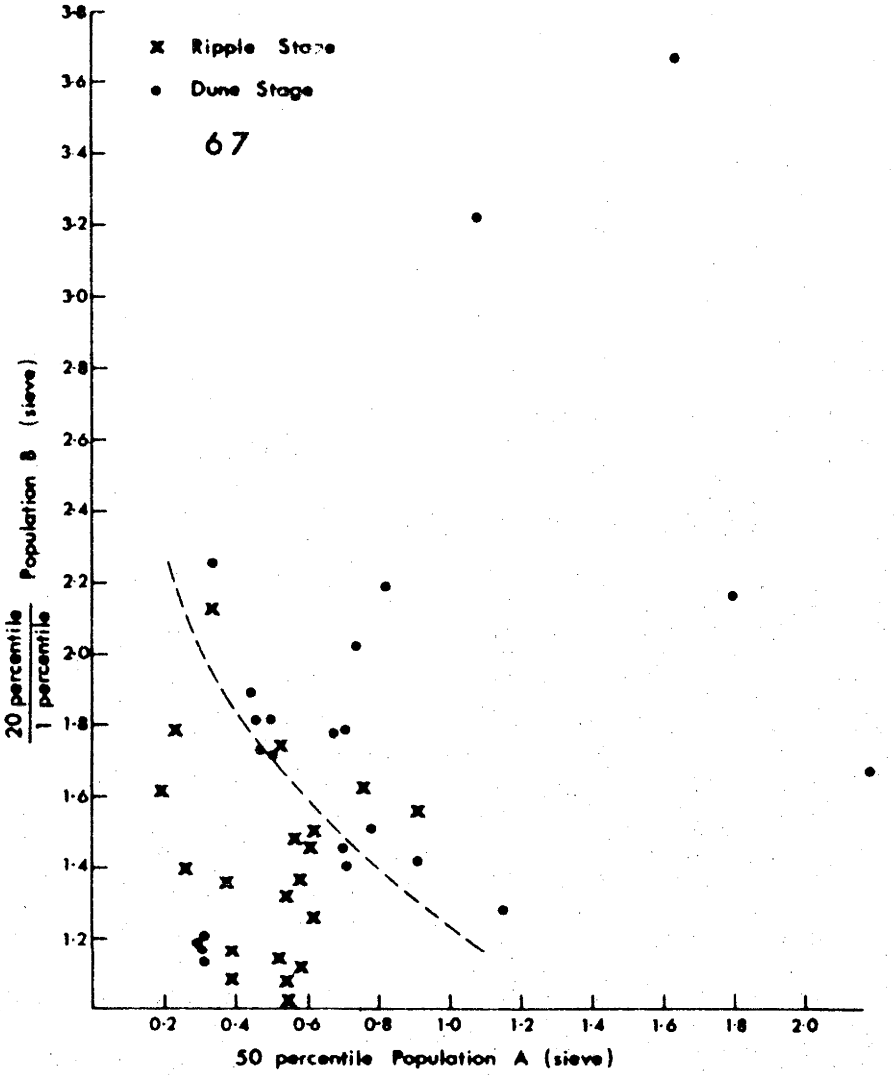

Fig. 67. The ratio of the twenty percentile of Population B to its one percentile versus the fifty percentile of Population A for natural ripple and dune stage samples.

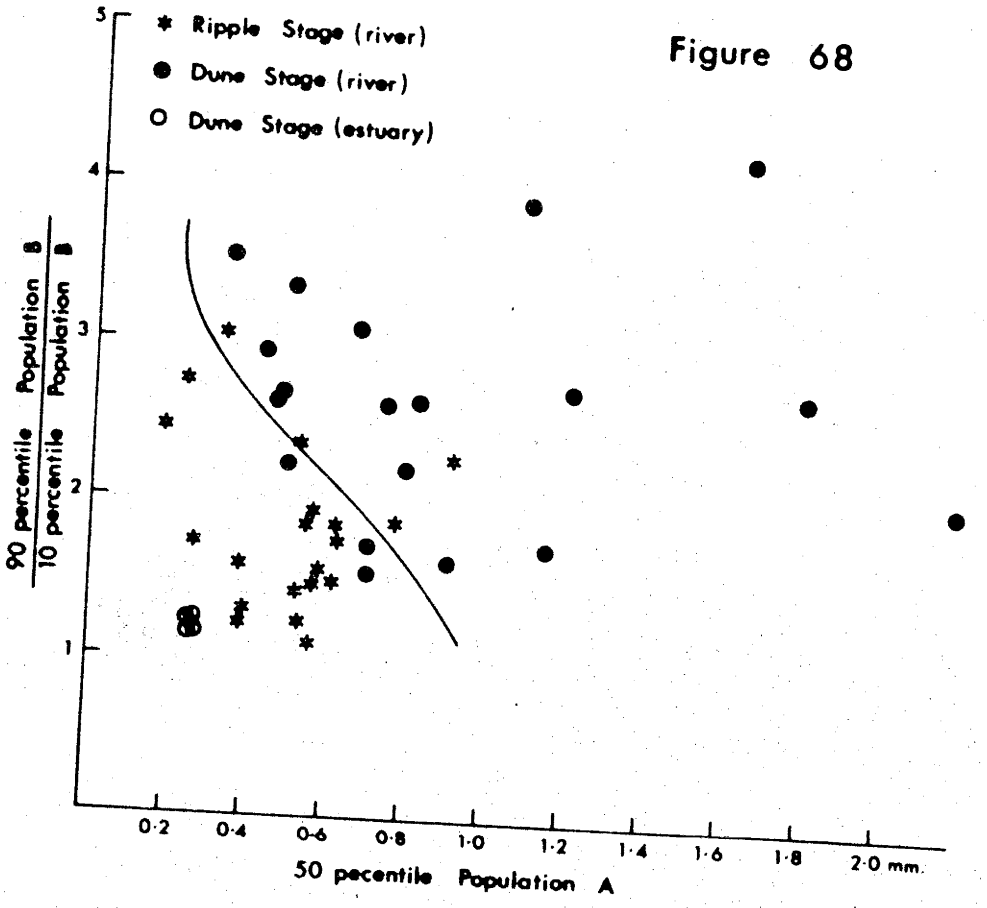

Fig. 68. The ratio of the ninety percentile of Population B to its one percentile versus the fifty percentile of Population A for natural ripple and dune stage samples.

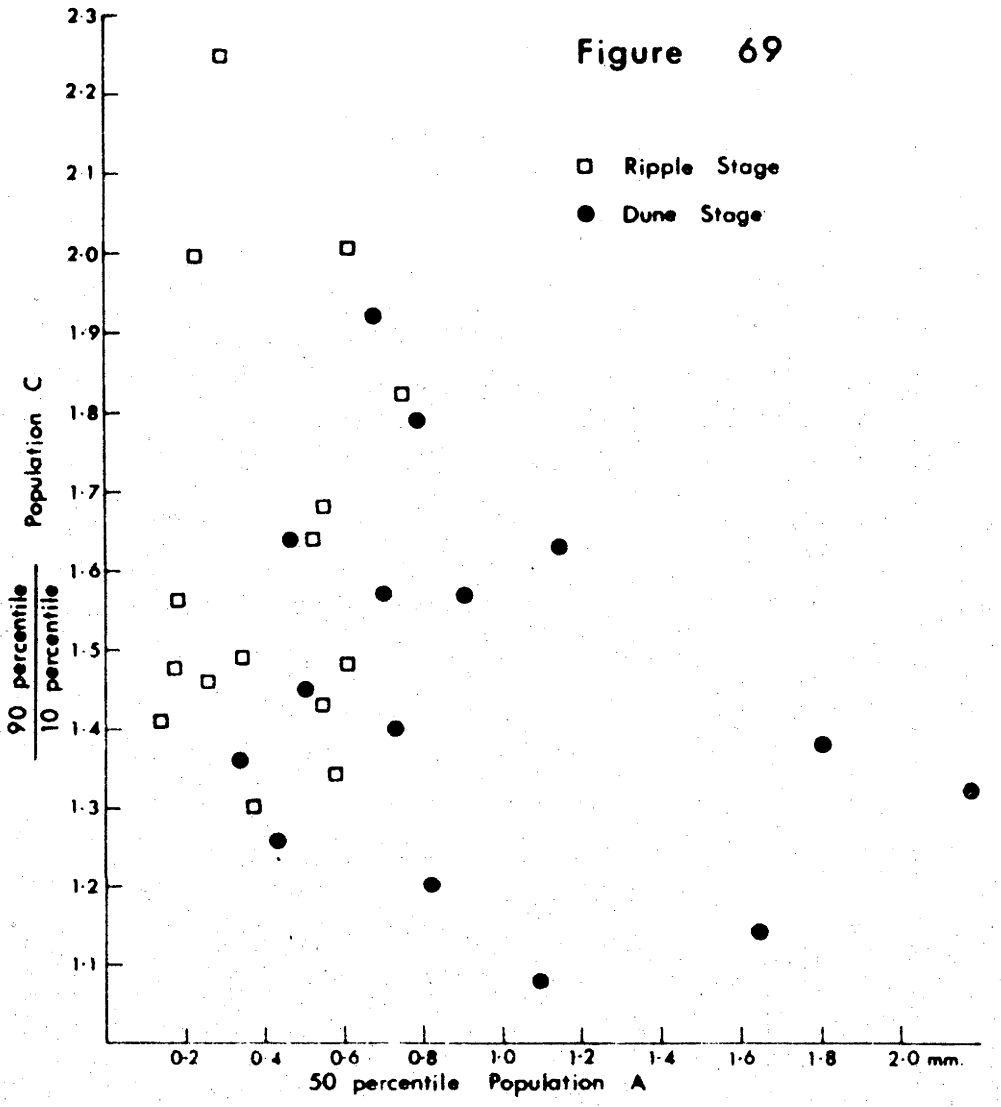

Fig. 69. The ratio of the ninety percentile of Population C to its ten percentile versus the fifty percentile of Population A for natural ripple and dune stage samples.

Figure 70

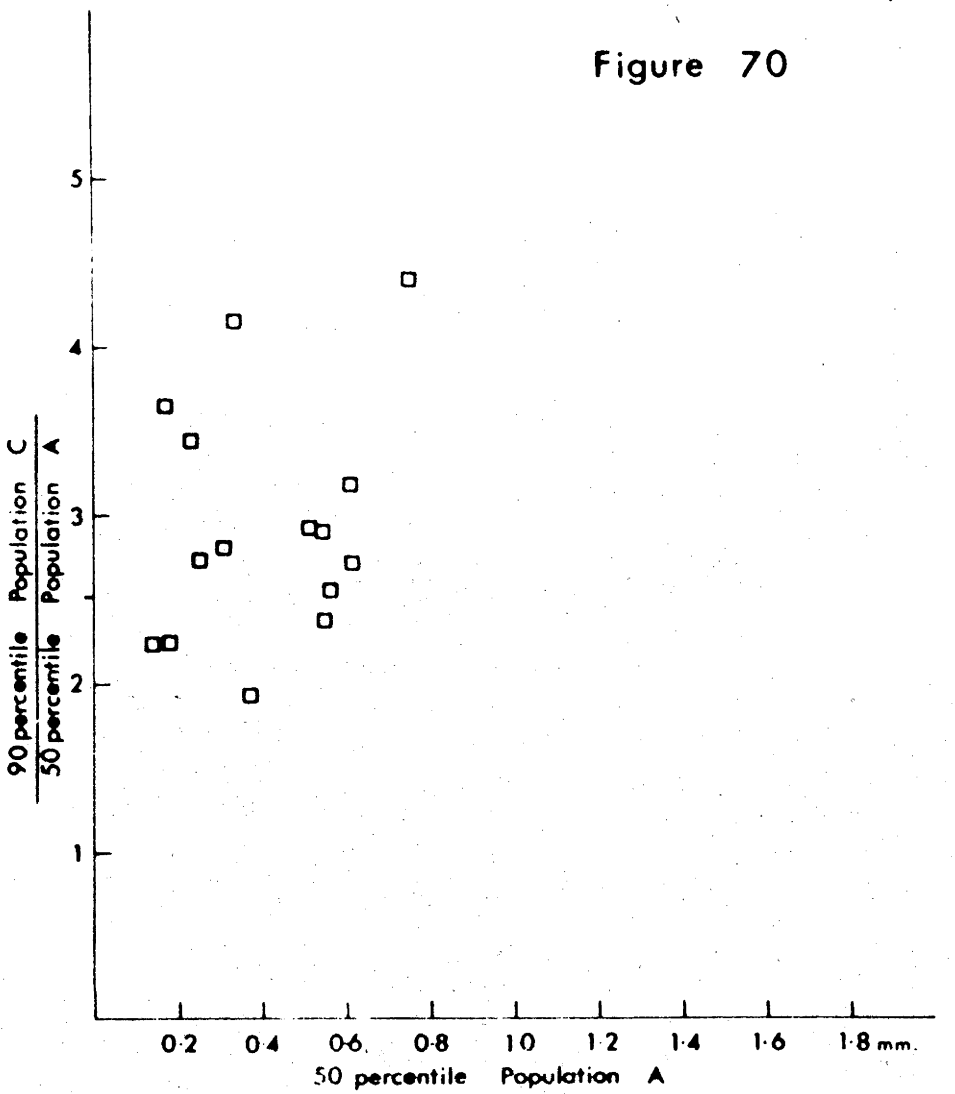

Fig. 70. The ratio of the ninety percentile of Population C to the fifty percentile of Population A versus the fifty percentile of Population A for natural ripple stage sands.

Figure 71

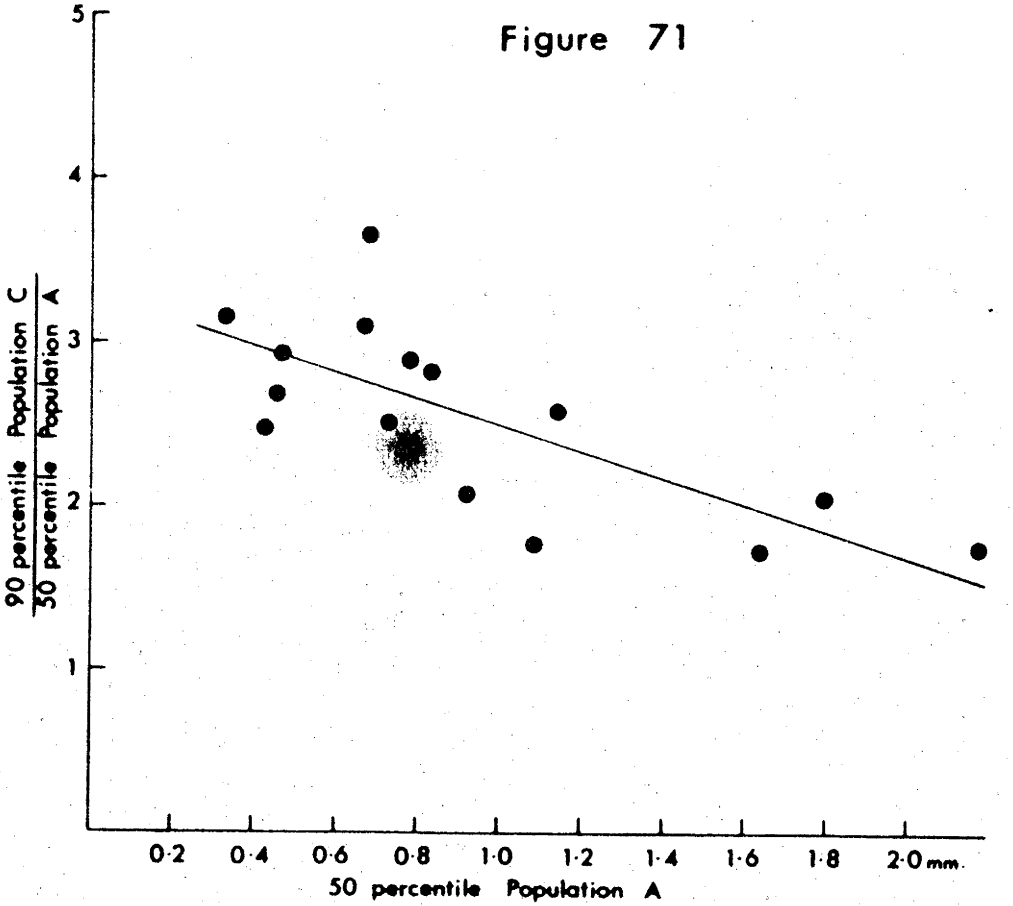

Fig. 71. Analogous plot to Fig. 70 but for natural dune stage sands. Correlation coefficient has a value of - 0.714.

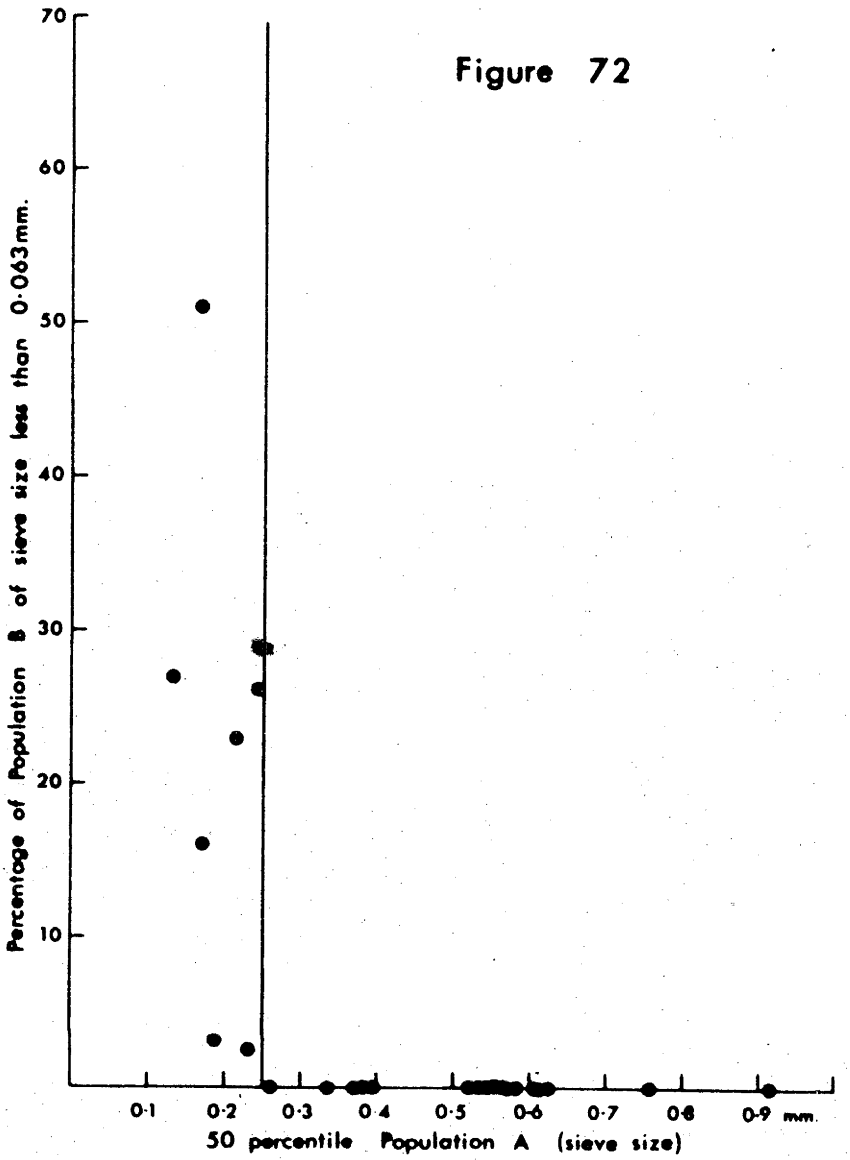

Fig. 72. Percentage of Population B of sieve size less than 0.063 mm versus the fifty percentile of Population A for natural ripple stage sediments.

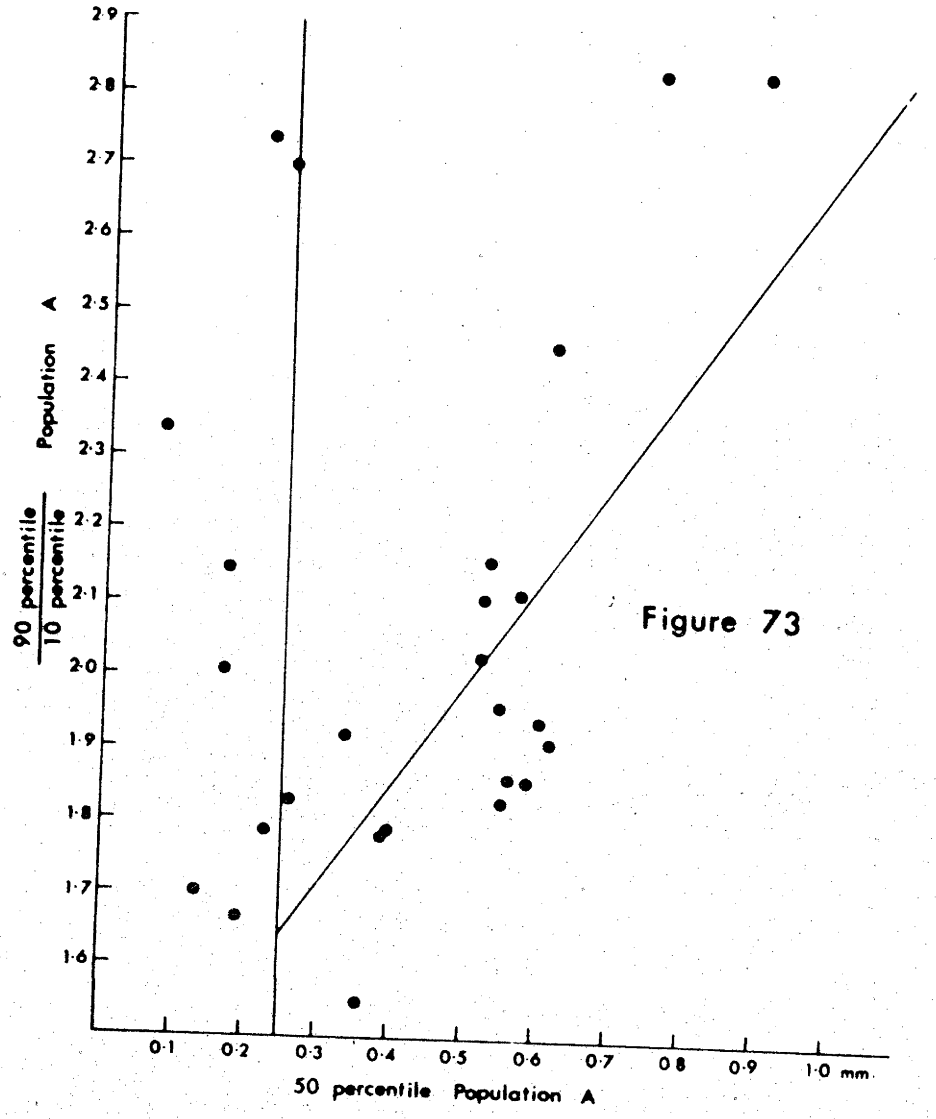

Figure 73

Fig. 73. Ratio of ninety percentile of Population A to its ten percentile versus the fifty percentile of Population A for natural ripple stage sediments. A least square linear curve is fitted for sediments with Population A fifty percentile over 0.25 mm, Correlation coefficient for these points is + 0.762.

Figure 74

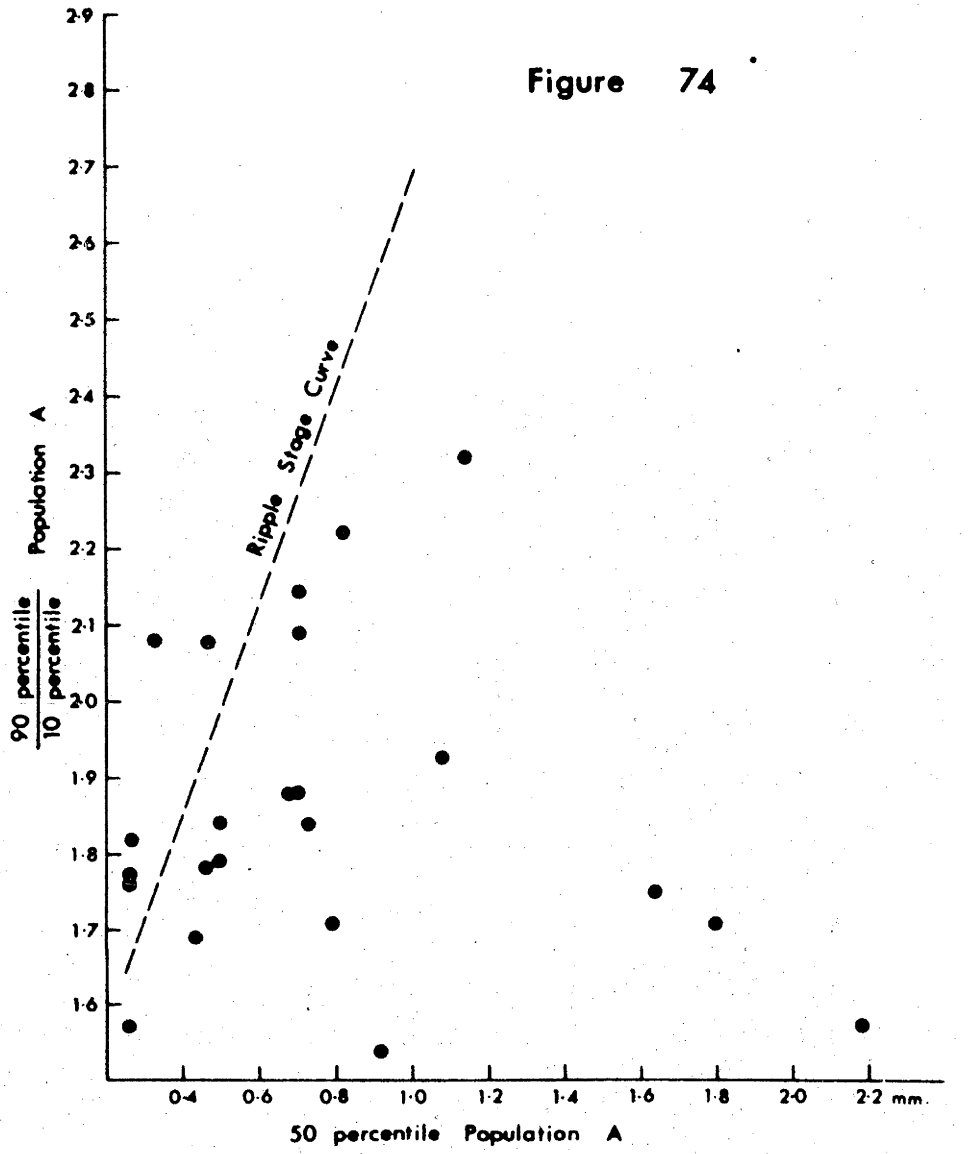

Fig. 74. Analogous plot to Fig. 73 for natural dune stage sands. The curve from Fig. 73 is inserted for comparative purposes.

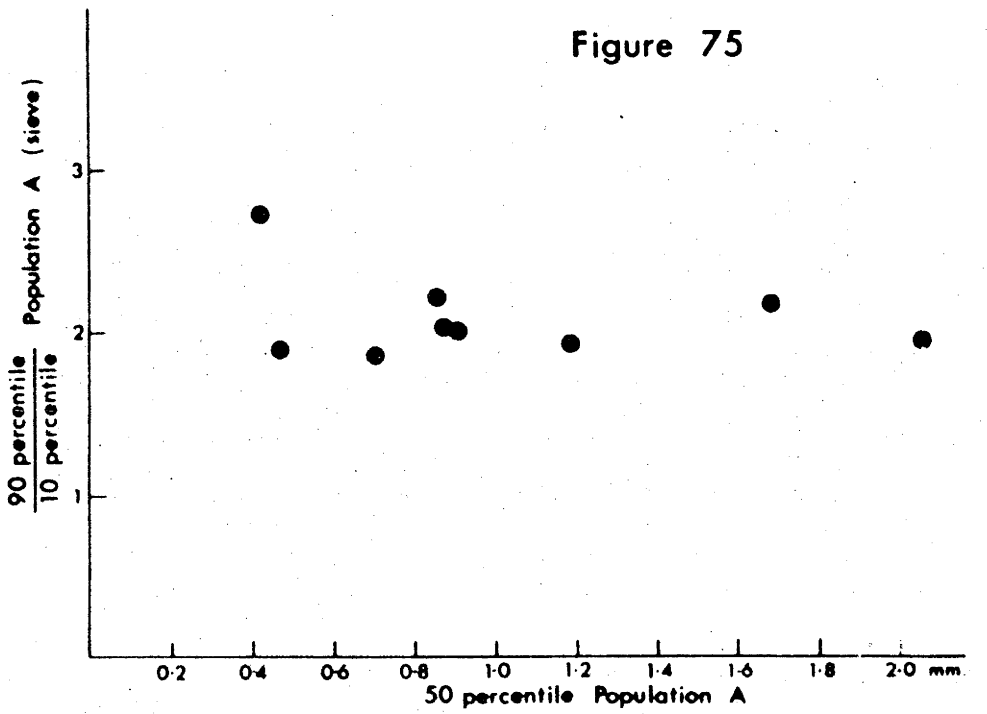

Fig. 75. Analogous plot to Fig. 73 for natural rheologic bed load deposits. No. 1162 was too coarse for the plot with a fifty percentile of 4.75 mm and a ratio of 2.19

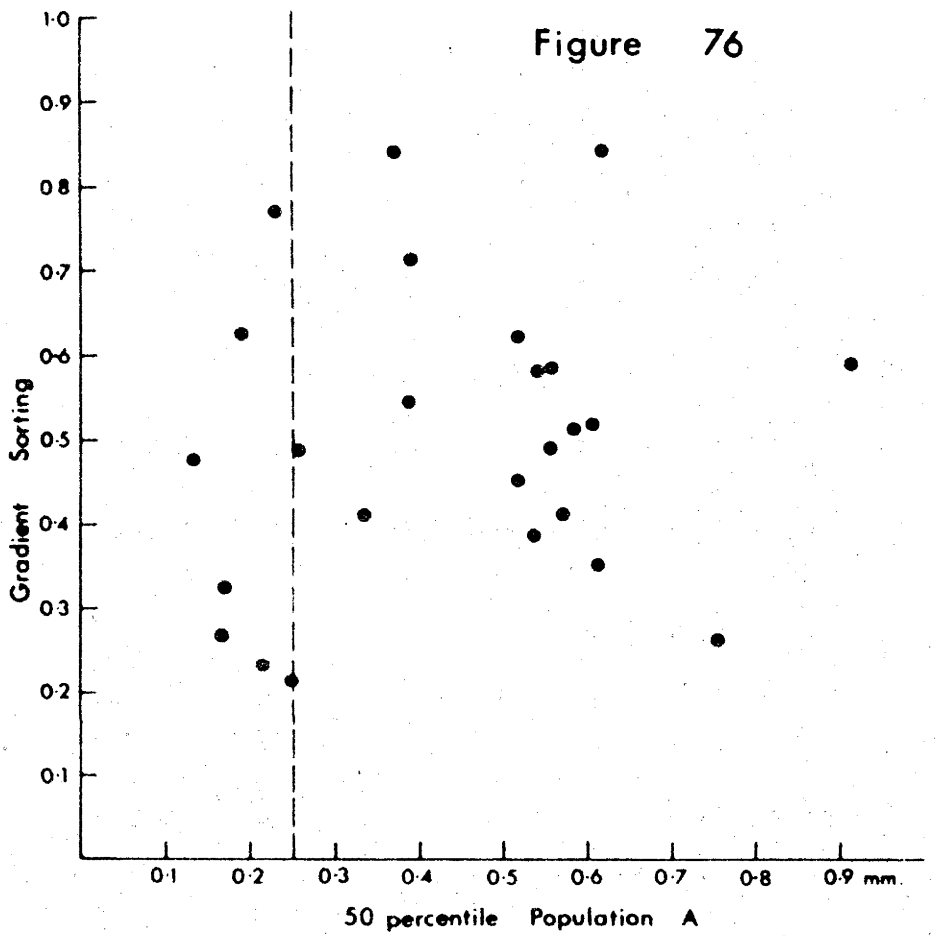

Fig. 76. Gradient sorting versus the fifty percentile of Population A for natural ripple stage sands. The correlation coefficient for those coarser than 0.25 mm is - 0.180.

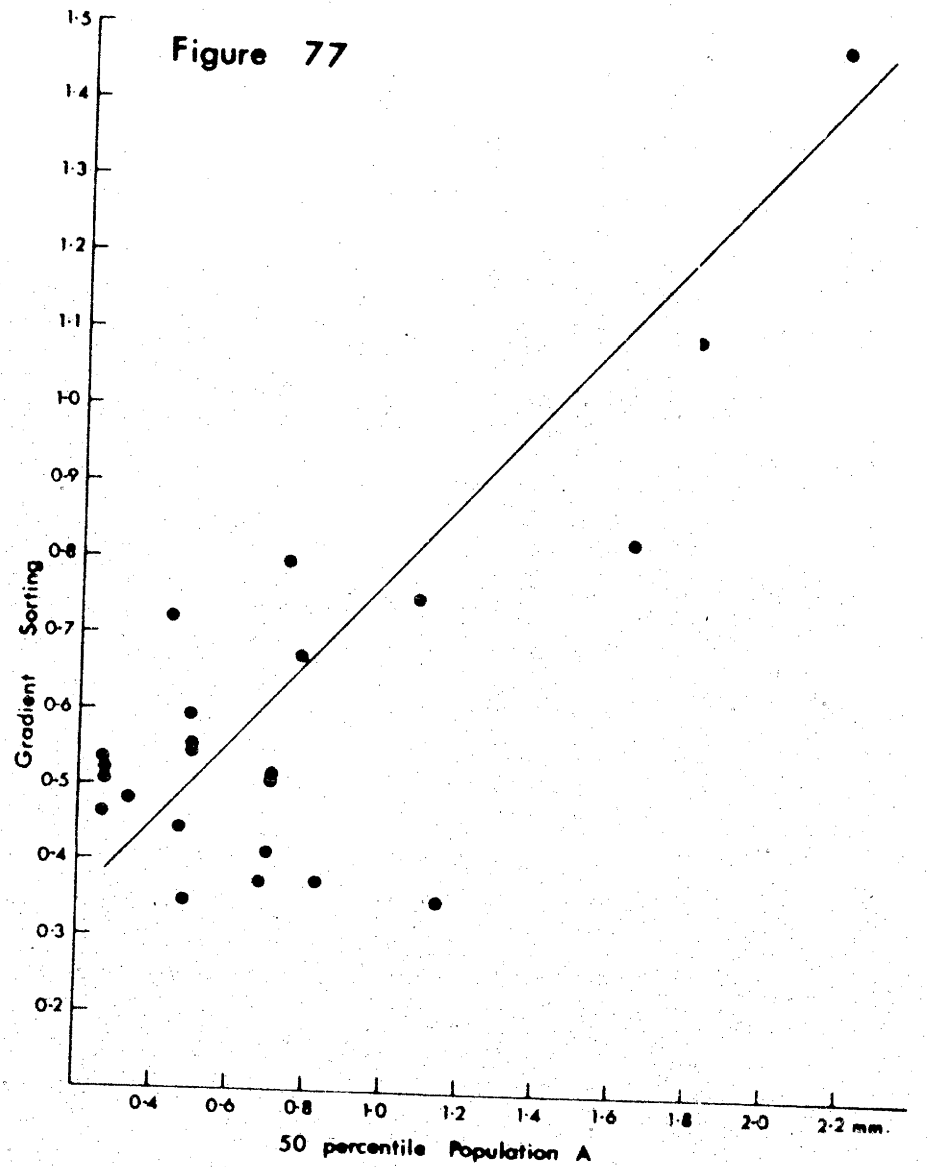

Fig. 77. Analogous plot to Fig. 76 for natural dune stage sands. A least squares linear curve is fitted to the data. Correlation coefficient is + 0.709.

Figure 78

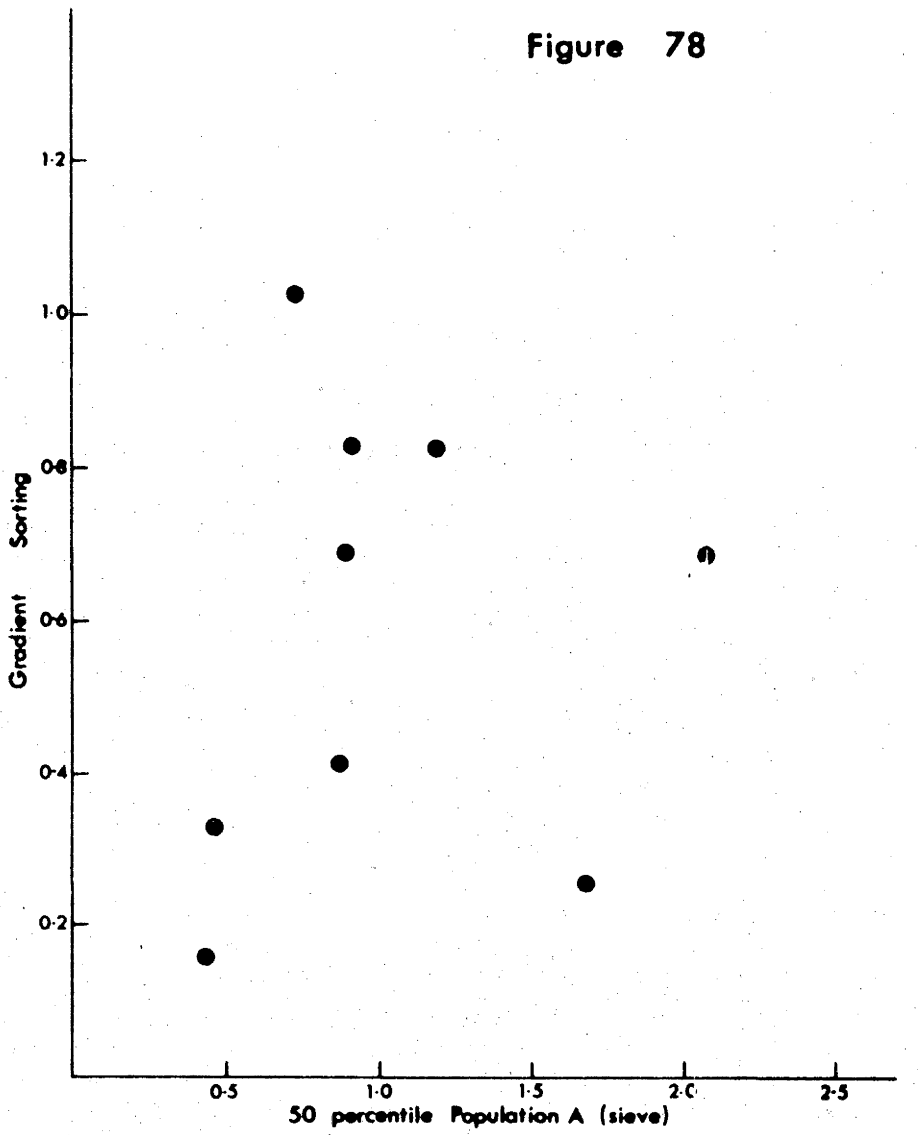

Fig. 78. Analogous plot to Fig. 76 for rheologic bed load sediments. No. 1162 could not be plotted as it was not covered by empirical settling velocity data

Figure 79

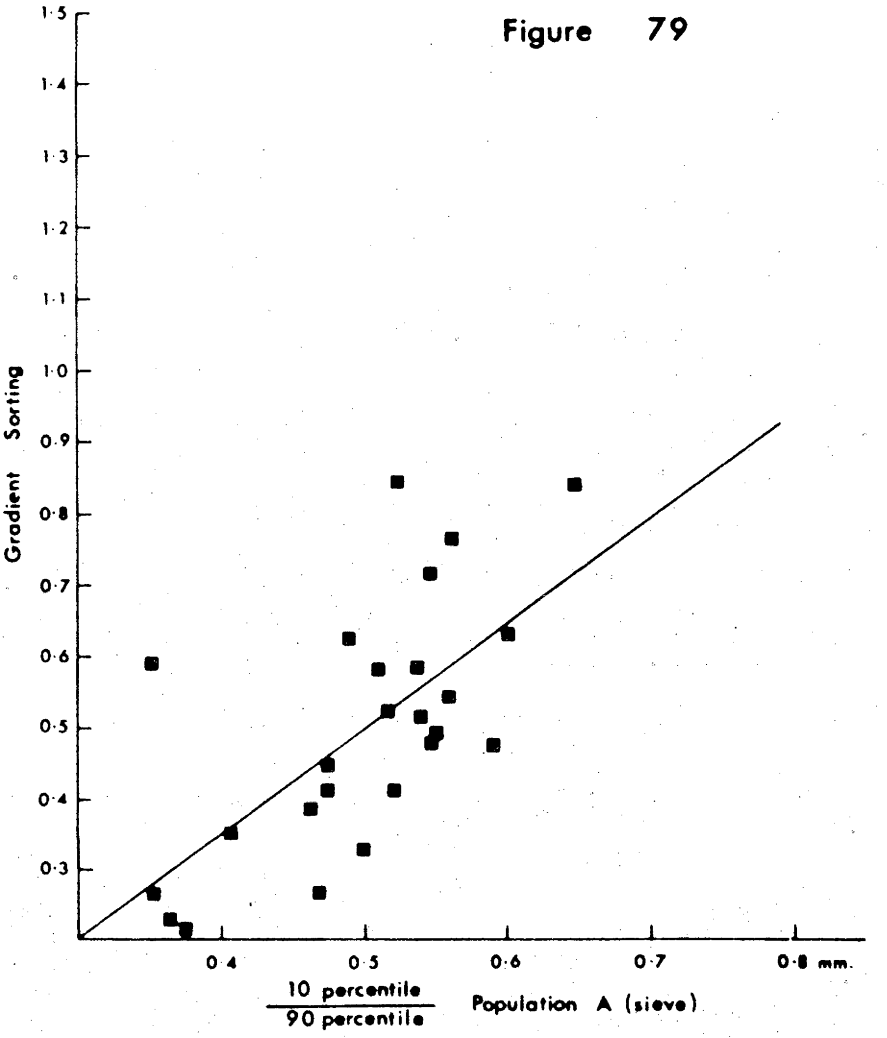

Fig. 79. Gradient sorting versus the ratio of the sieve ten percentile to the sieve ninety percentile of Population A for natural ripple stage sands. Correlation coefficient is + 0.649.

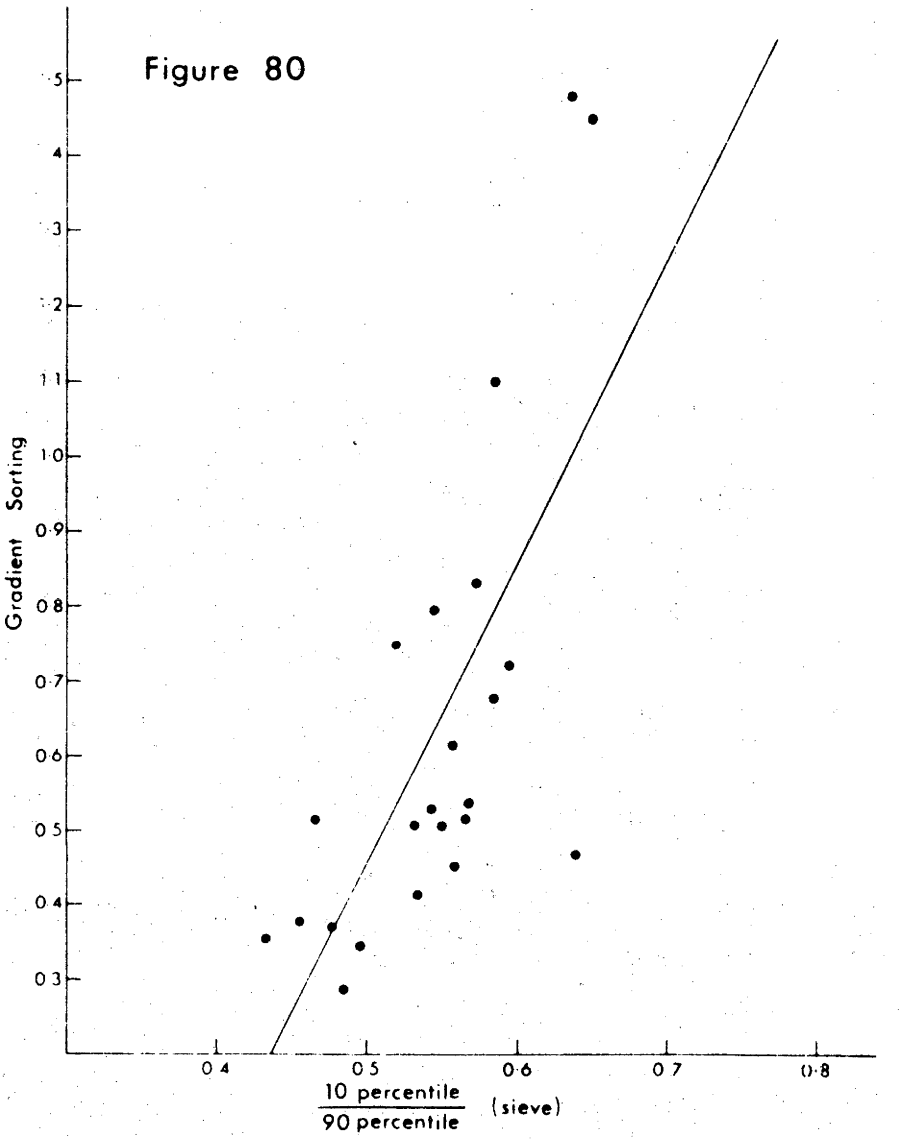

Fig. 80. Analogous plot to Fig. 74 for natural dune stage sands. Correlation coefficient is + 0.704.

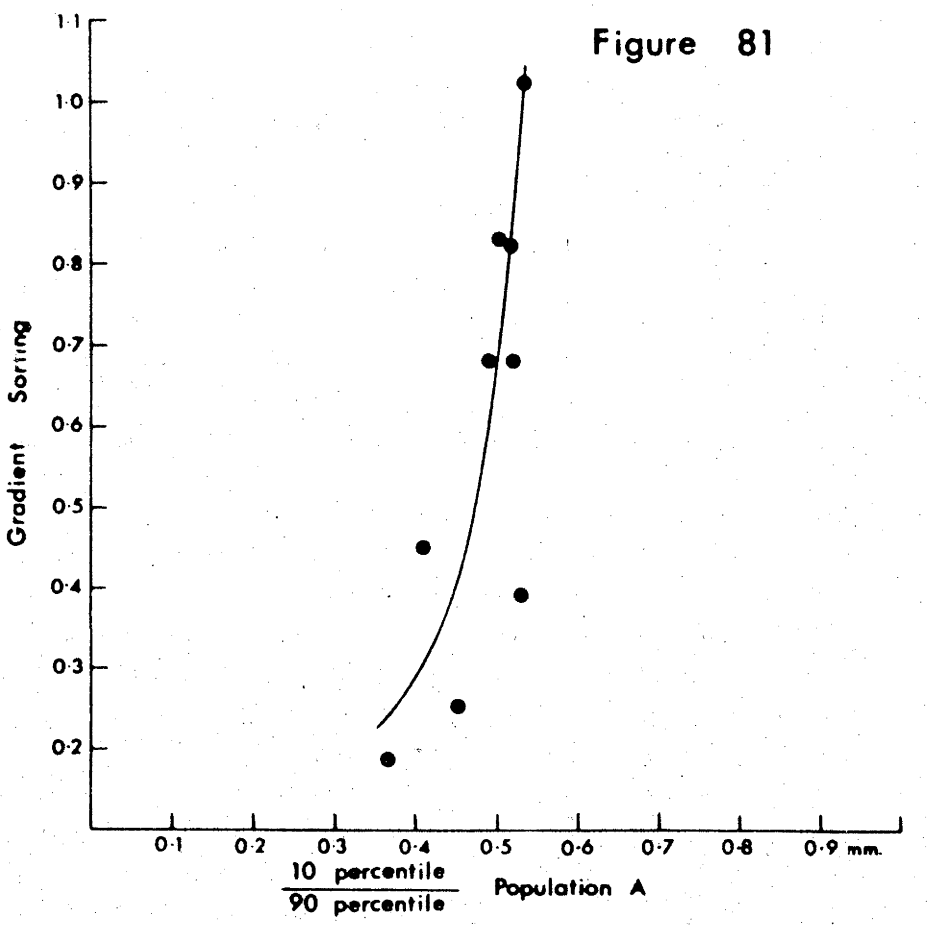

Fig. 81. Analogous plot to Fig. 79 for natural rheologic bed load sands.

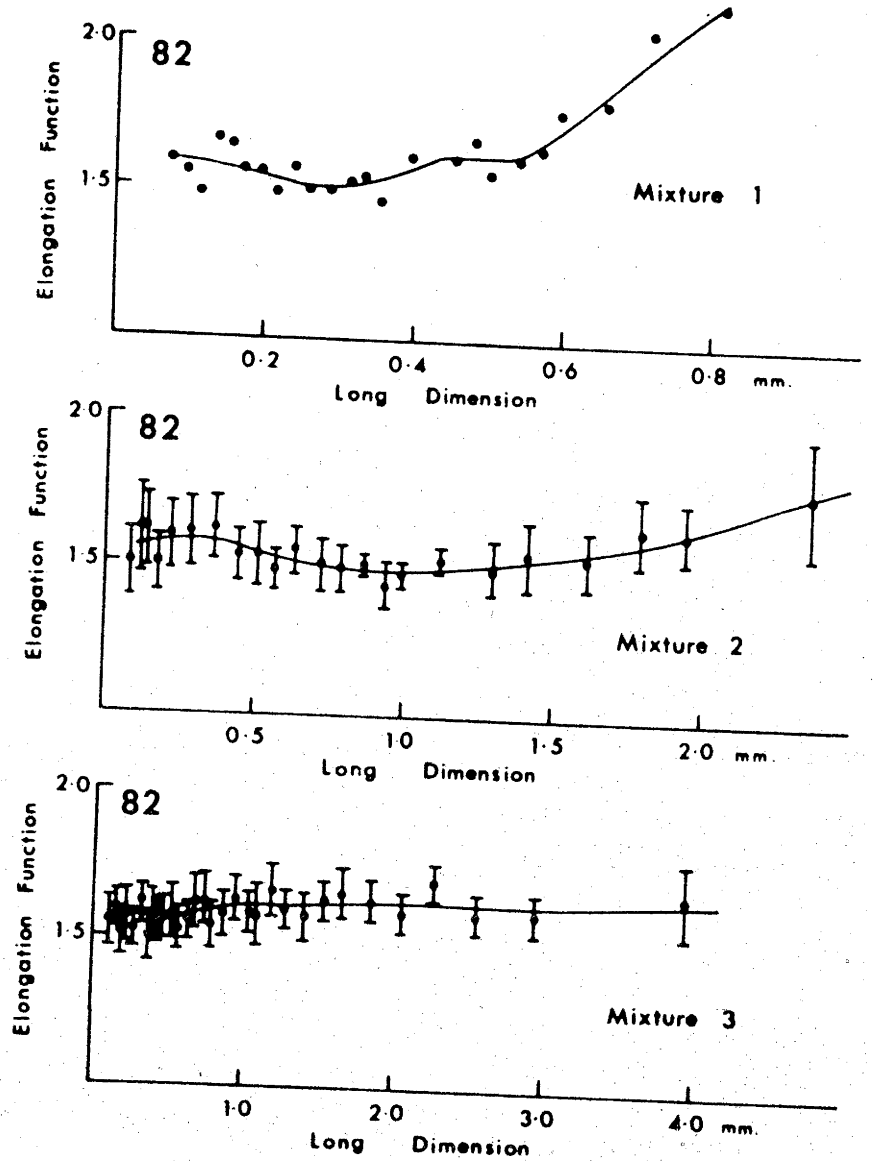

Fig. 82. Elongation function curves of the three mixtures used in the flume runs. 95% confidence limits are given for means for mixtures 2 and 3.

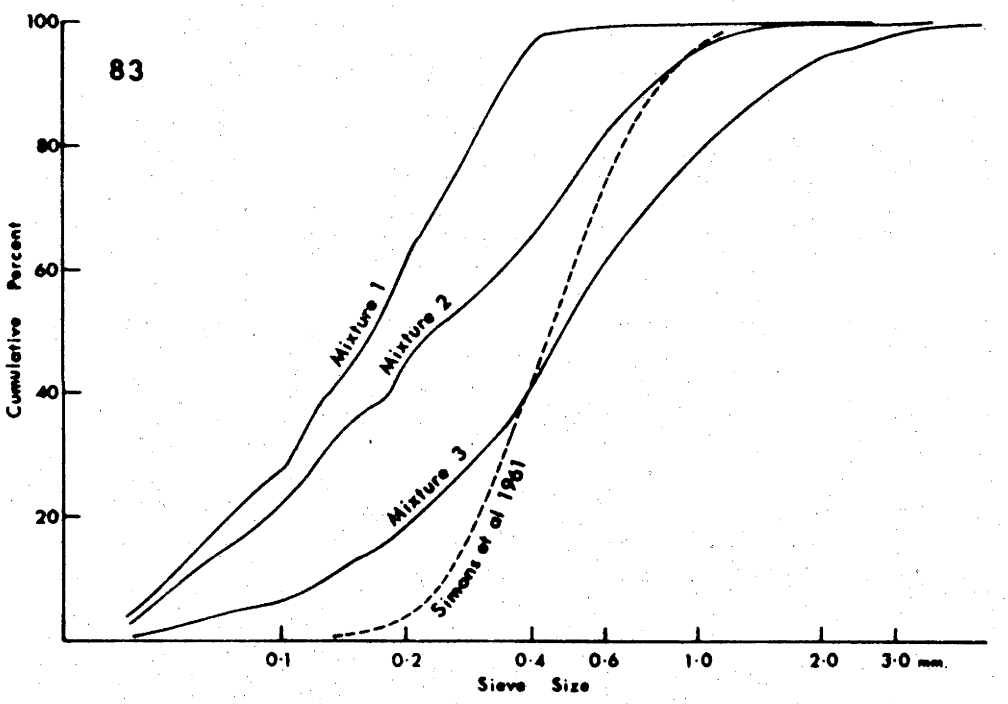

Fig. 83. Sieve cumulative curves of the three mixtures used in the flume runs. For comparison the curve for the sand used by Simons et al (1961) is added.

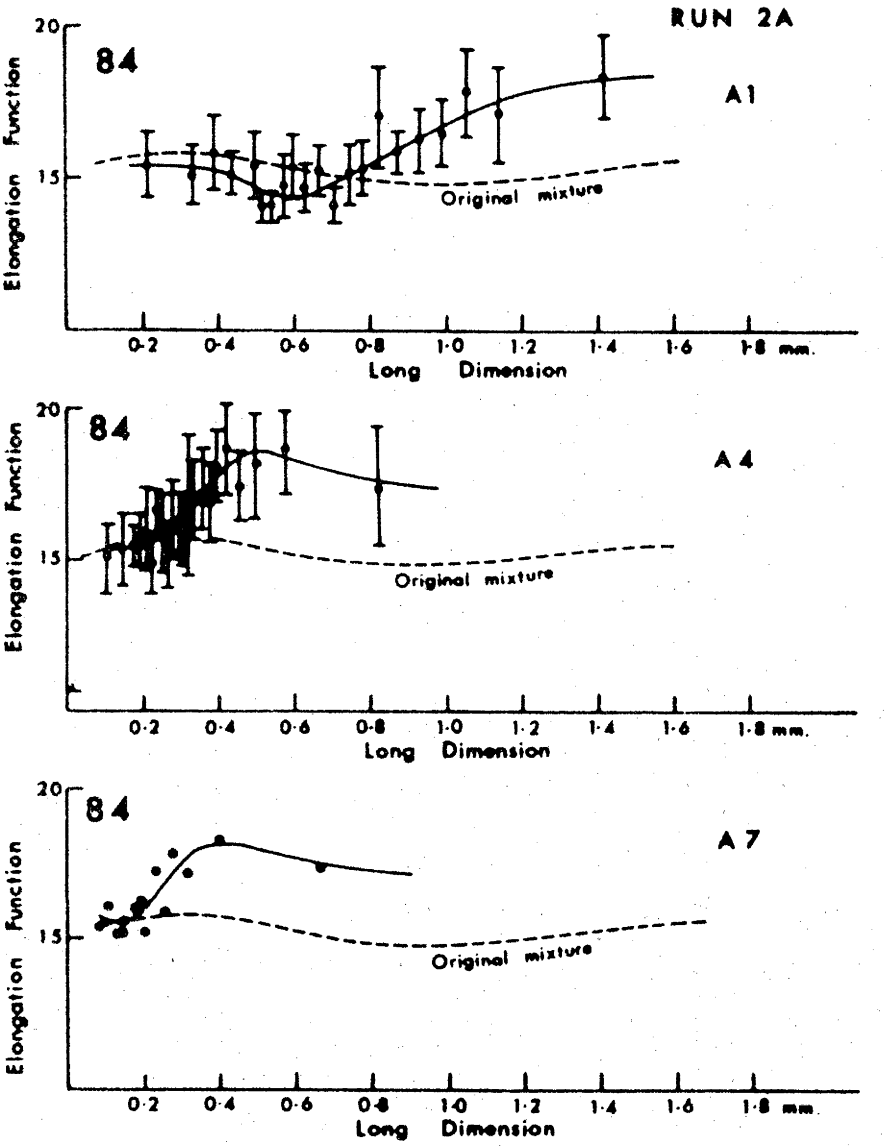

Fig. 84. Elongation function curves for Run 2A. 95% confidence limits are given for means for A1 and A4.

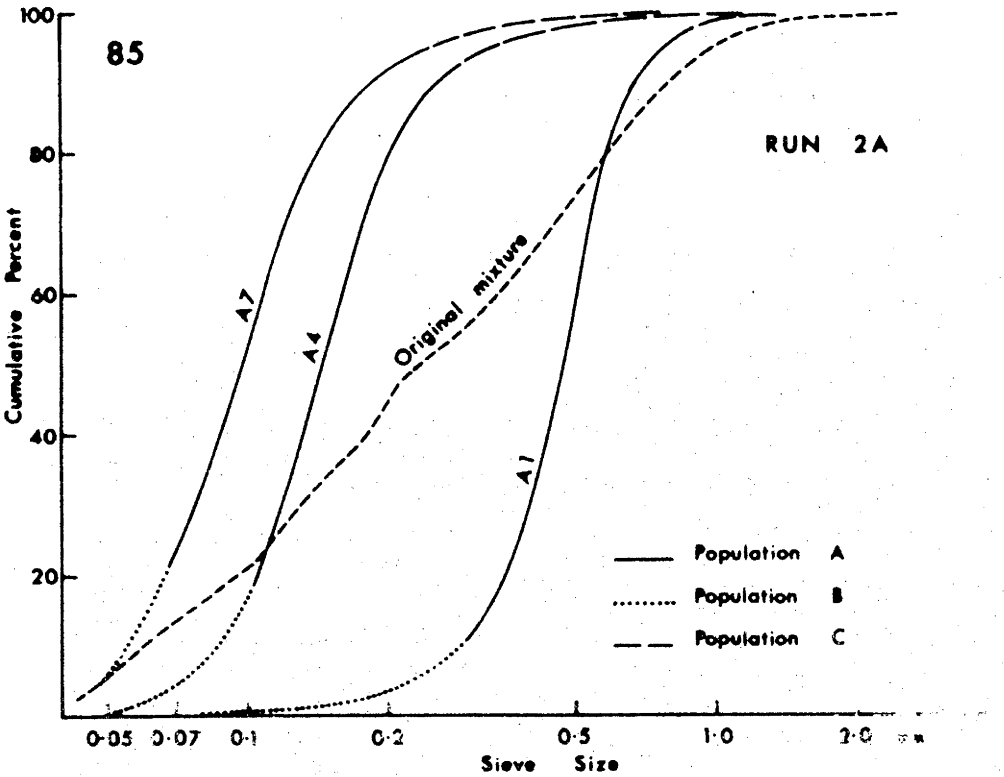

Fig. 85. Sieve cumulative curves for Run 2A.

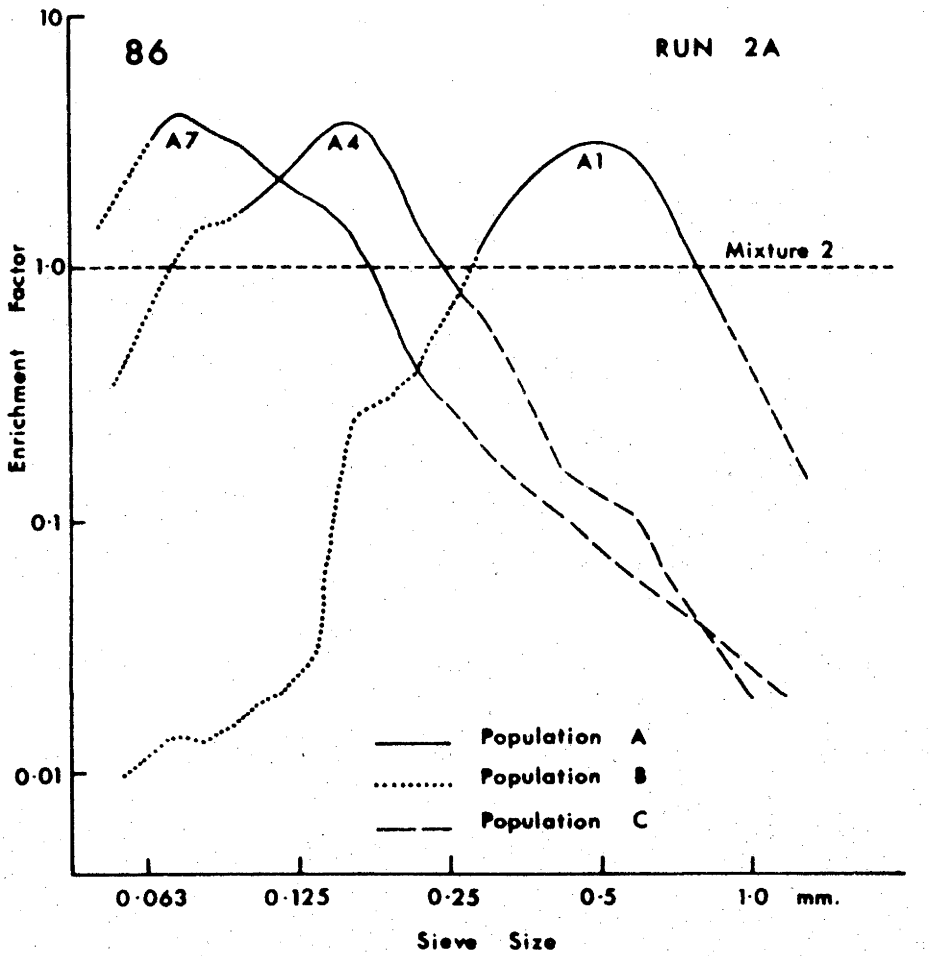

Fig. 86. Enrichment factors for Run 2A.

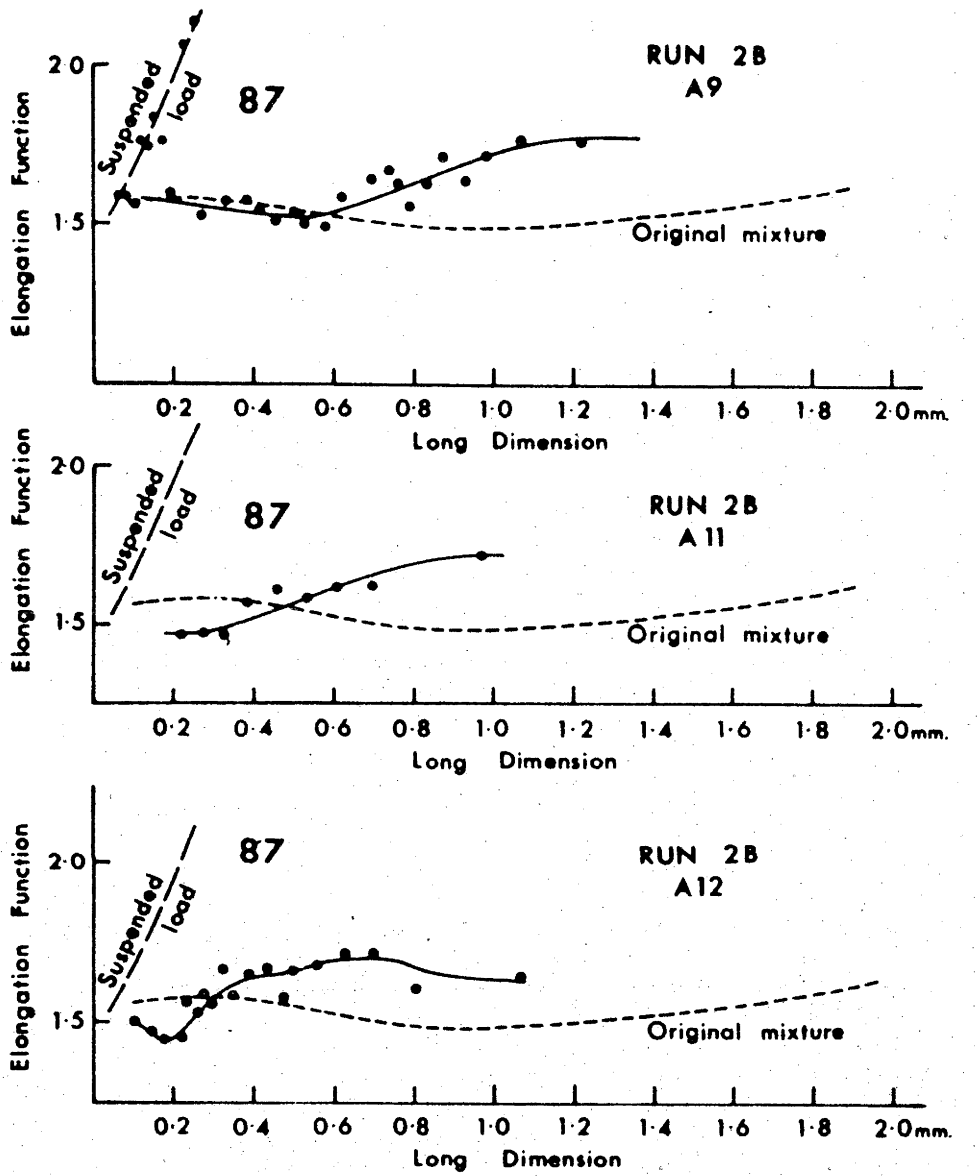

Fig. 87. Elongation function curves for Run 2B.

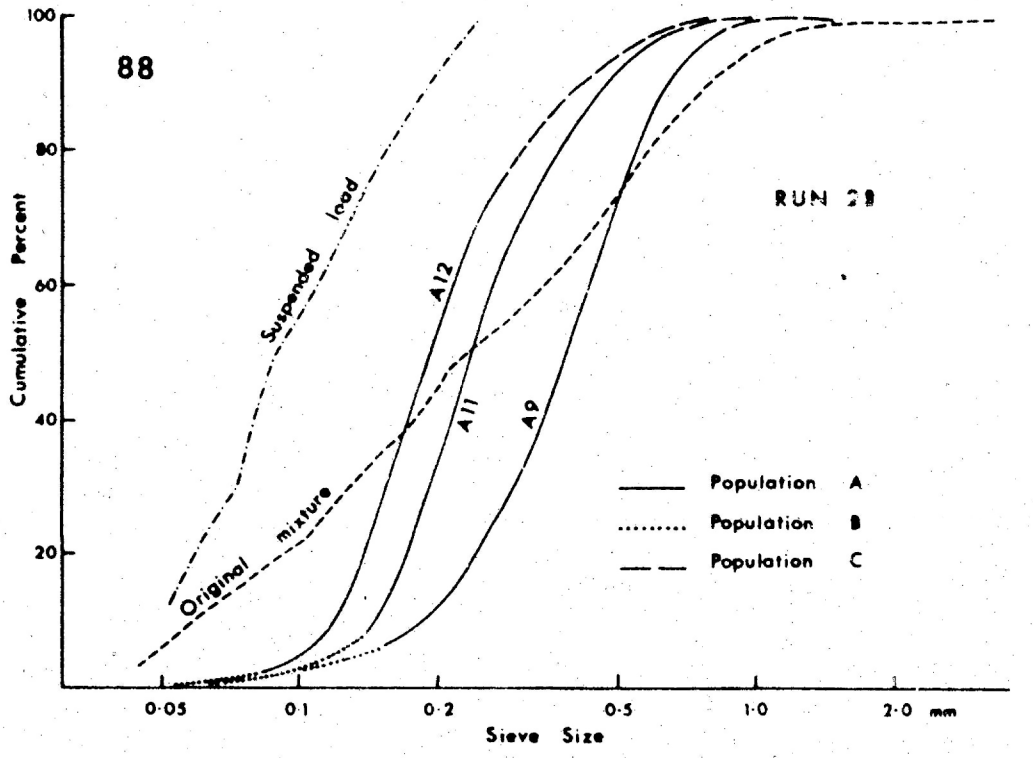

Fig. 88. Sieve cumulative curves for Run 2B.

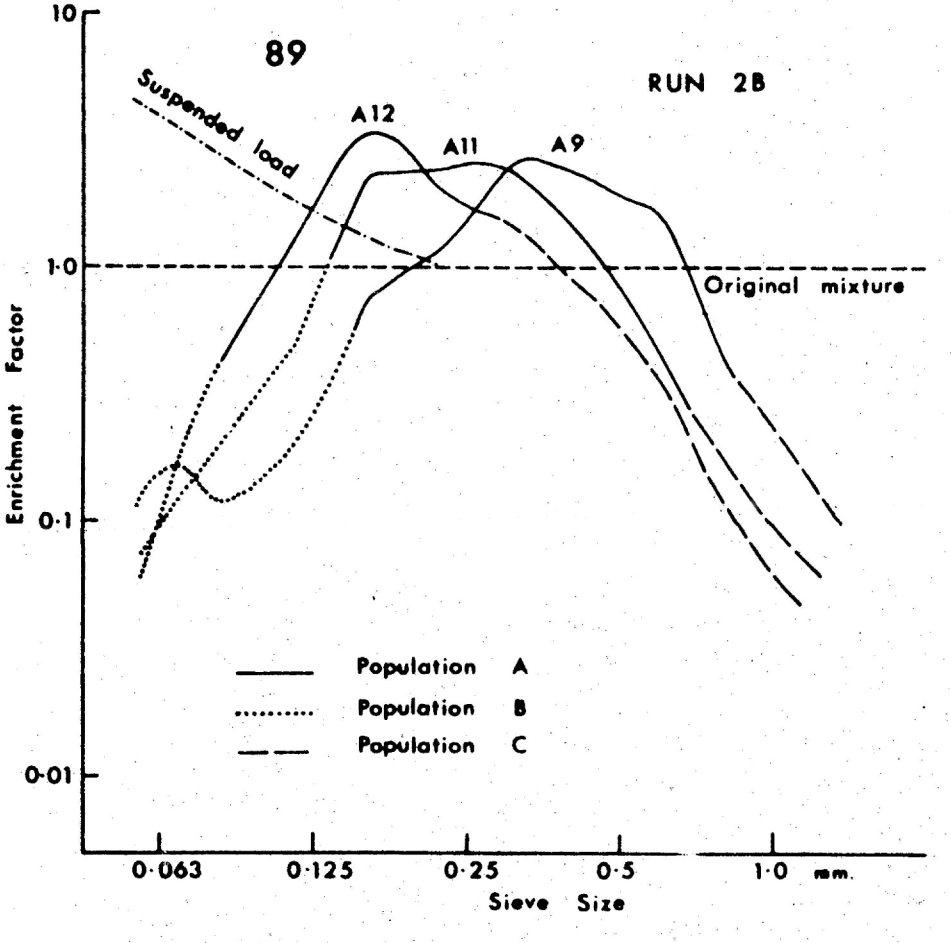

Fig. 89. Enrichment factors for Run 2B.

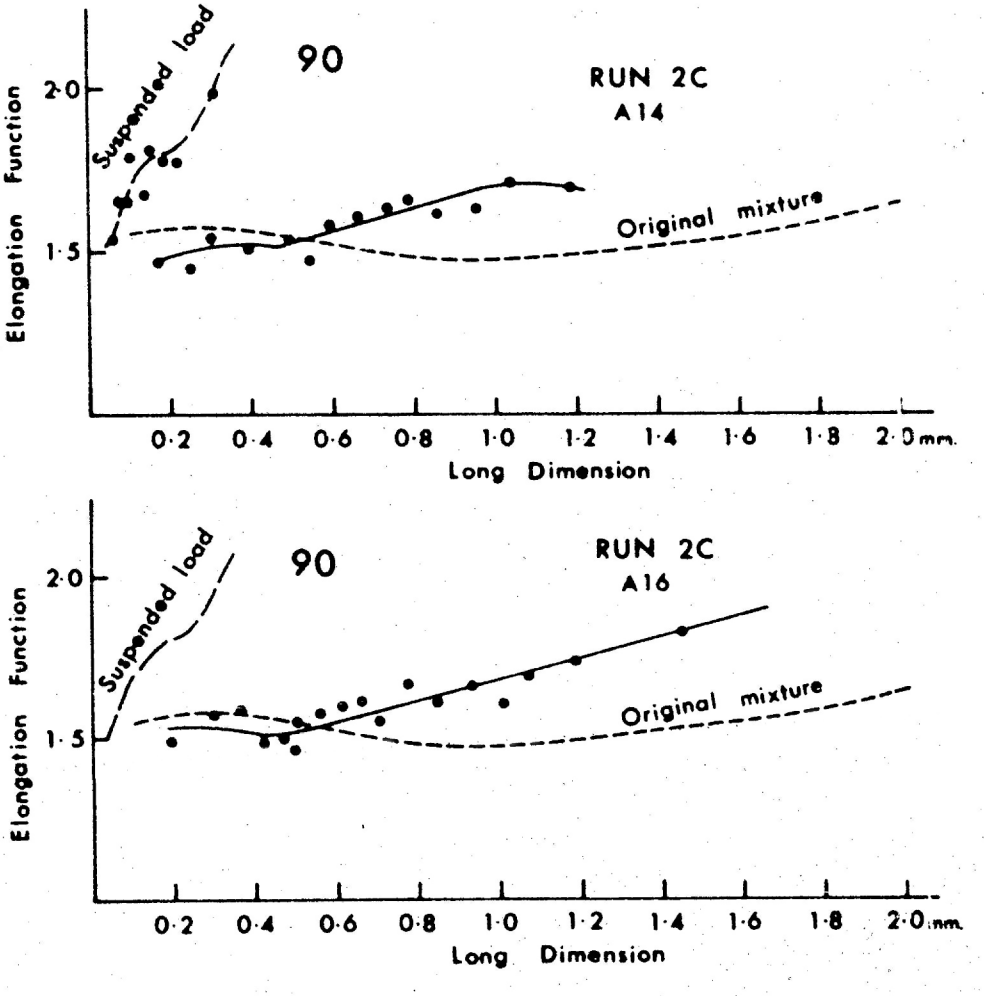

Fig. 90. Elongation function curves for Run 2C.

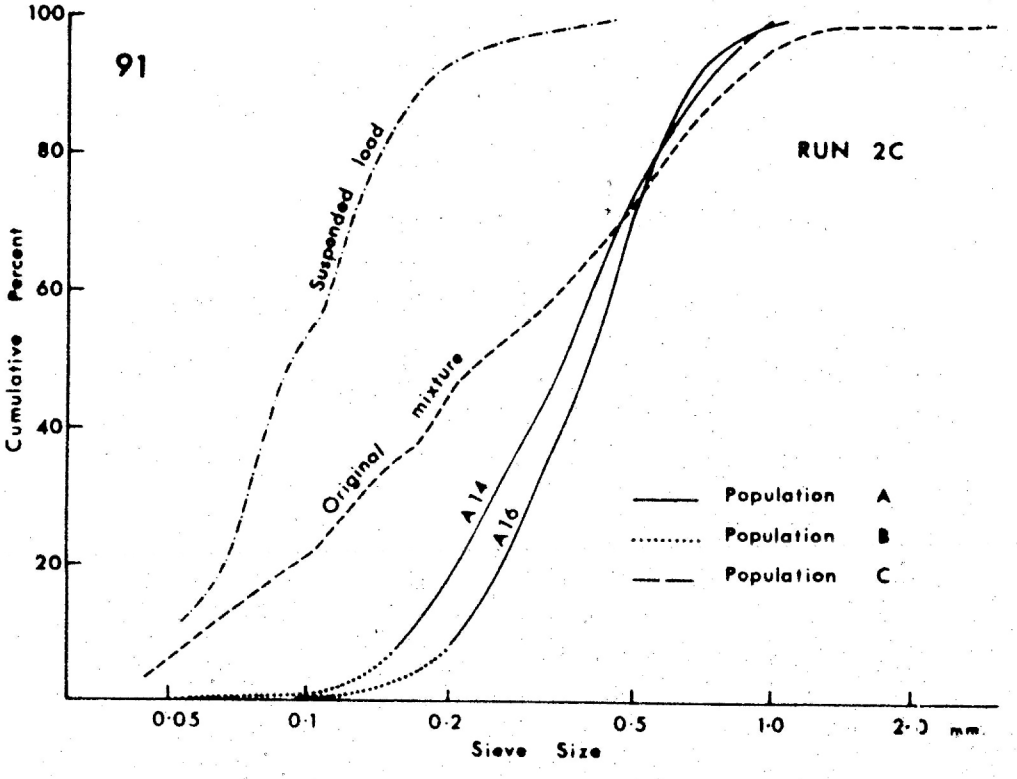

Fig. 91. Sieve cumulative curves for Run 2C.

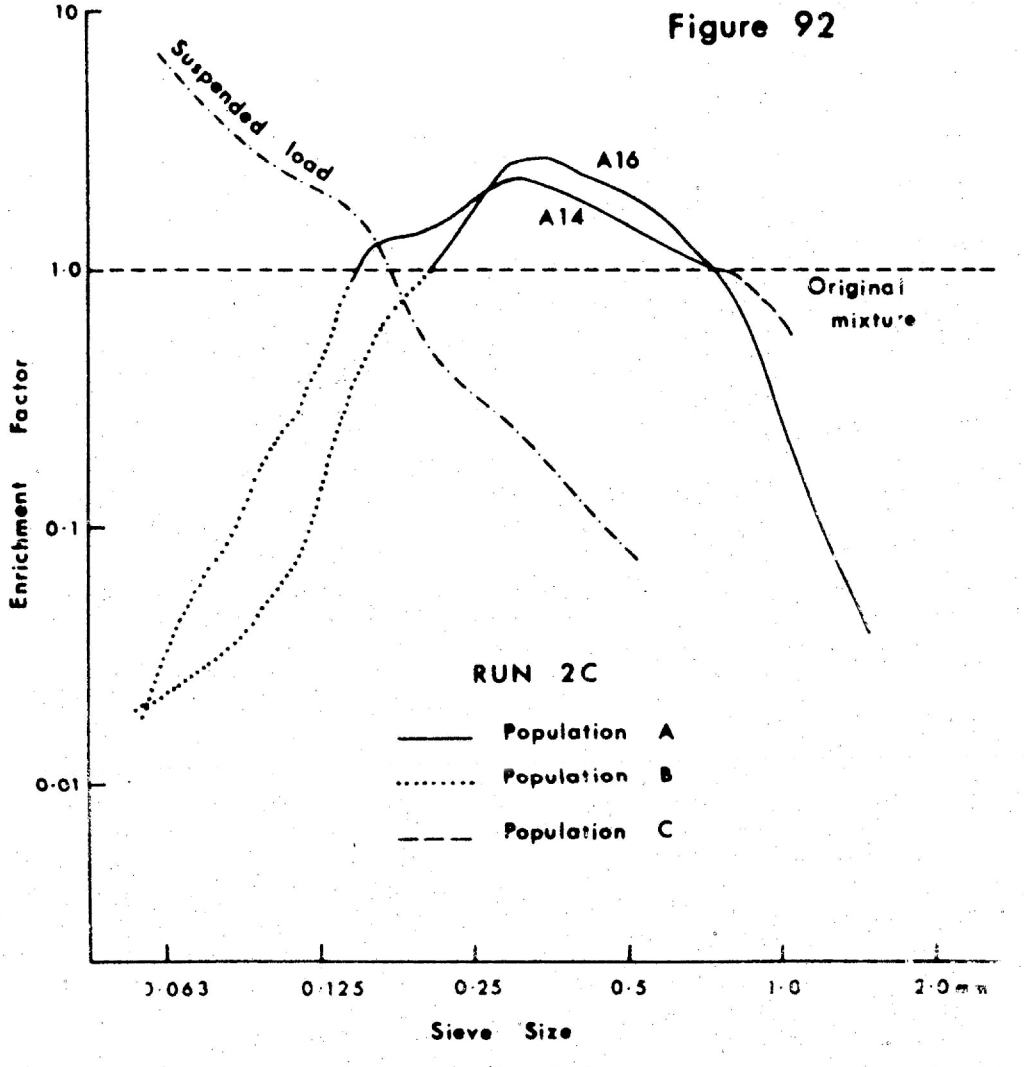

Fig. 92. Enrichment factors for Run 2C.

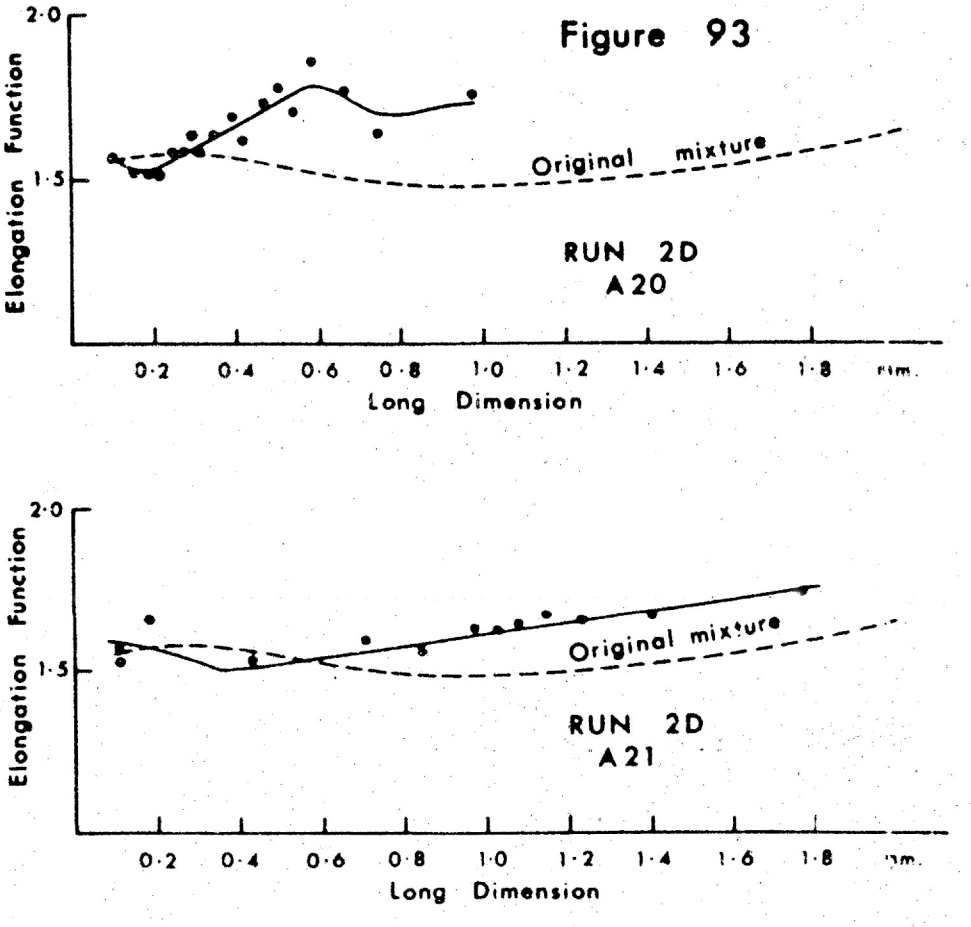

Fig. 93. Elongation function curves for Run 2D.

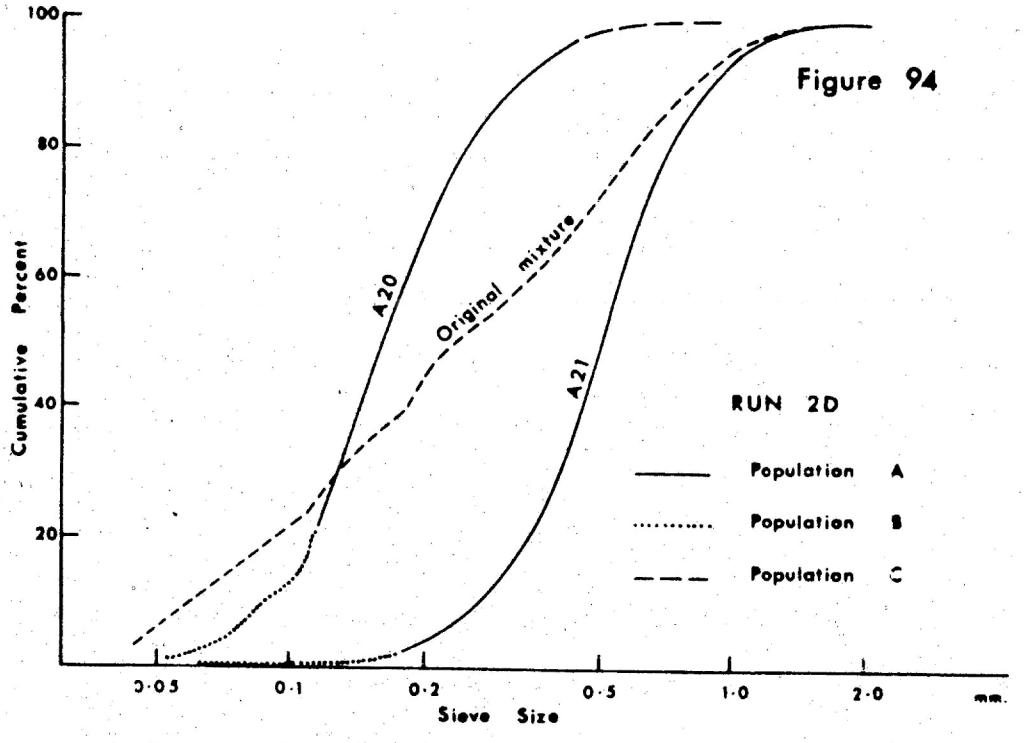

Fig. 94. Sieve cumulative curves for Run 2D.

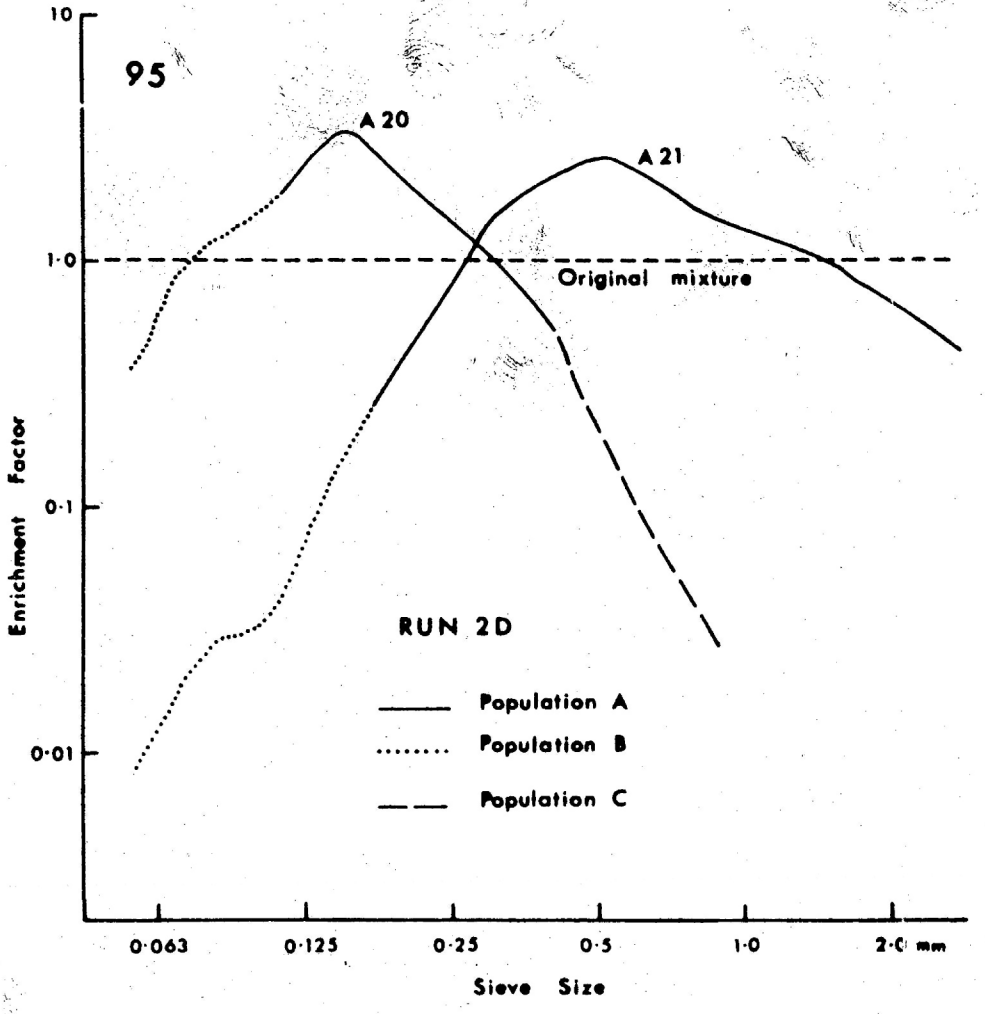

Fig. 95. Enrichment factors for Run 2D.

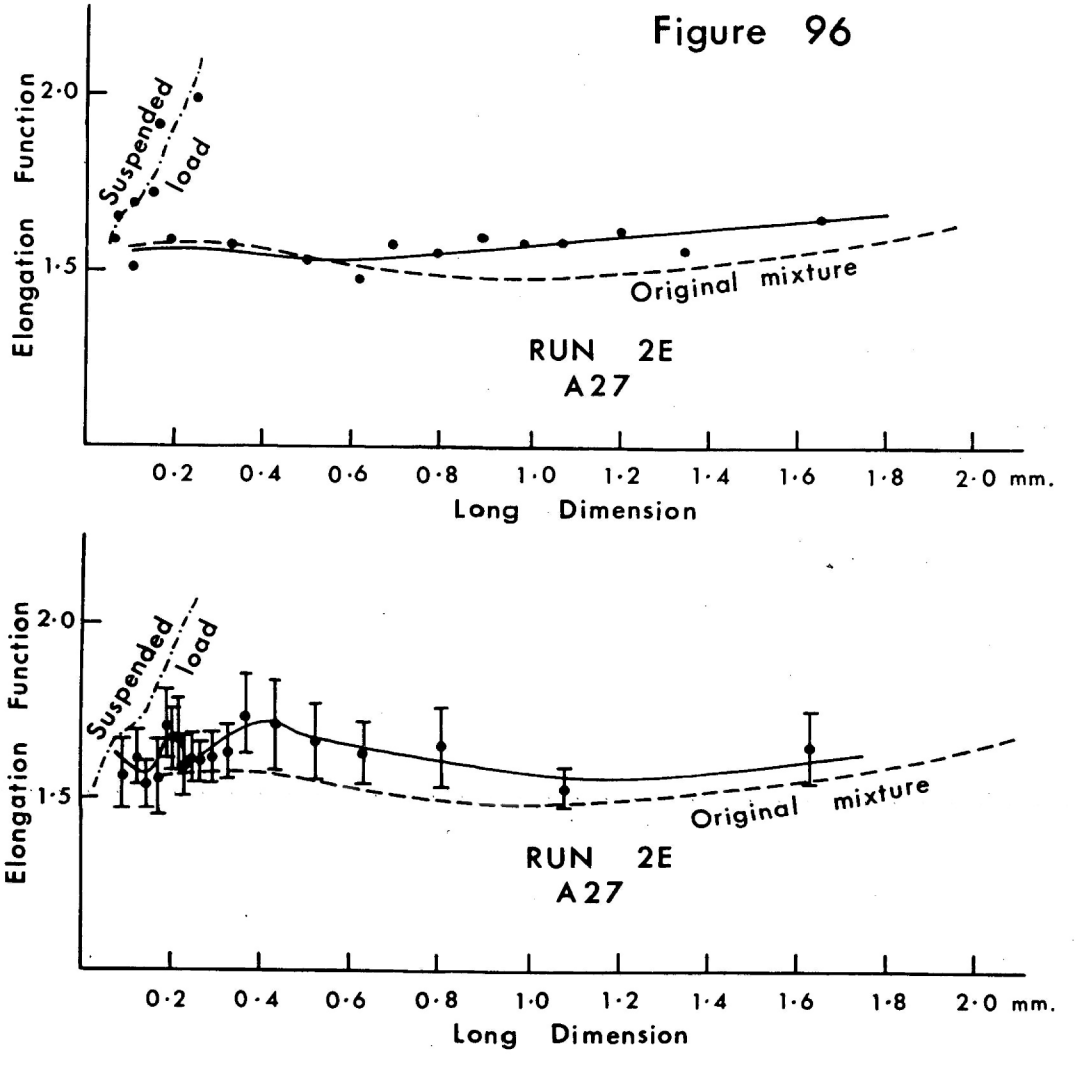

Fig. 96. Elongation function curves for Run 2E.

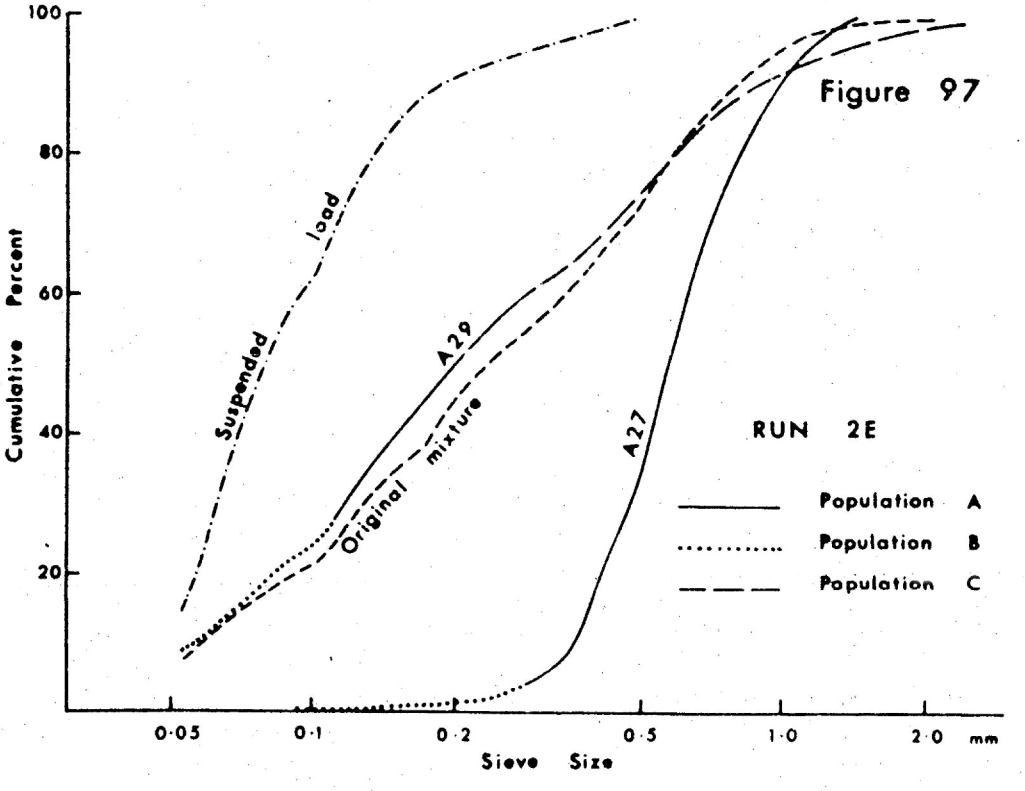

Fig. 97. Sieve cumulative curves for Run 2E.

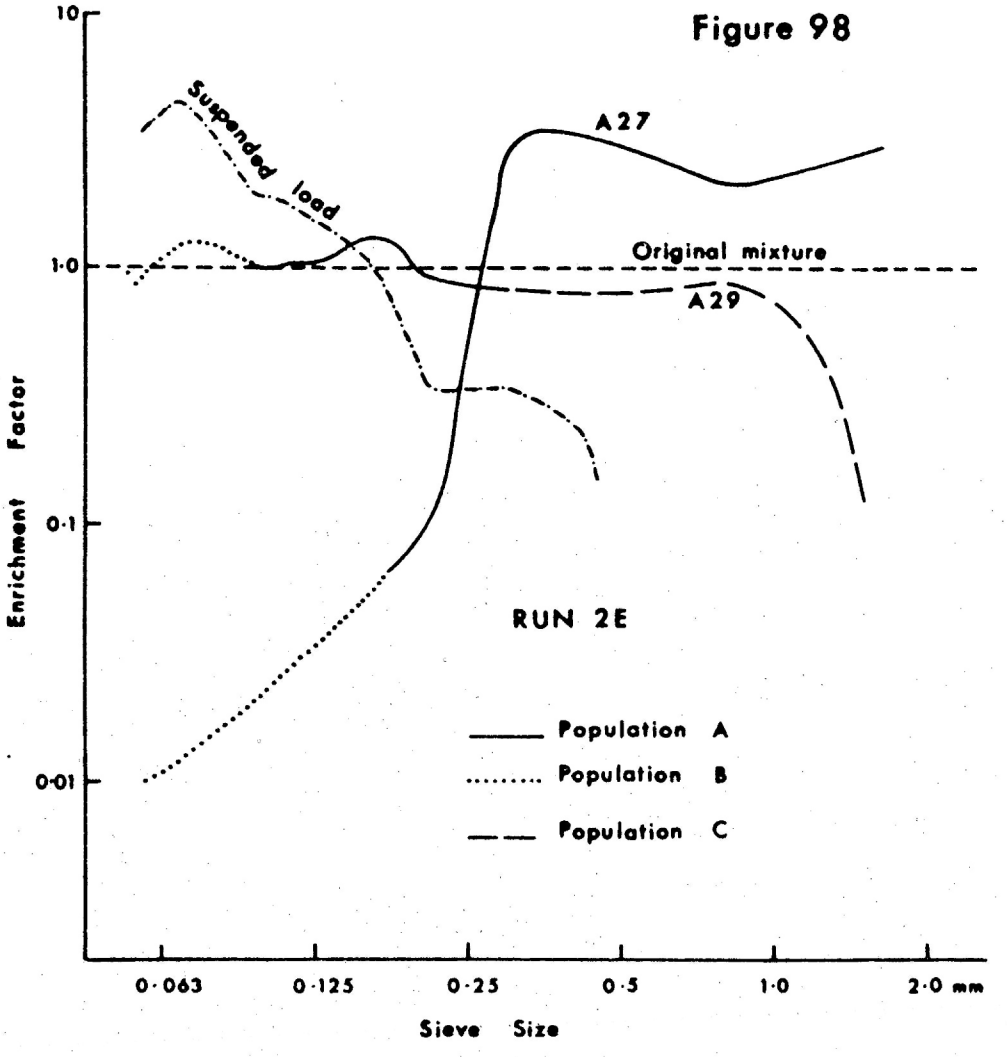

Fig. 98. Enrichment factors for Run 2E.

Figure 99

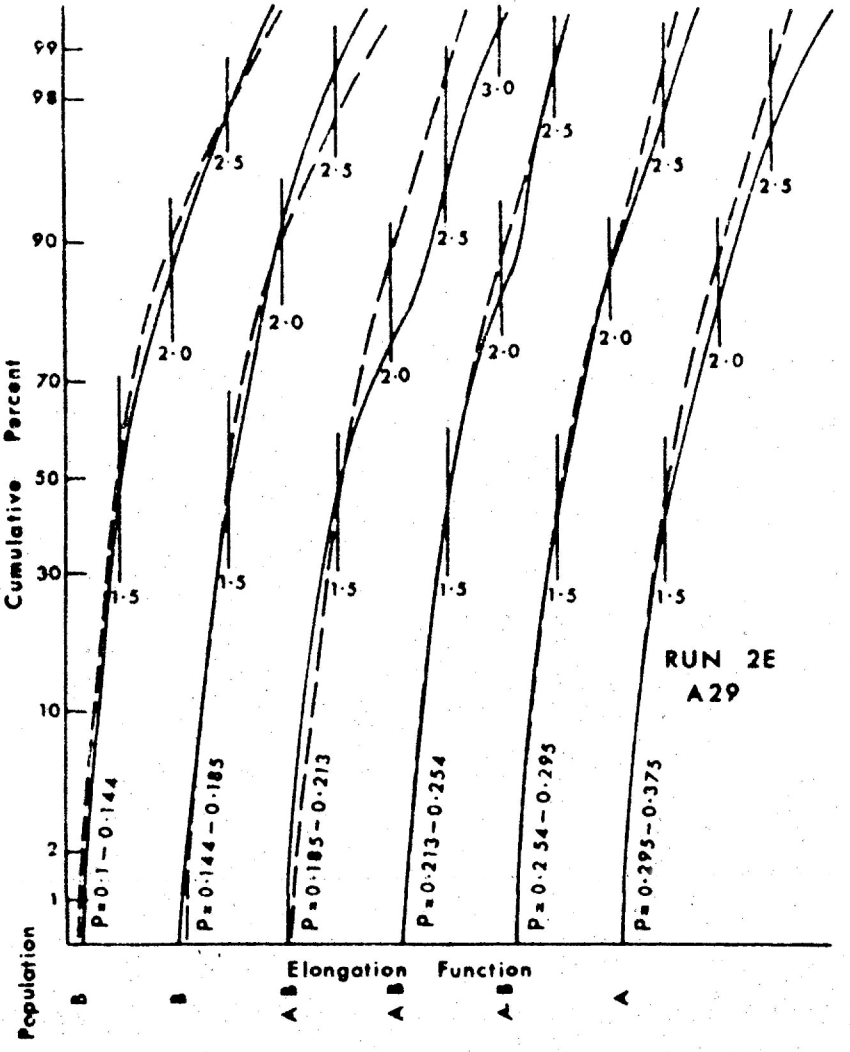

Fig. 99. Serial elongation function distribution sections, with respect to the long dimension, for A.29 compared with those of parent mixture. Long dimension range given for each curve.

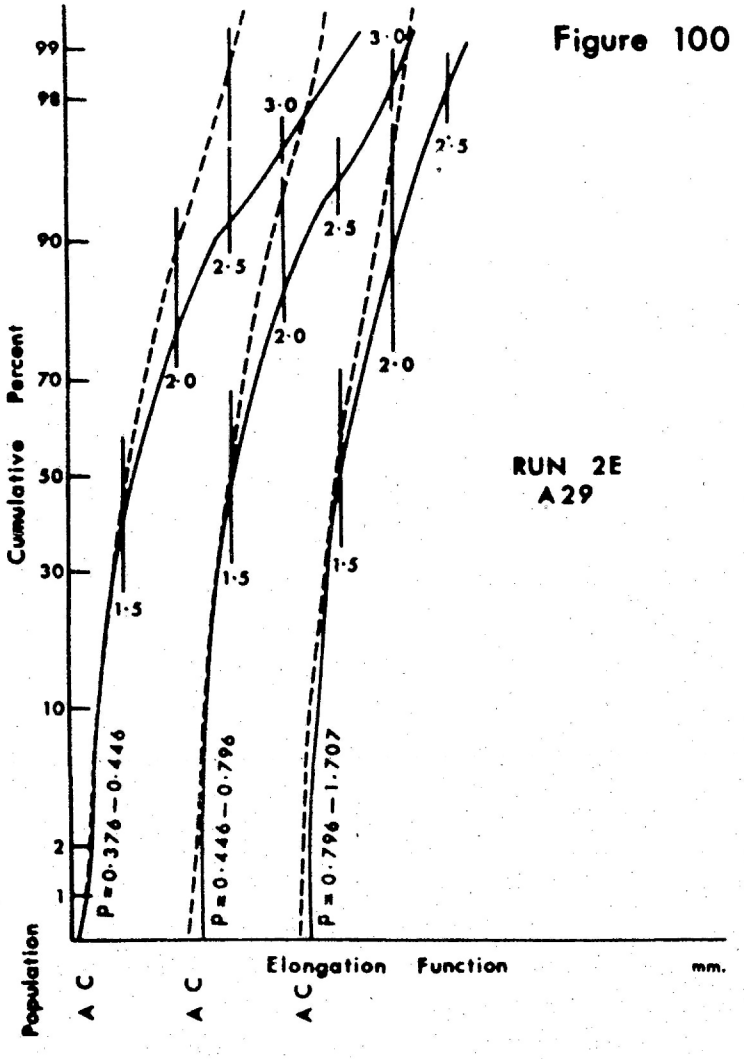

Fig. 100. As Fig. 99.

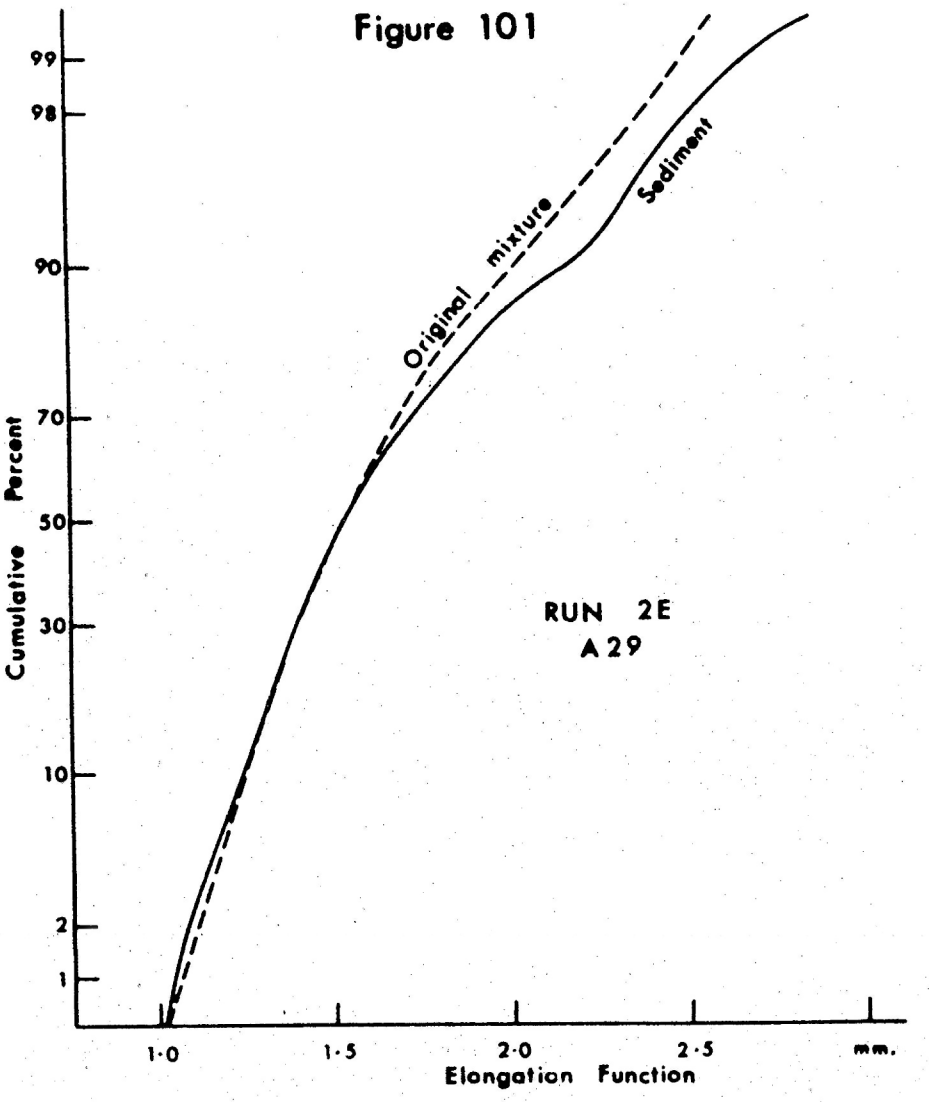

Fig. 101. Elongation function distribution, based on 360 grains, through feature 2 of A29 compared with distribution for parent mixture.

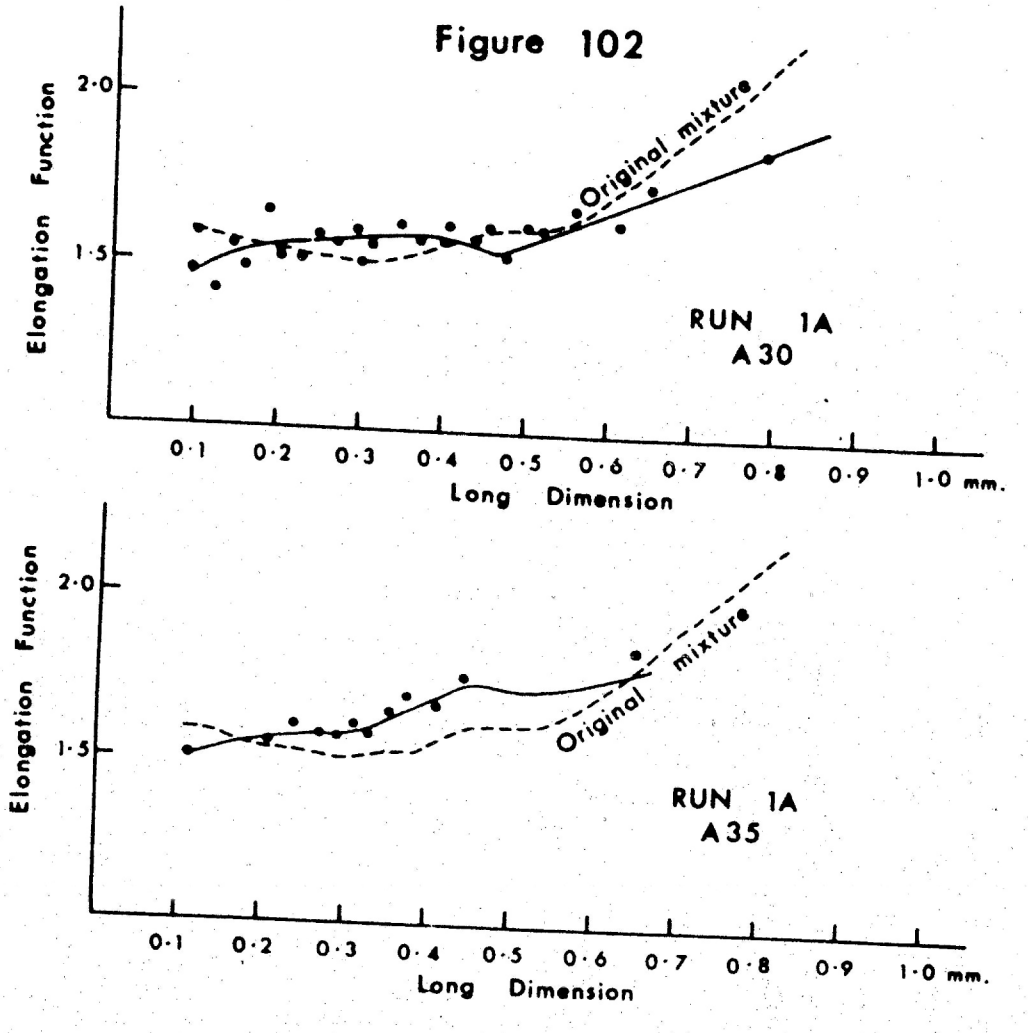

Fig. 102. Elongation function curves for Run 1A.

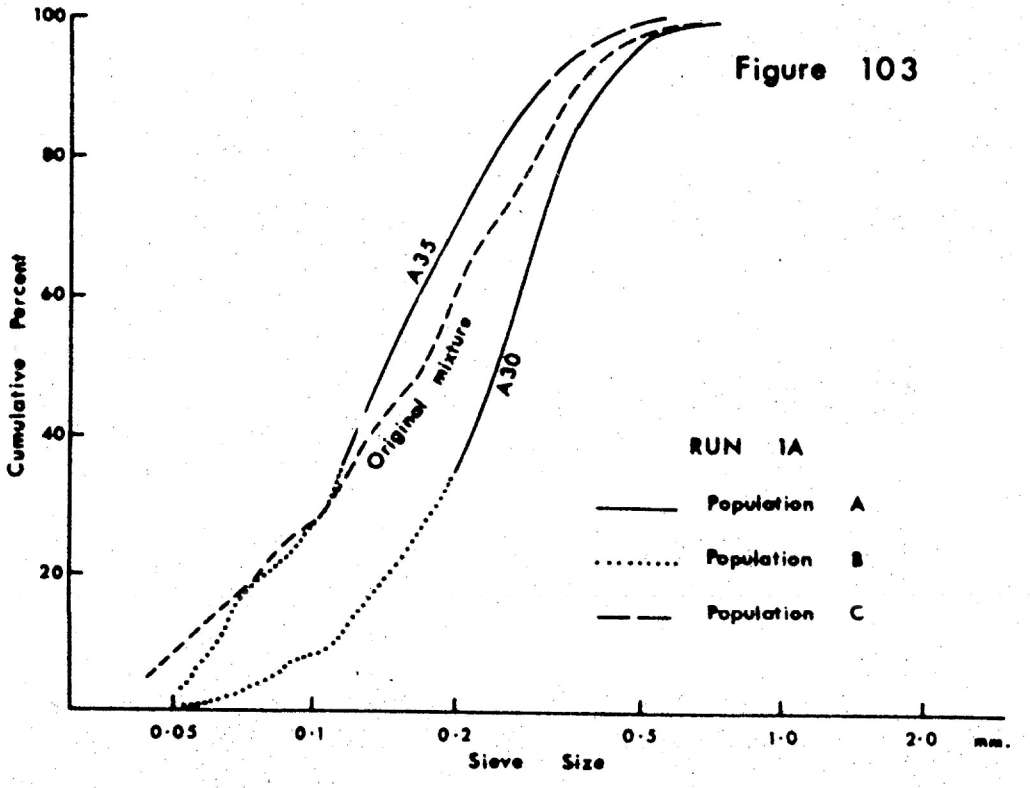

Fig. 103. Sieve cumulative curves for Run 1A.

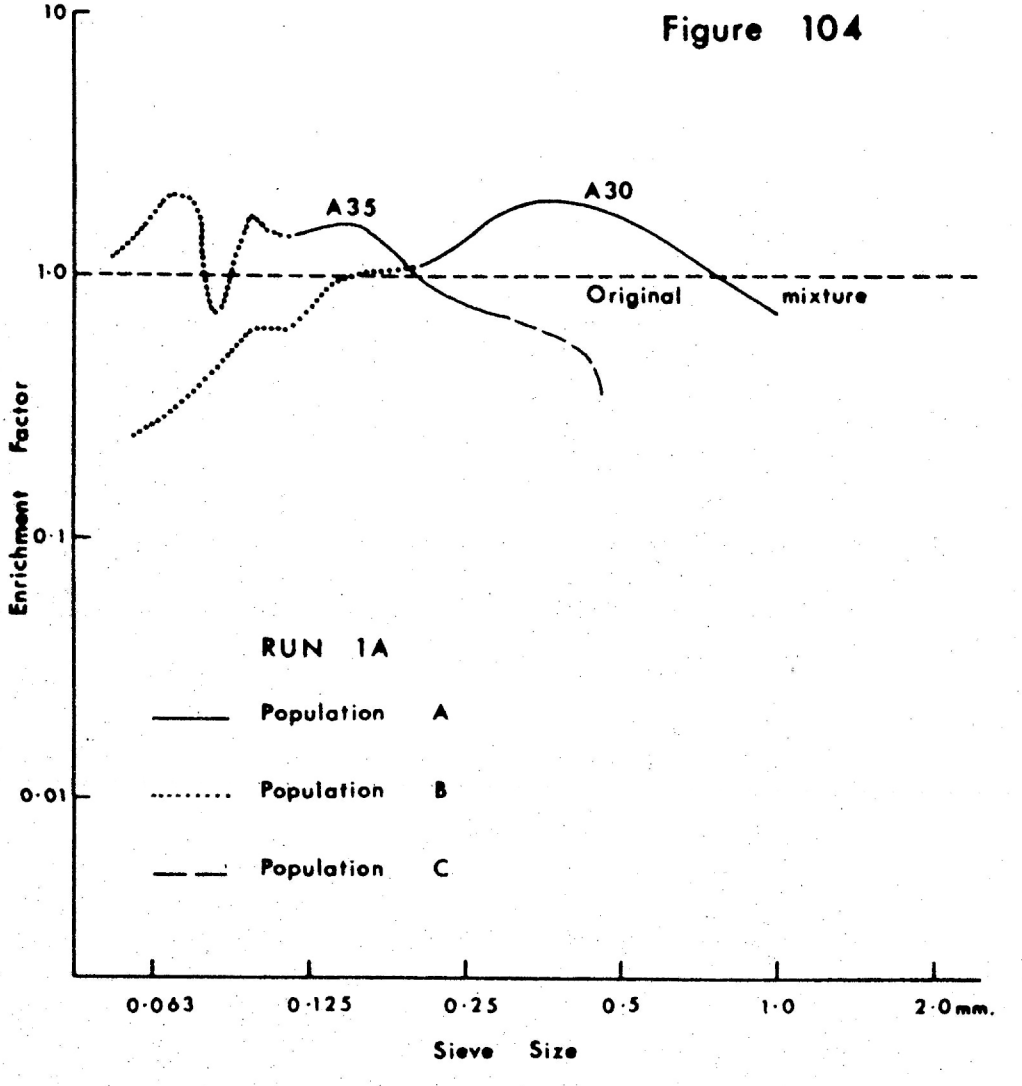

Fig. 104. Enrichment factors for Run 1A.

Fig. 105. Rippled bed after Run 1B, looking upstream.

Figure 106

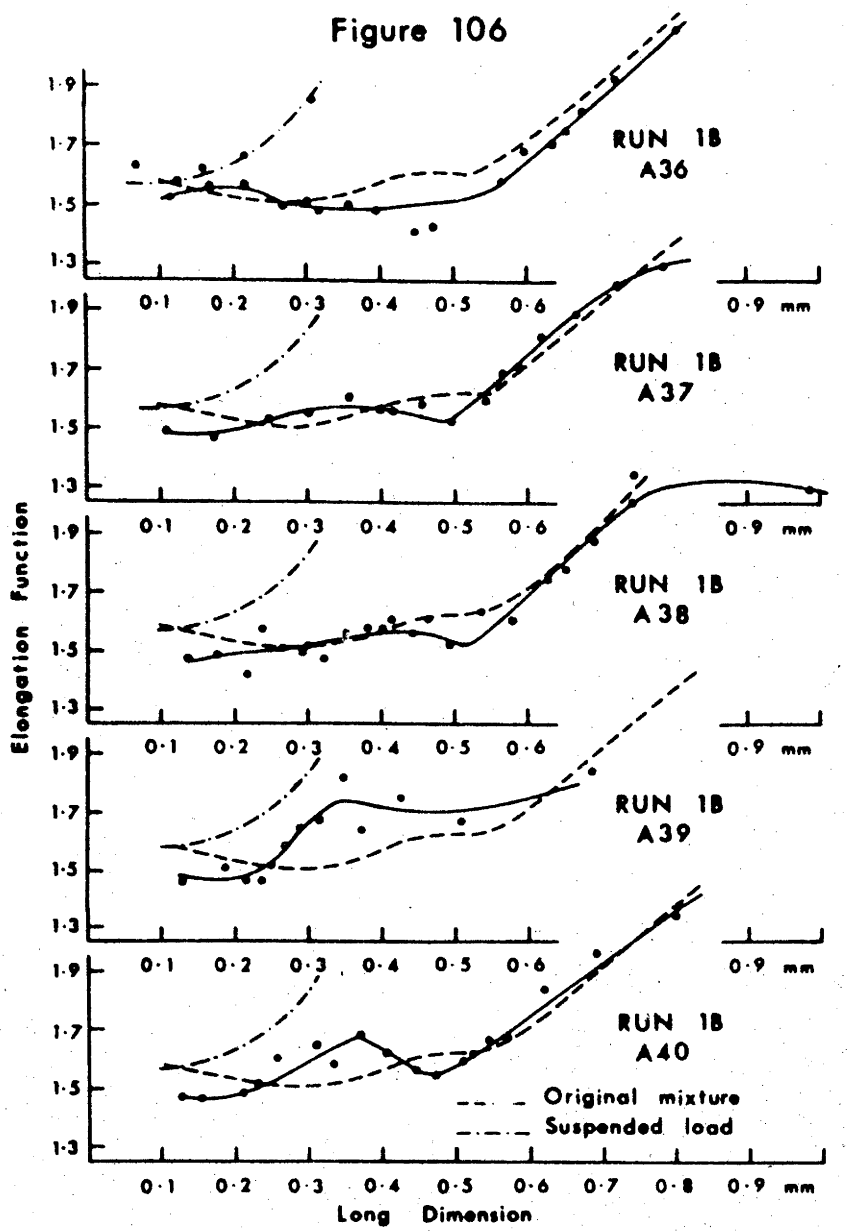

Fig. 106. Elongation function curves for Run 1B.

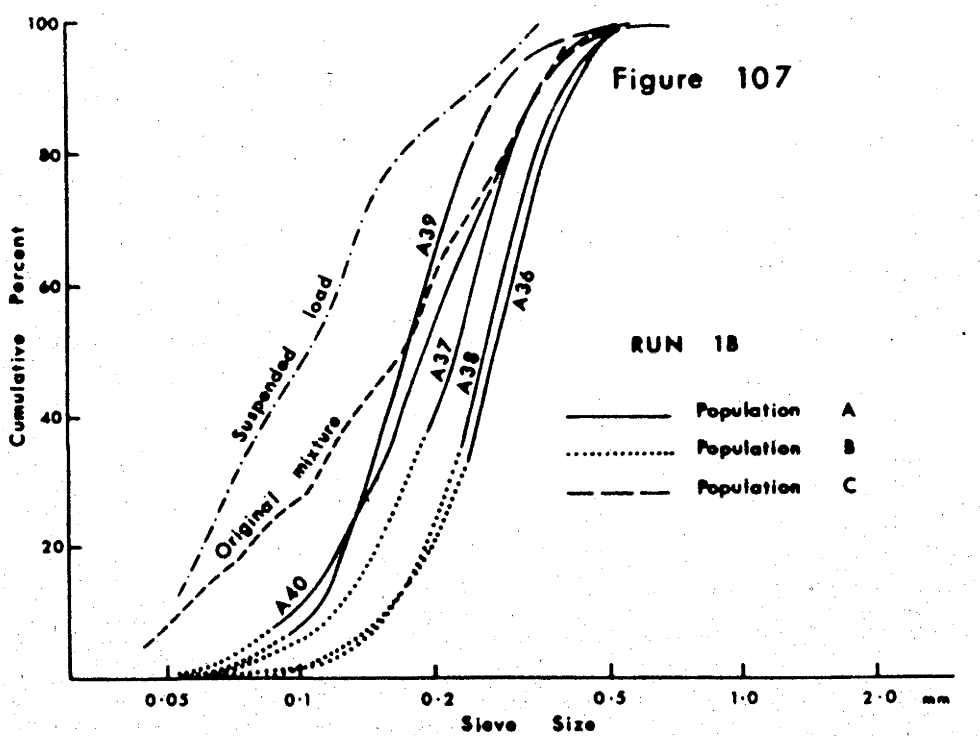

Fig. 107. Sieve cumulative curves for Run 1B.

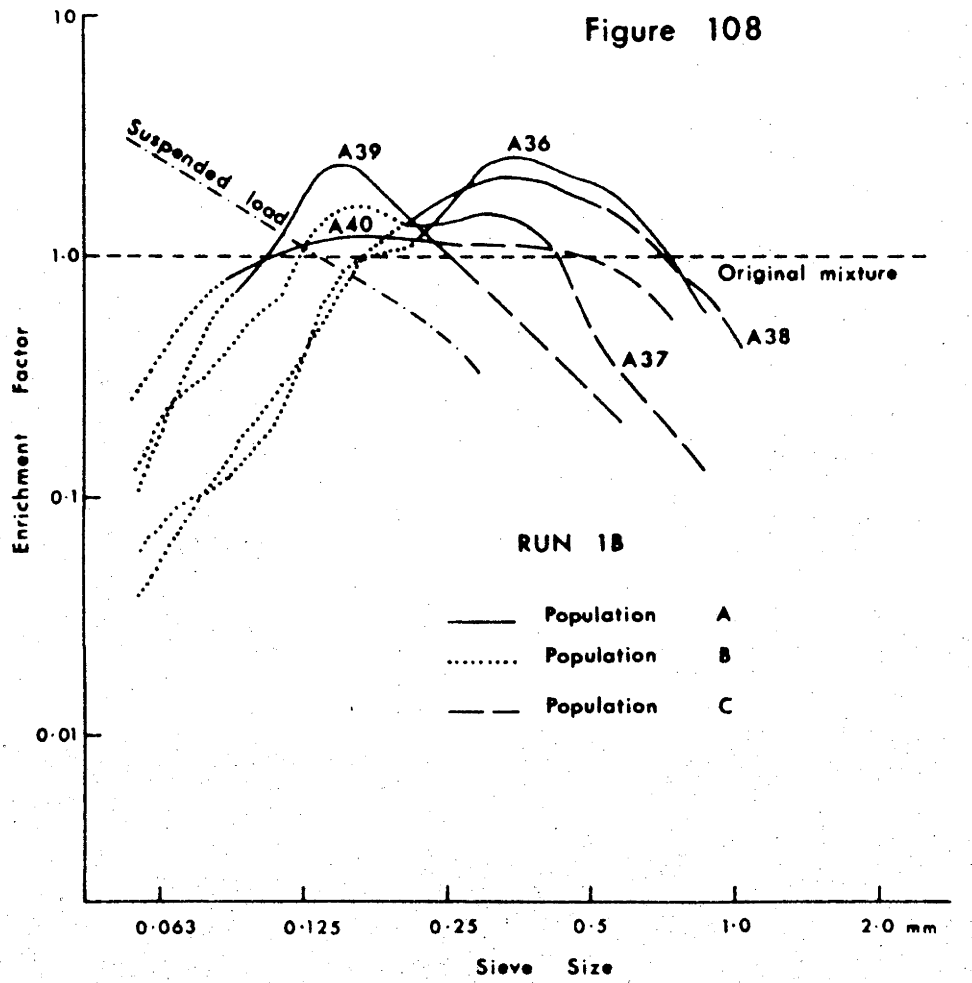

Fig. 108. Enrichment factors for Run 1B.

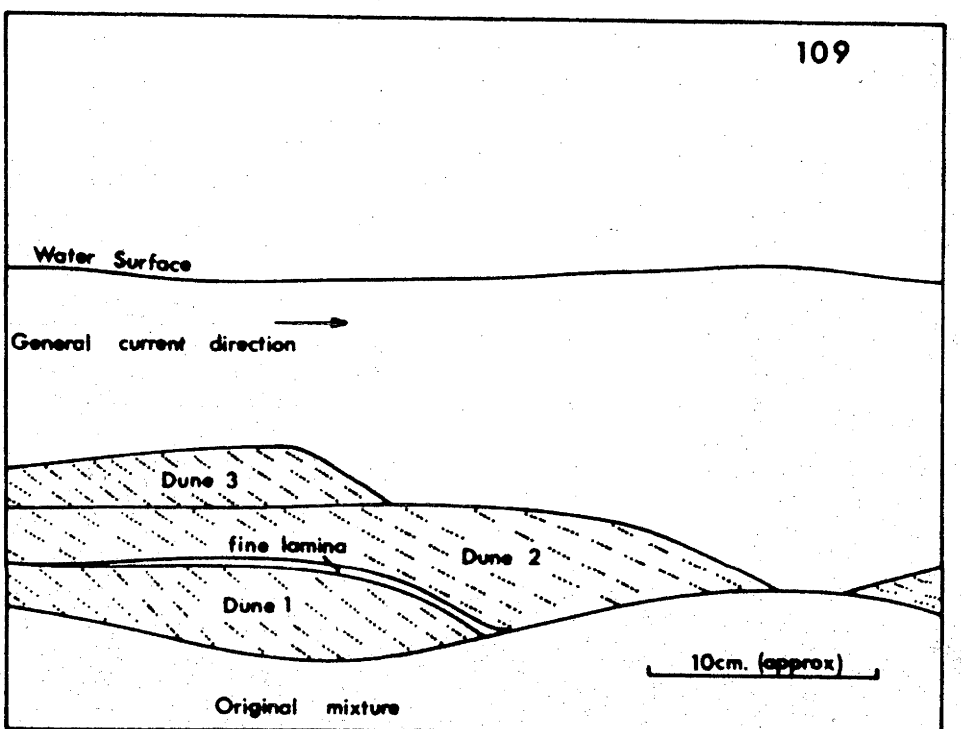

Fig. 109. Mechanism of dune capture as seen in Run 1C. Dune 1 was captured by Dune 2 which will, in turn, be captured by Dune 3.

Figure 110

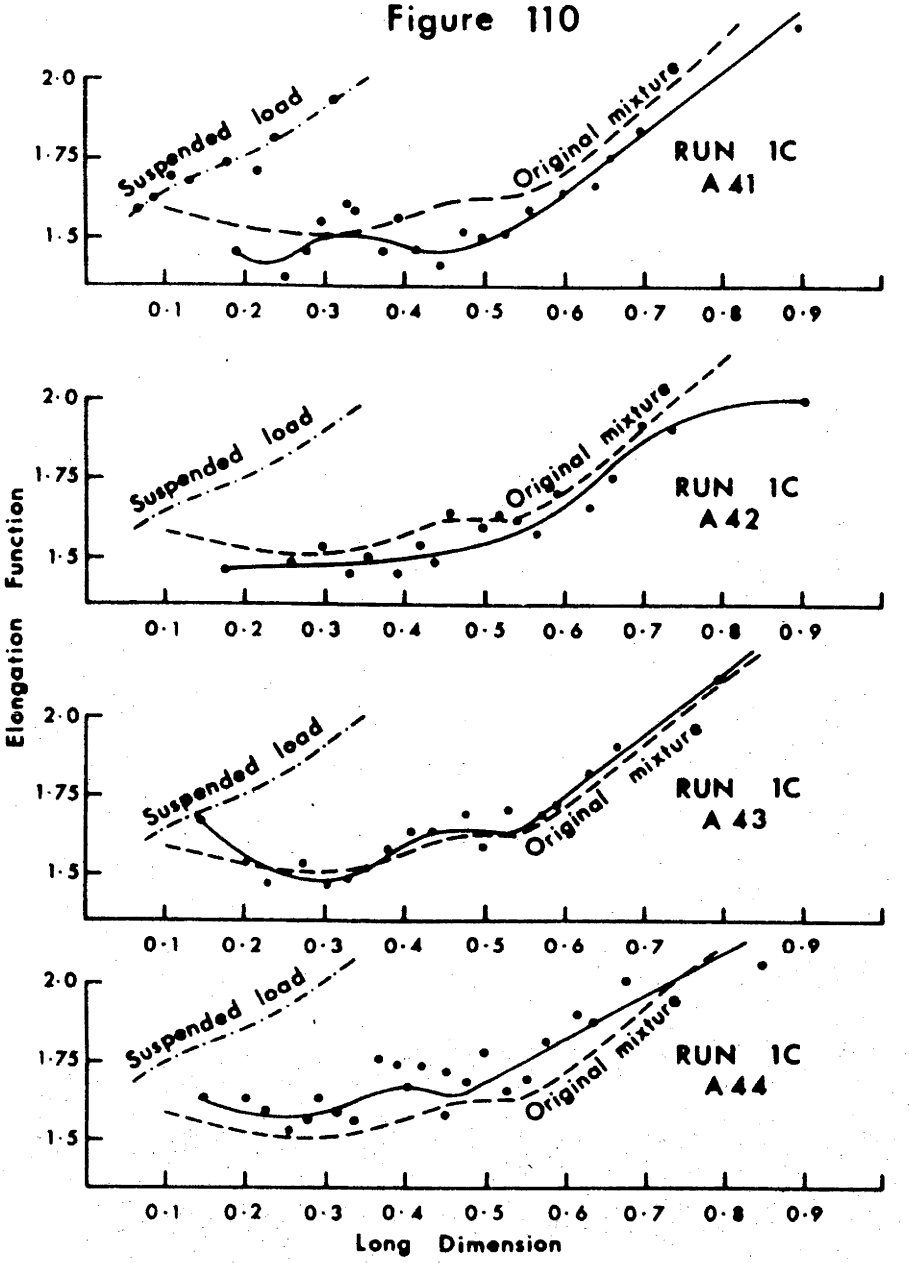

Fig. 110. Elongation function curves for Run 1C.

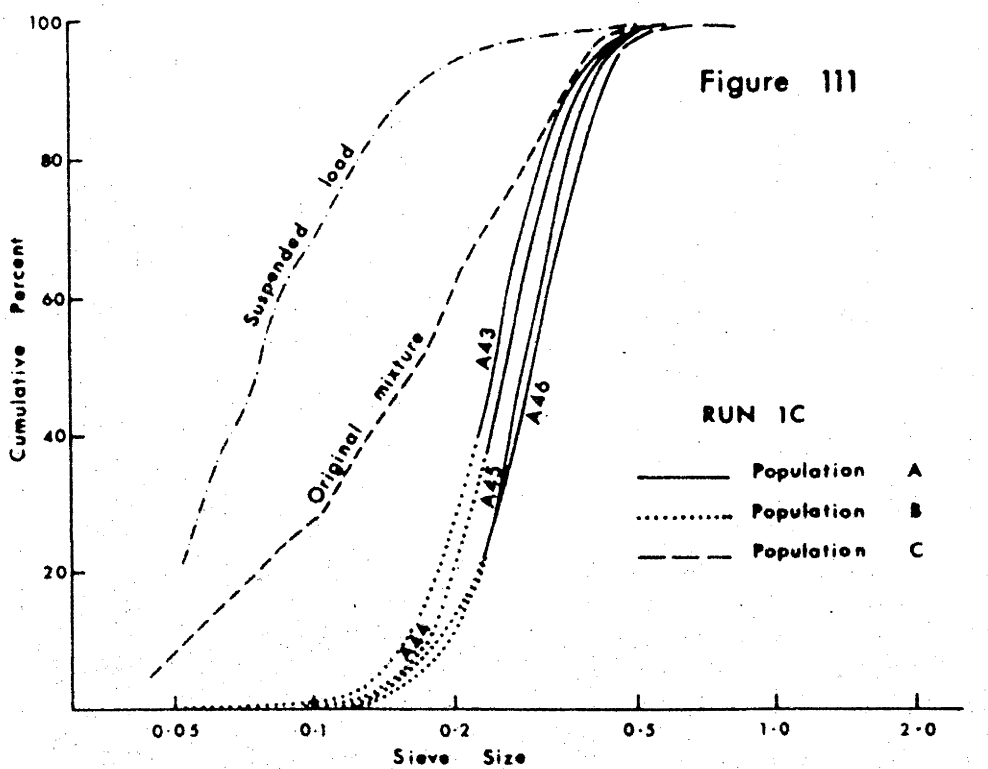

Fig. 111. Sieve cumulative curves for Run 1C.

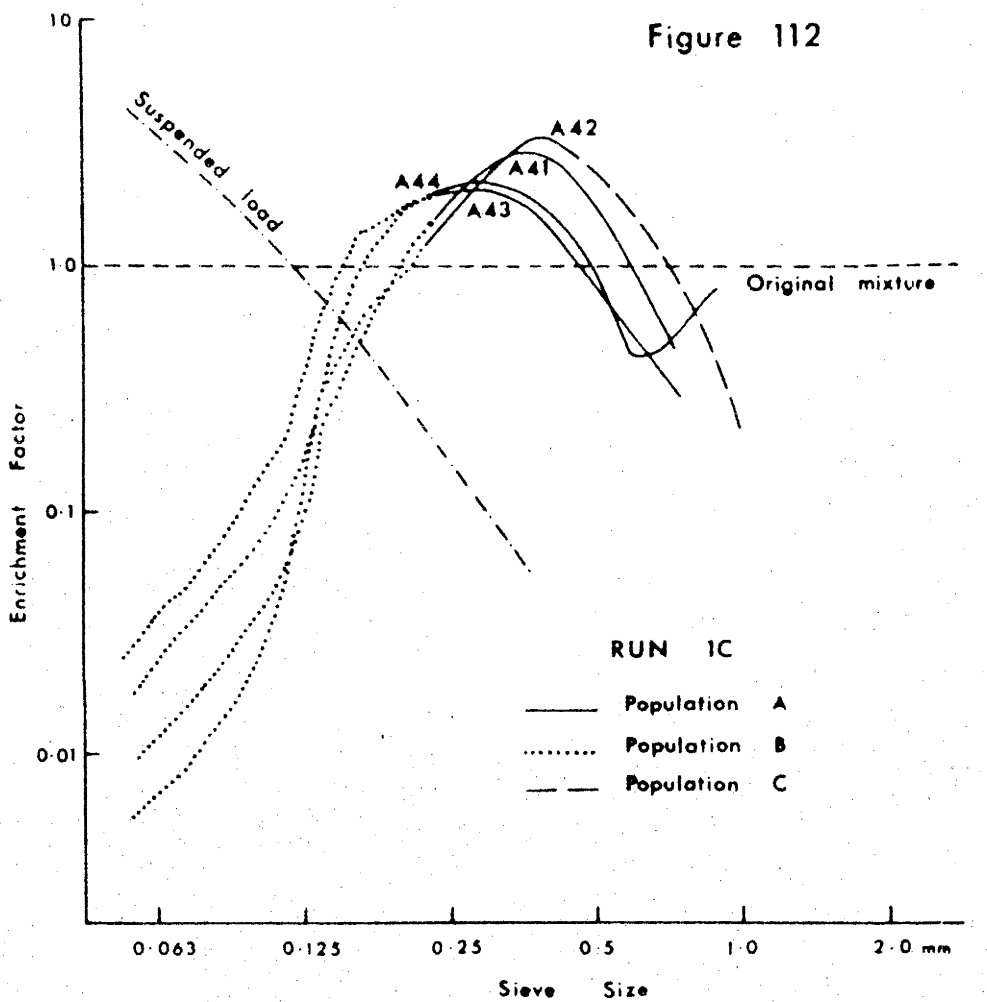

Fig. 112. Enrichment factors for Run 1C.

Figure 113

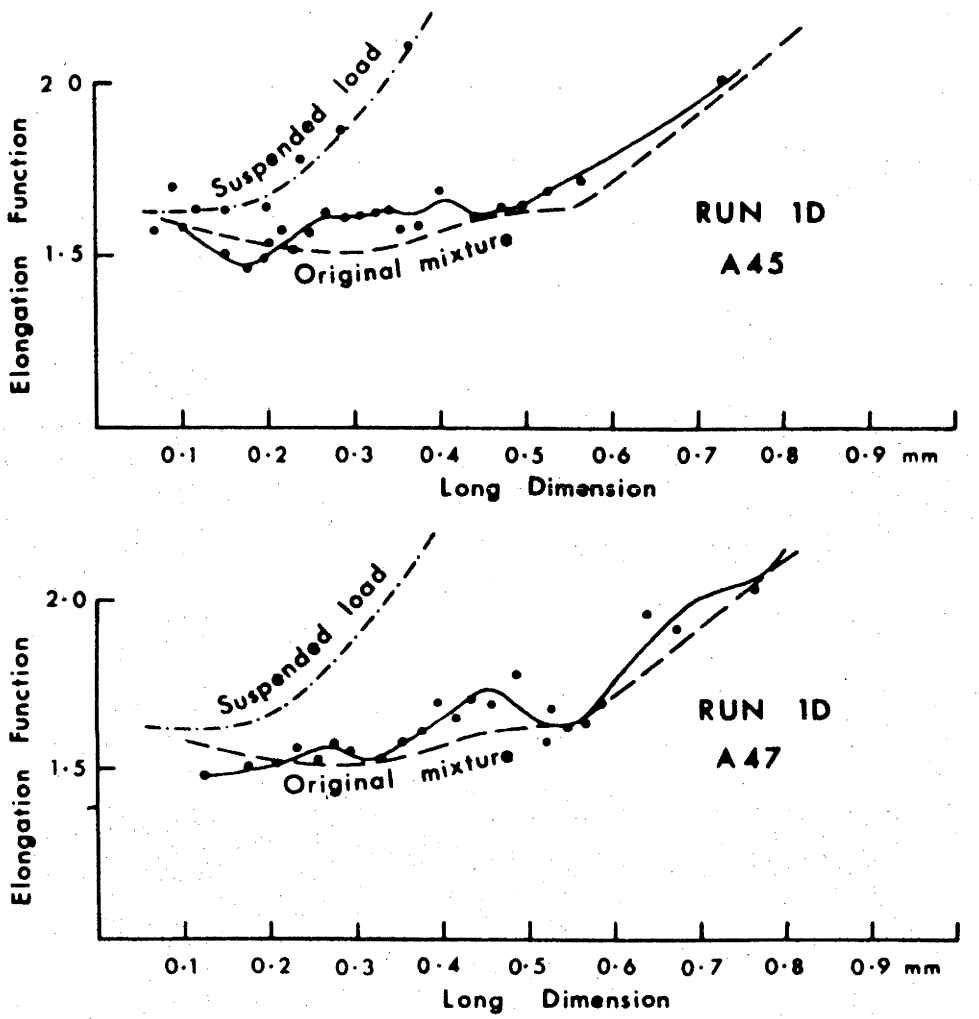

Fig. 113. Elongation function curves for Run 1D

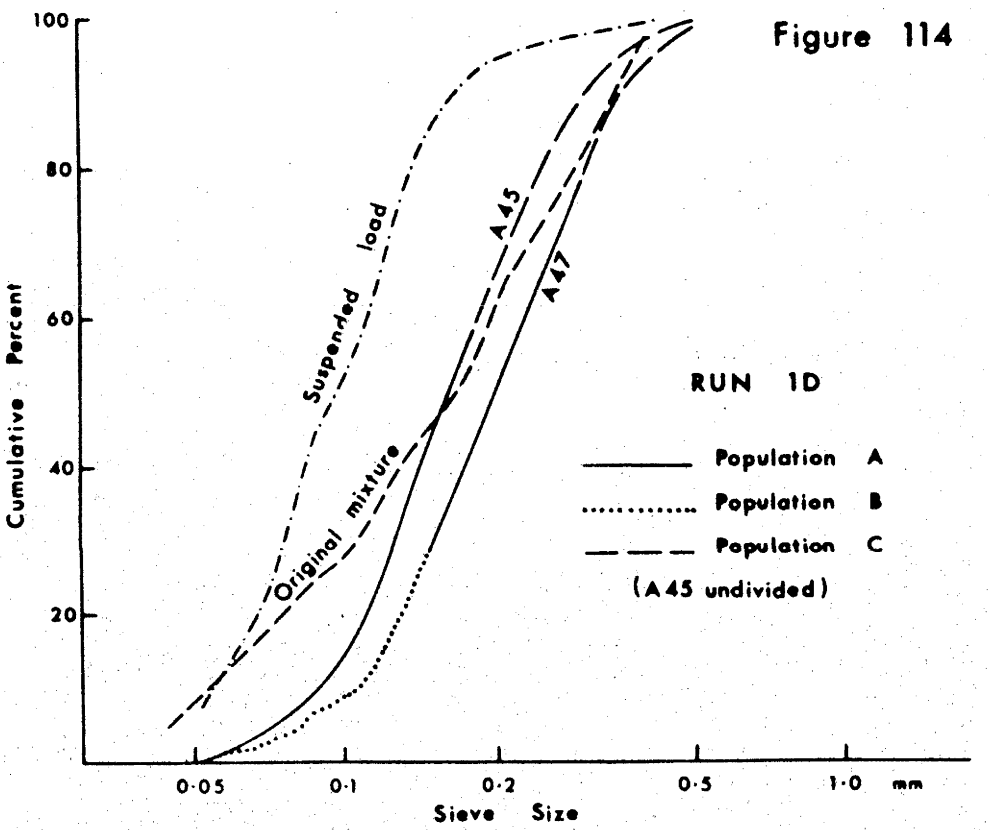

Fig. 114. Sieve cumulative curves for Run 1D.

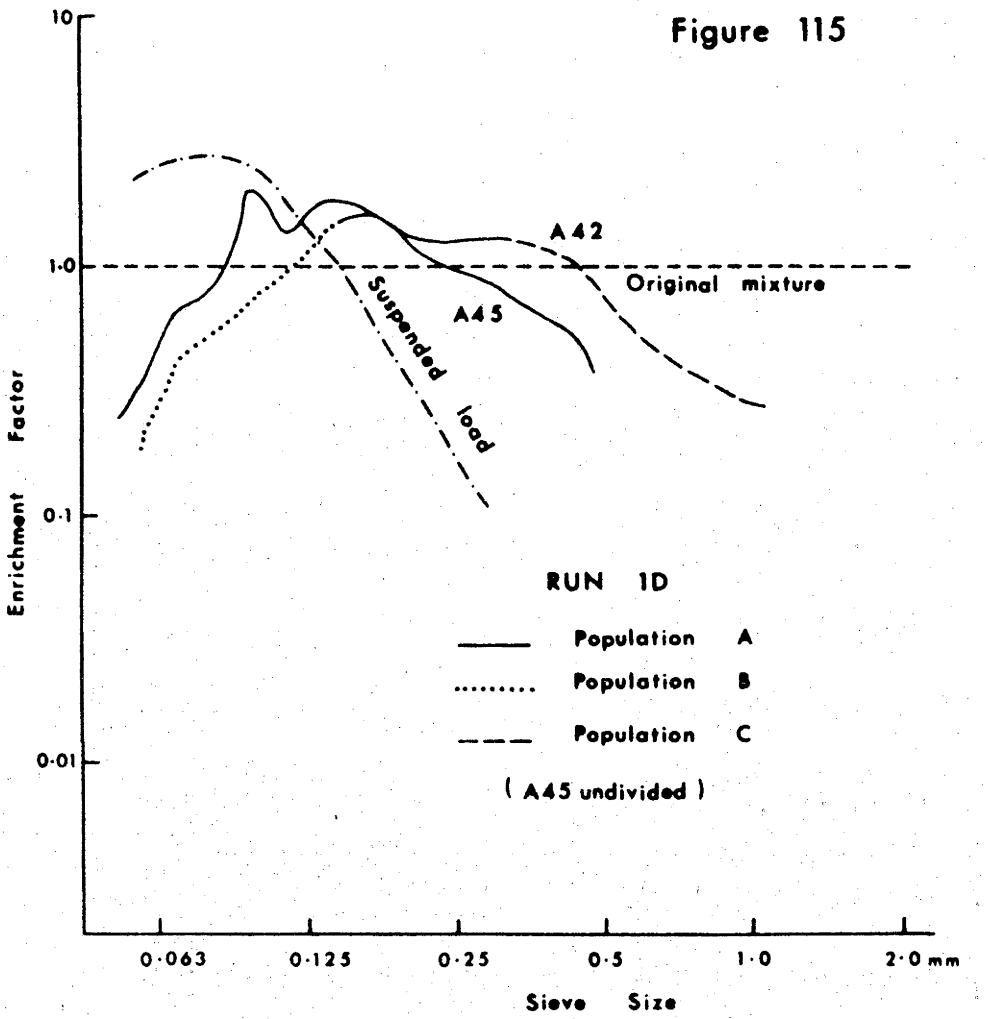

Fig. 115. Enrichment factors for Run 1D.

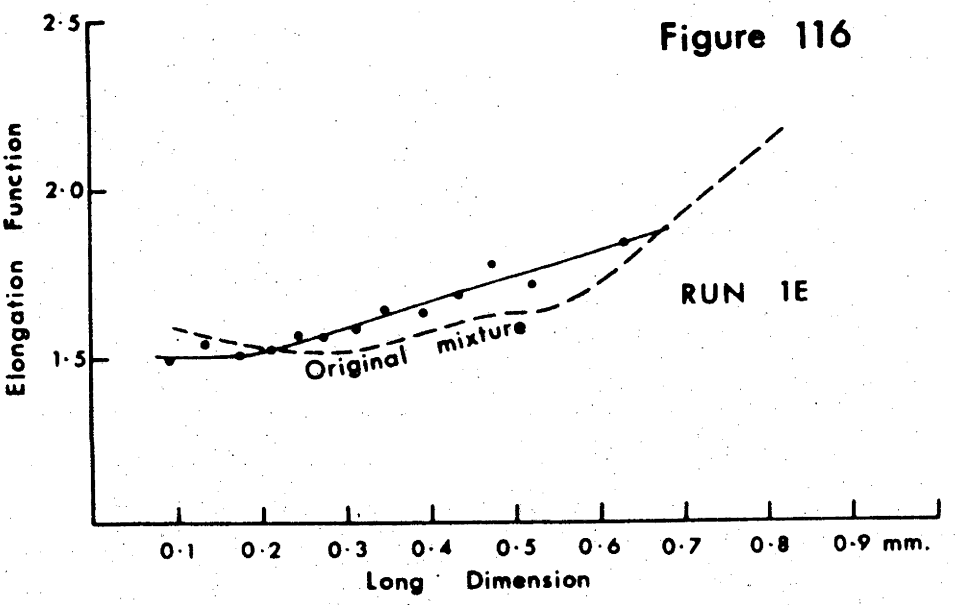

Fig. 116. Elongation function curves for Run 1E.

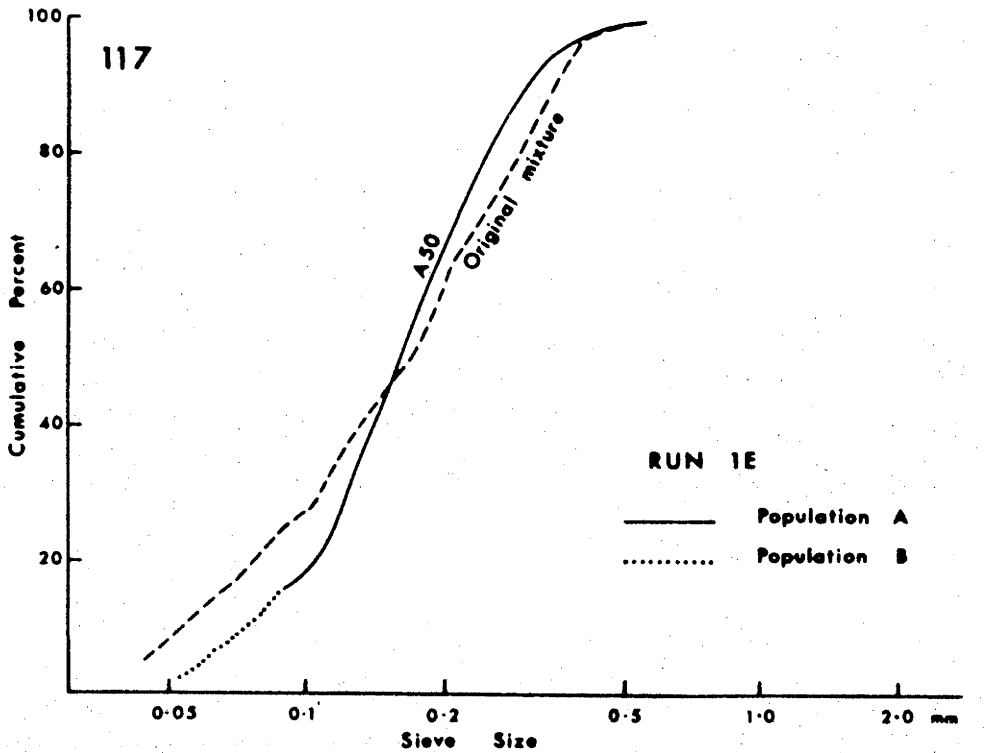

Fig. 117. Sieve cumulative curves for Run 1E.

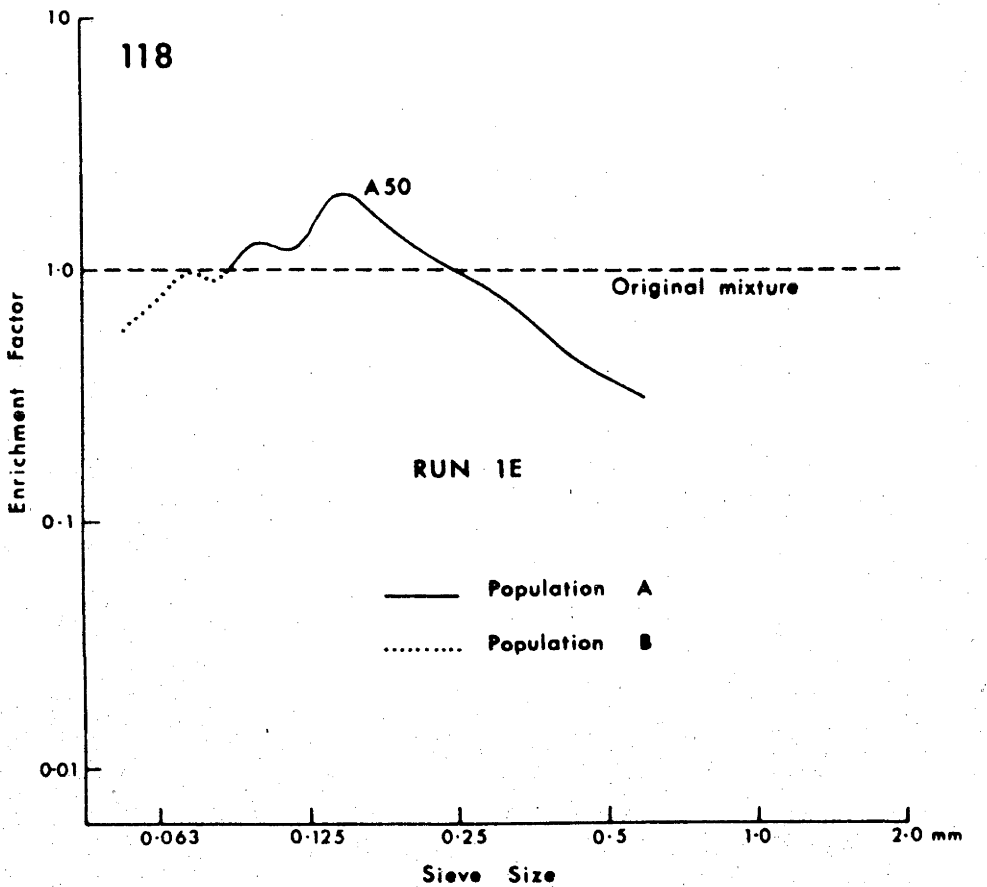

Fig. 118. Enrichment factors for Run 1E.

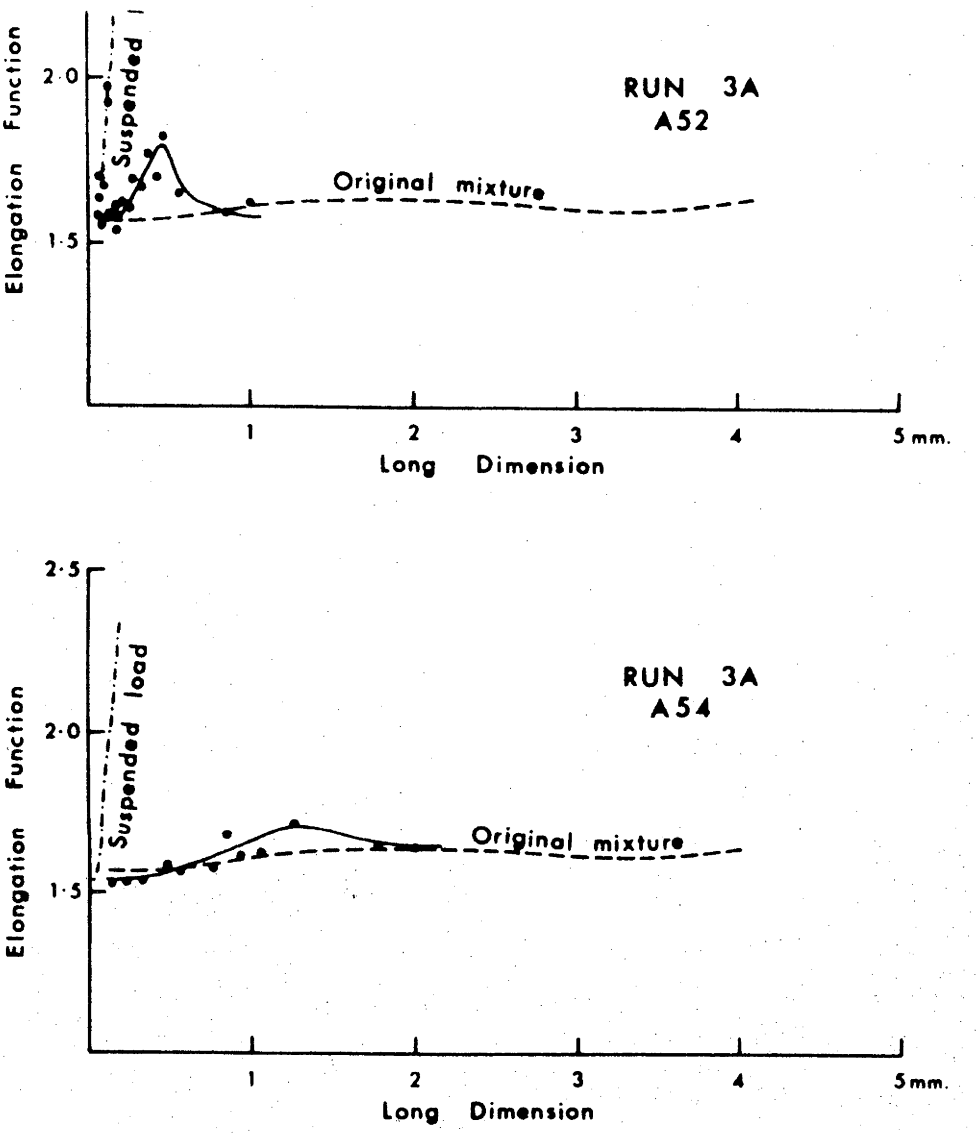

Fig. 119. Elongation function curves for Run 3A.

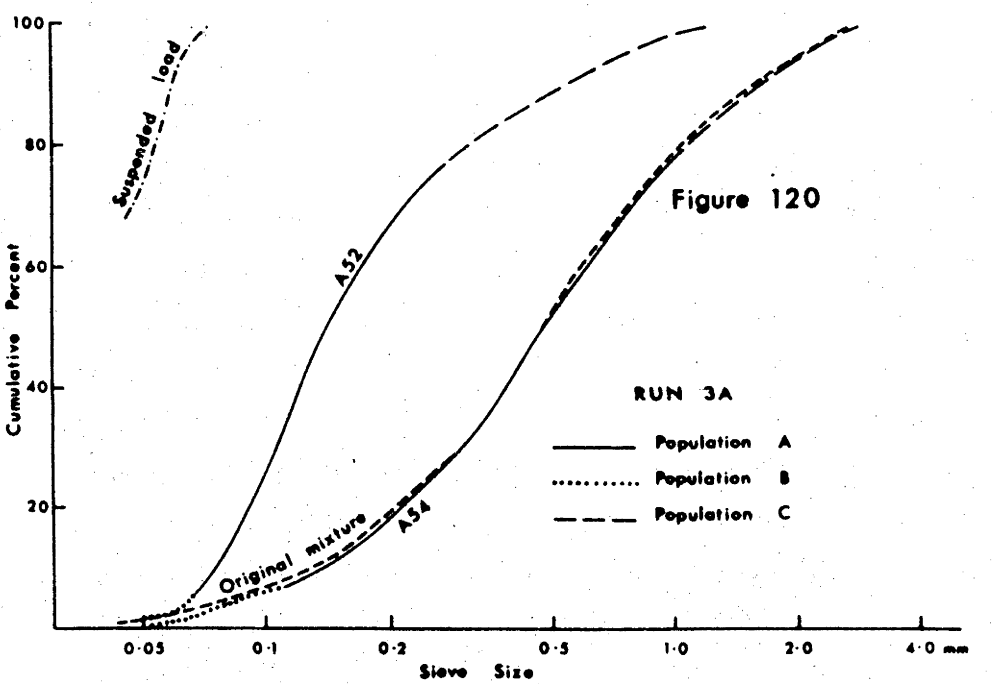

Fig. 120. Sieve cumulative curves for Run 3A.

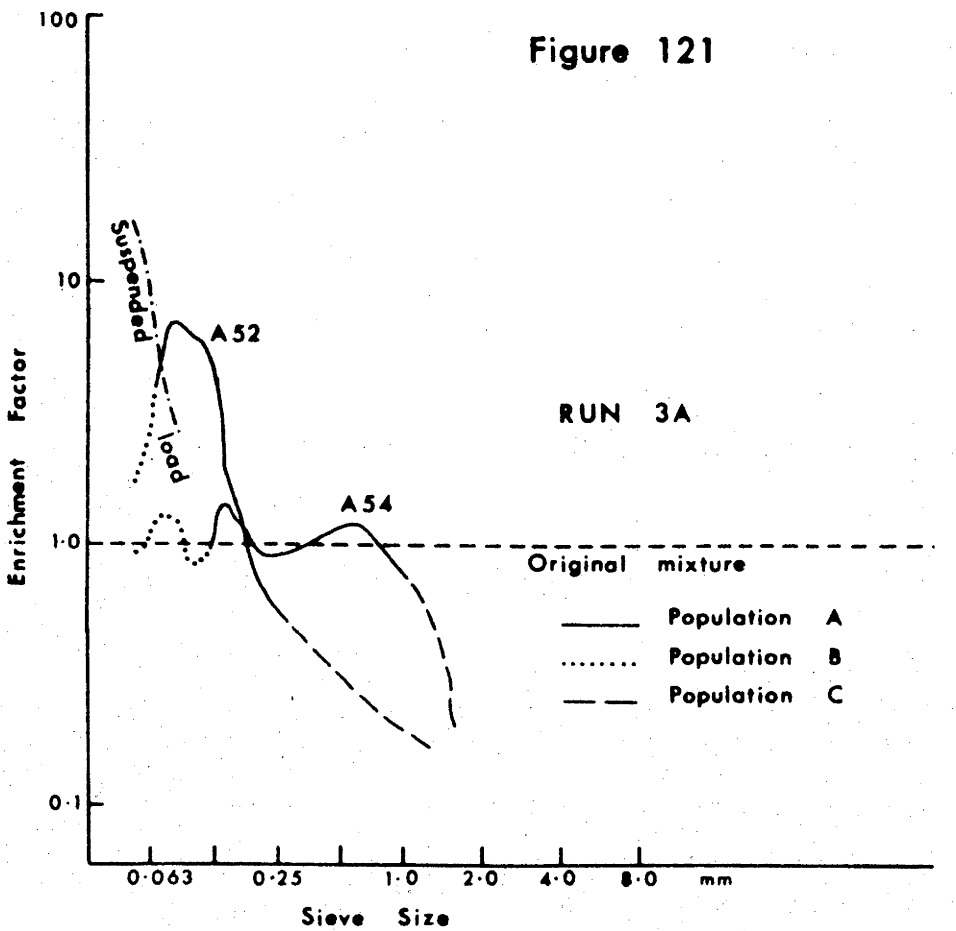

Fig. 121. Enrichment factors for Run 3A.

Fig. 122. Bed after Run 3B, looking upstream, ripples in foreground, dunes in background.

Fig. 123. Side view of dune in Run 3B. Apparently finer laminae result, in some cases, from large proportions of Population B in sediment formed immediately after feed addition. In other cases they represent a stage in dune capture.

Fig. 124. Junction of dunes and ripples in Run 3B.
Note grainsize difference.

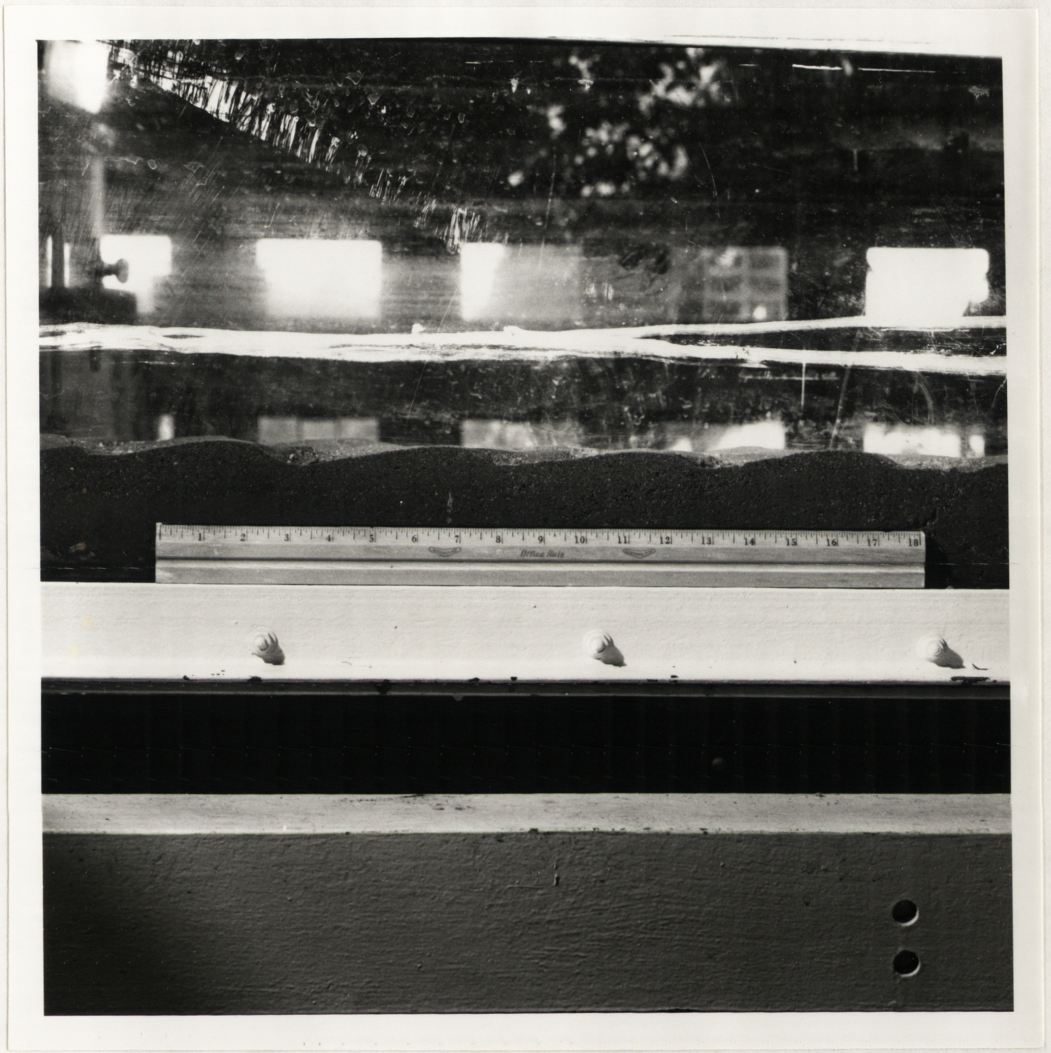

Fig. 125. Ripples in Run 3B.

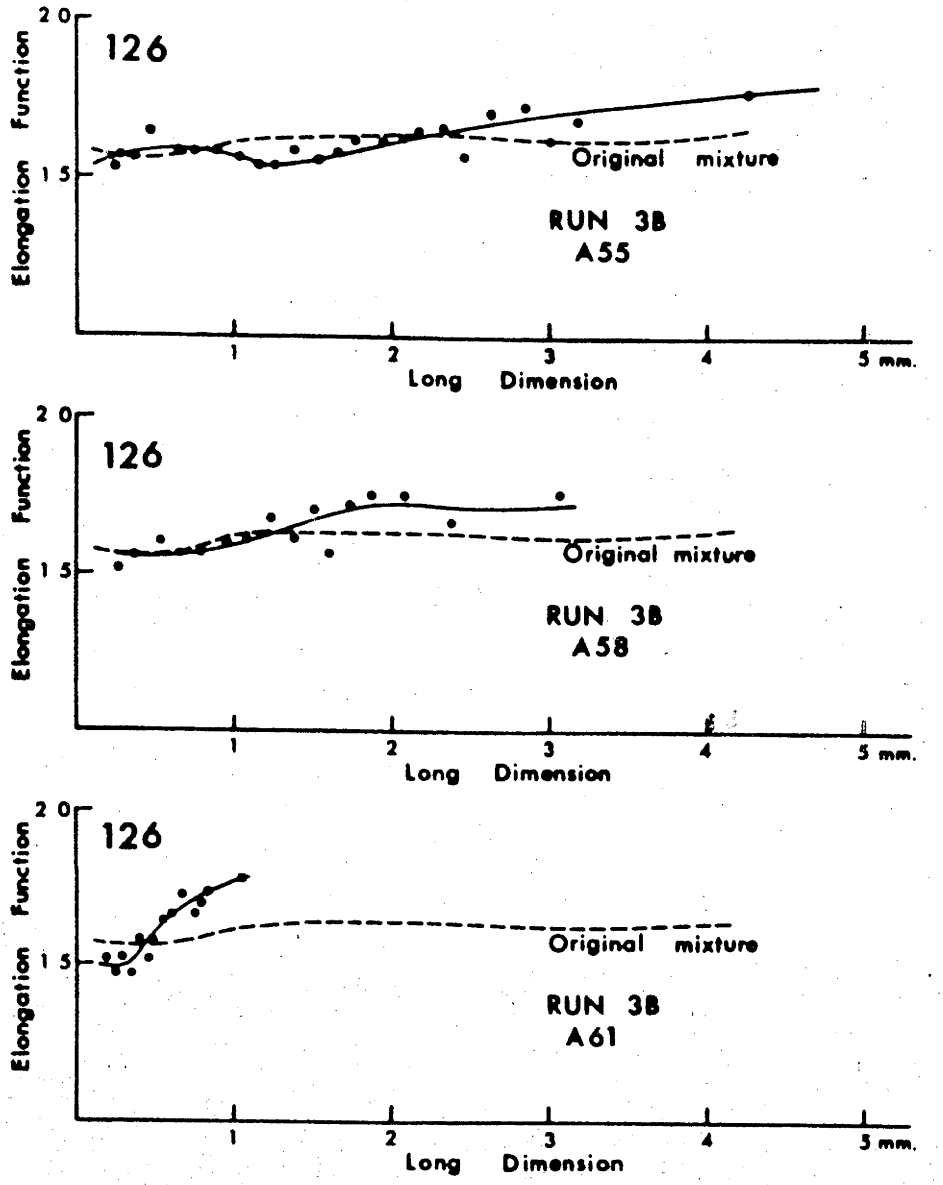

Fig. 126. Elongation function curves for Run 3B.

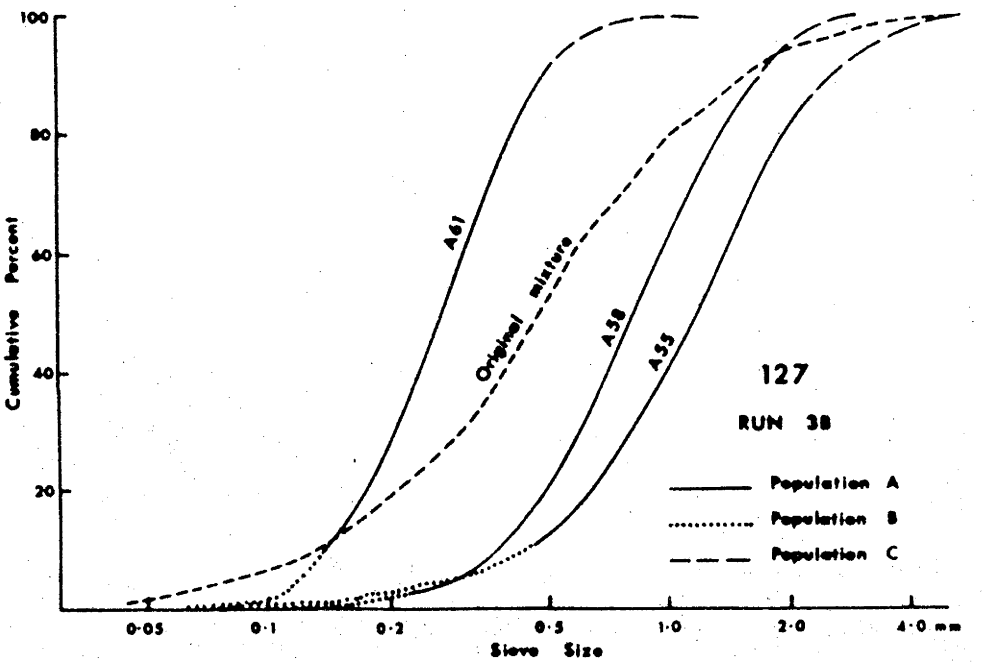

Fig. 127. Sieve cumulative curves for Run 38.

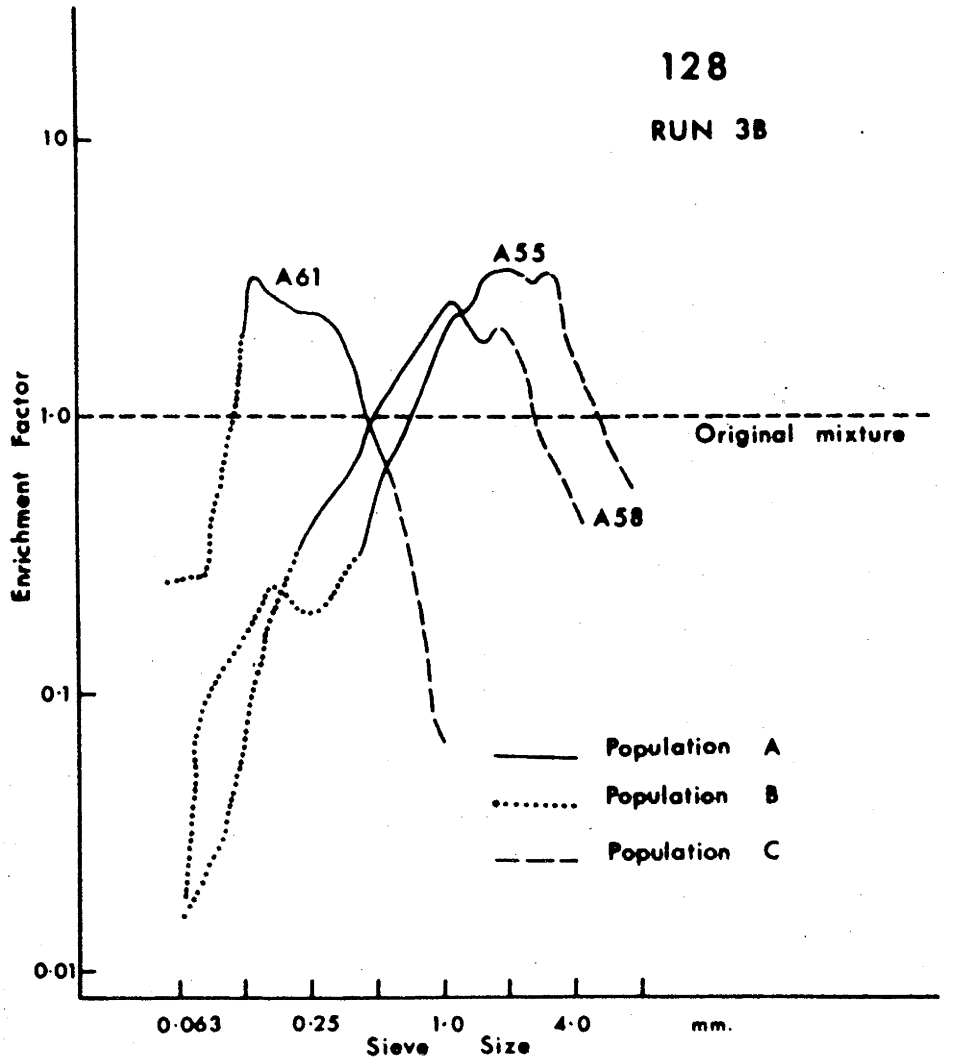

Fig. 128. Enrichment factors for Run 3B.

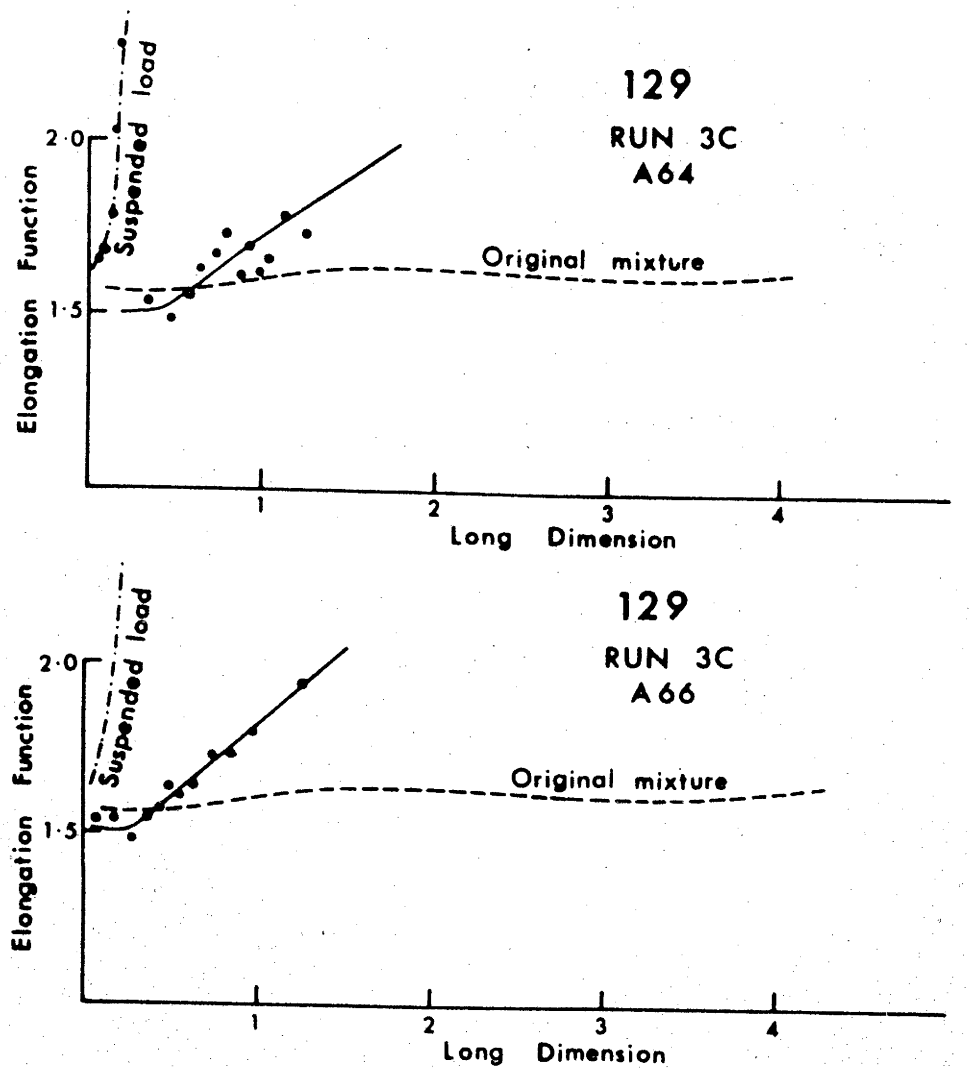

Fig. 129. Elongation function curves for Run 3C.

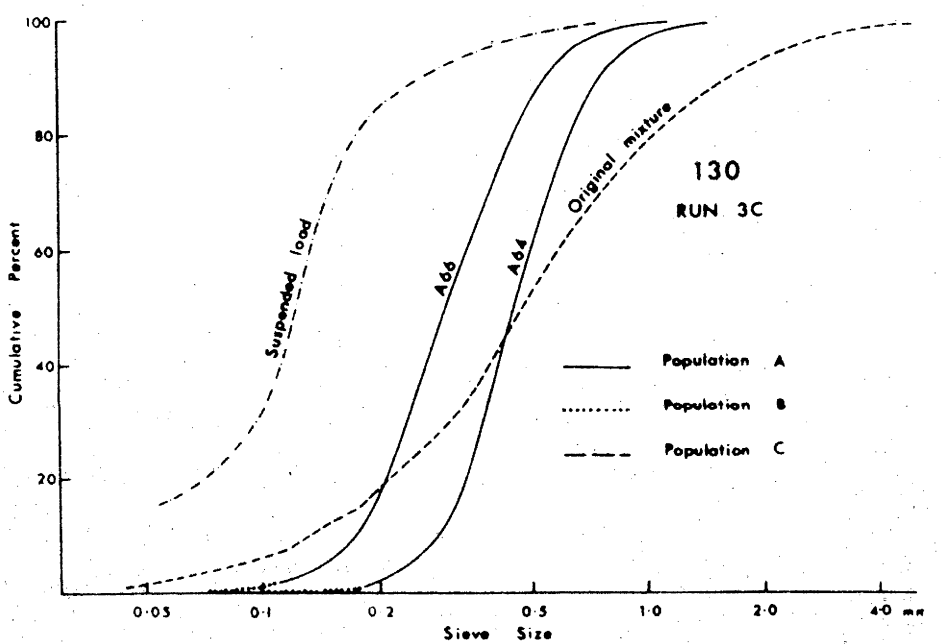

Fig. 130. Sieve cumulative curves for Run 3C.

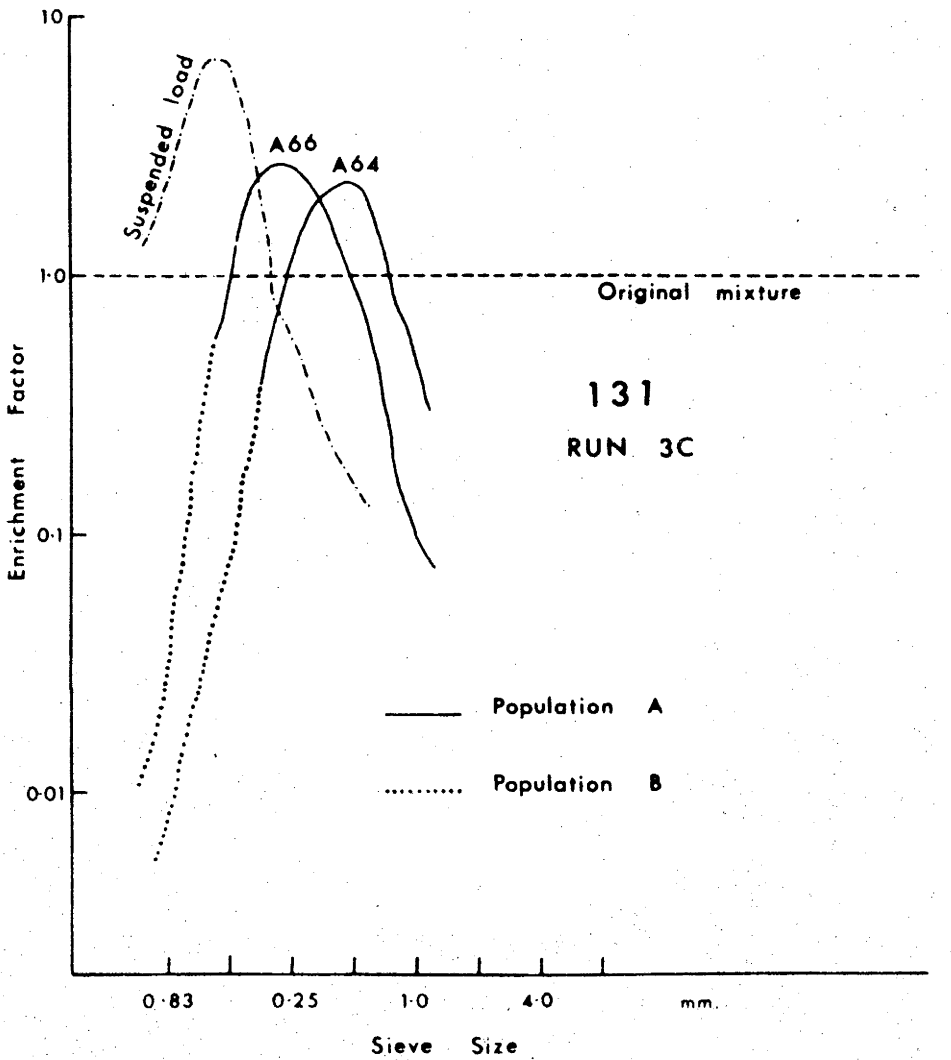

ig. 131. Enrichment factors for Run 3C.

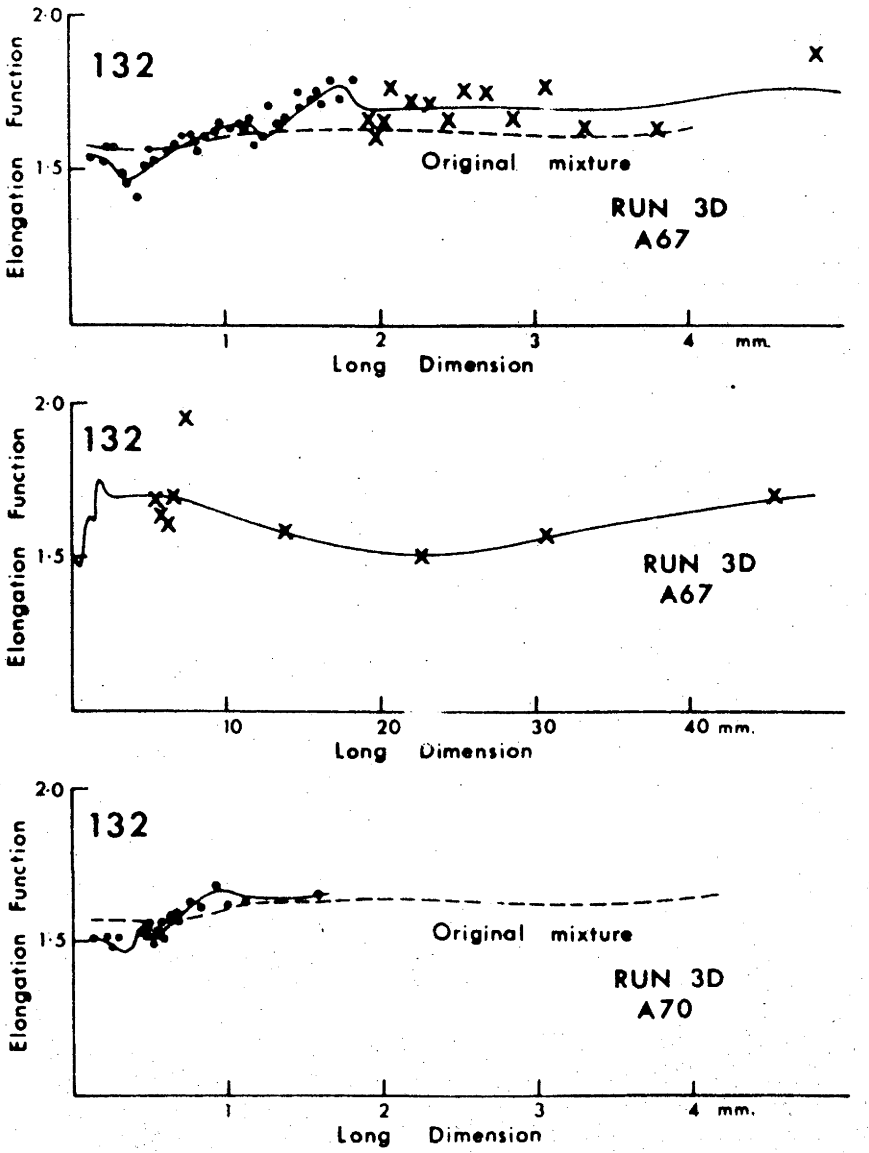

Fig. 132. Elongation function curves for Run 3D. That of A.67 is shown on two long dimension scales. For A.67 dots are means for 80 particles, crosses means for 20.

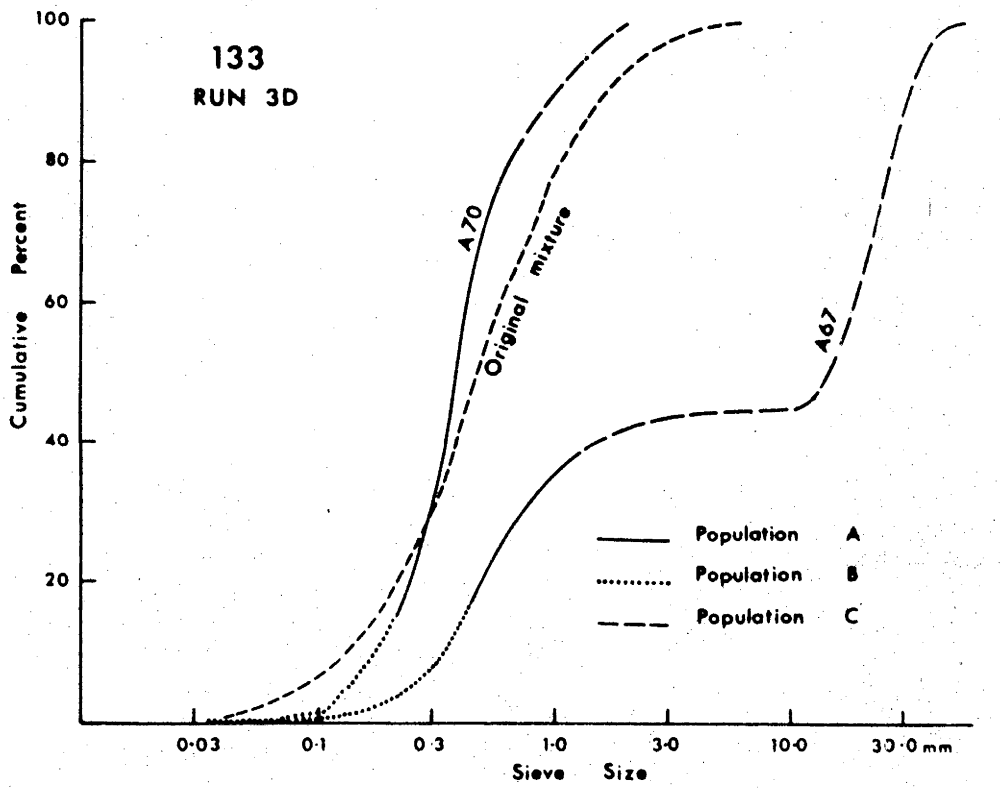

Fig. 133. Sieve cumulative curves for Run 3D.

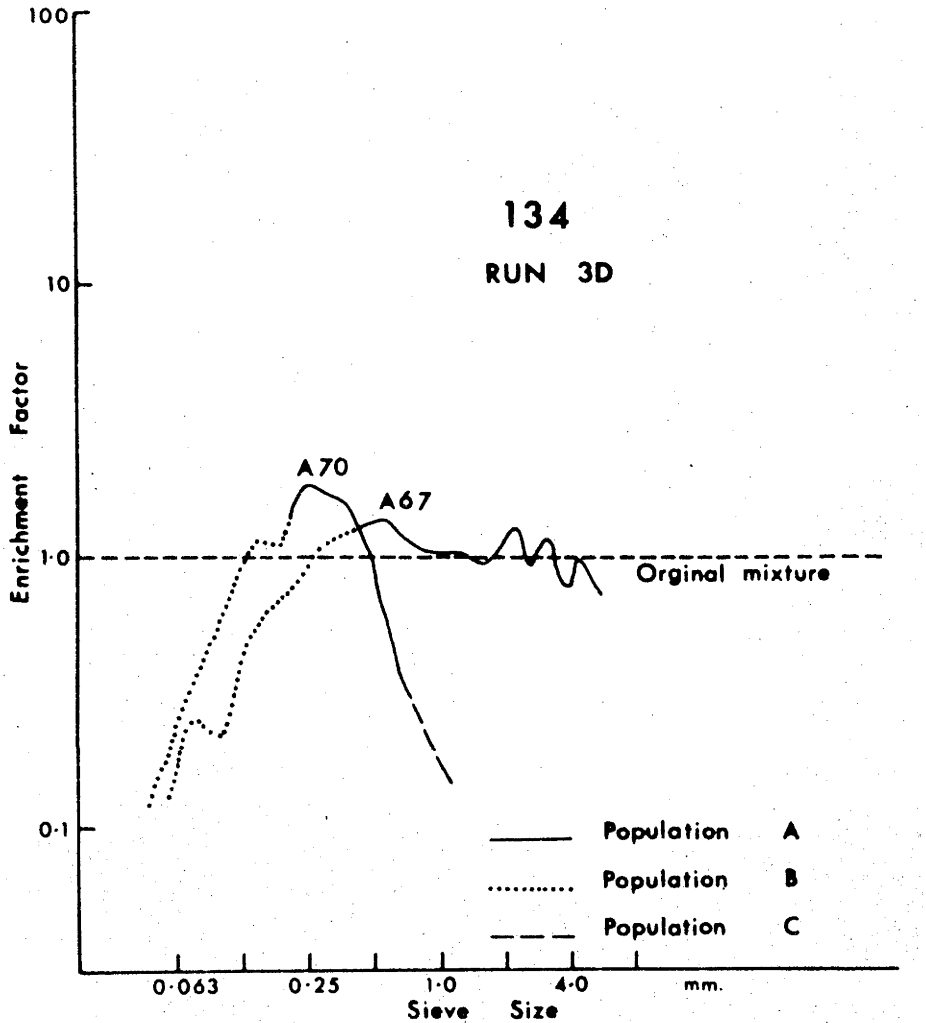

Fig. 134. Enrichment factors for Run 3D.

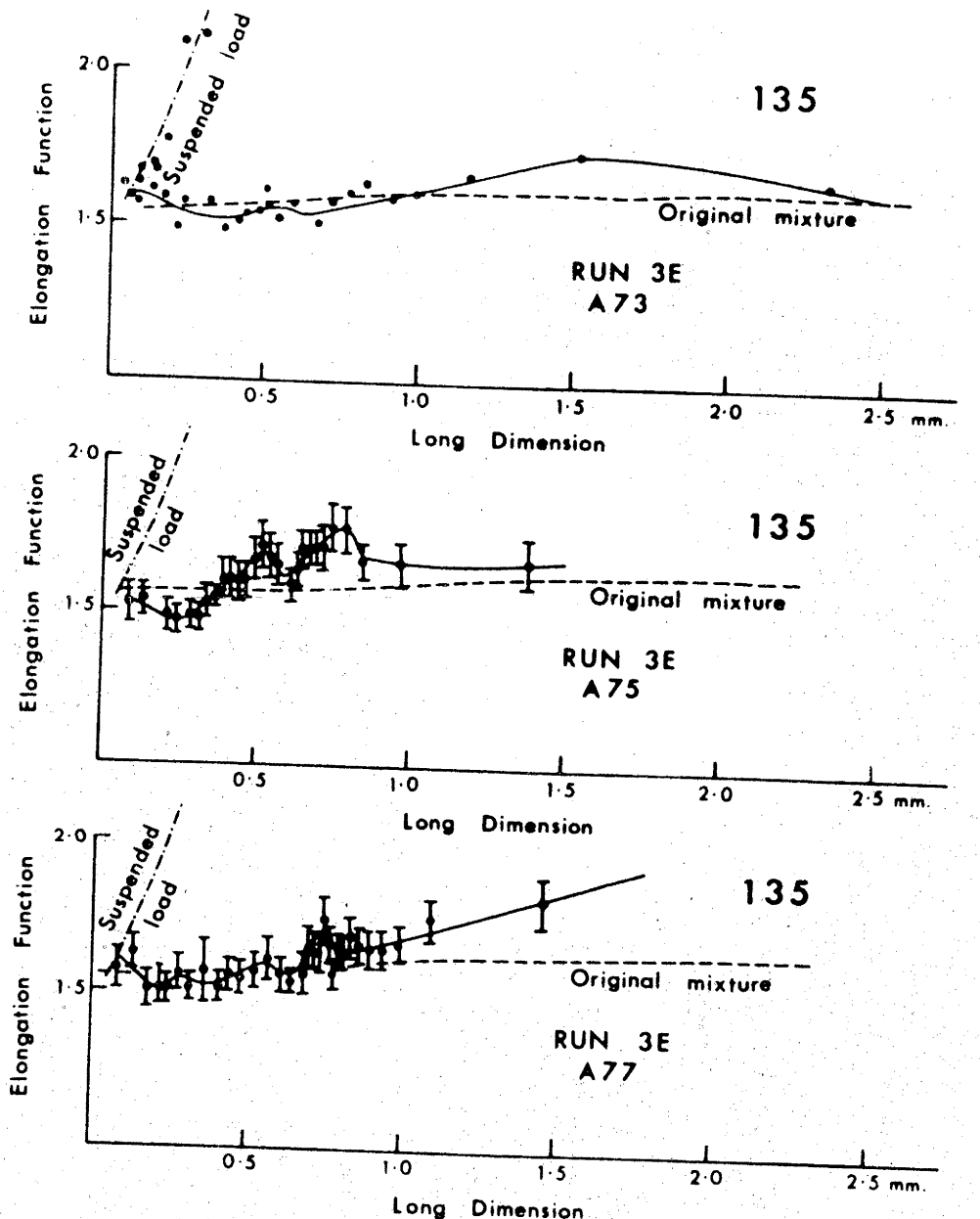

Fig. 135. Elongation function curves for Run 3E. 95% confidence limits given for A75 and A77.

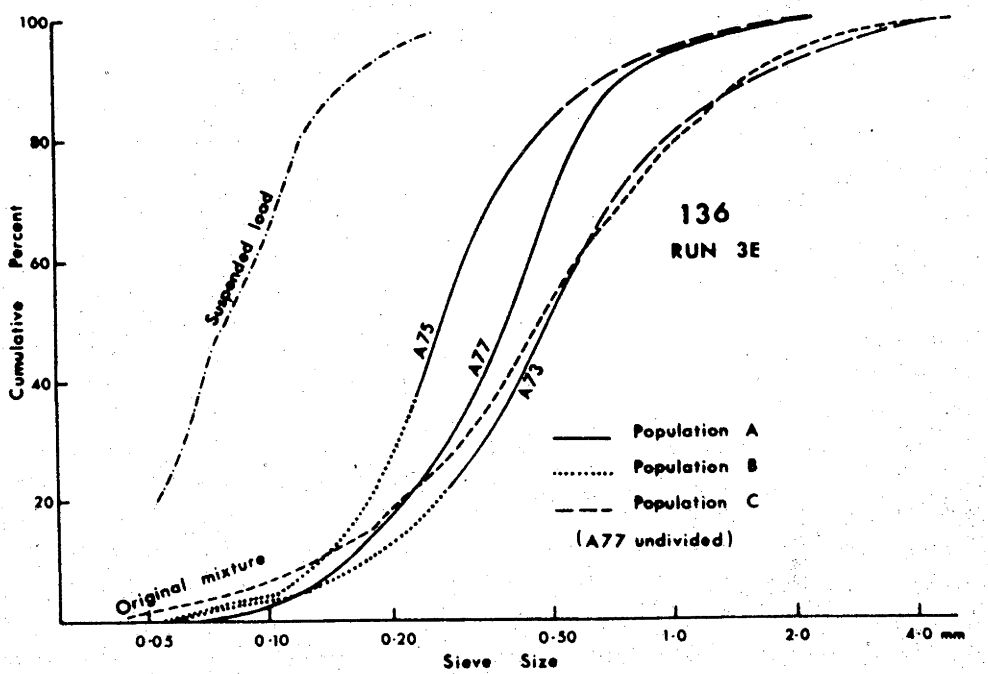

Fig. 136. Sieve cumulative curves for Run 3E.

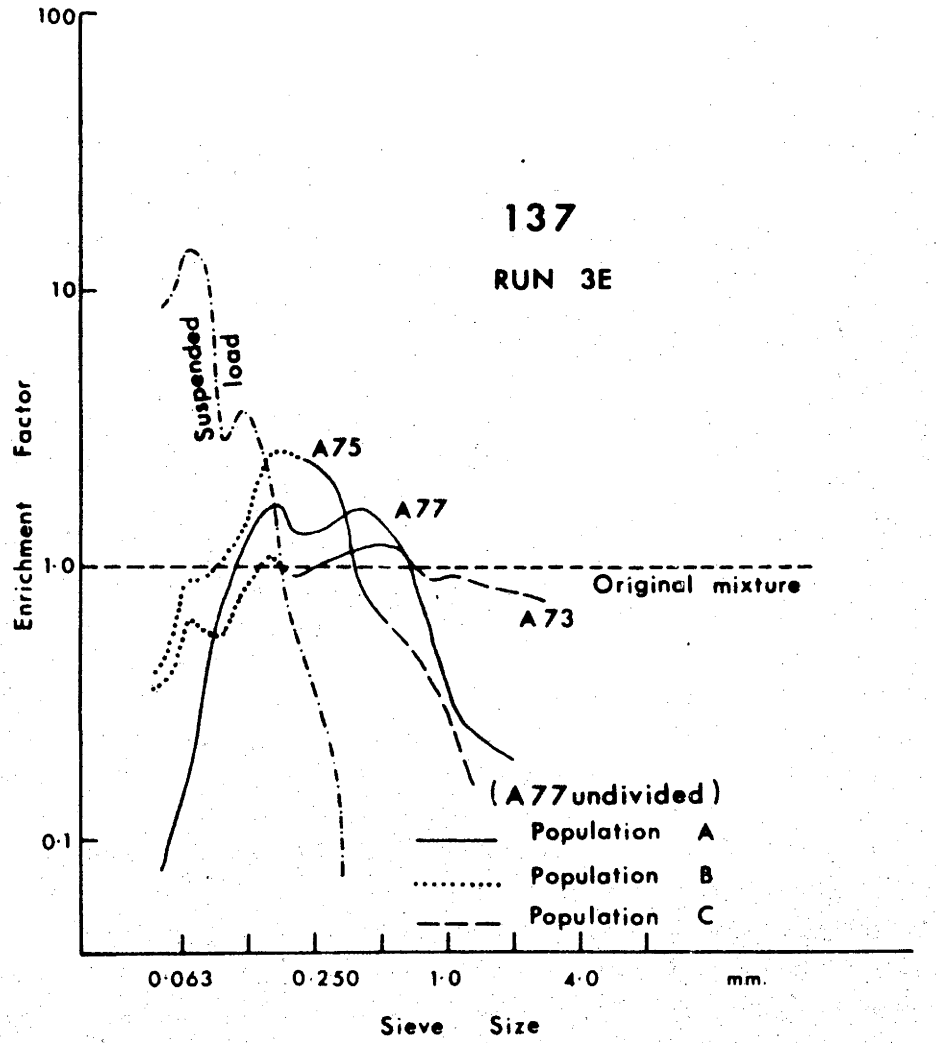

Fig. 137. Enrichment factors for Run 3E.

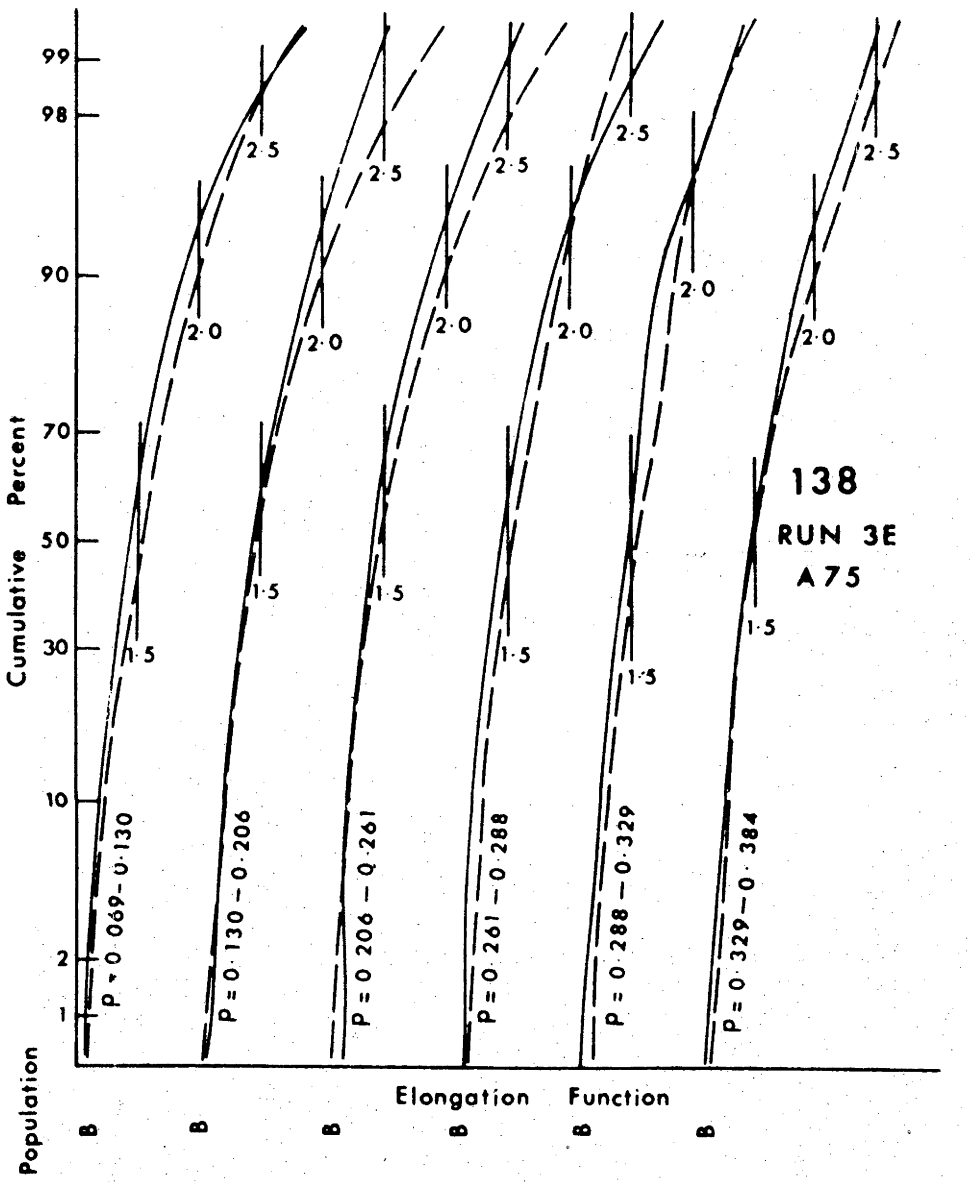

Fig. 138. Serial elongation function distribution sections, with respect to the long dimension. For A75 compared with those of parent mixture. Long dimension range given for each curve.

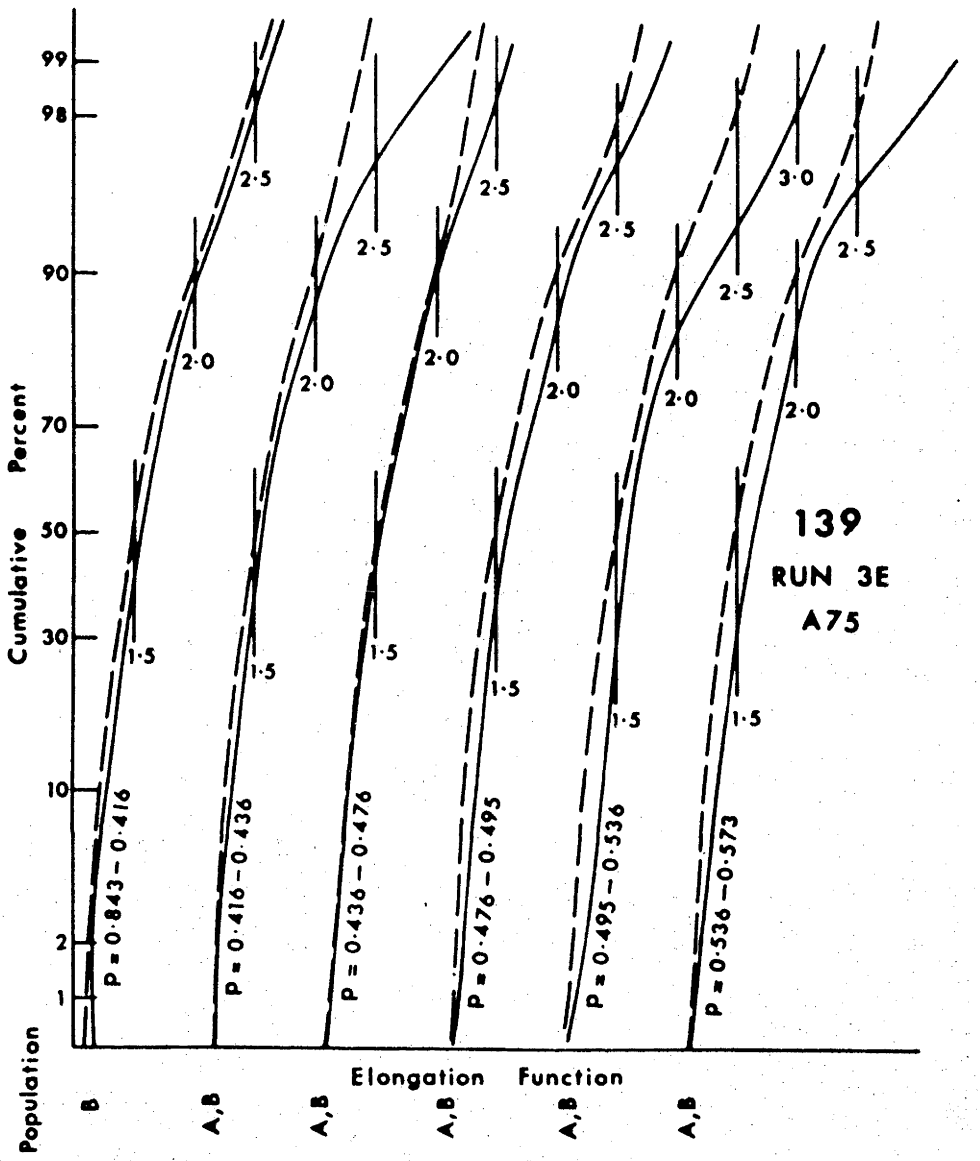

Fig. 139. As Fig. 138.

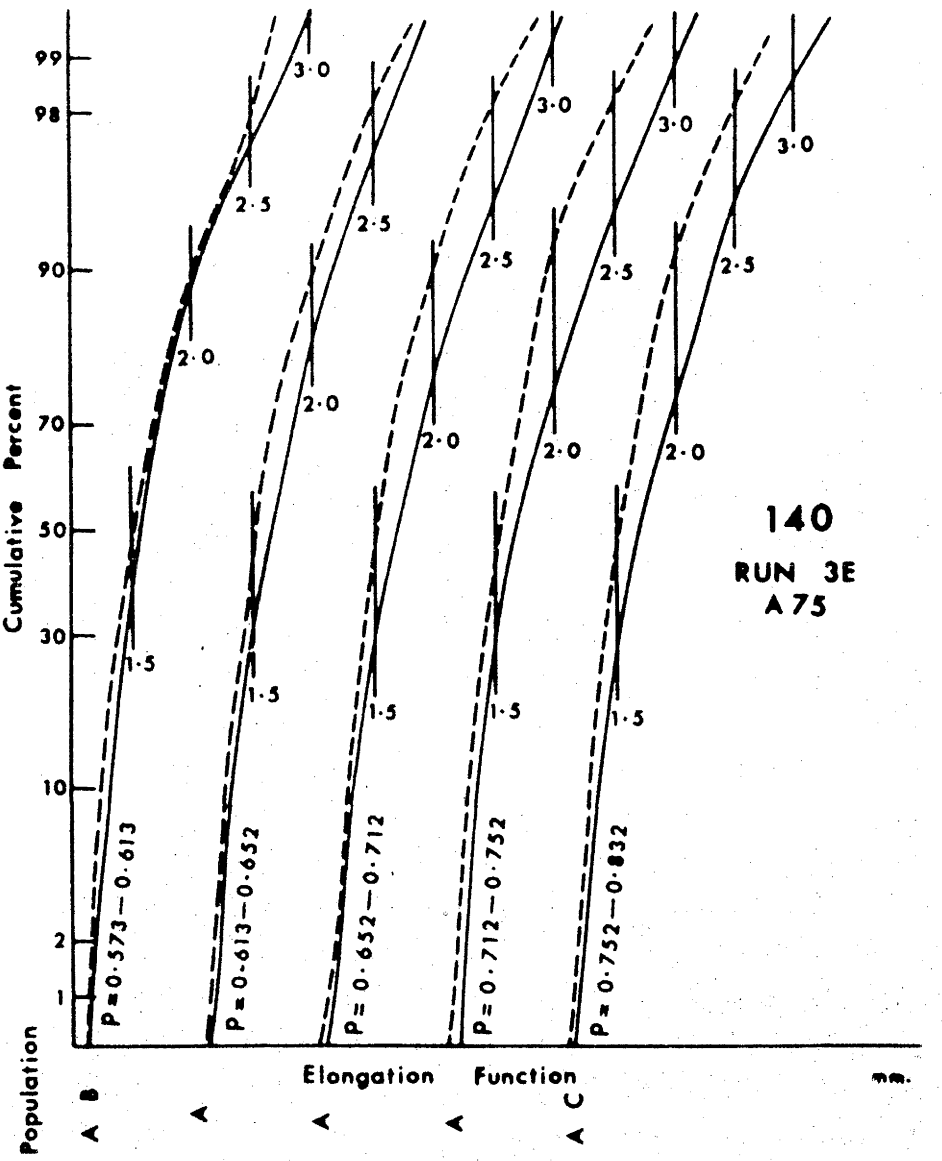

Fig. 140. As Fig. 138.

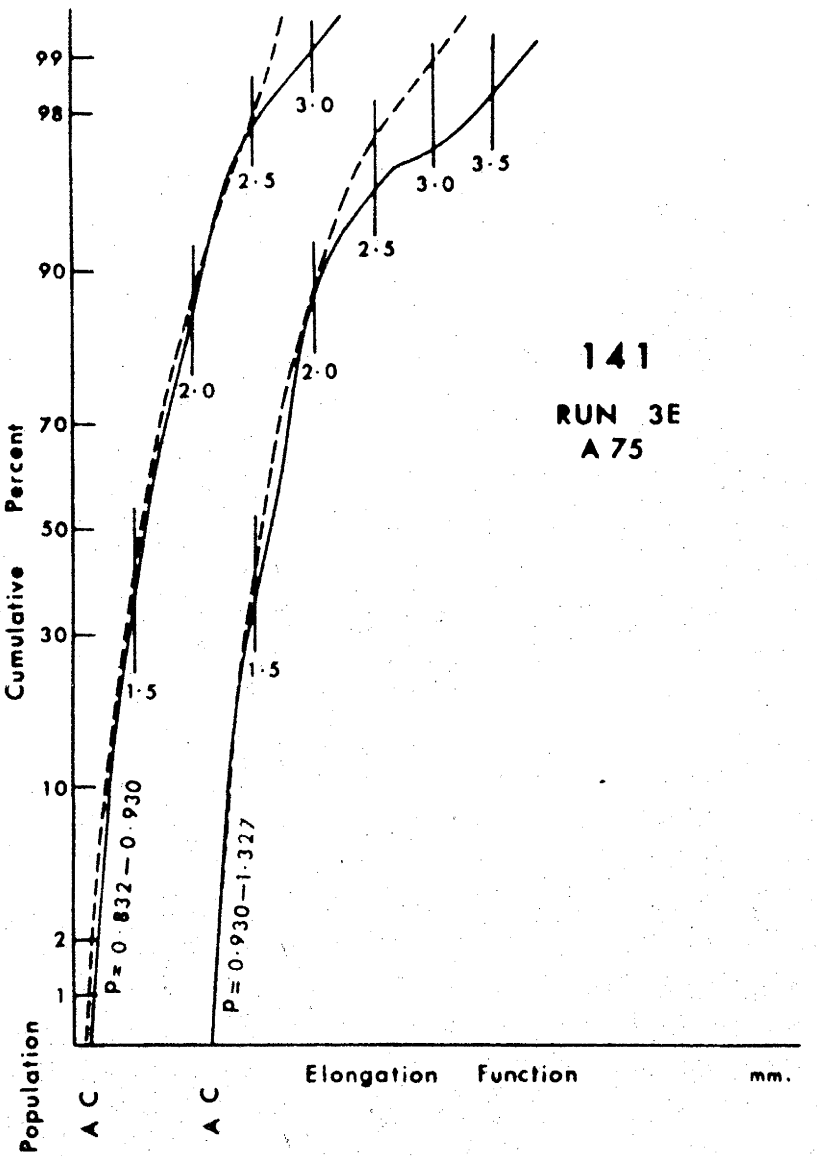

Fig. 141. As Fig. 138.

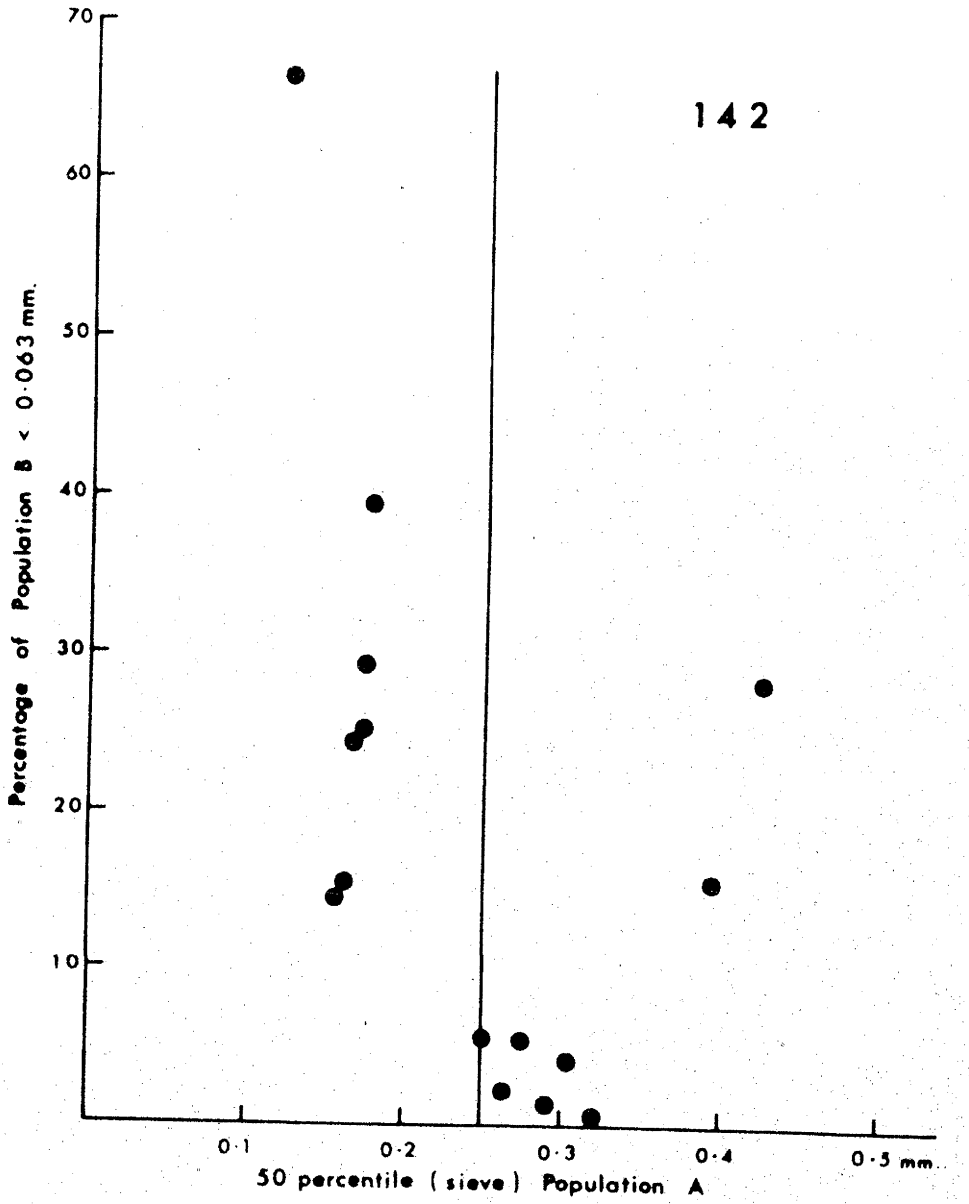

Fig. 142. Percentage of Population B less than 0.063 mm in sieve diameter plotted against the fifty percentile of Population A for artificial ripple stage sands.

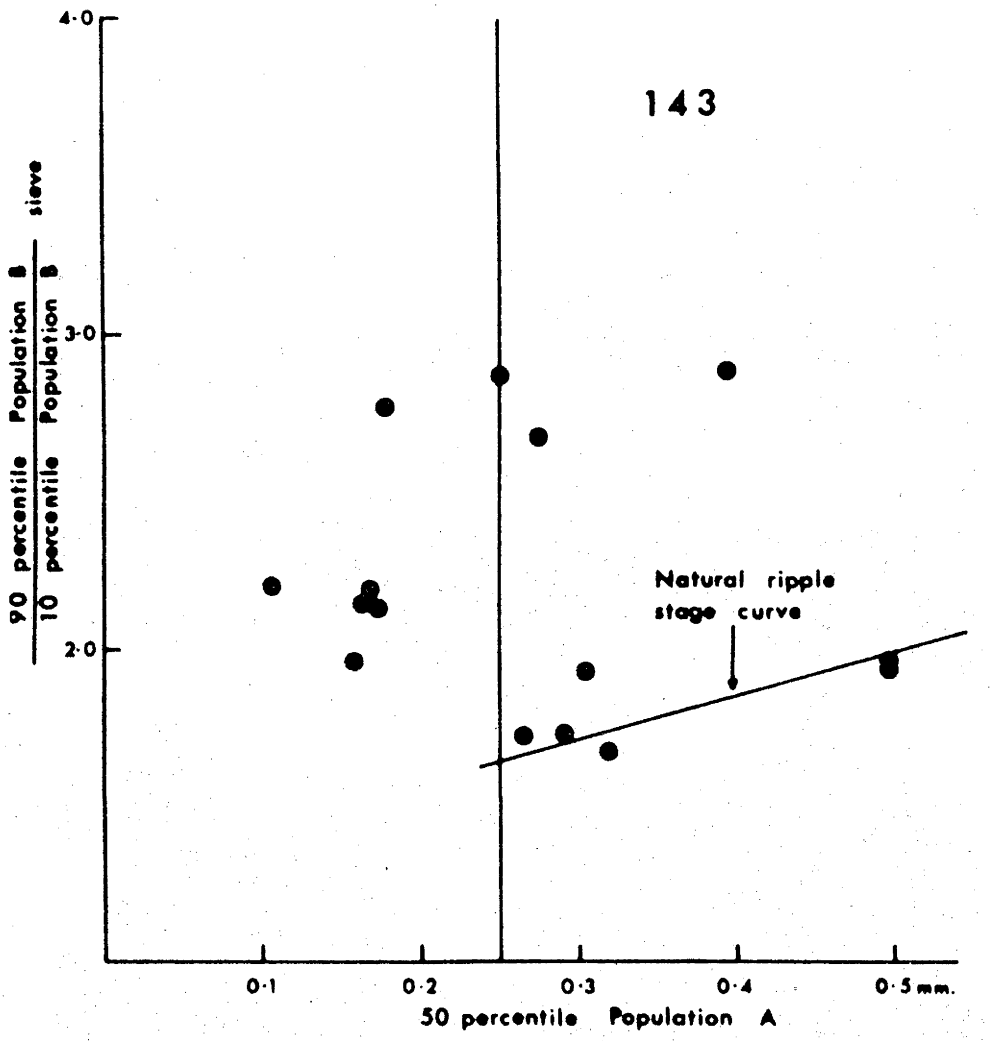

Fig. 143. Ratio of ninety percentile to ten percentile of Population A plotted against Population A fifty percentile for artificial ripple stage sands.

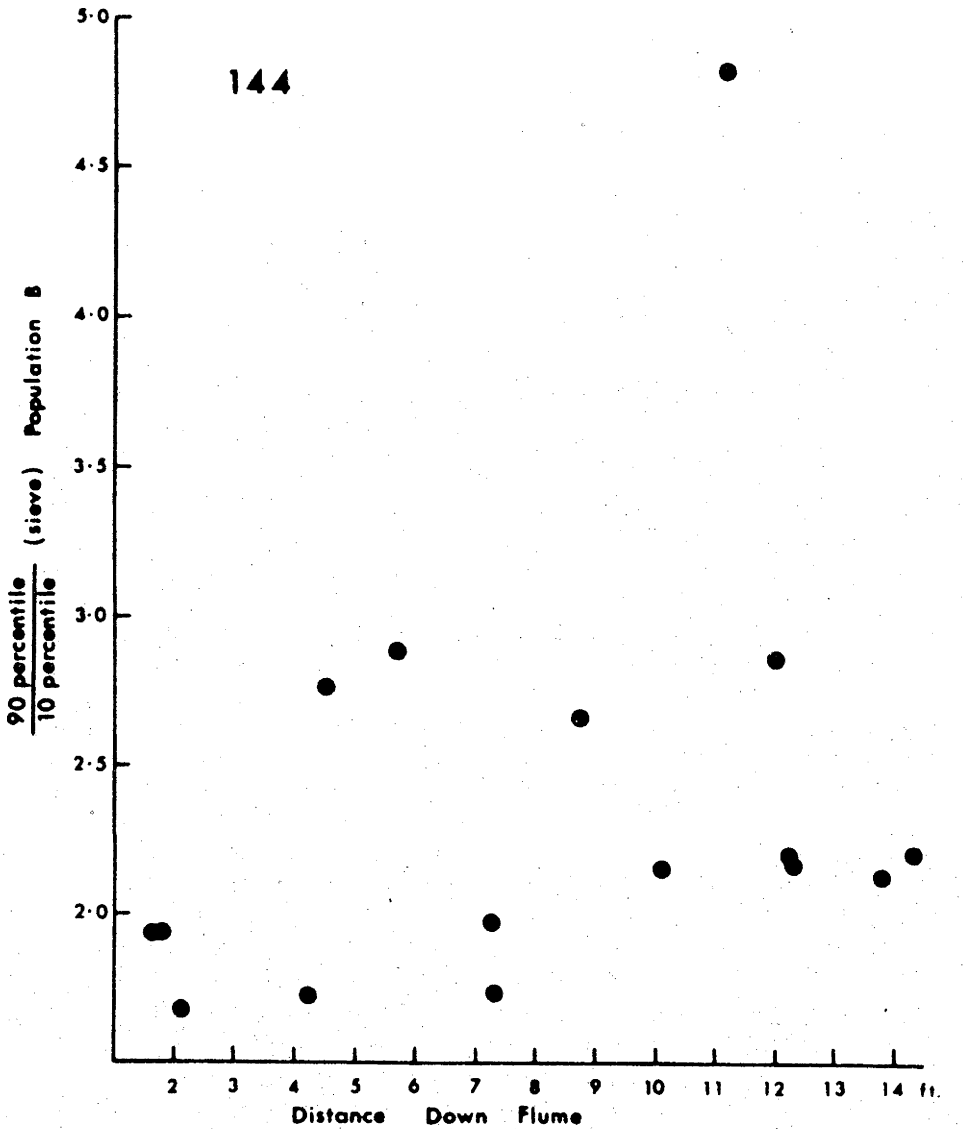

Fig. 144. Ratio of ninety percentile to ten percentile of Population A plotted against distance down flume for artificial ripple stage sediments.

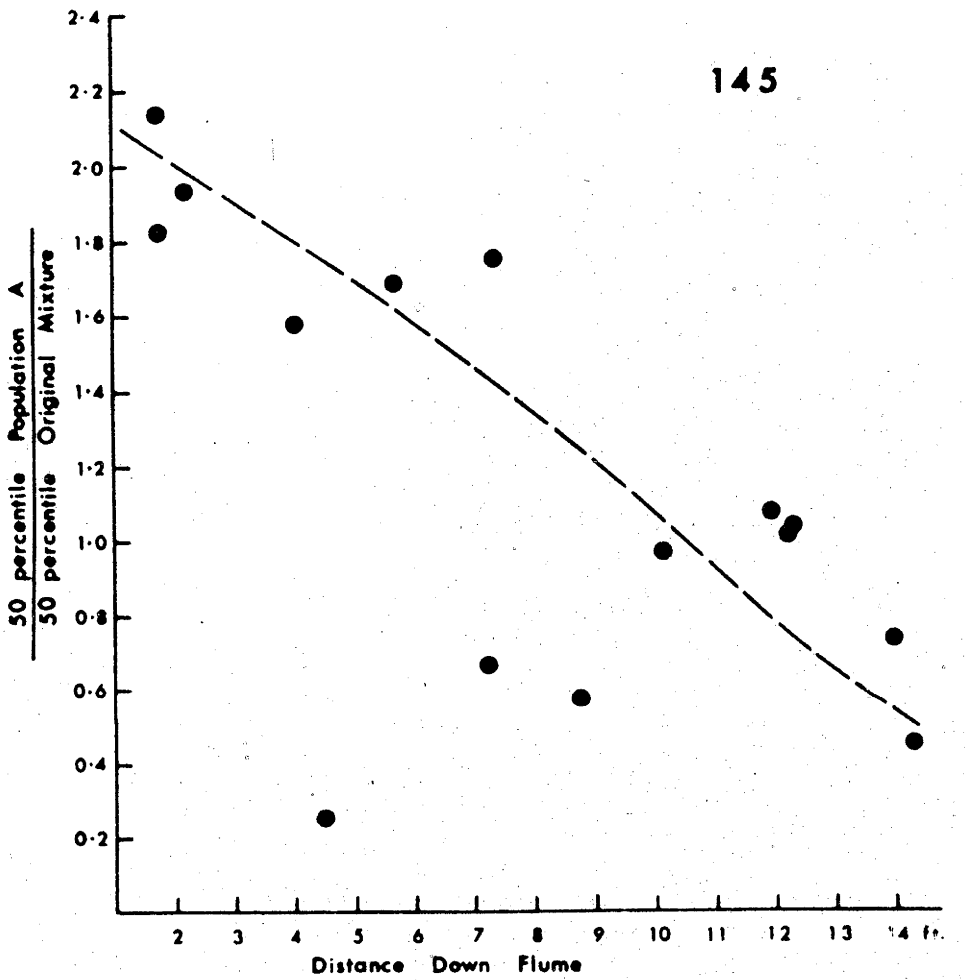

Fig. 145. Ratio of fifty percentile of Population A to fifty percentile of parent mixture versus distance down flume for artificial ripple stage sediments.

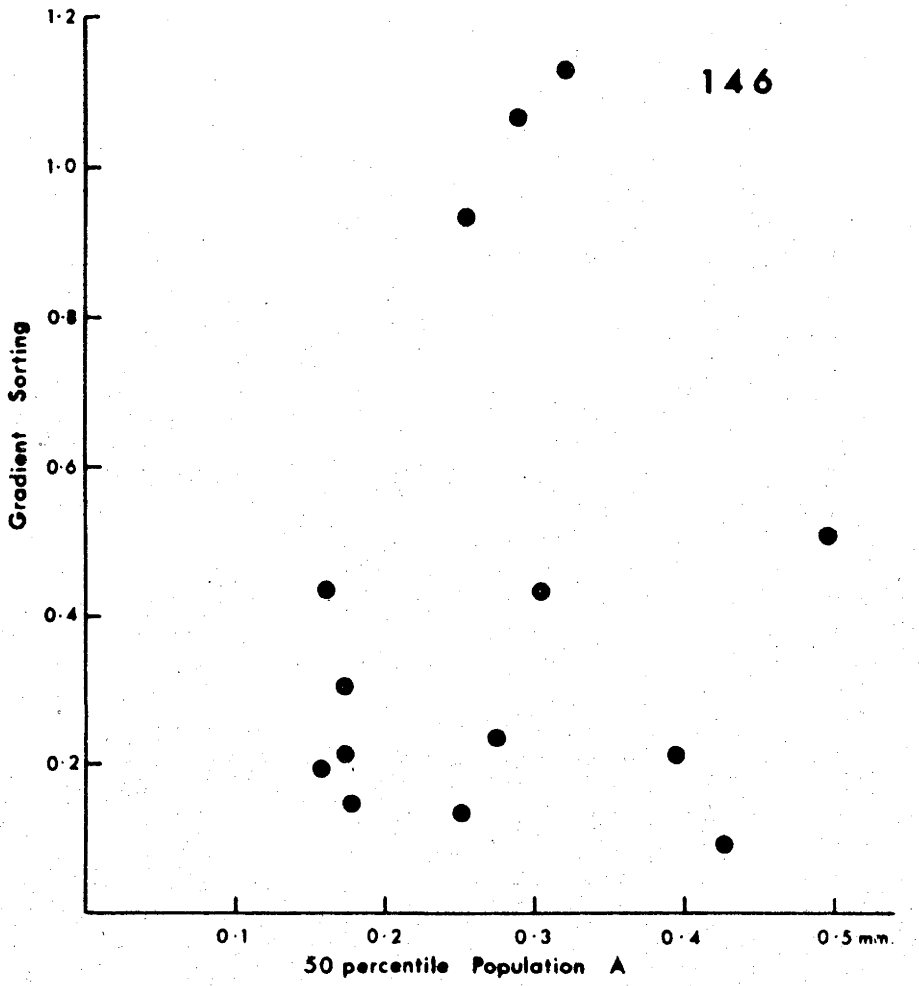

Fig. 146. Gradient sorting versus fifty percentile of Population A for artificial ripple stage sediments.

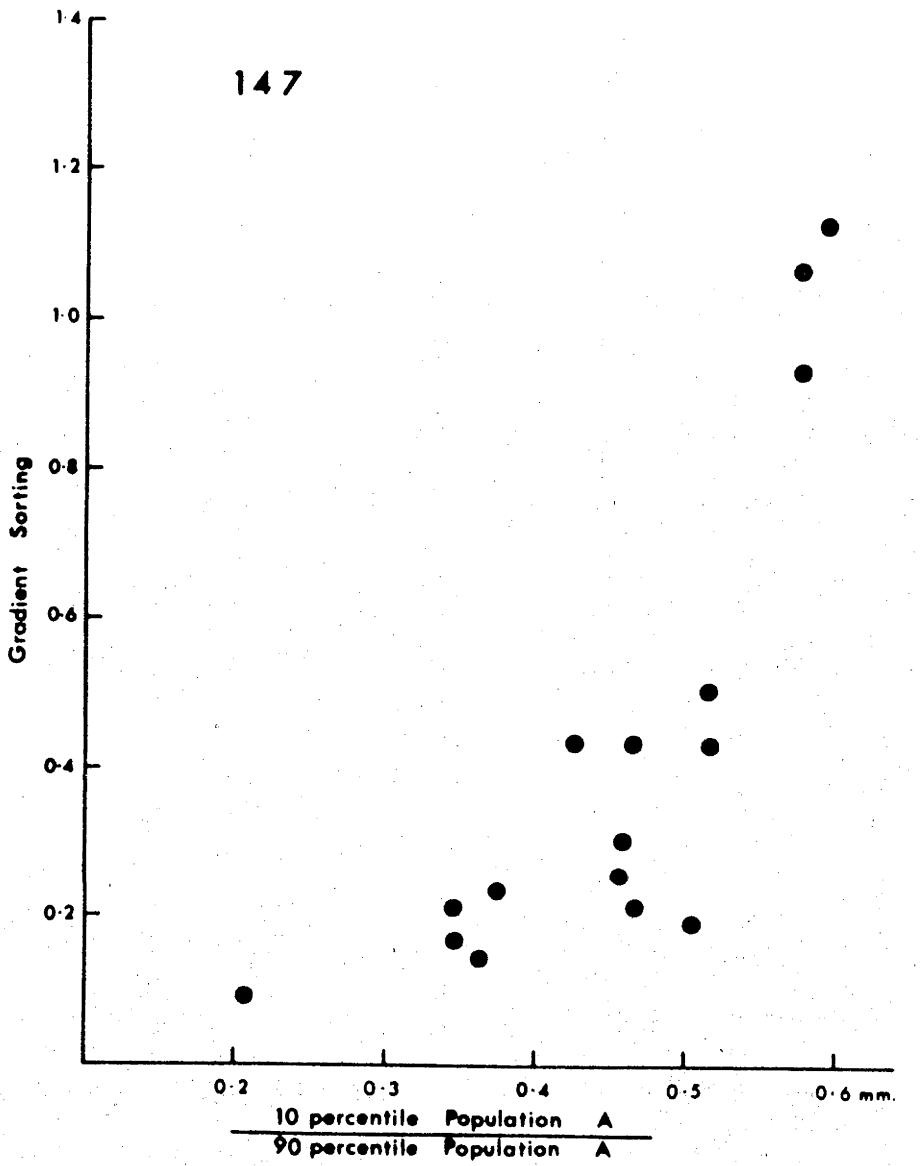

Fig. 147. Relationship between gradient sorting and the ratio of the ten to the ninety percentile (sieve) for artificial ripple stage sands. Correlation coefficient = +0.788.

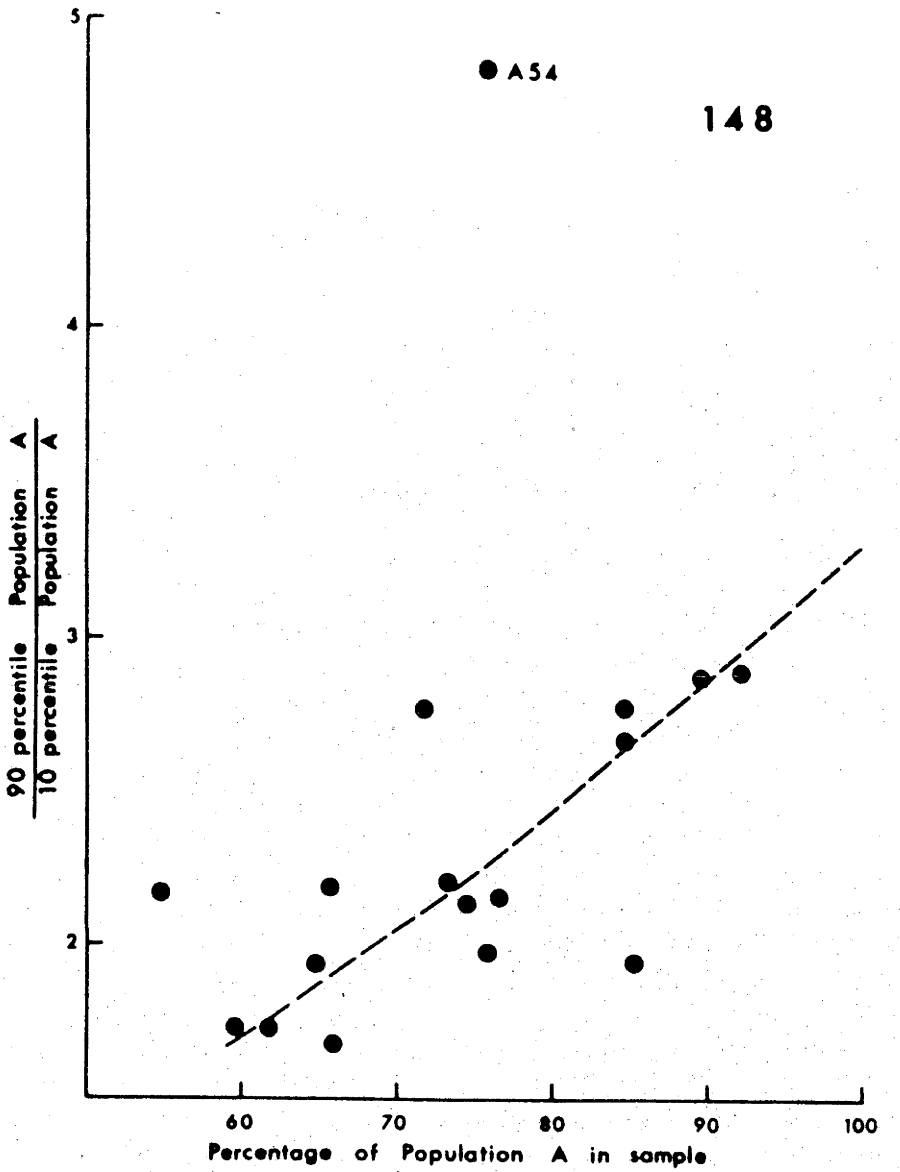

Fig. 148. Relationship between ratio of ninety to ten percentile (sieve) and percentage of Population A is sample for artificial ripple stage sands. Trend line sketched in.

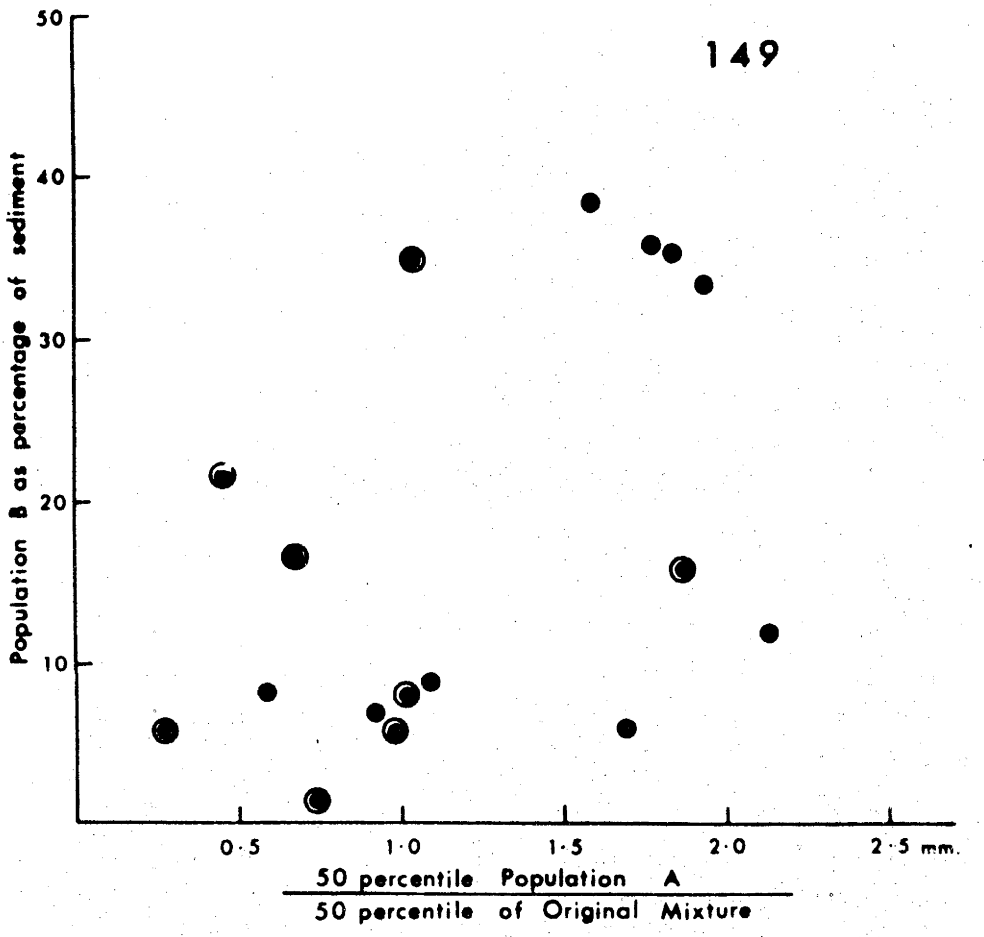

Fig. 149. Relationship between percentage of percentage of Population B in sample and the ratio of the fifty percentile of Population A to that of the parent mixture. Fine ripple stage sands are circled. Data for artificial ripple stage sediments.

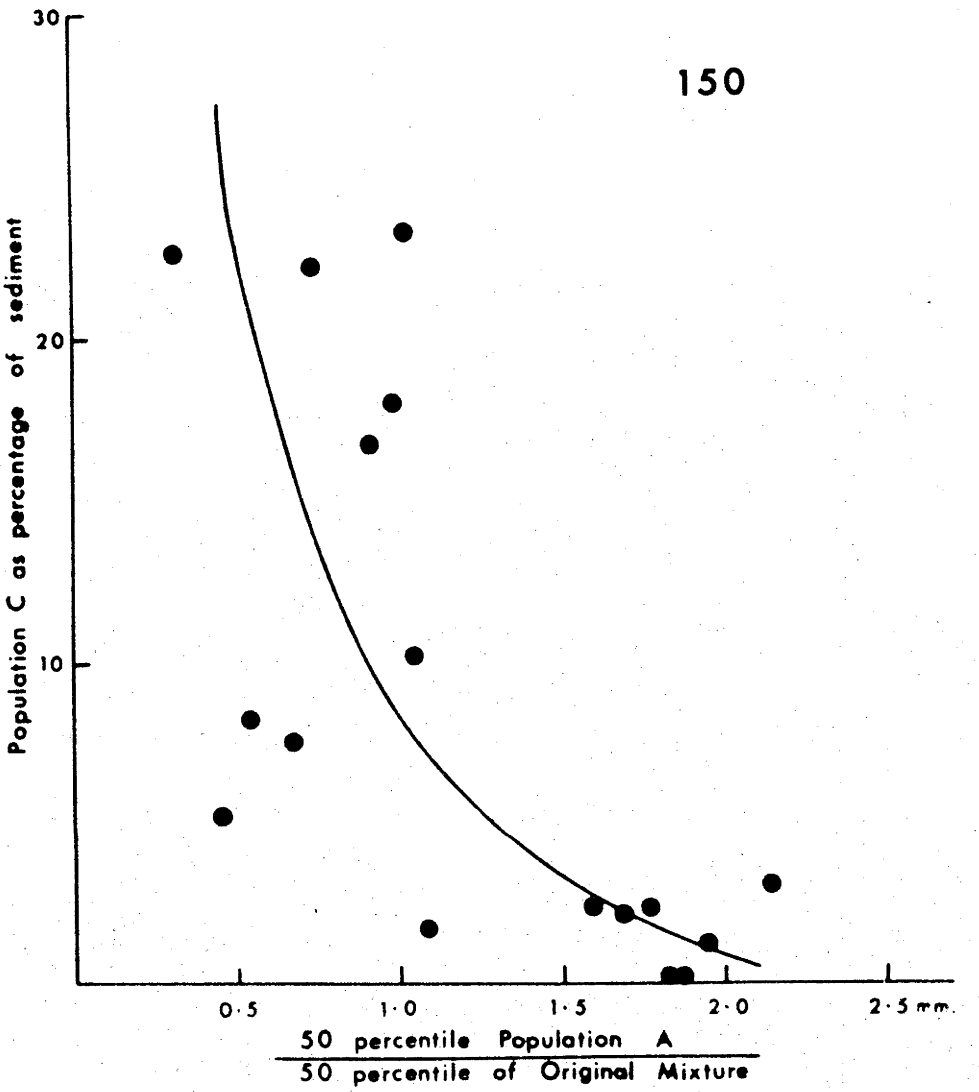

Fig. 150. Relationship between percentage of Population C in sample and the ratio of the fifty percentile of Population A to that of the parent mixture. Trend line is sketched. Data for artificial ripple stage sediments.

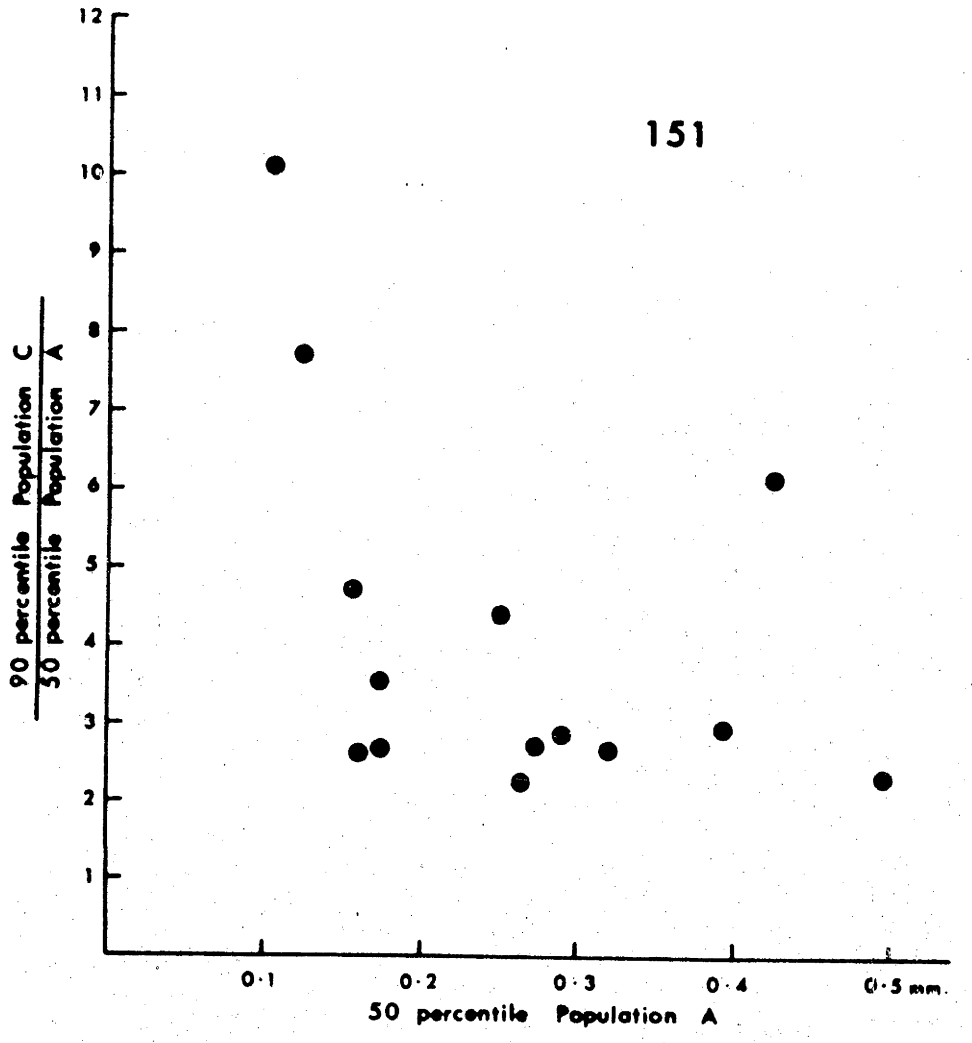

Fig. 151. Relationship between the ratio of the ninety percentile of Population C to the fifty percentile of Population A and the fifty percentile of Population A. Data for artificial ripple stage sands.

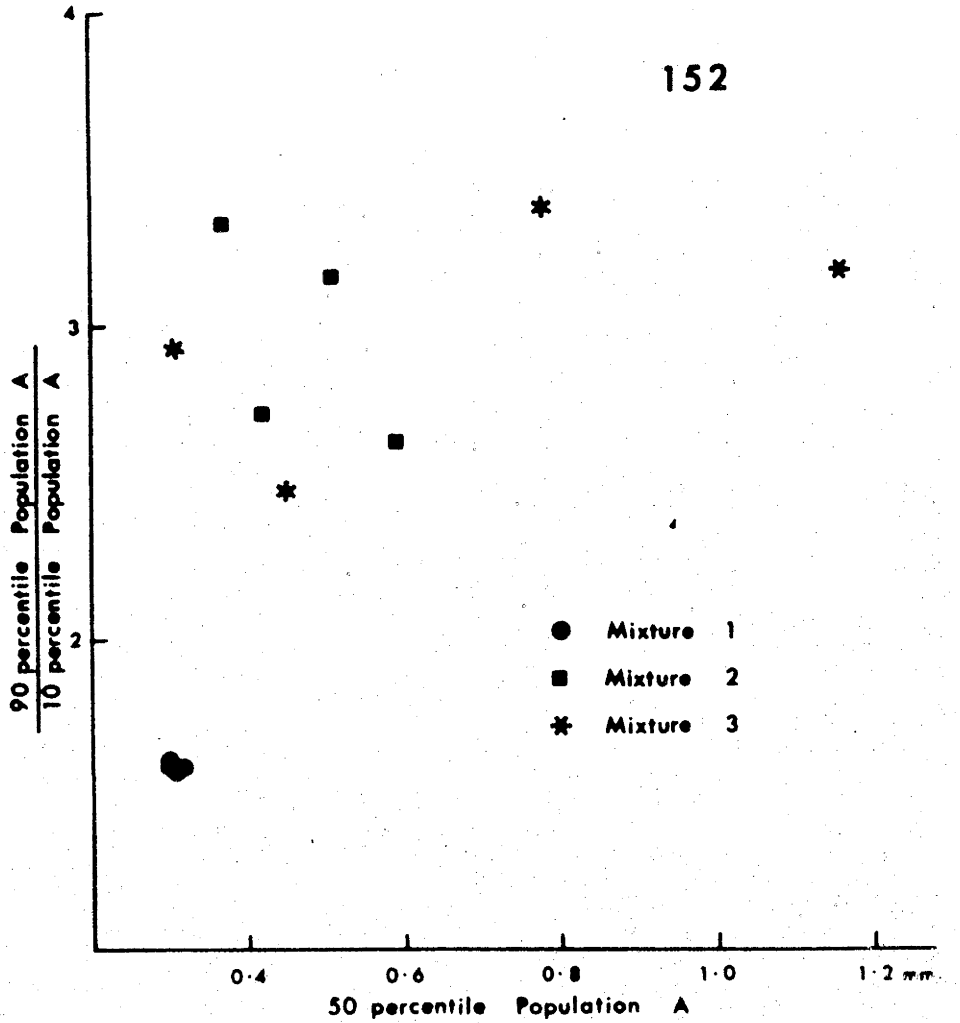

Fig. 152. Relationship between the ratio of the ninety to the ten percentile of Population A to its fifty percentile for artificial dune stage sands. Parent mixtures are indicated.

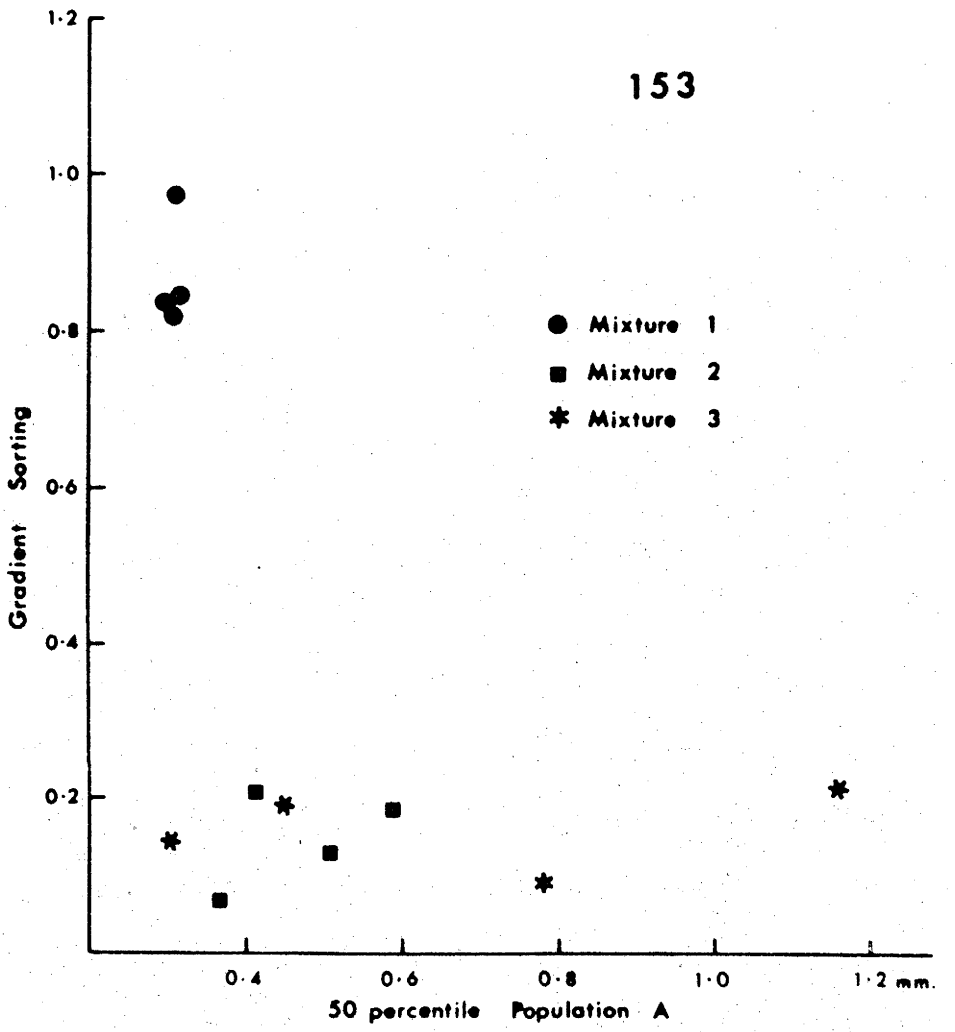

Fig. 153. Gradient sorting versus the fifty percentile of Population A for artificial dune stage sands. Parent mixtures are indicated.

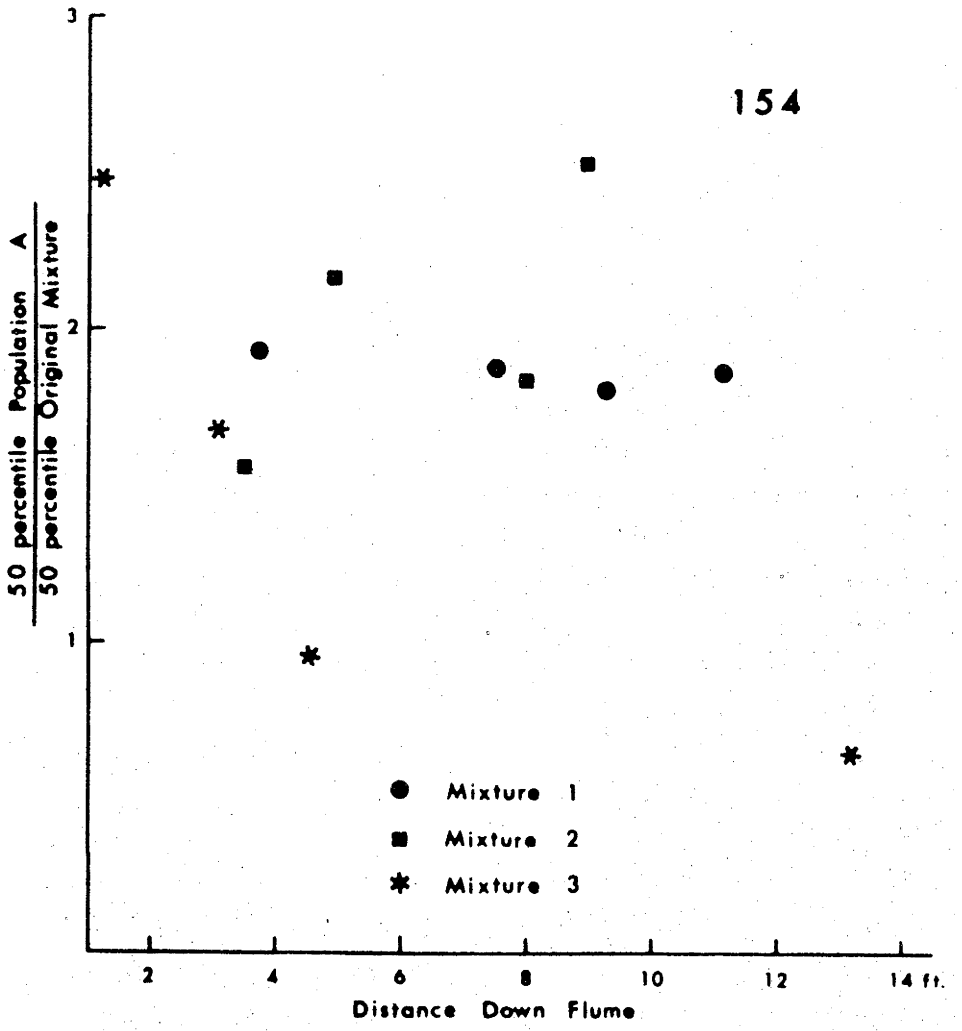

Fig. 154. Ratio of fifty percentile of Population A to that of parent mixture versus distance down flume. Parent mixtures are indicated. Data for artificial dune stage sediments.

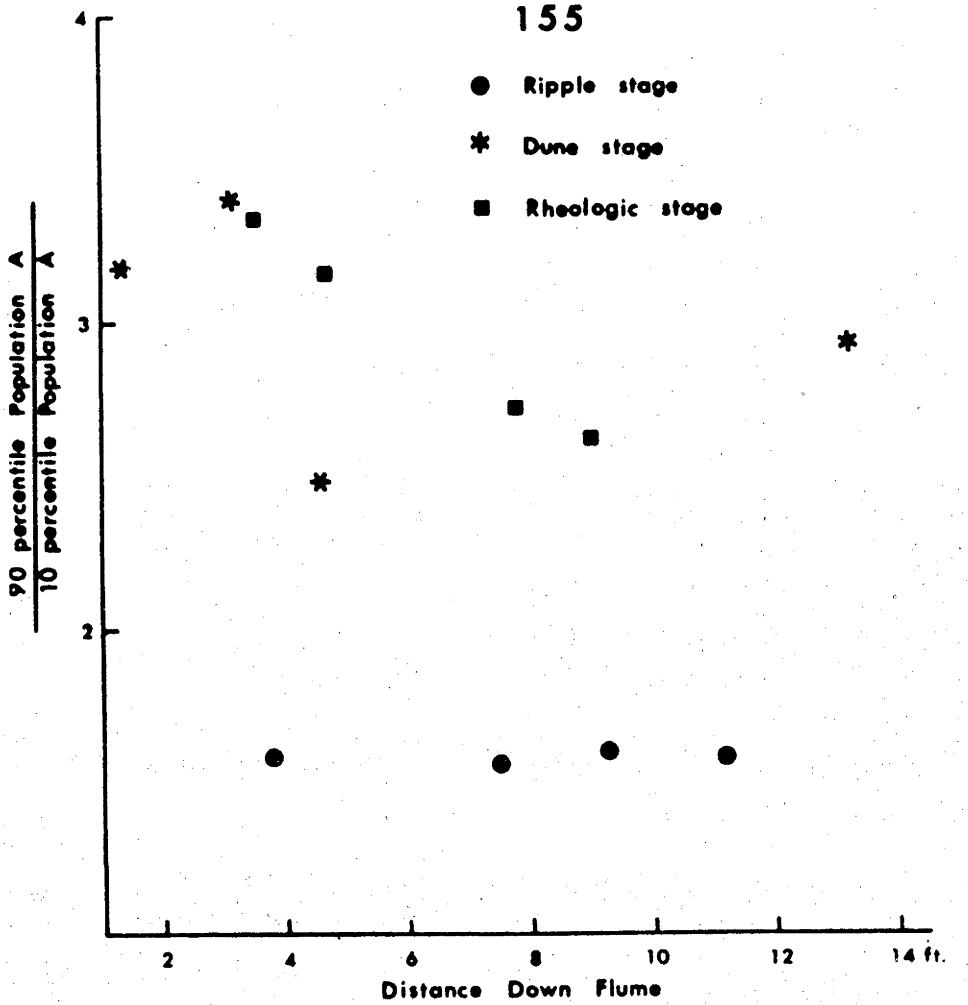

Fig. 155. Ratio of ninety to ten percentile of Population A versus distance down flume for artificial dune stage sediments.

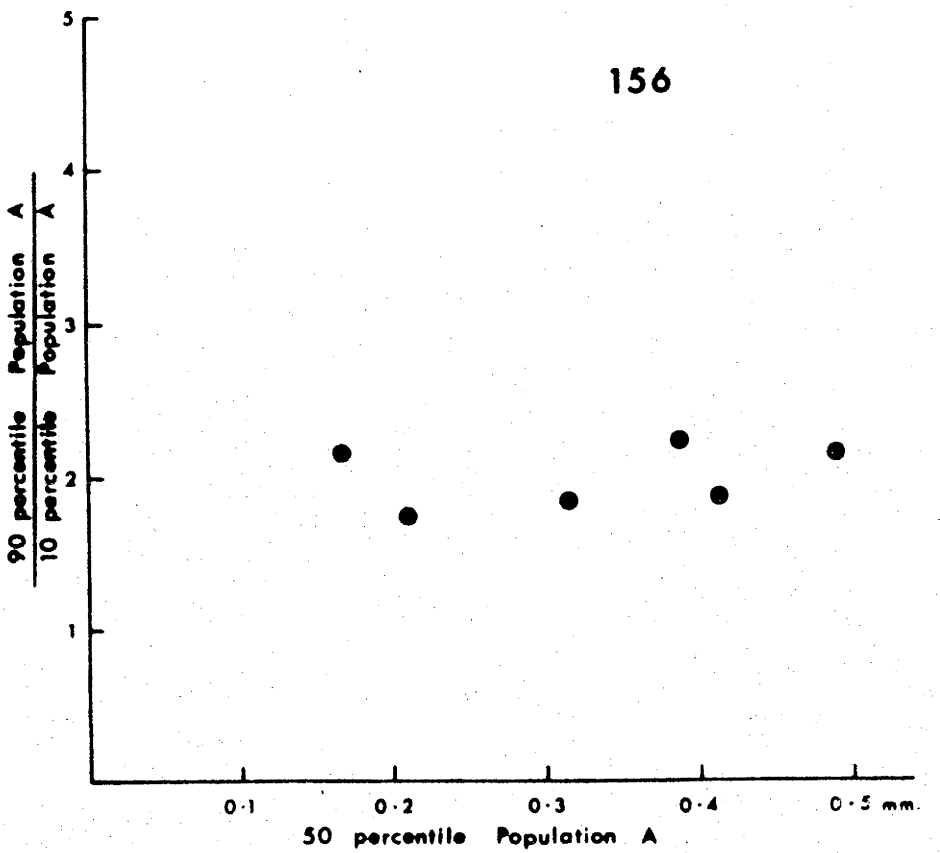

Fig. 156. Ratio of ninety to ten percentile of Population A versus fifty percentile of Population A for artificial rheologic bed load sediments.

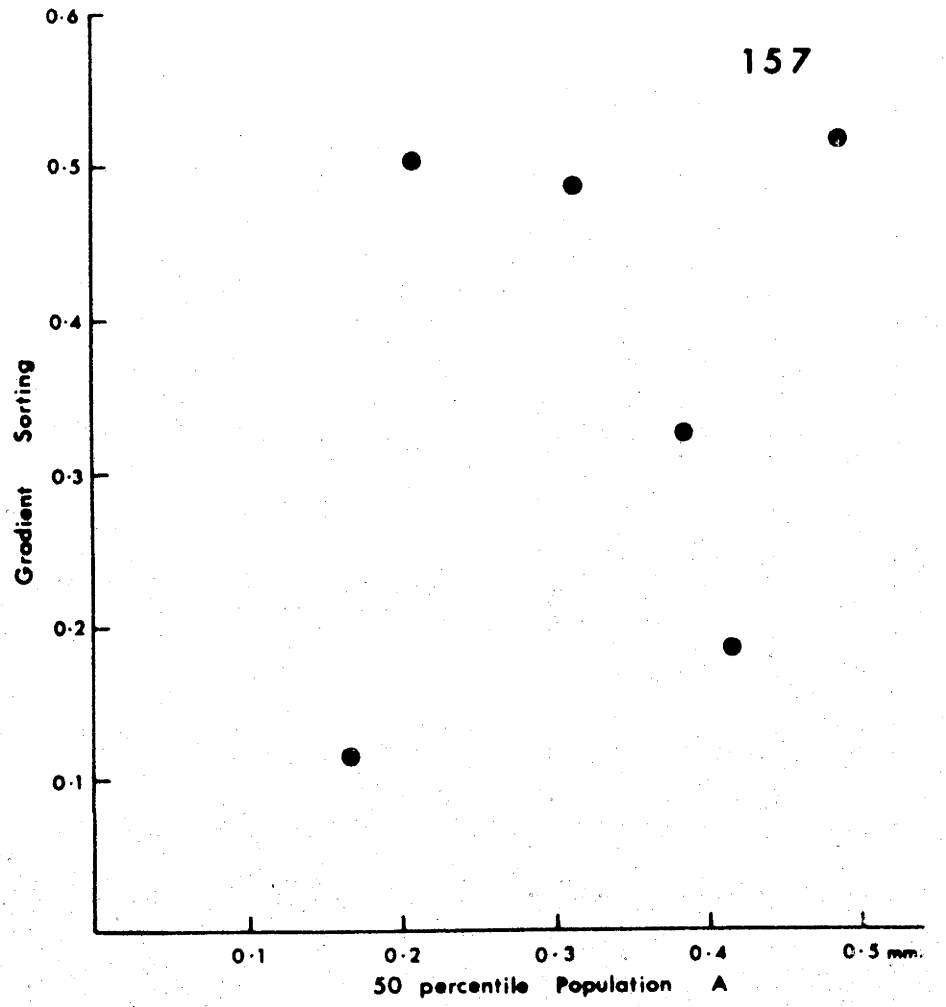

Fig. 157. Gradient sorting versus fifty percentile of Population A for artificial rheologic bed load sediments.

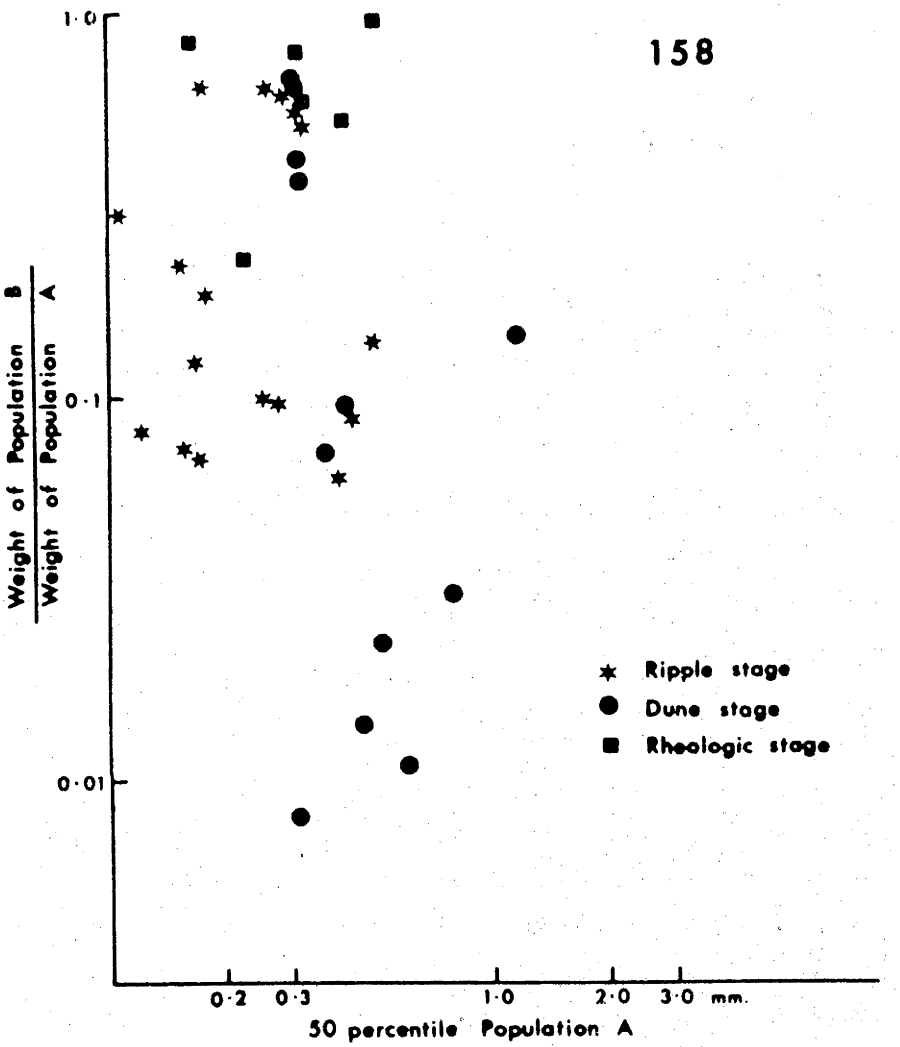

Fig. 158. Ratio of weight of Population B to weight of Population A versus fifty percentile of Population A for artificial sediments.

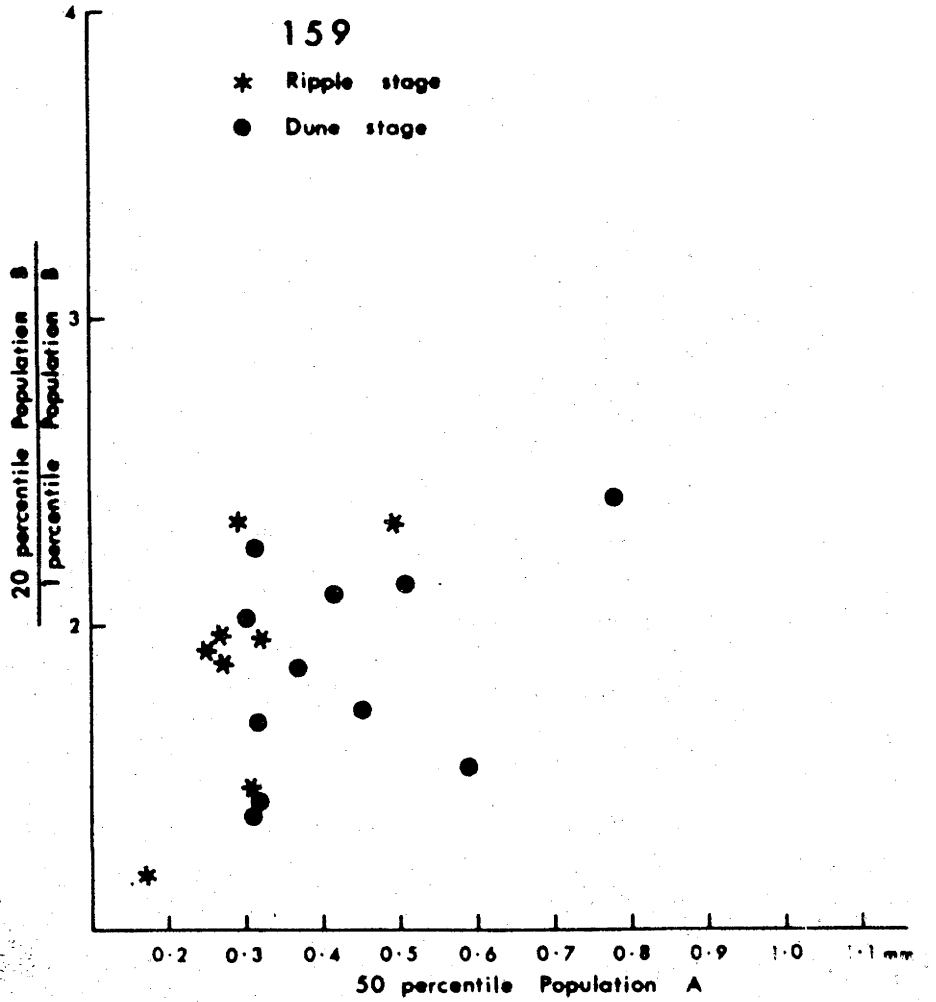

Fig. 159. Ratio of twenty to one percentile of Population B versus fifty percentile of Population A for artificial dune and ripple stage sediments.

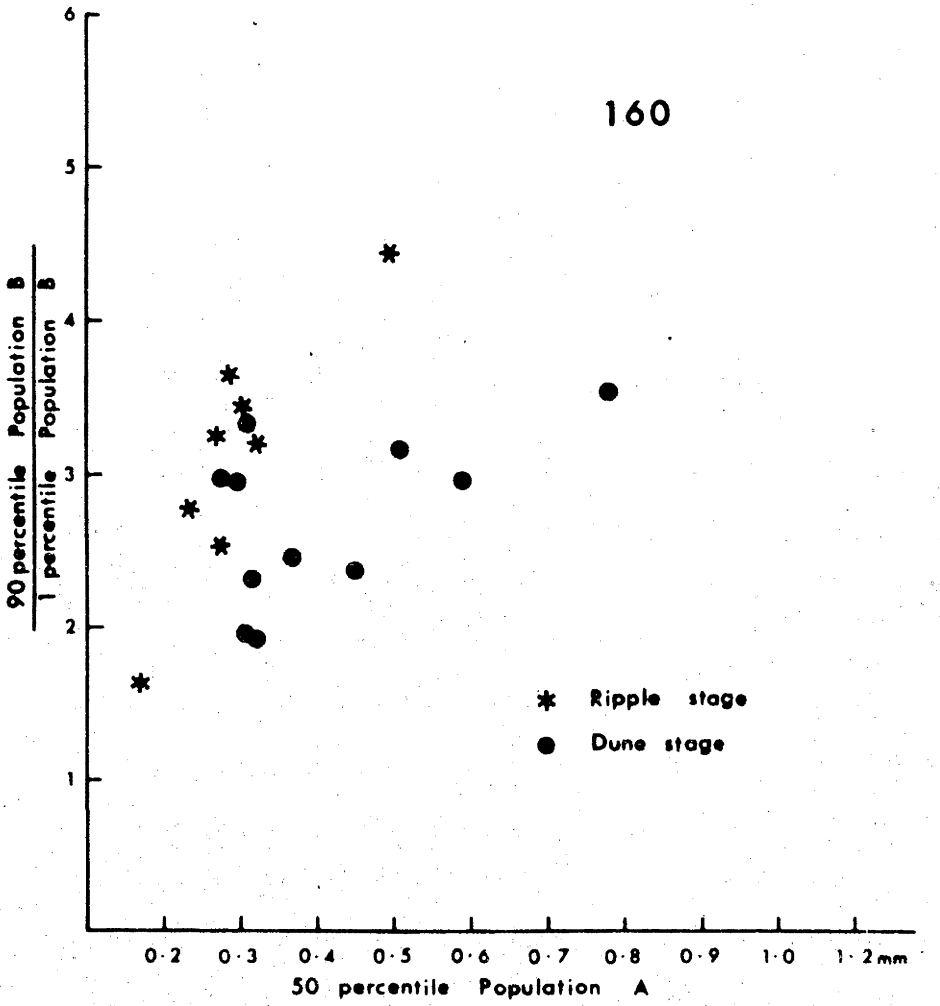

Fig. 160. Ratio of ninety to one percentile of Population B versus fifty percentile of Population A for artificial dune and ripple stage sediments.

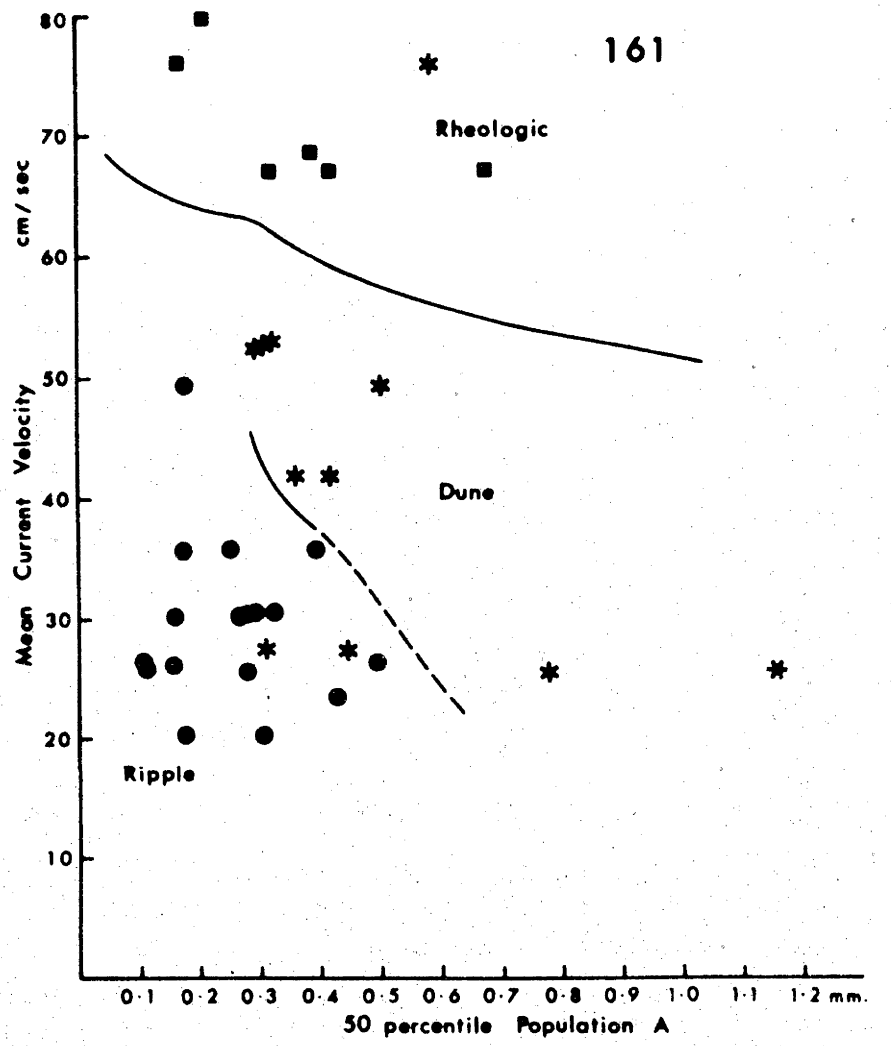

Fig. 161. Scatter diagram of mean current velocity versus fifty percentile of Population A for artificial sediments. Ripples shown by dots, dunes circled, rheologic bed load sands triangled.

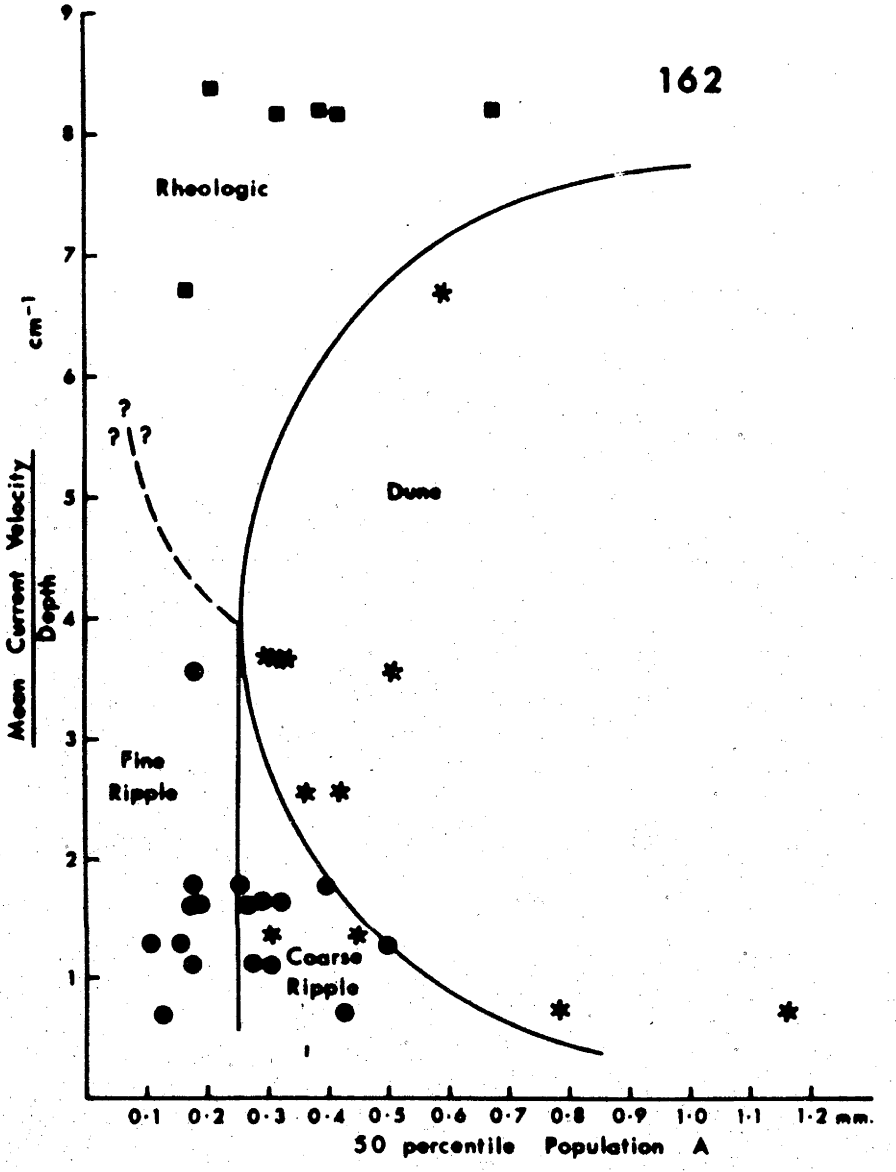

Fig. 162. Scatter diagram of ratio of mean current velocity to depth versus fifty percentile of Population A for artificial sediments. Legend as for Fig. 161.

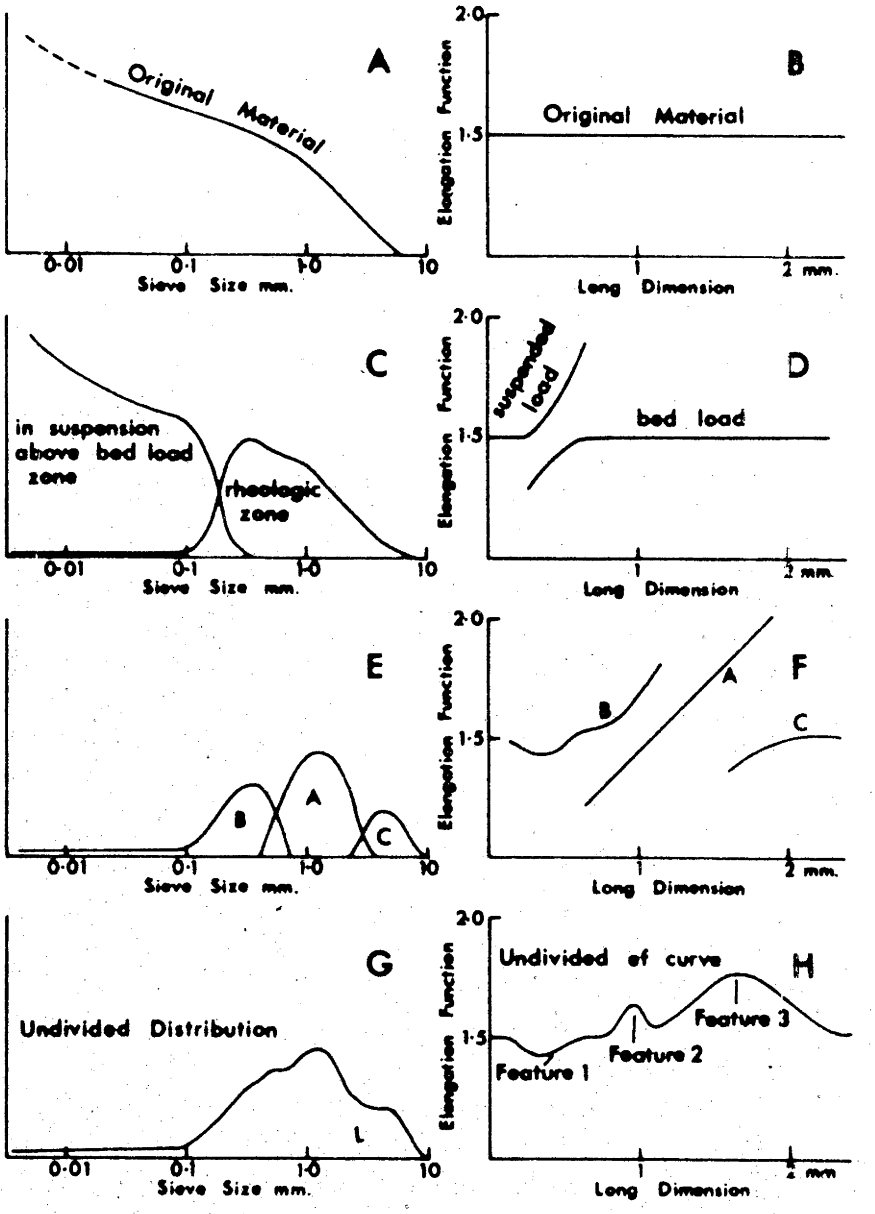

Fig. 163. Diagrams illustrating the suggested mode of origin of a rheologic bed load sediment. See text for detailed description.

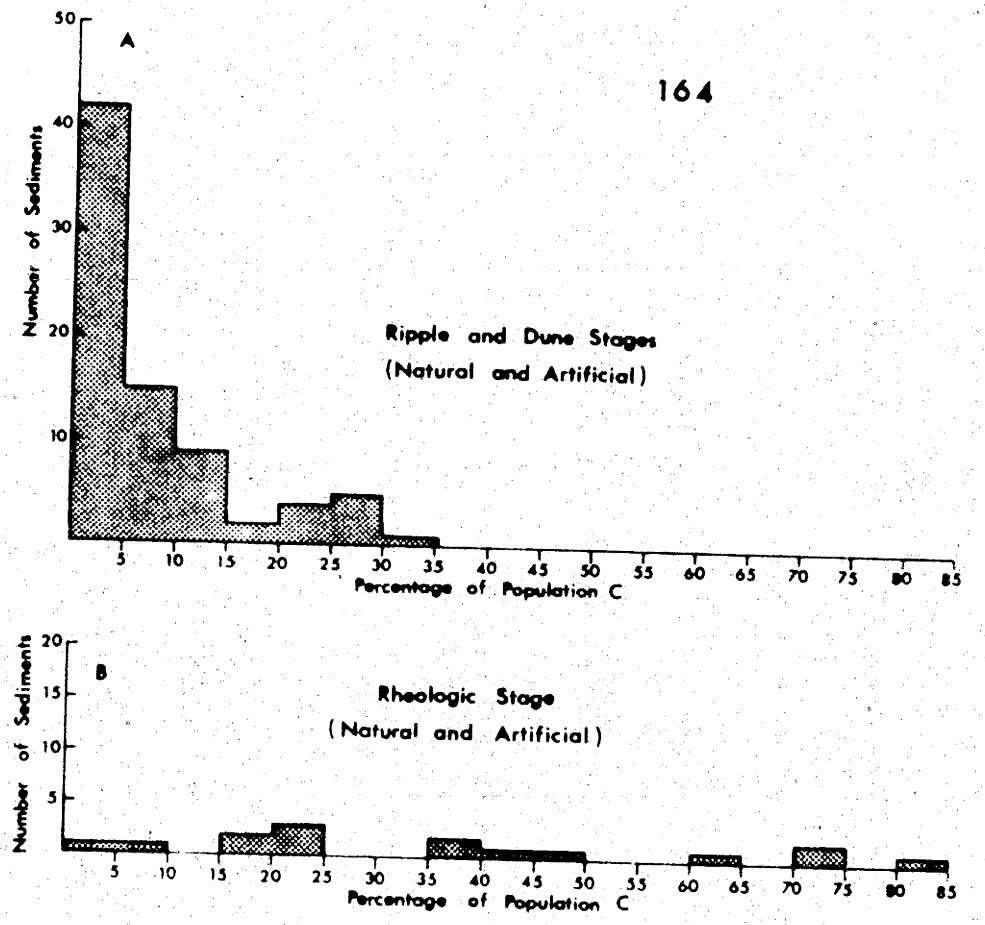

Fig. 164. Distribution of percentage of Population C in natural and artificial bed load sediments.

Fig. 165. Specimen of late Precambrian rippled sandstone from Ediacara, South Australia. Specimen about 20 cm across.

Fig. 166. Underside of specimen shown in Fig. 165 showing two medosoid specimens cast in fine sand. Specimens about 7 cm in diameter.

FIGURE 167

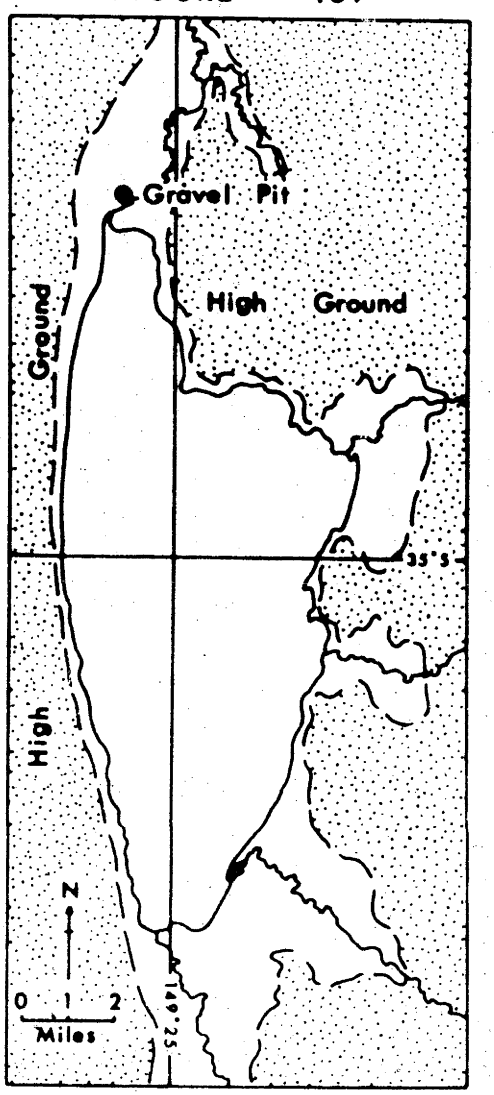

Fig. 167. Sketch map showing position of sampled gravel pit and general environment of Lake George.

Fig. 168. Photograph of face in gravel pit to north of Lake George. North to the right. Permeability variations cause variations in shade, due to dampness. Note current bedded unit.

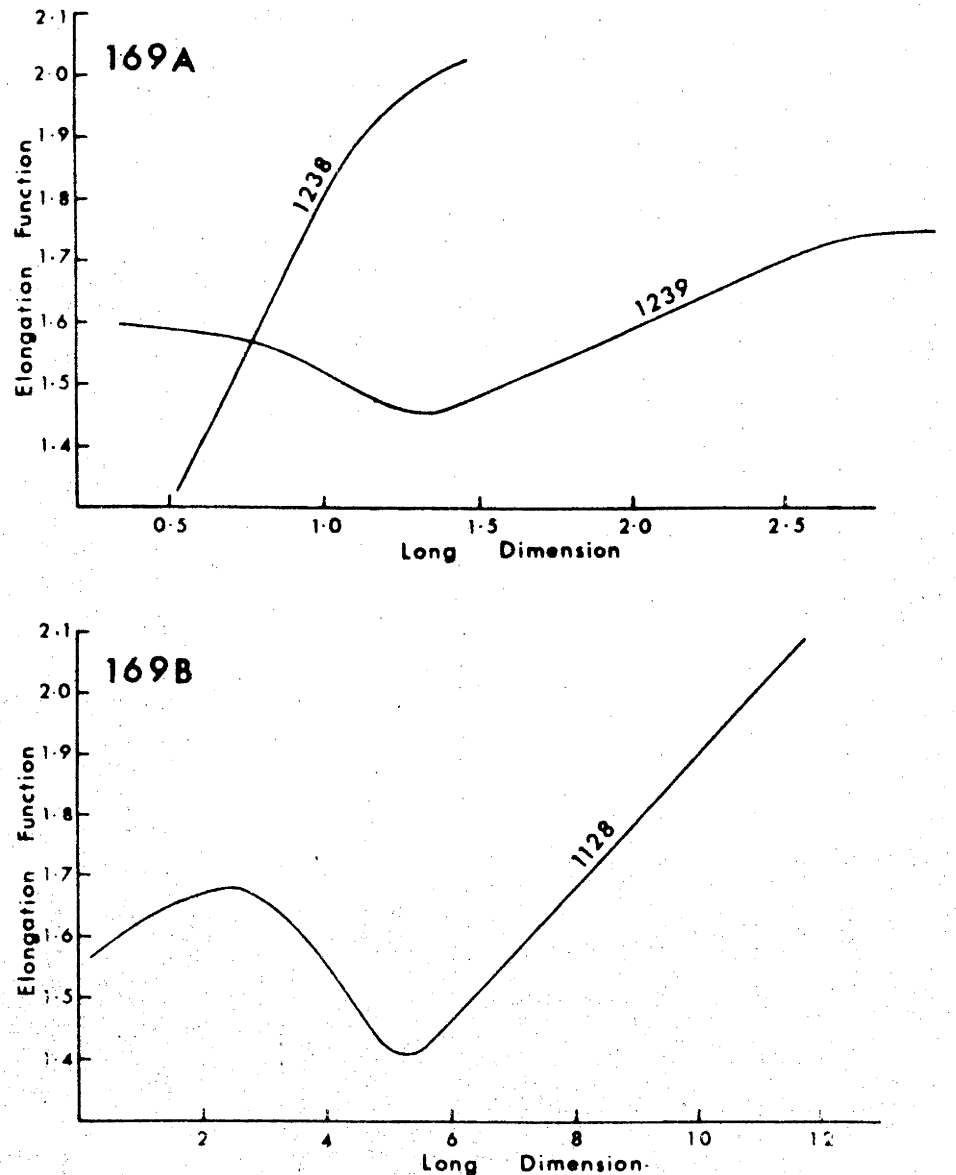

Fig. 169. Elongation function curves of a modern lake margin deposit (No. 1238) from Lake George and two samples from the investigated fossil deposit.

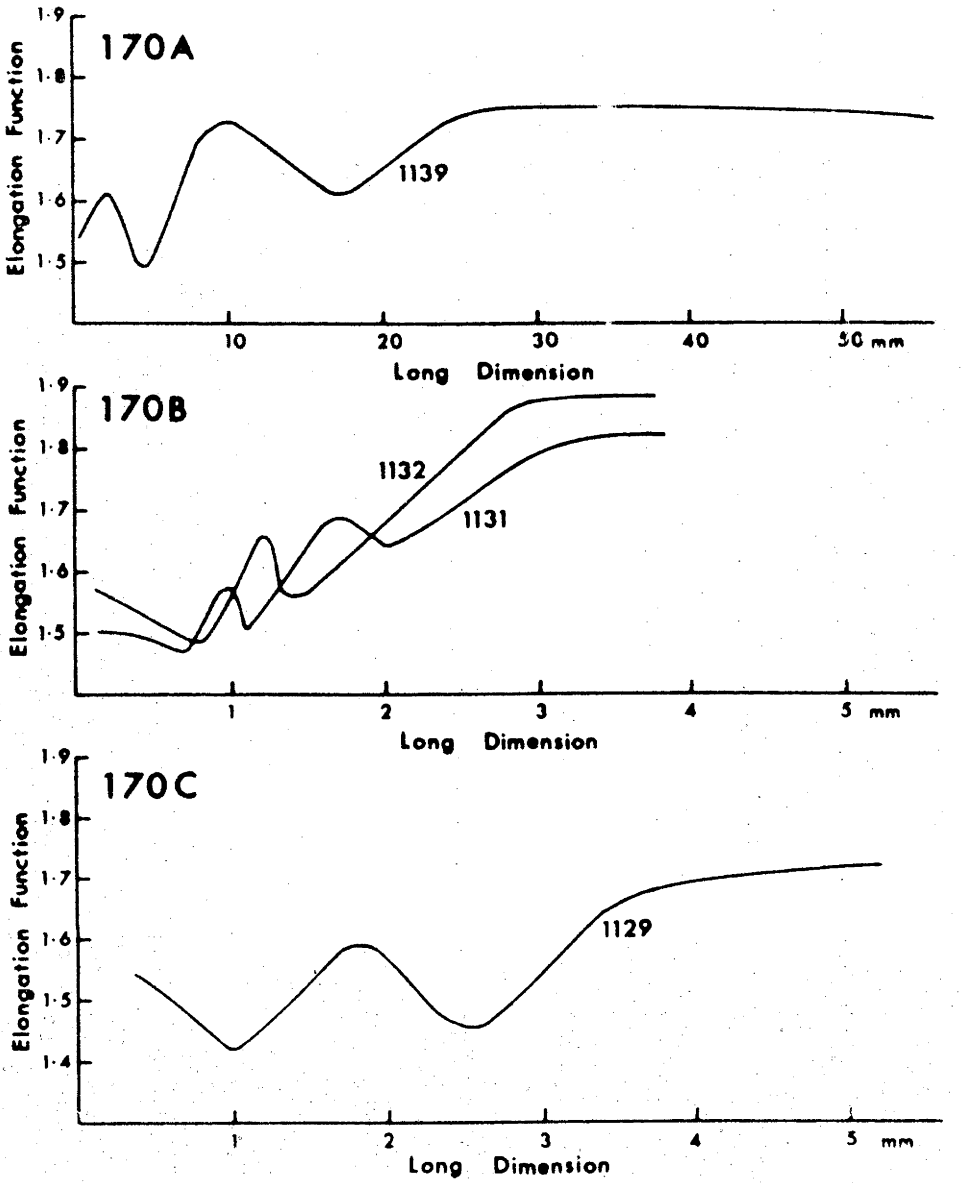

Fig. 170. Elongation function curves of fossil sediments from Lake George gravel pit.

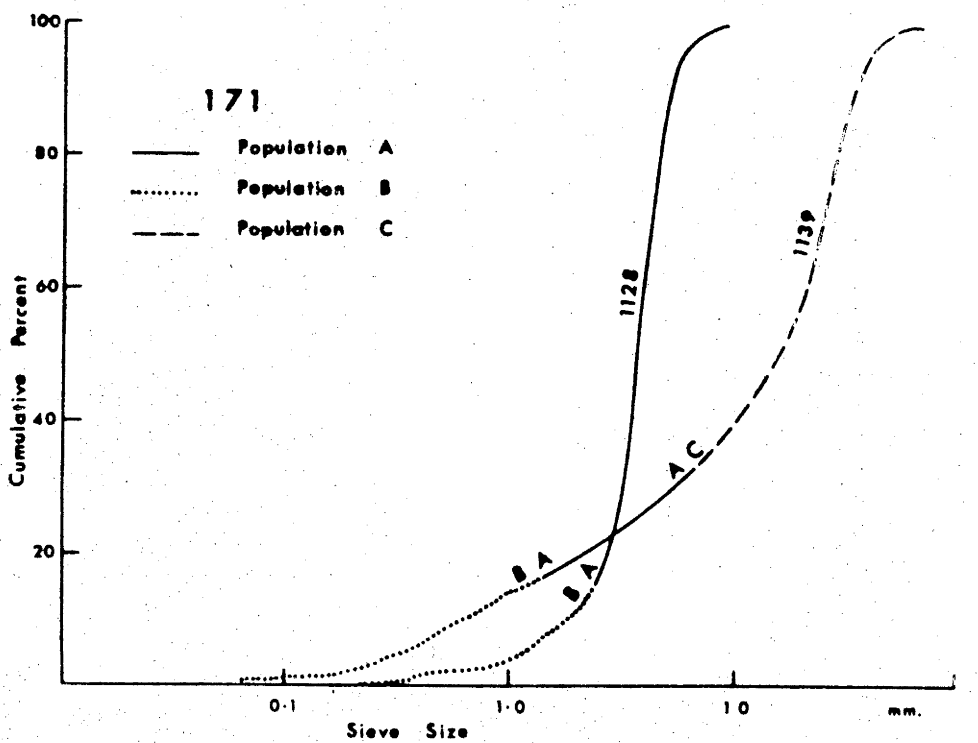

Fig. 171. Sieve cumulative curves of fossil sediments from Lake George gravel pit.

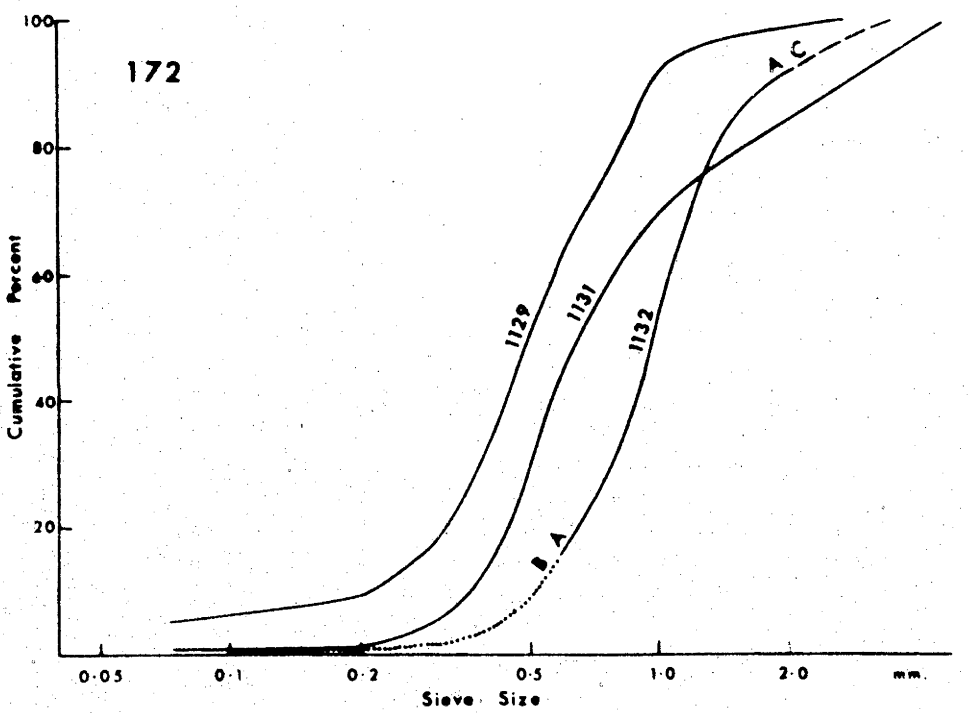

Fig. 172. Sieve cumulative curves of fossil sediments from Lake George gravel pit.

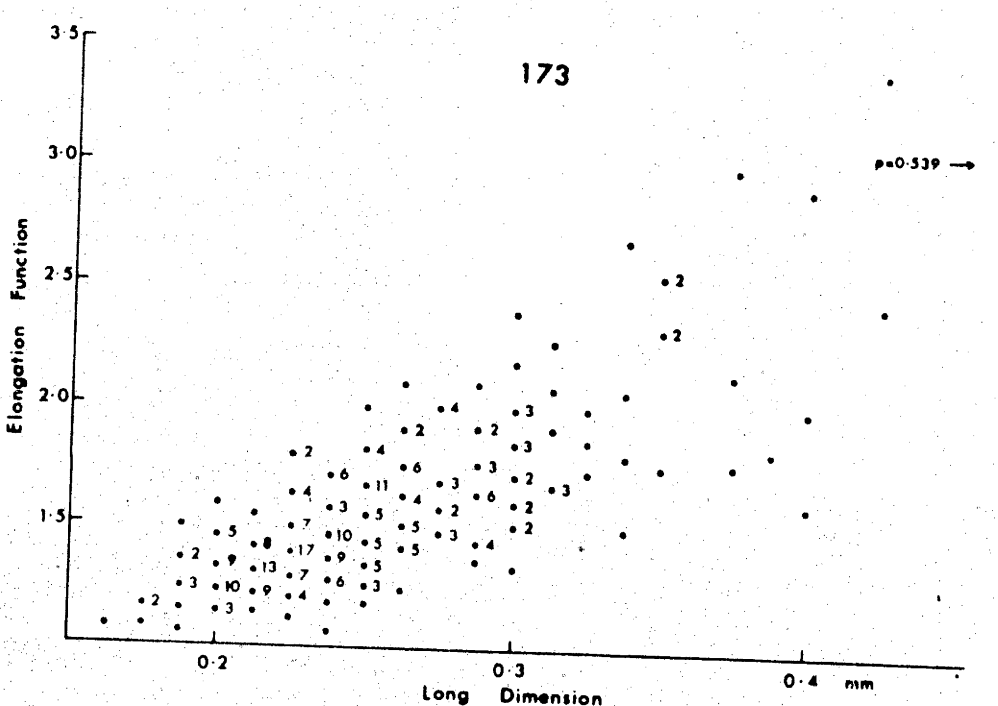

Fig. 173. Scatter plot of data for suite of quartz particles of nearly constant settling velocity. Curve shown in Figs. 1, 2 and 3. If point occurs more than once, number beside it indicates number of times.

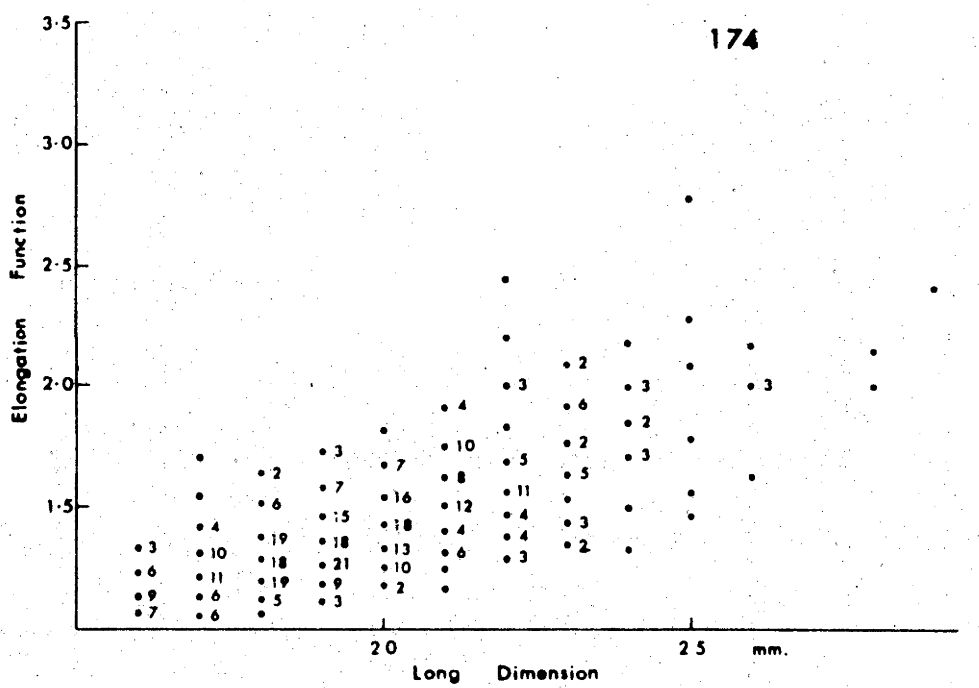

Fig. 174. Scatter plot of data for 400 pebbles of nearly constant mass. Curve shown in Fig. 5. Plotted as for Fig. 173.

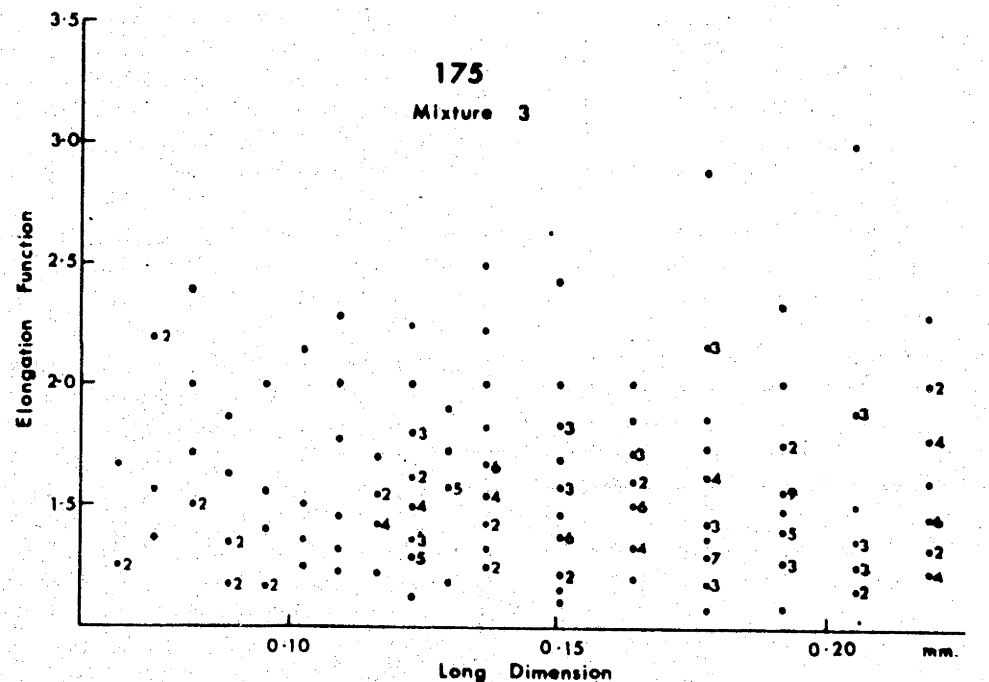

Fig. 175. Scatter plot for mixture 3. Plotted as for Fig. 173 but vertical dashed lines indicate boundaries between separate measured ranges.

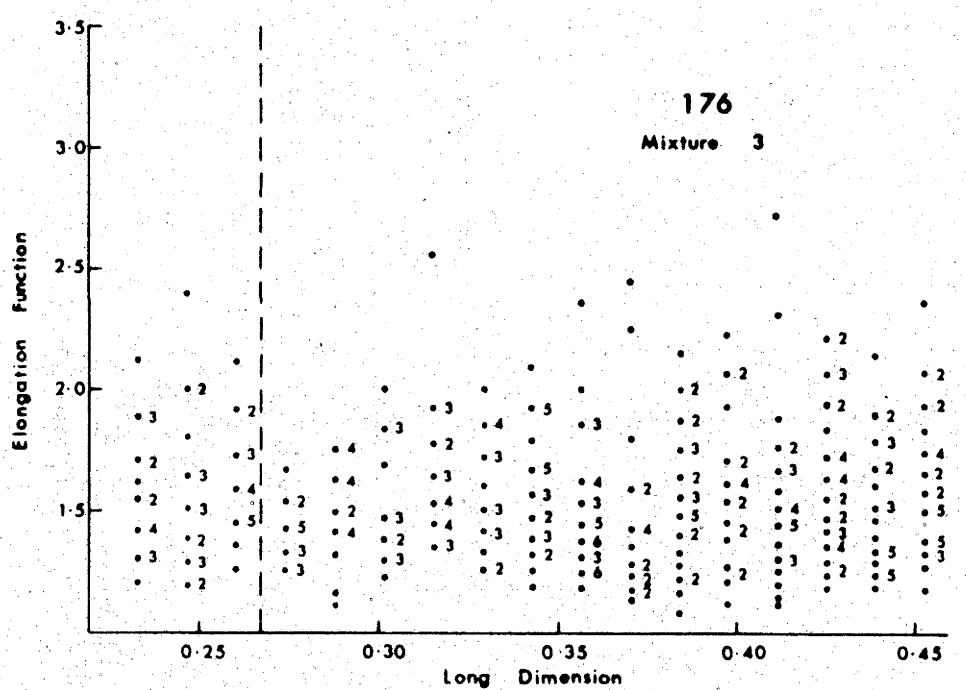

Fig. 176. As Fig. 175.

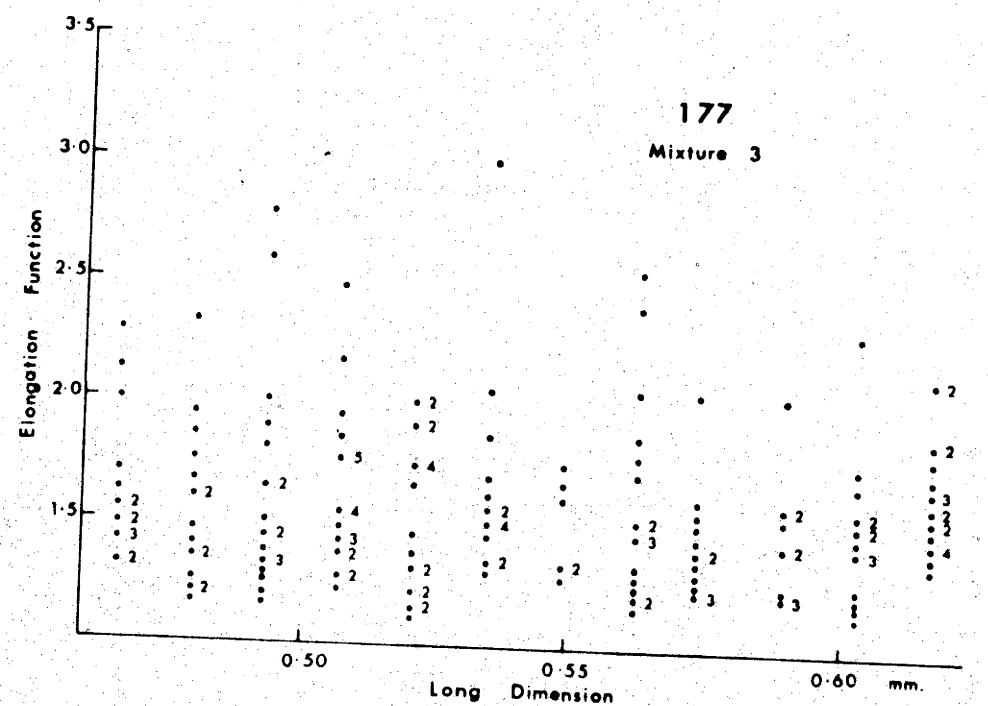

Fig. 177. As Fig. 175.

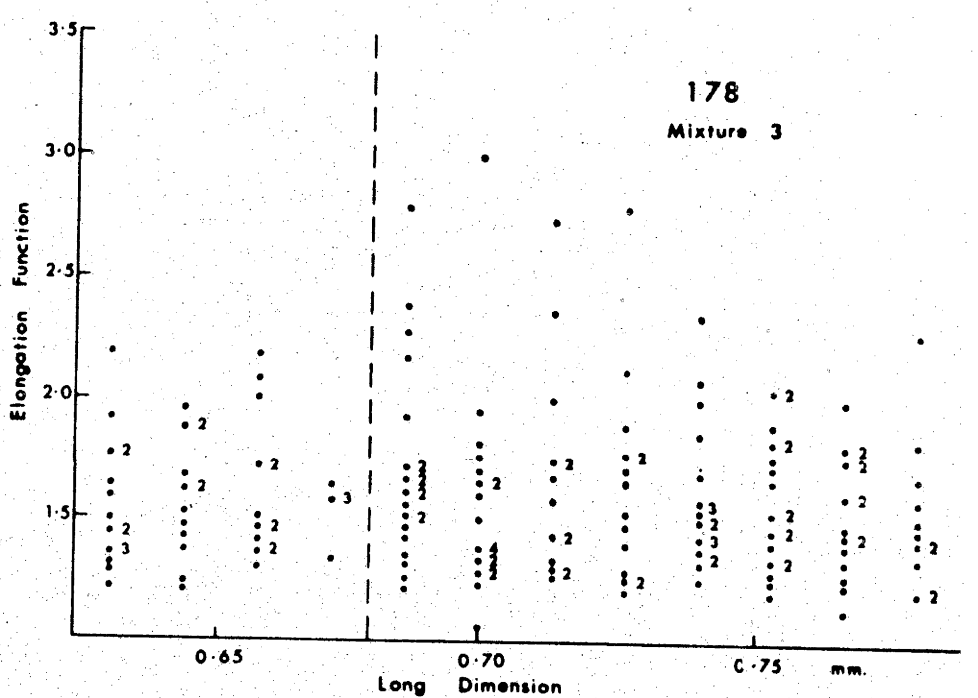

Fig. 178. As Fig. 175.

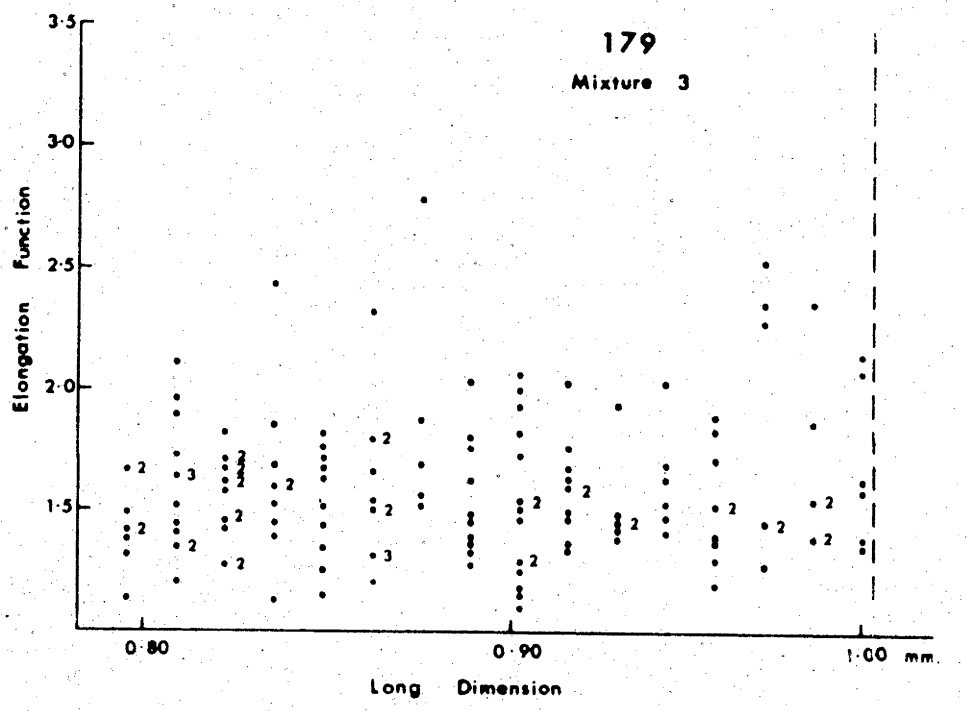

Fig. 179. As Fig. 175.

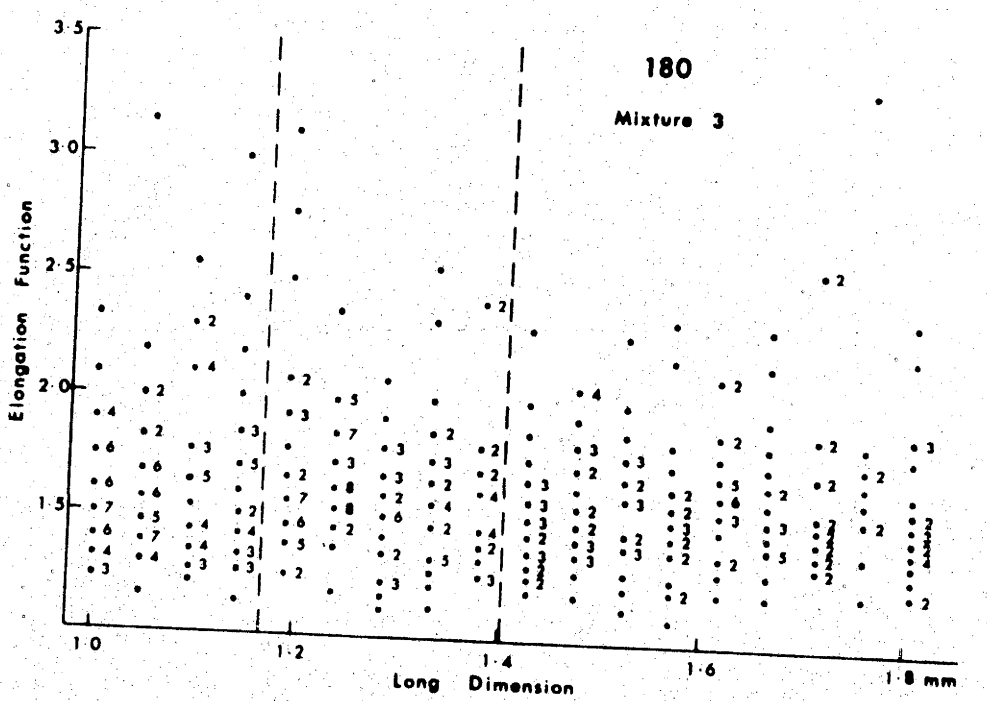

Fig. 180. As Fig. 175.

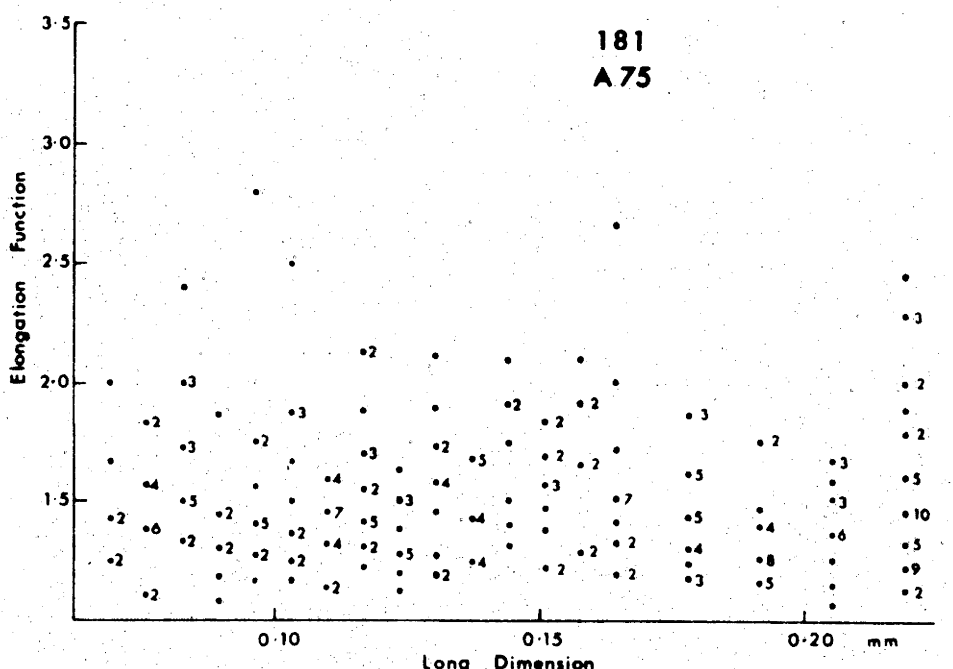

Fig. 181. Scatter plot for A.75. Plotted as for mixture 3.

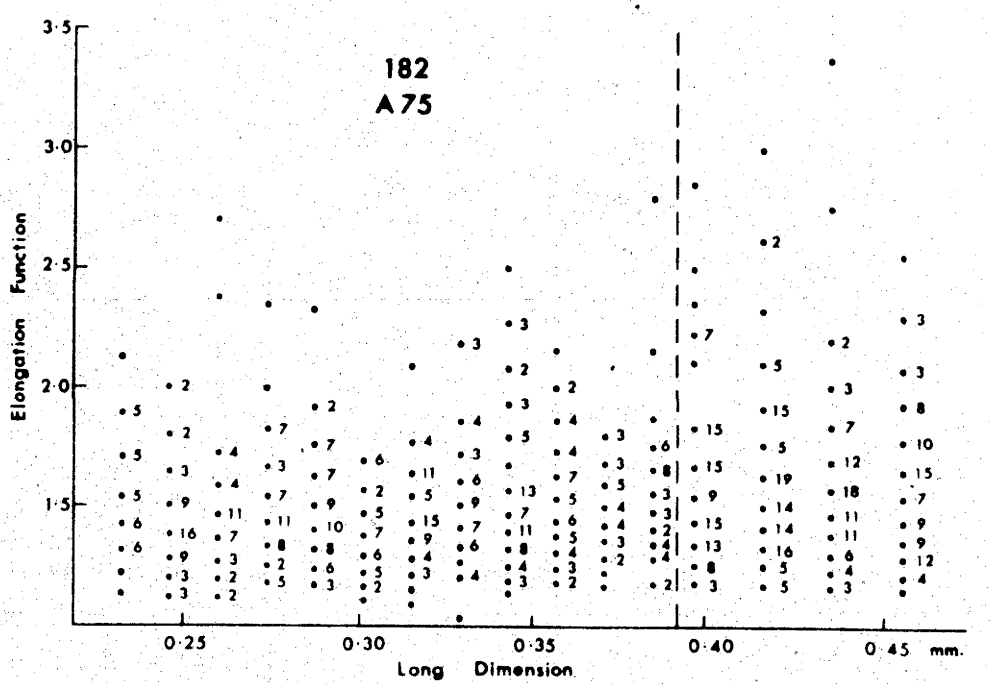

Fig. 182. As Fig. 181.

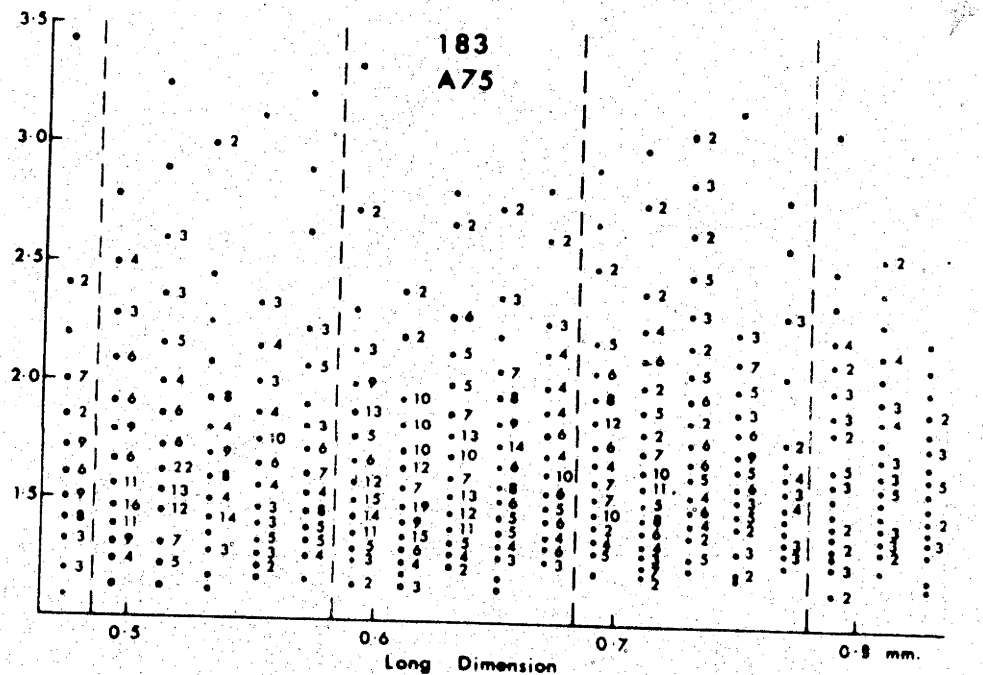

Fig. 183. As Fig. 181.

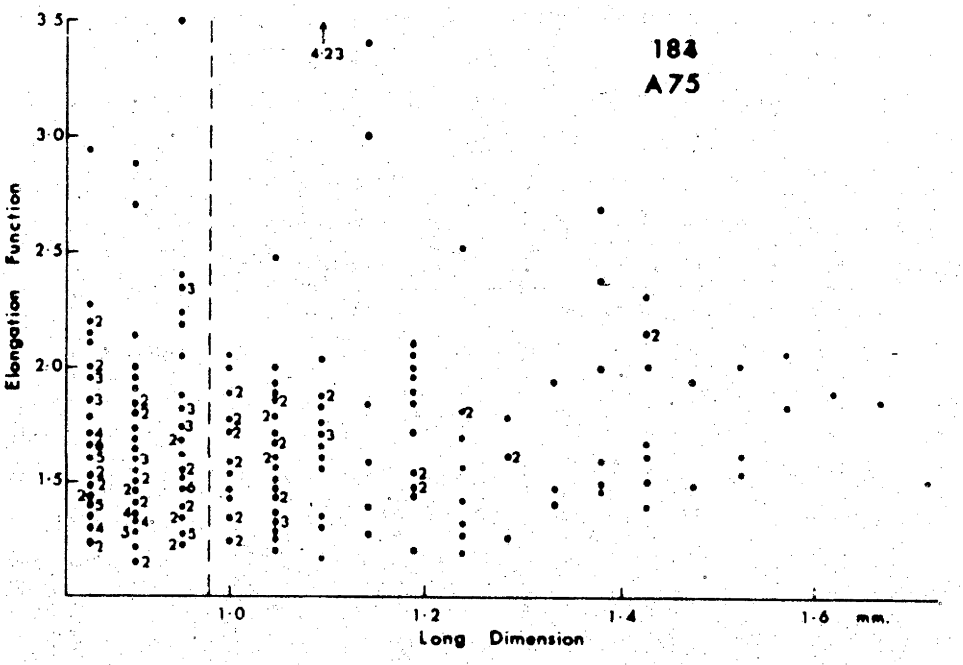

Fig. 184. As Fig. 181.

APPENDIX I

Sample Number	Locality and Description	Figures showing main results	Number of par-ticles measured
1110	Murrumbidgee River, Taemas Bridge, Yass, N.S.W. Ripple stage; ripple foreset	16,17	840
1111	Murrumbidgee River, Taemas Bridge, Yass, N.S.W. Ripple stage; level-bedded material closely associated with ripples	16,18	630
1113	Murrumbidgee River, Taemas Bridge, Yass, N.S.W. Ripple stage; fine sand from foreset of small ripple	15,18	540
1114	Murrumbidgee River, Taemas Bridge, Yass, N.S.W. Dune stage; nearly level lamina at base of excavated dune	25,26	600
1118	Murrumbidgee River, Taemas Bridge, Yass, N.S.W. Dune stage; topset of sectioned dune	25,28	600
1119	Murrumbidgee River, Taemas Bridge, Yass, N.S.W. Dune stage; topset of sectioned dune	25,28	600
1120	Murrumbidgee River, Taemas Bridge, Yass, N.S.W. Dune stage; foreset of sectioned dune	26,28	900
1121	Murrumbidgee River, Taemas Bridge, Yass, N.S.W. Dune stage; foreset of sectioned dune	25,27	780
1122	Murrumbidgee River, Taemas Bridge, Yass, N.S.W. Dune stage; foreset of sectioned dune	25,27	870

Sample Number	Locality and Description	Figures showing main results	Number of particles measured
1128	Gravel pit, northern end of Lake George, N.S.W. Openwork gravel deposit	169,171	630
1129	Gravel pit, northern end of Lake George, N.S.W. Level-bedded unit with scattered pebbles	170,172	510
1131	Gravel pit, northern end of Lake George, N.S.W. Current-bedded sand foreset in unit with scattered pebbles	170,172	720
1132	Gravel pit, northern end of Lake George, N.S.W. Current-bedded sand foreset in unit with scattered pebbles	170,172	600
1139	Gravel pit, northern end of Lake George, N.S.W. Level-bedded sandy gravel	170,171	1295
1141	Deep Creek, Lake George, N.S.W. Ripple stage; base of ripple foreset; see fig. 12	16,17	420
1142	Deep Creek, Lake George, N.S.W. Ripple stage, level bedded material; see fig. 12	16,18	420
1144	Deep Creek, Lake George, N.S.W. Ripple stage; mid-foreset of small deltaic structure; see fig. 12	16,18	330
1146	Deep Creek, Lake George, N.S.W. Ripple stage; low on foreset of small deltaic structure; see fig.12	16,18	540
1152	Naas River, Glencoe, A.C.T. Ripple stage; foreset of active ripple	16,17	390

Sample Number	Locality and Description	Figures showing main results	Number of particles measured
1153	Naas River, Glencoe, A.C.T. Rheologic bed load stage; level-bedded sandy gravel	41,45,46	1260
1156	Naas River, Glencoe, A.C.T. Rheologic bed load stage; level-bedded pebbly sand	39,49,50	1080
1159	Molonglo River, Foxlow, Captains Flat, N.S.W. Ripple stage; foreset of active ripple	15,17	360
1160	Molonglo River, Foxlow, Captains Flat, N.S.W. Rheologic bed load stage; level-bedded sandy gravel	38,49,50	1410
1162	Molonglo River, Foxlow, Captains Flat, N.S.W. Rheologic bed load stage; current bedded sandy gravel	39,52	1080
1170	Murrumbidgee River, Gumly-Gumly, Wagga Wagga, N.S.W. Ripple stage; foreset of small ripple	15,18	540
1172	Murrumbidgee River, Gumly-Gumly, Wagga Wagga, N.S.W. Ripple stage; level-bedded material	15,18	480
1175	Hillas Creek, Deltroit, Gundagai, N.S.W. Ripple stage; active ripple foreset	16,18	660
1176	Hillas Creek, Deltroit, Gundagai, N.S.W. Ripple stage; active ripple foreset	16,17	450

Sample Number	Locality and Description	Figures showing main results	Number of particles measured
1177	Hillas Creek, Deltroit, Gundagai, N.S.W. Ripple stage; level-bedded material	16,18	360
1179	Hillas Creek, Deltroit, Gundagai, N.S.W. Ripple stage, level-bedded material	16,17	360
1180	Murrumbidgee River, Riversdale, Gundagai, N.S.W. Rheologic bed load stage; level-bedded sandy gravel from beneath coarse pebble monolayer	34,47,48	3180
1181	Murrumbidgee River, Riversdale, Gundagai, N.S.W. Ripple stage; level-bedded	15,17	450
1184	Murrumbidgee River, Riversdale, Gundagai, N.S.W. Ripple stage; ripple foreset	13,15,18	570
1186	Murrumbidgee River, Riversdale, Gundagai, N.S.W. Ripple stage; level-bedded material	15,17	360
1187	Murrumbidgee River, Riversdale, Gundagai, N.S.W. Ripple stage; active ripple foreset	15,18	420
1188	Murrumbidgee River, Riversdale, Gundagai, N.S.W. Ripple stage; level-bedded material	14,16,18	420
1189	Murrumbidgee River, Riversdale, Gundagai, N.S.W. Ripple stage; level-bedded material	15,18	540
1190	Murrumbidgee River, Riversdale, Gundagai, N.S.W. Ripple stage; ripple foreset	15,17	360

Sample Number	Locality and Description	Figures showing main results	Number of particles measured
1191	Murrumbidgee River, Riversdale, Gundagai, N.S.W. Ripple stage; ripple foreset	15,17	540
1192	Murrumbidgee River, Riversdale, Gundagai, N.S.W. Ripple stage; ripple foreset	15,18	450
1193	Murrumbidgee River, Riversdale, Gundagai, N.S.W. Rheologic bed load deposit; level-bedded sand	41,51	1890
1194	Murrumbidgee River, Riversdale, Gundagai, N.S.W. Rheologic bed load deposit; level-bedded sand	40,51	2100
1201	Murrumbidgee River, 2 miles S. of Taemas Bridge, Yass, N.S.W. Dune stage; foreset of active dune	25,27	540
1210	Murrumbidgee River, 2 miles S. of Taemas Bridge, Yass, N.S.W. Dune stage; large foreset across entire flow	26,27	600
1212	Murrumbidgee River, 2 miles S. of Taemas Bridge, Yass, N.S.W. Dune stage; large foreset across entire flow	26,27	630
1215	Murrumbidgee River, 2 miles S. of Taemas Bridge, Yass, N.S.W. Dune stage; foreset of small, active dune	25,28	570
1217	Murrumbidgee River, 2 miles S. of Taemas Bridge, Yass, N.S.W. Dune stage; large foreset across entire flow	26,27	600
1218	Naas River, Tharwa, A.C.T. Dune stage; dune foreset	26,27	600

Sample Number	Locality and Description	Figures showing main results	Number of particles measured
1219	Naas River, Tharwa, A.C.T. Dune stage; dune foreset	26,27	510
1220	Naas River, Tharwa, A.C.T. Dune stage; dune foreset	26,27	510
1223	Naas River, Tharwa, A.C.T. Dune stage; level-bedded material	24,26,27	480
1224	Naas River, Tharwa, A.C.T. Dune stage; dune foreset	25,28	600
1225	Naas River, Tharwa, A.C.T. Dune stage; dune foreset	26,27	540
1226	Naas River, Tharwa, A.C.T. Dune stage; level-bedded material	26,28	570
1228	Goodradigbee River, Wee Jasper, N.S.W. Rheologic bed load stage; level-bedded sandy gravel	36,47,48	3000
1230	Murrumbidgee River, Jugiong, N.S.W. Rheologic bed load stage; level-bedded sand	34,43,44	1140
1232	Murrumbidgee River, Jugiong, N.S.W. Rheologic bed load stage; level-bedded sand	35,43,44	2100
1235	Murrumbidgee River, Angle Crossing, A.C.T. Rheologic bed load stage; current bedded foreset	37,43,44	1700
1236	Murrumbidgee River, Angle Crossing, A.C.T. Rheologic bed load stage; level bedded material	37,43,44	1740
1238	Western shore of Lake George, N.S.W. Recent lake margin deposit	169	720

Sample Number	Locality and Description	Figures showing main results	Number of particles measured
1239	Gravel pit, northern end of Lake George, N.S.W. Sand lamina gently inclined towards the lake	169	1200
1240	Estuary, Narooma, N.S.W. Dune stage; active dune foreset	25,28	1080
1241	Estuary, Narooma, N.S.W. Dune stage; active dune foreset	25,28	1020
1243	Estuary, Narooma, N.S.W. Dune stage; active dune foreset	25,27	1140
1245	Estuary, Narooma, N.S.W. Dune stage; symmetrical ripple-like structure atop active dune	25,28	1140

APPENDIX 2

Sample Number	Flume run; position on bed; description	Figures showing main results	Number of particles measured
Mixture 1	Fine mixture; parent material of samples A30 to A50; feed of all runs prefixed "1"	82, 83	750
Mixture 2	Medium mixture; parent material of samples A1 to A29; feed of all runs prefixed "2"	82, 83	690
Mixture 3	Coarse mixture; parent material of samples A52 to A77; feed of all runs prefixed "3"	82, 83	1840
A1	Run 2A; 1'9"; ripple stage; ripple foreset	84,85,86	600
A4	Run 2A; 7'3"; ripple stage; ripple foreset	84,85,86	660
A7	Run 2A; 14'4"; ripple stage; ripple foreset	84,85,86	840
A9	Run 2B; 5'8"; ripple stage; ripple foreset	87,88,89	660
A11	Run 2B; 12'0"; ripple stage; ripple foreset	87,88,89	570
A12	Run 2B; 14'0"; ripple stage; ripple foreset	87,88,89	600
A14	Run 2C; 3'6"; dune stage; dune foreset	90,91,92	1020
A16	Run 2C; 8'0"; dune stage; dune foreset	90,91,92	960
A20	Run 2D; 3'11"; probably ripple stage, antedating dune stage; horizontal lamina	93,94,95	1760
A21	Run 2D; 4'11"; dune stage; dune foreset	93,94,95	1040
A27	Run 2E; 9'0"; dune and rheologic stages; foreset of very low dune	96,97,98	720

Sample Number	Flume run; position on bed; description	Figures showing main results	Number of particles measured
A29	Run 2E; 14'3"; dune and rheologic stages; horizontal lamina	96,97,98, 99,100, 101	1110
A30	Run 1A; 1'9"; ripple stage; ripple foreset	102,103, 104	630
A35	Run 1A; 12'4"; ripple stage; ripple foreset	102,103, 104	810
A36	Run 1B; 2'2"; ripple stage; ripple foreset	106,107, 108	600
A37	Run 1B; 4'3"; ripple stage; ripple foreset	106,107, 108	810
A38	Run 1B; 7'4"; ripple stage; ripple foreset	106,107, 108	600
A39	Run 1B; 10'2"; ripple stage; ripple foreset	106,107, 108	690
A40	Run 1B; 12'3"; ripple stage; ripple foreset	106,107, 108	540
A41	Run 1C; 3'9"; dune stage; dune foreset	110,111, 112	600
A42	Run 1C; 7'6"; dune stage; dune foreset	110,111, 112	600
A43	Run 1C; 9'3"; dune stage; dune foreset	110,111, 112	540
A44	Run 1C; 11'2"; dune stage; dune foreset	110,111, 112	600
A45	Run 1D; 4'0"; rheologic stage; level lamina	113,114, 115	1840
A47	Run 1D; 9'0"; rheologic stage; level lamina	113,114, 115	1380
A50	Run 1E; ripple stage; "deltaic" foreset	116,117, 118	780

Sample Number	Flume run; position on bed; description	Figures showing main results	Number of particles measured
A52	Run 3A; 4'6"; ripple stage; level lamina	119,120, 121	840
A54	Run 3A; 11'3"; ripple stage; level lamina	119,120, 121	800
A55	Run 3B; 1'3"; dune and ripple stages; dune foreset	126,127, 128	1440
A58	Run 3B; 3'0"; dune and ripple stages; dune foreset	126,127, 128	960
A61	Run 3B; 8'9"; dune and ripple stages; ripple foreset	126,127,	840
A64	Run 3C; 4'7"; dune stage; dune foreset	129,130, 131	960
A66	Run 3C; 13'3"; dune stage; dune foreset	129,130, 131	940
A67	Run 3D; 6'6"; rheologic stage; level bed; (pebbles added to flume as well as mixture 3)	132,133, 134	3370
A70	Run 3D; 6'6"; rheologic stage; level bed	132,133, 134	2040
A73	Run 3E; 3'0"; rheologic stage; level bed	135,136,	2300
A75	Run 3E; 7'0"; rheologic stage; level bed	135,136, 137,138-141	2700
A77	Run 3E; 11'0"; rheologic stage; level bed	135,136, 137	3100
	Constant size sand grain suite	5, 7	125
	Constant size pebble suite	5, 7	400
	Settling velocity suites:-		
	0.68 - 0.74 cm/sec	3	260
	0.74 - 0.82 "	1,2,3	

Sample Number	Flume run; position on bed; description	Figures showing main results	Number of particles measured
	Settling velocity suites (cont):-		
	0.82 - 0.90 cm/sec	3	320
	0.90 - 0.99 "	3	280
	0.99 - 1.09 "	3	280
	1.09 - 1.20 "	3	320
	1.20 - 1.32 "	3	300
	1.32 - 1.45 "	3	260
	1.45 - 1.59 "	3	300
	1.59 - 1.75 "	3	300
	1.75 - 1.93 "	3	280
	1.93 - 2.12 "	3	280
	2.12 - 2.33 "	3	280
	2.33 - 2.57 "	3	320
	2.57 - 2.82 "	3	300
	2.82 - 3.11 "	3	280
	3.11 - 3.42 "	3	280
	3.42 - 3.75 "	3	300
	3.75 - 4.13 "	3	340
	4.13 - 4.54 "	3	300
	4.54 - 5.00 "	3	260
	5.00 - 5.50 "	3	320
	5.50 - 6.05 "	3	240
	6.05 - 6.65 "	3	340
	6.65 - 7.32 "	3	320

Sample Number	Flume run; position on bed; description	Figures showing main results	Number of particles measured
	Settling velocity suites (cont):-		
	7.32 - 8.05 cm/sec	3	260
	8.05 - 8.85 "	3	320
	8.85 - 9.72 "	3	300
	9.72 - 10.69 "	3	240

APPENDIX 3

reached if and when it was found that samples, from similar physical environments but different geographical locations, gave essentially similar results but that samples, from the same geographical location but different physical environments, gave quite different results. Statistically, the most important event in the investigation occurred when, after some thirty thousand particles had been measured, there was no reasonable doubt remaining as to the consistent reflection of environmental variation by the results produced by samples. It meant that there was considerable justification for formulating explanatory hypotheses, for testing such hypotheses, modifying them accordingly and, thereby, approaching more closely a rational explanation of the overall results. In terms of these hypotheses, flume experimentation could be planned to give much greater returns than would otherwise have been possible.

In the context of the above discussion, suppose that, in studying samples within a certain category (e.g. coarse ripple stage sands) there is time to measure 20,000 particles. Were one to measure all 20,000 from one sample, a very accurate curve would result but one would be quite unaware that the category, as a whole, existed and, for all one knew, the sample would be unique in the world. On the other hand, one could measure 20 particles from each of a thousand samples but find out virtually nothing because the resolution of individual curves would be very low. Both

these extremes are well nigh useless but, somewhere between them, lie compromise values for the number of particles per sample and the number of samples (whose product is 20,000) that gives the maximum amount of sedimentological information. Where this compromise lies depends largely on the complexity of the sediments for the more numerous the features of the elongation function curve the greater the number of data per sample needed to resolve them. This cannot be predicted in advance. Consequently a certain amount of guesswork is inevitable. Whatever the compromise used, as long as it was reasonably near the ideal compromise, it is the overall weight of the 20,000 data that counts.

In practice it was found that, although an intelligent guess had to be made in the first instance, as to the number of particles to be measured in each sample, three methods acted as a check and guide for later work. These were:-

1. For each batch of similar samples the 95% confidence limits for the individual elongation function means were evaluated in one or two cases. This process is time consuming but, if the raw material from which the sediments are made varies little and the general curve form is the same, then the results obtained give a general idea of the reliability for the number of data in the batch as a whole.

2. For one or two samples in each batch the number of particles measured was doubled or even trebled. This was a safeguard against losing curve detail through lack of resolution. Feature 1 was first resolved by this method.

3. Should any reasonable doubt occur as to the form of an elongation function curve over some part of the size range, then more grains would be measured across the size range until no reasonable doubt remained.

The general form of the elongation function curve is used in interpretation rather than the exact value of the elongation function at some particular value of the long dimension.

There is, of course, little or no justification for fitting a statistical curve to the size-shape data. As mentioned in the main text, the curve for a complex sediment is more analogous to a seismograph curve than to a simple mathematical relationship between two quantities. As size increases, first one physical influence asserts itself, then another. Thus an equation for the whole curve would have no useful physical meaning. Thus curve fitting by eye to a series of points, the accuracy of which was known either by direct statistical test or by close analogy, was the standard method used.

Computors were not used, largely because the pioneering nature of the project made it uncertain in advance how the data should be treated and adherence to a programme, to some extent, involved prejudgement.

A mechanical calculating machine was used for the calculations. Whether justifiably or not, it is felt that the extreme familiarity with first the grains, then the data which the somewhat tedious work of measuring and calculating allowed, gave some advantage in the interpretation of results.

It would take about a year to plot out the results of size-shape analysis accrued during the study in full. The full scatter plots have proved rather unhelpful and more can be learnt from elongation function curves and distribution plots. However, there is some point in viewing the full scatter of points and four samples have been thus plotted in Figures 173 to 184.

Figure 173 shows the scatter plot for the suite of grains of nearly constant settling velocity whose original curve was given in Figures 1 and 2. Figure 174 shows the equivalent plot for the 400 quartz pebbles of nearly equal size that were treated in the preliminary section of the thesis (Fig. 5). Of course, the materials from which the suites were derived were of rather different physical origin. Visual comparison of such large spreads of points appears to be rather difficult.

A more pertinent comparison can be made between the data for mixture 3 (Figures 175-180) and A75 (Figures 181-184), a rheologic bed load sediment derived from mixture 3. The original elongation function curves for these materials were given in Figures 82 and 135. In this case there do appear to be visible differences in

the scatter plots. Around p = 0.20 mm the sediment clearly shows a lack of elongate grains - this corresponds to feature 1. An excess of elongate grains occurs in the range p = 0.40 - 0.60 mm - due to feature 2 with its concentration of elongated grains in Population B. In this vicinity, the scatter appears to show some sign of bimodality with respect to the elongation function. At P = 0.60 mm the excess of elongate grains shown by the sediment suddenly ceases and, thereafter, there is evidently a steady overall climb in elongation function values to p = 0.80 mm. This represents pure Population A. Feature 3 occurred at p = 0.80 mm and the scatter seems to show elongate grains becoming relatively rarer beyond this point.

In retrospect, it is felt that all the features shown on the scatter plots have been made much more vividly apparent by the other methods of data-handling that have been used. The work involved in plotting these scatters does not appear to be justifiable on available evidence.

All data and samples used in the present study are retained by the author. The data are being kept because they could well shed light on topics that have not yet come to mind. The samples are kept because it may save much time to apply other techniques to suites of particles about which much is already known.